GRATINGS WITH MULTIPLE, INDEPENDENTLY APODIZED LAYERS

Thomas L. Gradishar

Thesis submitted to the Faculty of the
Virginia Polytechnic Institute and State University
in partial fulfillment of the requirements for the degree of

Master of Science
in
Electrical Engineering

Ahmad Safaai-Jazi, Chair
Ioannis M. Besieris
Lee W. Johnson

Blacksburg, Virginia

Key words: Gratings, optical fiber communications

GRATINGS WITH MULTIPLE, INDEPENDENTLY APODIZED LAYERS

Thomas L. Gradishar

(ABSTRACT)

An index grating is a periodic perturbation of the refractive index in a waveguide's axial direction. Gratings have important roles in optical communication as spectral filters and dispersion compensators. The spectral response characteristics of gratings can be controlled by shaping the profile of the index modulation, a process called apodization.

Apodizing different layers of the grating using different apodizing functions is proposed for adding more degrees of freedom to the design. An approach to designing a two-layer separately apodized grating that yields virtually the same reflectivity and dispersion responses as an arbitrary zero-"dc", apodized, un-chirped grating is proposed. A design example is presented, and coupled-mode theory is employed to compute the reflectivity responses of the original zero-"dc" design and the nearly equivalent separately-apodized design proposed in this thesis.

An approach to designing a four-layer separately apodized grating that yields virtually the same reflectivity and dispersion responses as an arbitrary chirped grating is proposed. The largest bandwidth a four-layer separately-apodized grating designed using this approach can yield is as large as the largest bandwidth a variable-period conventional design can yield. Also, a similar, less-capable design approach is proposed for two-layer separately apodized gratings that are equivalent to conventional, chirped gratings. Design examples are presented.

For all of the separately apodized gratings designed, the layers have a varying "dc" index change that is proportional to the varying "ac" index change. Furthermore, the period, which is the same in every layer, is constant, i.e. independent of the position. Both considerations enhance the prospects of fabricating the separately-apodized designs using a simple, reproducible technique. One such technique is proposed that separately-apodizes halves of the waveguide, instead of layers, but the design approaches are easily adjusted to this case.

To the memory of my twin sister, Theresa

Acknowledgements

My heartfelt gratitude goes out to Dr. Ahmad Safaai-Jazi for the countless hours he spent advising me and reviewing my work. I will never forget that above all he was concerned that I would benefit. He set an example I would like to follow if I have a chance to pass on what I have learned later in my career.

I also acknowledge the assistance of my other committee members, Dr. Ioannis Besieris and Dr. Lee Johnson. The classes I took with them were some of the best I had, and they were always helpful to me.

Contents

Tables

Figures

Chapter 1

Introduction

Germania-doped optical fibers and planar waveguide devices exhibit the property of photosensitivity. The refractive index permanently increases in response to UV irradiation. By illuminating the fiber or planar waveguide through the side or top, respectively, by two intersecting beams of UV light, an interference pattern is formed. This writes a corresponding periodic grating, a perturbation of the refractive index along the waveguide's length.

A light wave incident on the grating is reflected by successive, coherent scattering from the crests in the index perturbation. In the simplest case, the incident wave couples to an identical, counterpropagating mode – hence, it is reflected. However, coupling to any of the supported modes is possible. Because a fiber grating is simply a diffraction grating [1], a simple, qualitative ray-optic picture describes the interactions. The grating diffracts the incident wave with a bounce angle of θ_1 into a wave with a bounce angle of θ_2. Given the angle θ_1 and the period of the grating, the familiar grating equation [1] determines the angle θ_2. If the waveguide supports a mode with a bounce angle of θ_2 at the wavelength of the incident wave, a strong interaction between the modes occurs. If not, then the interference is non-constructive and the grating is transparent to the incident wave. Grating devices are essentially narrowband, hence the interaction occurs within a narrow spectral window centered on the wavelength satisfying the grating equation as described. When the incident wave couples to a counterpropagating like mode, the grating is called a Bragg grating and the wavelength satisfying the grating equation is called the Bragg wavelength.

Fiber gratings have found applications in sensor systems too. The Bragg wavelength is sensitive to external disturbances, such as strain, temperature, and pressure [2] which change the modal propagation constants or grating period. However, this thesis concentrates on applications that gratings have found in optical communications. A grating is a stopband filter in the transmission mode and a passband filter in the reflection mode. Narrowband optical filters have an important role in wavelength

division multiplexing, single-mode semiconductor lasers, and optical spectrum analyzers [3].

Fiber gratings offer compatibility with the transmission medium [2] [4]. However, photosensitivity has also been detected in planar glass optical waveguides, which offer high stability and reproducibility [5]. Considerable interest is directed toward combining planar waveguide devices with narrowband gratings for applications in wavelength division multiplexed (WDM) fiber optic communication systems [5]. In this thesis, all of the analysis is carried out for multi-clad planar waveguides. However, the refractive-index profile is assumed symmetric, increasing the correspondence with the fiber geometry. Furthermore, in the coupled-wave formalism used to compute the gratings' filter characteristics, the dependence on the waveguide geometry is confined to the coupling coefficients and the modal propagation constants. Thus, the methods of the analyses and the design techniques proposed, in particular for apodizing different layers in the waveguide separately as discussed below, are widely applicable to various geometries.

Chapter 2 derives the field solutions and dispersion curves for the TE modes in multi-clad, symmetric planar waveguides with no gratings. It is possible but difficult to solve for the exact modal fields of a mutli-clad, symmetric planar waveguide with gratings using Maxwell's equations. An easier approach that is approximate in nature but surprisingly accurate is to write the fields of the waveguide with gratings as a superposition of the modal fields of the identical waveguide without gratings. The field amplitudes are no longer constant as when gratings are absent, but couple to each other and vary with the axial coordinate. We use this approach, and the coupled-mode theory that is its foundation, to compute all of the quantitative results. Chapter 3 reviews coupled-mode theory, then uses it to derive an expression for the reflectivity of uniform gratings. It is assumed the phase of the index perturbation is the same in every layer of the waveguide. Furthermore, it is assumed the incident wave is TE_0 and couples to a counterpropagating like mode. This second assumption is made every time the reflectivity spectrum is computed in this thesis. Numerous articles and texts have previously solved this problem for different geometries, but the dependence of the analysis and solution on the geometry is confined to the coupling coefficients. Chapter 3

also presents a series of plots of the reflectivity versus normalized wavelength that facilitates an understanding of its dependence on the waveguide parameters.

Chapter 4 repeats the problem solved in Chapter 3, but assumes the phase of the index change is not the same in different layers. No available fabrication techniques can achieve this for the type of gratings we consider -- index modulation, not surface corrugation. The rationale for carrying out this analysis is threefold. Interesting theoretical results could motivate new fabrication techniques, the method of the analysis and the principles behind the results are readily extended to the surface corrugation type of gratings, and the analysis paves the way for the analysis in Chapter 7. The significant, useful results of the thesis are contained in Chapter 7.

The spectral response characteristics of gratings can be controlled by shaping the profile of the index modulation along the length of the grating. This process is called apodization. The reflectivity spectrum of a uniform, i.e. unapodized and unchirped, grating has sidelobes on both sides of the main reflection peak, which are undesirable in applications like WDM. Apodizing the grating by controlling the irradiation dose spatially eliminates the sidelobes on the long wavelength side of the main peak, but gives rise to very different sidelobes on the short wavelength side. They are due to the variation in the "dc" index change. That is, the form of the index modulation, with an apodizing function $f(z)$, is given by $f(z)[1+\cos(\ )]$ since the intensity of the UV light used to fabricate the grating is always non-negative. The "dc" index change is proportional to the "ac" index change. The required form of the index modulation to eliminate the sidelobes from both sides of the main peak is $X + f(z)\cos(\ )$, where the "dc" index change equals a constant, X. Holding the "dc" index change constant depends on using a second exposure or otherwise increasing the complexity of the fabrication technique.

Considerable interest is directed toward using "chirped" gratings as dispersion compensators. As a light pulse propagates through a fiber, it is dispersed, meaning its width is broadened. The longer wavelength light lags the shorter wavelength light. The period of a chirped grating varies linearly with position. Since the grating period determines the wavelength of the light reflected, the longer wavelength light is reflected

near the front of the grating, while the shorter wavelength light is reflected near the back. Thus, all the wavelengths in the light pulse exit the chirped grating at the same time.

Chapter 5 presents the coupled-wave equations for apodized, chirped gratings. They encompass non-chirped gratings, as well. It is assumed that the apodizing function and the dependence of the phase of the index change on position are the same in every layer of the grating. However, a constant phase shift between layers is allowed. The forms of the coupled-wave equations for a "dc" index change that varies in proportion to the "ac" index change, and for a "dc" index change equal to zero ($X = 0$), are presented. Chapter 7 extends the coupled-wave equations to the case where the "dc" index change varies independently of the "ac" index change. Chapter 6 presents the matrix method for solving the coupled-wave equations in Chapter 5. Specifically, the matrix method computes the power reflectivity, the group delay, and the dispersion of the grating (but not the field amplitudes.)

In Chapter 7, it is assumed the apodizing function and the dependence of the phase of the index change on position are different in every layer of the grating. This adds more degrees of freedom to the design. The coupled-wave equations and the matrix method for solving them in Chapters 5 and 6 are adapted to this situation. We present a design approach which allows the "dc" index change to vary in proportion with the "ac" index change without the negative consequences described above. We also present two approaches for designing dispersion compensators without varying the grating period. Separately apodizing the layers is not possible using available fabrication techniques using UV light. However, we propose a fabrication technique that separately apodizes the halves of the waveguide. The design approaches for separately-apodized layers are readily extended to separately-apodized halves, since the analysis and behavior are not substantially changed.

Chapter 2
Field Solutions for Multiclad Symmetric Planar Waveguides

2.1 Geometry

The field solutions for the multi-clad symmetric planar dielectric waveguide shown in Figure 2-1a are determined in this chapter. In later chapters, gratings are added to this waveguide which are viewed as perturbations, and the fields are written as a superposition of the fields in the unperturbed waveguide analyzed here. Each layer extends to infinity along the positive and negative directions of both the y and z axes. The refractive index $n = \sqrt{\varepsilon_r}$, where $\varepsilon_r = \varepsilon/\varepsilon_o$ is the relative permittivity. The refractive index profile is assumed symmetric to increase the correspondence with the fiber geometry, and one possibility is illustrated in Figure 2-1b. The waveguide, then, is described by

$$n(x) = \begin{cases} n_1, & |x| < a_1 \\ n_2, & a_1 < |x| < a_2 \\ n_3, & a_2 < |x| < a_3 \\ n_4, & a_3 < |x| \end{cases} . \qquad (2.1)$$

The region with refractive index n_1 is the core, while the regions with refractive indices n_2, n_3, and n_4 are layers of cladding. n_1, n_2, n_3, and n_4 are nearly equal – their values lie within a few percent of each other. This is the case for so-called "weakly guiding" dielectric waveguides. Although $n_1 = n_3 > n_2 = n_4$ in Figure 2-1b, this is not a requirement. The only constraint is $n_4 < \max\{n_1, n_2, n_3\}$, otherwise the waveguide does not support guided modes as explained later. All layers are nonmagnetic with $\mu = \mu_o$. Although any number of cladding layers could be considered, here we take just three to reduce the complexity of analysis and the computer algorithm required to compute the field solutions. Three cladding layers (six layers if not considering the symmetry in profile) are sufficient to examine the phenomena within the scope of this thesis. This

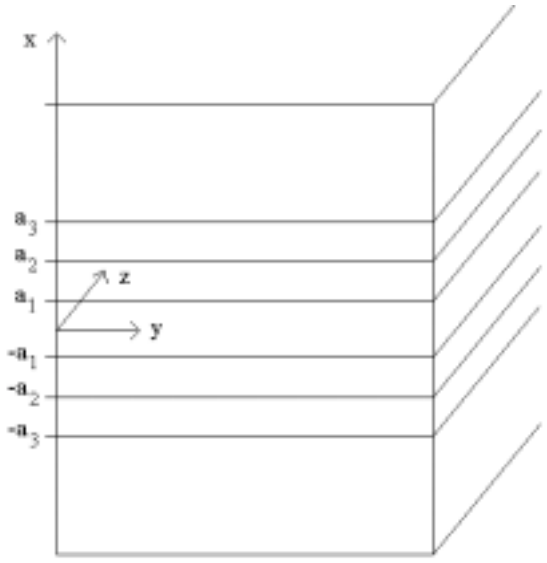

(a)

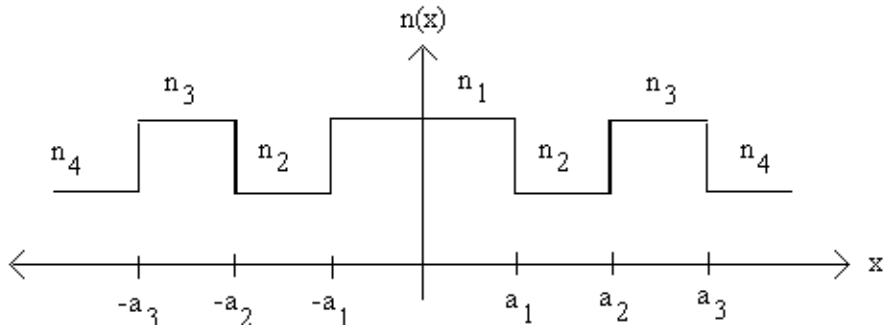

(b)

Figure 2-1 (a) Geometry and (b) sample refractive index profile of the waveguide described in Section 2.1.

choice of profile also serves as a two-dimensional model for a coaxial fiber that can accommodate two parallel gratings.

2.2 Introduction to Field Solutions

Assuming time-harmonic fields with $e^{j\omega t}$ dependence and wave propagation along the positive z-axis, the electric and magnetic fields can be expressed in phasor form as

$$\begin{aligned}\mathbf{E}(x,y,z) &= \mathbf{e}(x,y)\,e^{-j\beta z} = \left[\mathbf{a}_x e_x(x,y) + \mathbf{a}_y e_y(x,y) + \mathbf{a}_z e_z(x,y)\right] e^{-j\beta z} \\ &= \left[\mathbf{e}_t(x,y) + \mathbf{a}_z e_z(x,y)\right] e^{-j\beta z}\end{aligned} \tag{2.2a}$$

$$\mathbf{H}(x,y,z) = \mathbf{h}(x,y)\,e^{-j\beta z} = \left[\mathbf{a}_x h_x(x,y) + \mathbf{a}_y h_y(x,y) + \mathbf{a}_z h_z(x,y)\right] e^{-j\beta z}$$
$$= \left[\mathbf{h}_t(x,y) + \mathbf{a}_z h_z(x,y)\right] e^{-j\beta z} \qquad (2.2b)$$

where β is an unknown called propagation constant. A set of fields having this separable form which satisfy Maxwell's equations and remain finite when x and/or y approach infinity is called a mode. Guided modes are one type of modes – they carry the electromagnetic energy along the z-direction and exponentially decay to zero as x approaches positive or negative infinity. Radiation modes are the other type of modes. They do not diminish to zero exponentially when x approaches positive or negative infinity.

Many readers will already be familiar with the basics of planar waveguide theory. All others are referred to Appendix A which reviews the theory underlying the remainder of this chapter.

2.3 Solutions for the TE Guided Modes

This section determines the field solutions for the TE guided modes. Appendix A is a primer for the theory underlying the analysis provided for the benefit of readers lacking prior exposure.

2.3.1 Complete Expression for the Axial Component of the TE Modes

A complete expression for the axial component of the TE modes is written. Due to symmetry, it suffices to consider field expressions and boundary conditions for $x > 0$ only. The form in the core, that is for $0 < x < a_1$, depends upon whether the modes under consideration are even or odd. It follows

$$h_z = \begin{cases} \left.\begin{array}{ll} A_1 \sin u_1 x & \text{if EVEN, if } n_1 > \bar{\beta} \\ A_1 \sinh u_1 x & \text{if EVEN, if } n_1 < \bar{\beta} \\ A_1 \cos u_1 x & \text{if ODD, if } n_1 > \bar{\beta} \\ A_1 \cosh u_1 x & \text{if ODD, if } n_1 < \bar{\beta} \end{array}\right\} & 0 < x < a_1 \\ \left.\begin{array}{ll} A_2 \sin u_2 x + A_3 \cos u_2 x & \text{if } n_2 > \bar{\beta} \\ A_2 \sinh u_2 x + A_3 \cosh u_2 x & \text{if } \mathrm{n}_2 < \bar{\beta} \end{array}\right\} & a_1 < x < a_2 \\ \left.\begin{array}{ll} A_4 \sin u_3 x + A_5 \cos u_3 x & \text{if } n_3 > \bar{\beta} \\ A_4 \sinh u_3 x + A_5 \cosh u_3 x & \text{if } n_3 < \bar{\beta} \end{array}\right\} & a_2 < x < a_3 \\ A_6 e^{-u_4 x} & a_3 < x \end{cases} \tag{2.3}$$

where u_1, u_2, u_3, and u_4 are given by (A.26a) through (A.26d), $\bar{\beta} = \dfrac{\beta}{k_o}$ is the normalized propagation constant, and A_1 through A_6 are unknown constants.

2.3.2 Transverse E Field and Boundary Conditions

Using (2.3) in (A.21) gives

$$\frac{1}{j\omega\mu_o} e_y = \begin{cases} \left.\begin{array}{ll} \dfrac{A_1}{u_1}\cos u_1 x & \text{if EVEN, if } n_1 > \bar{\beta} \\ -\dfrac{A_1}{u_1}\cosh u_1 x & \text{if EVEN, if } n_1 < \bar{\beta} \\ -\dfrac{A_1}{u_1}\sin u_1 x & \text{if ODD, if } n_1 > \bar{\beta} \\ -\dfrac{A_1}{u_1}\sinh u_1 x & \text{if ODD, if } n_1 < \bar{\beta} \end{array}\right\} & 0 < x < a_1 \\ \left.\begin{array}{ll} \dfrac{A_2}{u_2}\cos u_2 x - \dfrac{A_3}{u_2}\sin u_2 x & \text{if } n_2 > \bar{\beta} \\ -\dfrac{A_2}{u_2}\cosh u_2 x - \dfrac{A_3}{u_2}\sinh u_2 x & \text{if } \mathrm{n}_2 < \bar{\beta} \end{array}\right\} & a_1 < x < a_2 \\ \left.\begin{array}{ll} \dfrac{A_4}{u_3}\cos u_3 x - \dfrac{A_5}{u_3}\sin u_3 x & \text{if } n_3 > \bar{\beta} \\ -\dfrac{A_4}{u_3}\cosh u_3 x - \dfrac{A_5}{u_3}\sinh u_3 x & \text{if } n_3 < \bar{\beta} \end{array}\right\} & a_2 < x < a_3 \\ \dfrac{A_6}{u_4} e^{-u_4 x} & a_3 < x \end{cases} \tag{2.4}$$

Using (2.3) and (2.4), the continuity of the tangential $\mathbf{E}$ and $\mathbf{H}$ fields at the $x = a_1, a_2,$ and a_3 interfaces is enforced. The result is a system of six equations and six unknowns (six amplitude coefficients). For example, supposing $n_4 \le n_2 < \bar{\beta} < n_3 \le n_1$, then for even modes the six equations are

$$A_1 \sin u_1 a_1 = A_2 \sinh u_2 a_1 + A_3 \cosh u_2 a_1$$

$$A_2 \sinh u_2 a_2 + A_3 \cosh u_2 a_2 = A_4 \sin u_3 a_2 + A_5 \cos u_3 a_2$$

$$A_4 \sin u_3 a_3 + A_5 \cos u_3 a_3 = A_6 e^{-u_4 a_3}$$

$$\frac{A_1}{u_1} \cos u_1 a_1 = -\frac{A_2}{u_2} \cosh u_2 a_1 - \frac{A_3}{u_2} \sinh u_2 a_1$$

$$-\frac{A_2}{u_2} \cosh u_2 a_2 - \frac{A_3}{u_2} \sinh u_2 a_2 = \frac{A_4}{u_3} \cos u_3 a_2 - \frac{A_5}{u_3} \sin u_3 a_2$$

$$\frac{A_4}{u_3} \cos u_3 a_3 - \frac{A_5}{u_3} \sin u_3 a_3 = \frac{A_6}{u_4} e^{-u_4 a_3}.$$

These six equations are expressed as one matrix equation

$$\left[\mathbf{M}_{ij}\right] \begin{bmatrix} A_1 \\ A_2 \\ A_3 \\ A_4 \\ A_5 \\ A_6 \end{bmatrix} = 0, \quad i \text{ and } j = 1,2,...6 \qquad (2.5)$$

where $\mathbf{M}_{ij}$ is given in Table 2-1. In order for this matrix equation to have a nontrivial solution it is necessary that

$$\left|\mathbf{M}_{ij}\right| = f\left(\bar{\beta}\right) = 0 \qquad (2.6)$$

where $\left| \quad \right|$ denotes the determinant. A root finding algorithm is used to find values of $\bar{\beta}$ that satisfy this necessary condition. It is established in Section A.4.3 that for guided modes $\bar{\beta} > n_4$. Another well established fact is that no real solution exists unless $\bar{\beta} < \max\{n_1, n_2, n_3\}$. Then, for a given frequency, or equivalently for a given $\lambda_o = \frac{2\pi}{k_o}$, a root finding algorithm locates a finite number of discrete normalized propagation

Table 2-1 Matrix $\mathbf{M}_{ij}$ in equation (2.5)

$\sin u_1 a_1$ if even, if $n_1 > \bar{\beta}$ $\sinh u_1 a_1$ if even, if $n_1 < \bar{\beta}$ $\cos u_1 a_1$ if odd, if $n_1 > \bar{\beta}$ $\cosh u_1 a_1$ if odd, if $n_1 < \bar{\beta}$	$-\sin u_2 a_1$ if $n_2 > \bar{\beta}$ $-\sinh u_2 a_1$ if $n_2 < \bar{\beta}$	$-\cos u_2 a_1$ if $n_2 > \bar{\beta}$ $-\cosh u_2 a_1$ if $n_2 < \bar{\beta}$	0	0	0
0	$\sin u_2 a_2$ if $n_2 > \bar{\beta}$ $\sinh u_2 a_2$ if $n_2 < \bar{\beta}$	$\cos u_2 a_2$ if $n_2 > \bar{\beta}$ $\cosh u_2 a_2$ if $n_2 < \bar{\beta}$	$-\sin u_3 a_2$ if $n_3 > \bar{\beta}$ $-\sinh u_3 a_2$ if $n_3 < \bar{\beta}$	$-\cos u_3 a_2$ if $n_3 > \bar{\beta}$ $-\cosh u_3 a_2$ if $n_3 < \bar{\beta}$	0
0	0	0	$\sin u_3 a_3$ if $n_3 > \bar{\beta}$ $\sinh u_3 a_3$ if $n_3 < \bar{\beta}$	$\cos u_3 a_3$ if $n_3 > \bar{\beta}$ $\cosh u_3 a_3$ if $n_3 < \bar{\beta}$	$-e^{-u_4 a_3}$
$\frac{1}{u_1}\cos u_1 a_1$ if even, if $n_1 > \bar{\beta}$ $-\frac{1}{u_1}\cosh u_1 a_1$ if even, if $n_1 < \bar{\beta}$ $-\frac{1}{u_1}\sin u_1 a_1$ if odd, if $n_1 > \bar{\beta}$ $-\frac{1}{u_1}\sinh u_1 a_1$ if odd, if $n_1 < \bar{\beta}$	$-\frac{1}{u_2}\cos u_2 a_1$ if $n_2 > \bar{\beta}$ $\frac{1}{u_2}\cosh u_2 a_1$ if $n_2 < \bar{\beta}$	$\frac{1}{u_2}\sin u_2 a_1$ if $n_2 > \bar{\beta}$ $\frac{1}{u_2}\sinh u_2 a_1$ if $n_2 < \bar{\beta}$	0	0	0
0	$\frac{1}{u_2}\cos u_2 a_2$ if $n_2 > \bar{\beta}$ $-\frac{1}{u_2}\cosh u_2 a_2$ if $n_2 < \bar{\beta}$	$-\frac{1}{u_2}\sin u_2 a_2$ if $n_2 > \bar{\beta}$ $-\frac{1}{u_2}\sinh u_2 a_2$ if $n_2 < \bar{\beta}$	$-\frac{1}{u_3}\cos u_3 a_2$ if $n_3 > \bar{\beta}$ $\frac{1}{u_3}\cosh u_3 a_2$ if $n_3 < \bar{\beta}$	$\frac{1}{u_3}\sin u_3 a_2$ if $n_3 > \bar{\beta}$ $\frac{1}{u_3}\sinh u_3 a_2$ if $n_3 < \bar{\beta}$	0
0	0	0	$\frac{1}{u_3}\cos u_3 a_3$ if $n_3 > \bar{\beta}$ $-\frac{1}{u_3}\cosh u_3 a_3$ if $n_3 < \bar{\beta}$	$-\frac{1}{u_3}\sin u_3 a_3$ if $n_3 > \bar{\beta}$ $-\frac{1}{u_3}\sinh u_3 a_3$ if $n_3 < \bar{\beta}$	$-\frac{1}{u_4}e^{-u_4 a_3}$

constants lying between $n_4 < \bar{\beta} < \max\{n_1, n_2, n_3\}$. Each value of $\bar{\beta}$ corresponds to a different mode – hence at a given frequency the number of guided modes is finite.

Choosing one amplitude coefficient, say A_1, as an independent variable, the remaining coefficients $A_2, A_3, \ldots A_6$ are determined in terms of A_1. Assuming $A_1 = 1$, we obtain

$$\begin{bmatrix} A_2 \\ A_3 \\ A_4 \\ A_5 \\ A_6 \end{bmatrix} = -\left[\mathbf{M}_{ij} : i \in [1,5],\ j \in [2,6]\right]^{-1} \left[\mathbf{M}_{ij} : i \in [1,5],\ j = 1\right] A_1 . \tag{2.7}$$

$K \begin{bmatrix} A_1 & A_2 & A_3 & A_4 & A_5 & A_6 \end{bmatrix}$ where K is any constant is also a solution. K is determined by the waveguide's excitation.

2.3.3 When $\bar{\beta}$ Equals the Refractive Index in One Layer

When $\bar{\beta} = n_i$, then in layer i (A.12) and (A.13) reduce to

$$\frac{\partial^2 e_y}{\partial x^2} = 0 ,$$

$$\frac{\partial^2 h_z}{\partial x^2} = 0 .$$

The corresponding solutions are

$$e_y = K_1 x + K_2 , \tag{2.8a}$$

$$h_z = K_3 x + K_4 \tag{2.8b}$$

where $K_1, K_2, K_3,$ and K_4 are constants which are not independent. Unfortunately we cannot determine the dependence using (A.21) because $T = 0$ though this equation seems to require $\frac{\partial h_z}{\partial x} = 0$, that is $K_3 = 0$. In fact only two independent constants are permissible in each of layers 2 and 3 and only one independent constant is permissible in each of layers 1 and 4 so the matrix $\mathbf{M}$ will be square.

Equations (2.8), which are the solutions to equations (A.12) and (A.13) when $\overline{\beta} = n_i$, have different forms than equations (2.3) and (2.4) which are the solutions in the more ordinary case of $\overline{\beta} \neq n_i$. What remains is to determine the dependence of the constants $K_1, K_2, K_3,$ and K_4 in equations (2.8). Consider equations (2.3) and (2.4) in region i and a neighboring region in the limit as $u_i \to 0$. For example consider $i = 2$, corresponding to $a_1 < x < a_2$, and use region 1, corresponding to $0 < x < a_1$ for the neighboring region. Also let the even modes be the modes under consideration and assume $n_1 > \overline{\beta}$ and $n_2 > \overline{\beta}$. The pertinent expressions are

$$h_z = \begin{cases} A_1 \sin(u_1 x) & 0 < x < a_1 \\ A_2 \sin(u_2 x) + A_3 \cos(u_2 x) & a_1 < x < a_2 \end{cases}, \qquad (2.9)$$

$$e_y = j\omega\mu_o \begin{cases} \dfrac{A_1}{u_1}\cos(u_1 x) & 0 < x < a_1 \\ \dfrac{A_2}{u_2}\cos(u_2 x) - \dfrac{A_3}{u_2}\sin(u_2 x) & a_1 < x < a_2 . \end{cases} \qquad (2.10)$$

Now finding an expression for the ratio $\dfrac{A_2}{A_3}$ by enforcing the continuity of the tangential components of the $\mathbf{E}$ and $\mathbf{H}$ fields at the $x = a_1$ interface yields

$$A_2 \sin(u_2 a_1) + A_3 \cos(u_2 a_1) = A_1 \sin(u_1 a_1)$$

$$A_2 \cos(u_2 a_1) - A_3 \sin(u_2 a_1) = \frac{u_2}{u_1} A_1 \cos(u_1 x)$$

$$\frac{A_2 \sin(u_2 a_1) + A_3 \cos(u_2 a_1)}{A_2 \cos(u_2 a_1) - A_3 \sin(u_2 a_1)} = \frac{u_1}{u_2}\frac{\sin(u_1 a_1)}{\cos(u_1 a_1)}$$

$$\frac{\dfrac{A_2}{A_3}\tan(u_2 a_1) + 1}{\dfrac{A_2}{A_3} - \tan(u_2 a_1)} = \frac{u_1}{u_2}\tan(u_1 a_1)$$

$$\frac{A_2}{A_3}\left[\tan(u_2 a_1) - \frac{u_1}{u_2}\tan(u_1 a_1)\right] = -1 - \frac{u_1}{u_2}\tan(u_1 a_1)\tan(u_2 a_1)$$

$$\frac{A_2}{A_3} = \frac{1 + \frac{u_1}{u_2}\tan(u_1 a_1)\tan(u_2 a_1)}{\frac{u_1}{u_2}\tan(u_1 a_1) - \tan(u_2 a_1)}$$

$$\lim_{u_2 \to 0}\left(\frac{A_2}{A_3}\right) = 0$$

Therefore $A_2 = 0$. Putting this result into (2.9) and (2.10) to determine h_z and e_y in layer 2 when $u_2 = 0$, we obtain

$$h_z = \lim_{u_2 \to 0}\left(A_3 \cos u_2 x\right) = A_3$$

$$e_y = \lim_{u_2 \to 0}\left[j\omega\mu_o\left(\frac{A_2}{u_2}\cos(u_2 x) - \frac{A_3}{u_2}\sin(u_2 x)\right)\right] = j\omega\mu_o A_3\left[-x + \frac{1 + a_1 u_1 \tan(u_1 a_1)}{u_1 \tan(u_1 a_1)}\right]$$

since

$$\lim_{u_2 \to 0}\left(\frac{A_2}{u_2}\right) = \lim_{u_2 \to 0} A_3\left[\frac{1 + u_1 \tan(u_1 a_1)\frac{\tan(u_2 a_1)}{u_2}}{u_1 \tan(u_1 a_1) - u_2 \tan(u_2 a_1)}\right] = A_3 \frac{1 + a_1 u_1 \tan(u_1 a_1)}{u_1 \tan(u_1 a_1)}.$$

To generalize these expressions for any combination of assumptions i.e. even or odd modes plus $n_1 < \overline{\beta}$ or $n_2 > \overline{\beta}$, the following equations for h_z and e_y are used in layer 2

$$h_z = A_3$$

$$e_y = -j\omega\mu_o A_3 x + A_2.$$

These expressions fit (2.8) but with the requisite two or fewer constants.

In a similar manner it can be shown that when $\overline{\beta} = u_4$ the solutions in layer 4 i.e. $a_3 < x$ become

$$h_z = 0 \qquad \text{(2.11a)}$$

$$e_y = A_6. \qquad \text{(2.11b)}$$

which is predictable because the fields must remain finite as $x \to \infty$. Equations (2.11) can be used to find the cuttoff frequencies of the modes i.e. λ_o when $\overline{\beta} = u_4$.

2.3.4 Matlab Programs For Determining the Field Solutions for the TE Guided Modes

A Matlab program called slab.m that implements most of the procedure described in section 2.3.2 is now presented. A second program to be presented later performs the last few steps and can be run after slab.m. The inputs to slab.m are $n_1, n_2, n_3,$ and n_4 plus $a_1, a_2,$ and a_3 for the slab guide described in section 2.1. The outputs are the discrete normalized propagation constants for the TE guided modes for λ_o lying between $\lambda_{o_{\min}}$ and $\lambda_{o_{\max}}$, which are the two other inputs. As described in section 2.3.2, a 6x6 determinant $\left|\mathbf{M}_{i\,j}\right|$ can be calculated given λ_o and $\overline{\beta}$. If λ_o is fixed then $\left|\mathbf{M}_{i\,j}\right| = f\left(\overline{\beta}\right)$, i.e. a function of $\overline{\beta}$ which has roots at a finite number of points lying within $n_4 < \overline{\beta} < \max\{n_1, n_2, n_3\}$. These are the discrete normalized propagation constants corresponding to the particular value of λ_o.

Slab.m calls several original (not built into Matlab) Matlab functions. The main program slab.m has several nested loops. The outermost of these toggles between even and odd modes as is explained in Appendix B. The second outermost nested loop fixes λ_o at $\lambda_{o\,\min}$ and finds all the roots of $f\left(\overline{\beta}\right)$ when $\lambda_o = \lambda_{o\,\min}$. Nested within this second loop is a loop which to begin with fixes λ_o at $\left(\lambda_{o\,\min} + \Delta\lambda_o\right)$ where, for example, $\Delta\lambda_o = \dfrac{\lambda_{o\,\max} - \lambda_{o\,\min}}{50}$ if 50 steps are desired. All the roots of $f\left(\overline{\beta}\right)$ with λ_o fixed at this new value are found. Then λ_o is set to $\lambda_{o\,\min} + 2\Delta\lambda_o$ and the roots are found, then $\lambda_{o\,\min} + 3\Delta\lambda_o$, etc. until the roots of $f\left(\overline{\beta}\right)$ are known for all $\lambda_o = \lambda_{o\,\min} + n\Delta\lambda_o$, $n = 0,1,2,\ldots,\ \lambda_o < \lambda_{o\,\max}$. Connecting the dots a plot of the dispersion curves such as the one shown in Figure 2-2 is obtained. Further details of slab.m and a program listing are presented in Appendix B.

The plot resulting from an example run of slab.m is shown in Figure 2-2. The top curve is always designated TE_0 and is always an even mode. TE_0 has the lowest cutoff frequency i.e. the highest value of λ_o where it intersects the line $\overline{\beta} = n_4$ -- we know it

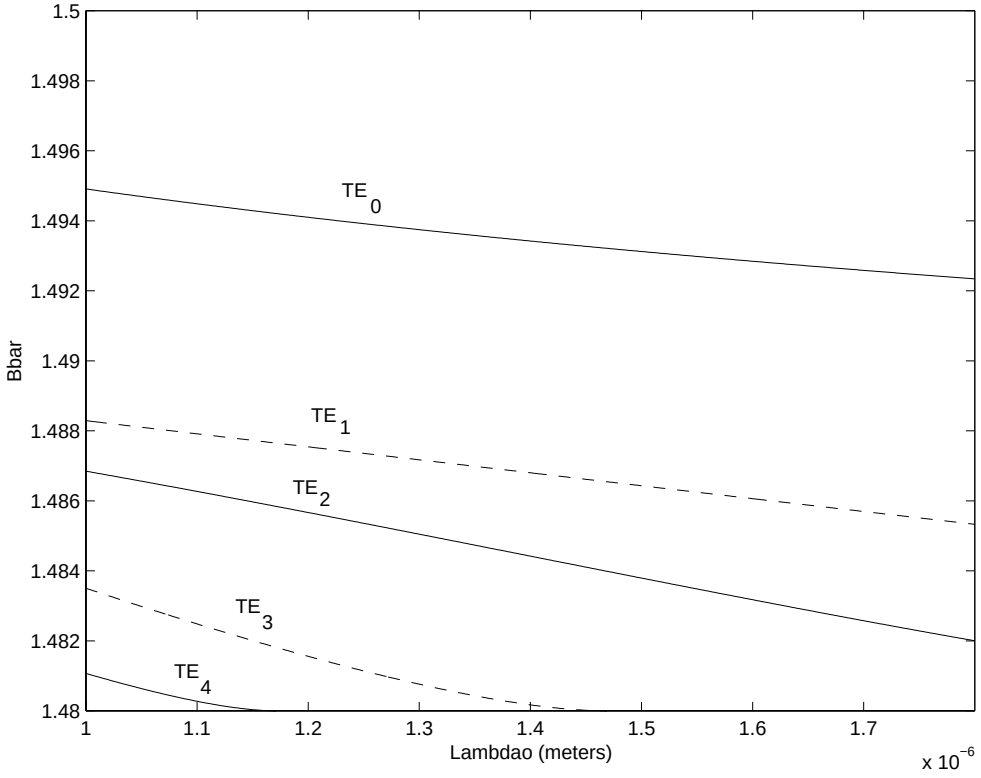

Figure 2-2 Example dispersion curve calculated by slab.m for a waveguide with $n_1 = 1.5$, $n_2 = 1.49$, $n_3 = 1.485$, $n_4 = 1.48$, $a_1 = 1 \times 10^{-6}$ m, $a_2 = 5 \times 10^{-6}$ m, $a_3 = 7 \times 10^{-6}$ m

extends no further but ends there (for the particular case of symmetric waveguide, the cutoff frequency for even TE_0 mode is zero). Recall that no real solutions exist when $\overline{\beta} < n_4$. The line below TE_0 is always an odd mode and is designated TE_1. Its cutoff frequency is higher than for TE_0. The next curve is an even mode and is designated TE_2; even and odd modes alternate. The last two modes in the example shown are TE_3 and TE_4.

Another program call fdist.m has been written which plots the field distributions corresponding to any one of the points on one of the dispersion curves generated by slab.m. Slab.m stores the values of $\overline{\beta}$ in a 3-dimensional matrix called Bbar; the only inputs to fdist.m are a row and column reference plus a third coordinate denoting even or odd. The indices $n_1, n_2, n_3,$ and n_4 and the dimensions $a_1, a_2,$ and a_3 are still in memory after running slab.m. The even modes all have a third coordinate equal to one; the $\overline{\beta}$ for the TE_0 mode fill the first column, for TE_2 the second, etc. of a 2-dimensional matrix

which conceptually is stacked on top of a similar 2-D matrix for the odd modes TE_1, TE_3, etc. The third coordinate for the odd modes equals two and the $\overline{\beta}$ for TE_1 fills the first column, for TE_3 the second, etc. Some or all of TE_1, TE_2, TE_3, … are padded with zeros because for them cutoff occurs at $\lambda_o < \lambda_{o\,\max}$, therefore their columns have fewer nonzero elements than TE_0. TE_0 itself may cutoff at $\lambda_o < \lambda_{o\,\max}$ though the higher order modes then still have shorter columns as they cutoff at lower values of λ_o. Then the coordinates entered correspond to a value of $\overline{\beta}$ which fdist.m retrieves from memory. Then it calculates λ_o using the row coordinate and calls the function UevalM.m which computes the $\mathbf{M}_{i\,j}$ matrix. Fdist.m then assumes $A_1 = 1$ and calculates $[A_2, A_3, A_4, A_5, A_6]$ using the procedure described in Section 2.3.2. Next the field distributions for $|e_y|$ and $|h_z|$ are computed using (2.4) and (2.3) respectively. Each is normalized, that is scaled, so $\max(abs(e_y)) = \max(abs(h_z)) = 1$, then each is plotted. A legend applies the correct label to the mode being plotted. A program listing of fdist.m is presented in Appendix B.

The plots resulting from an example run of fdist.m are shown in Figures 2-3a through 2-3e. Note that neither mode TE_0 nor TE_1 crosses through zero, modes TE_2 and TE_3 both cross through zero once, and mode TE_4 crosses through zero twice. This is a general result.

2.3.5 Field Solutions for $x < 0$

Fields for $x < 0$ can be obtained using the following symmetry considerations:

a) axial field components are even and odd functions of x for odd and even modes, respectively

b) transverse field components are even and odd functions of x for even and odd modes, respectively.

2.3.6 TM modes

So far in part 2 of this chapter only the TE modes have been considered. (A.13) was written for h_z obtaining (A.25) which we solved, obtaining (2.3). Next (2.27) was used in (A.21), yielding (2.4).

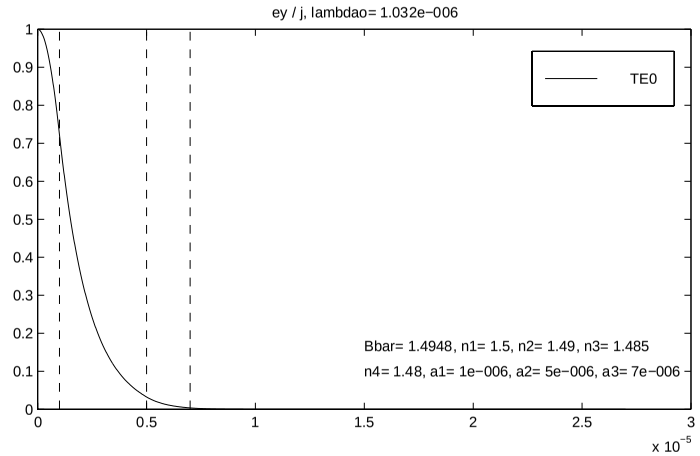

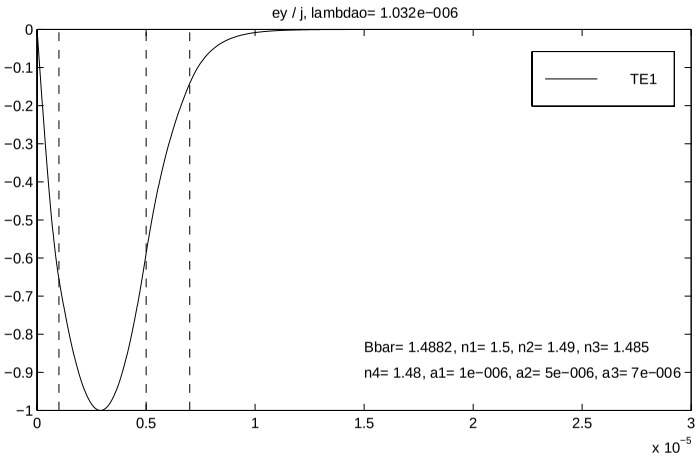

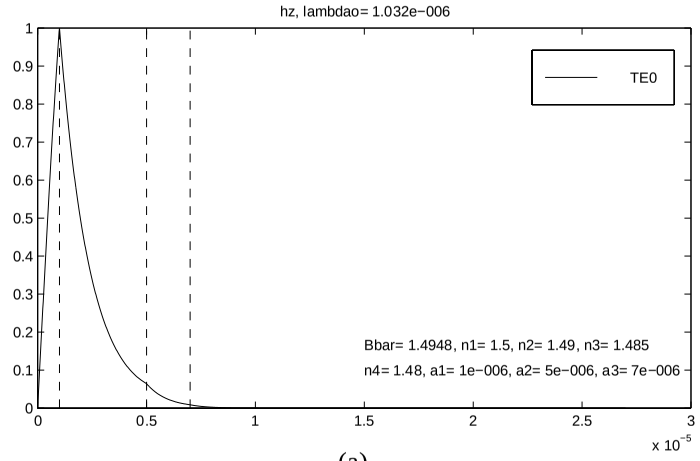

(a)

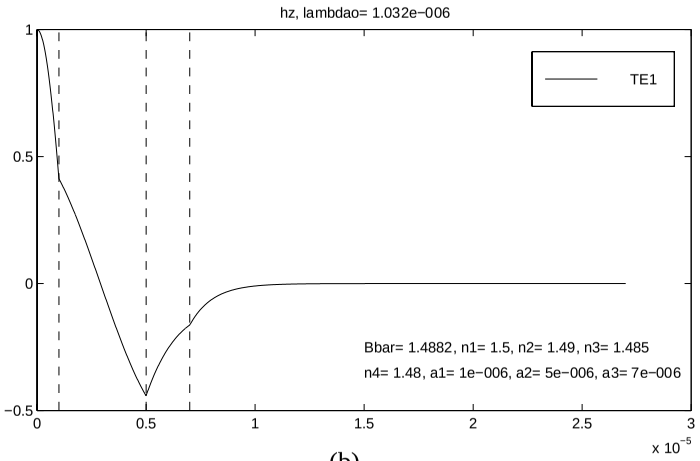

(b)

Figure 2-3 Field distributions of the (a) TE0 (b) TE1 (c) TE2 (d) TE3 (e) TE4 mode at free-space wavelength equal 1.032 μm corresponding to one point in Figure 2-2.

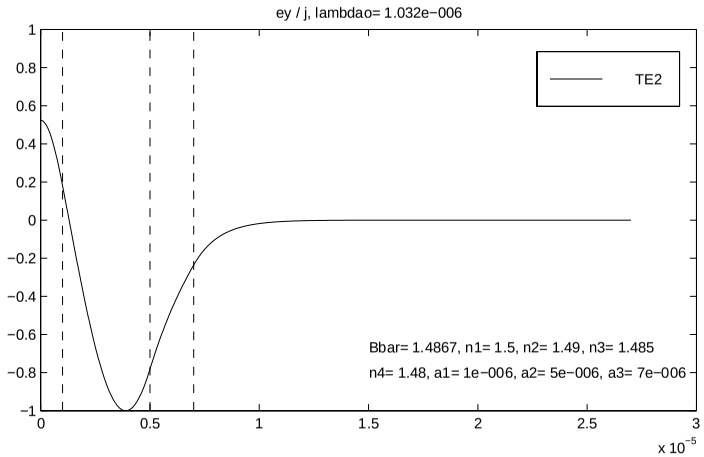

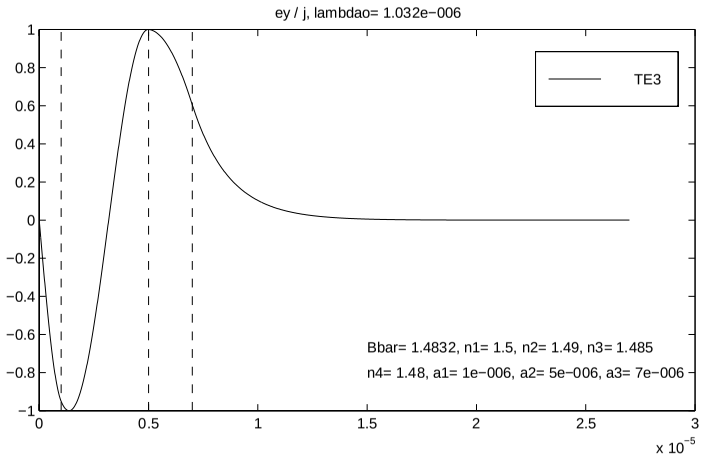

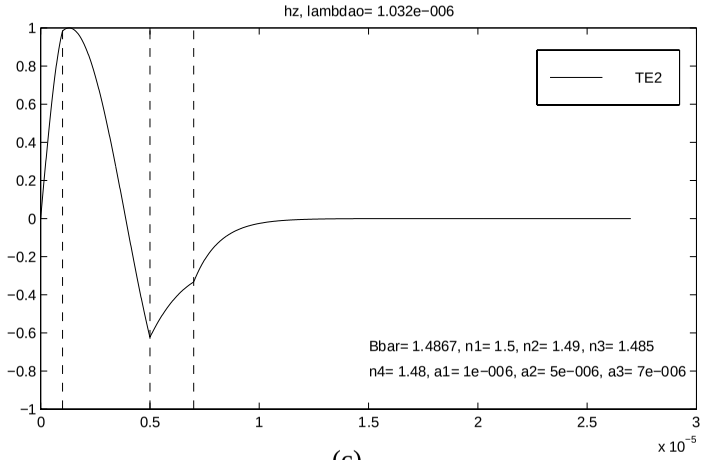

(c)

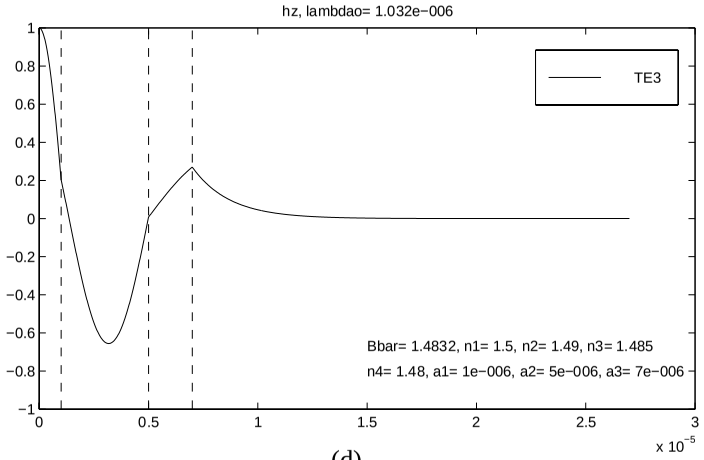

(d)

Figure 2-3 Continued

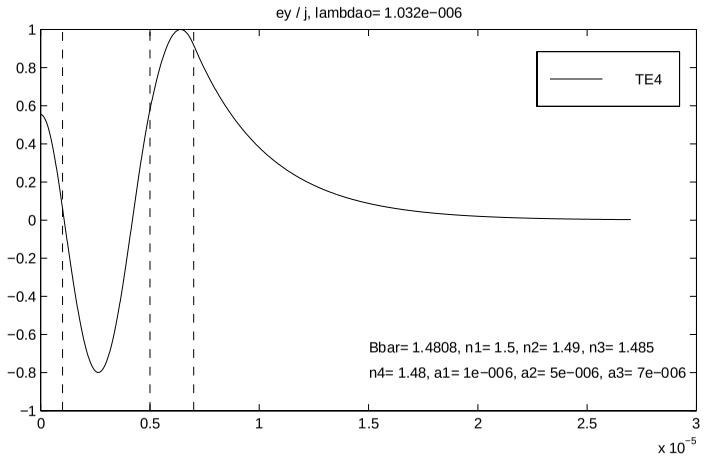

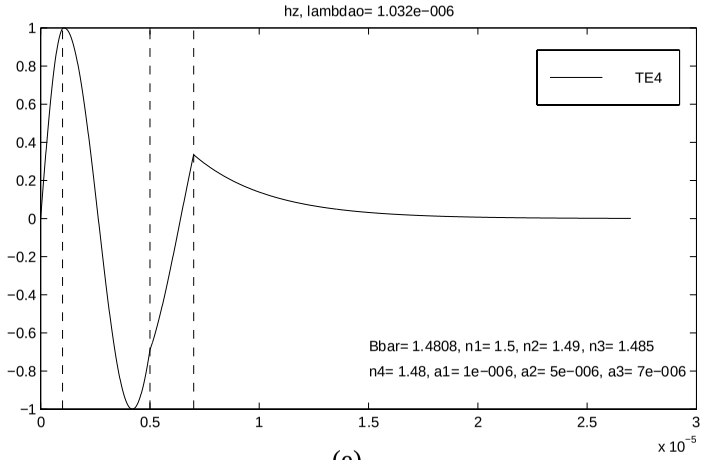

(e)

Figure 2-3 Continued

The field solutions for the TM modes can be determined in a similar manner. First (A.12) is written for e_y -- the result is exactly the same as (A.25) if h_z is replaced with e_z. Solving, e_z equals the right-hand-side of (2.3). Looking ahead, the first 3 rows of $\mathbf{M}_{ij}$ will be the same as for the TE modes.

Next, h_y is solved using (A.23). This equation is comparable to (A.21) used at this stage in the analysis of the TE modes. Next, the boundary conditions on e_z and h_y are applied to form $\mathbf{M}_{ij}$. Just as $(j\omega\mu_o)$ in (A.21) cancelled out of the $\mathbf{M}_{ij}$ matrix formed in the TE analysis the constant term $(-j\omega\varepsilon_o)$ cancels out of $\mathbf{M}_{ij}$ here. (n^2) also nearly cancels since $n_1, n_2, n_3,$ and n_4 are nearly equal. Hence $\mathbf{M}_{ij}$ is very nearly the same as before and consequently the dispersion curves are very nearly the same. We say that the TM and TE modes are degenerate.

2.3.7 Review of Choices in Analysis

A couple of the choices made in the formulation of the analysis are reviewed here. First, $u_1, u_2, u_3,$ and u_4 are taken to be positive as was noted at the end of Appendix A. Because of the radical signs in their definitions we are at liberty to make them negative instead. Supposing this is done the rest of the formulation stays the same except that now the term $B_1' e^{-u_4 x}$ is dropped and $B_2' e^{u_4 x}$ is retained in (A.29). Then equations (2.3) and (2.4) stay the same except that in the expression for $a_3 < x$ in (2.3) the negative sign is removed in front of u_4; in (2.4) the same is done to the expression for $a_3 < x$ and also it is multiplied by (-1). After $\mathbf{M}_{ij}$ is modified accordingly the roots of $f(\bar{\beta}) = |\mathbf{M}_{ij}|$ can be found. As might be expected, these turn out to be the same roots as when $u_1, u_2, u_3,$ and u_4 were taken to be positive.

Clearly if $A_1, A_2,$ and A_4 reverse their signs then evaluating (2.3) and (2.4) yields the same result as before the signs of $u_1, u_2, u_3,$ and u_4 were reversed. It was stated that $K[A_1, A_2, A_3, A_4, A_5, A_6]$ where K is any constant is also a solution. This was the justification for assuming $A_1 = 1$. Let us set $A_1 = 1$ as we did previously.

$[A_1, A_2, A_3, A_4, A_5, A_6]$ are determined using the same technique as before. It turns out that $[A_1, A_2, A_3, A_4, A_5, A_6]$ are the same as before the signs of $u_1, u_2, u_3,$ and u_4 were reversed except that the signs of $A_3, A_5,$ and A_6 are reversed. This fields solution is completely equivalent to the solution obtained before the signs of $u_1, u_2, u_3,$ and u_4 were reversed if the sign of K is reversed. K is determined by the waveguide's excitation.

Now the absolute value signs which were included in the definitions of u_i are considered. If these were omitted, specifically if $u_i = k_o\sqrt{\bar{\beta}^2 - n_i^2}$, then h_z in each layer would have the expression

$$h_z = K\sinh u_i x + M\cosh u_i x \qquad K, M \text{ constants} \qquad (2.12)$$

except in the first layer where $K = 0$ for odd modes or $M = 0$ for even modes and in the last layer where $h_z = A_6 e^{-u_4 x}$. "If $n_i > \bar{\beta}$" and "if $n_i < \bar{\beta}$" statements such as were used in (2.3) are no longer required. If $\bar{\beta} > n_i$ then $u_i =$ real but if $\bar{\beta} < n_i$ then $u_i = j\bar{u}_4$ where $\bar{u}_4 = k_o\sqrt{n_i^2 - \bar{\beta}^2} =$ real. Because of the relations

$$\sinh jx = j\sin x,$$

$$\cosh jx = \cos x,$$

when $\bar{\beta} < n_i$, (2.12) would have the correct sinusoidal nature with K absorbing the factor of j. If this scheme is used then after solving for $[A_1, A_2, A_3, A_4, A_5, A_6]$ it is discovered that at least one of them is imaginary whereas before they were all positive.

2.3.8 Heuristic Proof That if $\bar{\beta}$ is Purely Real Then $\bar{\beta} > n_4$

The second portion of the previous section has prepared us for the heuristic proof that for guided modes $\bar{\beta} > n_4$ which was promised in section A.4.3. Suppose the absolute value signs are omitted from the definitions of $u_1, u_2, u_3,$ and u_4. Then

$$h_z = A_6 e^{-u_4 x}, \qquad x > a_3,$$

$$u_4 = k_o\sqrt{\bar{\beta}^2 - n_4^2}, \qquad \bar{\beta} = \frac{\beta}{k_o}, \quad k_o = \frac{2\pi}{\lambda_o}.$$

This is the case whether $\bar{\beta} > n_4$ or $\bar{\beta} < n_4$ though u_4 is purely imaginary if $\bar{\beta} < n_4$.

If $\bar{\beta} > n_4$ then u_4 is purely real. The expression for h_z could be

$$h_z = A_6 e^{-u_4 x} + A_7 e^{u_4 x}$$

except that the field must remain bounded when $x \to \infty$. So the term $\left(A_7 e^{u_4 x}\right)$ is deleted.

If $\bar{\beta} < n_4$ then u_4 is purely imaginary. Let us introduce the variable $\bar{u}_4$

$$u_4 = k_o \sqrt{(-1)\left(n_4{}^2 - \bar{\beta}^2\right)} = jk_o \sqrt{n_4{}^2 - \bar{\beta}^2} = j\bar{u}_4 .$$

The expression for h_z becomes

$$h_z = A_6 e^{-j\bar{u}_4 x} + A_7 e^{j\bar{u}_4 x}, \qquad x > a_3 .$$

Reinserting the $e^{-j\beta z}$ dependence yields

$$h_z = A_6 e^{-j\beta z - j\bar{u}_4 x} + A_7 e^{-j\beta z + j\bar{u}_4 x} .$$

This represents two plane waves propagating in the directions of the vectors

$$\frac{\bar{u}_4 \mathbf{a}_x + \beta \mathbf{a}_z}{\sqrt{\bar{u}_4{}^2 + \beta^2}} \text{ and } \frac{-\bar{u}_4 \mathbf{a}_x + \beta \mathbf{a}_z}{\sqrt{\bar{u}_4{}^2 + \beta^2}} .$$

Now the energy is no longer confined to the core region. A_6 and A_7 are both retained, i.e. neither is set equal to zero, because the fields remain finite as $x \to \infty$ without eliminating either. The given mode is a "radiation" mode, and one more arbitrary constant is present than before. Consequently, for radiation modes $\bar{\beta}$ can have any value in the range $\left|\bar{\beta}\right| < n_4$, not just a finite number of discrete values, and we say that a continuum of radiation modes exist. However, when $\bar{\beta} < n_4$ radiation modes arise to the exclusion of guided modes, therefore for guided modes $\bar{\beta} > n_4$.

Chapter 3

Reflectivity Spectra of Uniform Gratings in Multiclad Symmetric Waveguides

3.1 Introduction

An index grating is a periodic perturbation of the refractive index in the waveguide's axial direction. Fiber gratings are fabricated by illuminating the fiber from the side with two intersecting beams of UV light which interfere producing a periodic interference pattern. The index in germanium doped layers of the fiber is changed permanently by irradiation. Hence the interference pattern produces a corresponding periodic index grating in the fiber. In a planar waveguide gratings can be formed by illuminating from the top.

The planar waveguide shown in Figure 2-1 has refractive index given by (2.1). If this waveguide is perturbed, a new waveguide results with refractive index given by

$$n'(x,z) = n(x) + \Delta n(x,z) \tag{3.1a}$$

where

$$\Delta n(x,z) = \begin{cases} \Delta n_{l1}(z) = \overline{\Delta n_{l1}}\left[1+\cos\left(\dfrac{2\pi}{\Lambda_{l1}}z+\phi_{l1}\right)\right], & |x| < a_1 \\ \Delta n_{l2}(z) = \overline{\Delta n_{l2}}\left[1+\cos\left(\dfrac{2\pi}{\Lambda_{l2}}z+\phi_{l2}\right)\right], & a_1 < |x| < a_2 \\ \Delta n_{l3}(z) = \overline{\Delta n_{l3}}\left[1+\cos\left(\dfrac{2\pi}{\Lambda_{l3}}z+\phi_{l3}\right)\right], & a_2 < |x| < a_3 \\ \Delta n_{l4}(z) = \overline{\Delta n_{l4}}\left[1+\cos\left(\dfrac{2\pi}{\Lambda_{l4}}z+\phi_{l4}\right)\right], & a_3 < |x| \end{cases} . \tag{3.1b}$$

The new waveguide described by $n'(x,z)$ represents the old waveguide described by $n(x)$ with gratings added. $\Delta n(x,z)$ is small relative to $n(x)$. For completeness, gratings are included in the outer cladding layer $a_3 < |x|$, which is not standard, but they may be eliminated by setting $\overline{\Delta n_{l4}} = 0$.

Note that $\overline{\Delta n_{l1}}$, $\overline{\Delta n_{l2}}$, $\overline{\Delta n_{l3}}$, and $\overline{\Delta n_{l4}}$ do not depend on z, therefore we are considering "uniform" gratings for now. Also, $\phi_{l1}, \phi_{l2}, \phi_{l3}, \text{and } \phi_{l4}$ do not depend on z, therefore we are considering unchirped gratings. $\overline{\Delta n_{l1}}$, $\overline{\Delta n_{l2}}$, $\overline{\Delta n_{l3}}$, and $\overline{\Delta n_{l4}}$ are constants dependant on several factors including the intensity of irradiating light and the composition of the silica material forming the core and cladding layers [2]. Pure, undoped SiO_2 has a value of refractive index denoted by n_{SiO_2} and is not photosensitive. By introducing GeO_2 dopant the refractive index is increased in proportion to the concentration of dopant. Planar dielectric waveguides including waveguides described by (2.1) are formed by doping each layer within which we desire $n > n_{SiO_2}$ with the correct concentration of GeO_2. SiO_2, when doped with GeO_2, also becomes photosensitive, a property that is exploited to fabricate gratings. As has already been described, the slab waveguide is illuminated with two intersecting beams of UV light that interfere producing a periodic interference pattern. A corresponding periodic grating is formed in every doped layer since the UV light penetrates all layers. The magnitude of the refractive index change in each layer is proportional to the concentration of dopant in each layer. In accordance with the above discussion regarding the two effects of GeO_2 dopant $\overline{\Delta n_{l1}}$, $\overline{\Delta n_{l2}}$, $\overline{\Delta n_{l3}}$, and $\overline{\Delta n_{l4}}$ in (3.2b) are given by

$$\begin{cases} \overline{\Delta n_{l1}} = \alpha\left(n_1 - n_{SiO_2}\right) \\ \overline{\Delta n_{l2}} = \alpha\left(n_2 - n_{SiO_2}\right) \\ \overline{\Delta n_{l3}} = \alpha\left(n_3 - n_{SiO_2}\right) \\ \overline{\Delta n_{l4}} = \alpha\left(n_4 - n_{SiO_2}\right) \end{cases}, \qquad (3.2)$$

$$n_{SiO_2} = 1.44691047 \text{ at } \lambda_o = 1.30\ \mu m$$

where α depends on the intensity and exposure time of the irradiating light which is equal for all layers. The refractive index change Δn produced by illuminating doped SiO_2 is never negative, hence the $1+\cos(\ )$ form of (3.1b) as opposed to simply $\cos(\ )$.

It is possible but difficult to solve for the exact modal fields of the waveguide with gratings using Maxwell's equations. An easier approach that is approximate in nature but surprisingly accurate is to write the fields of the waveguide with gratings as a

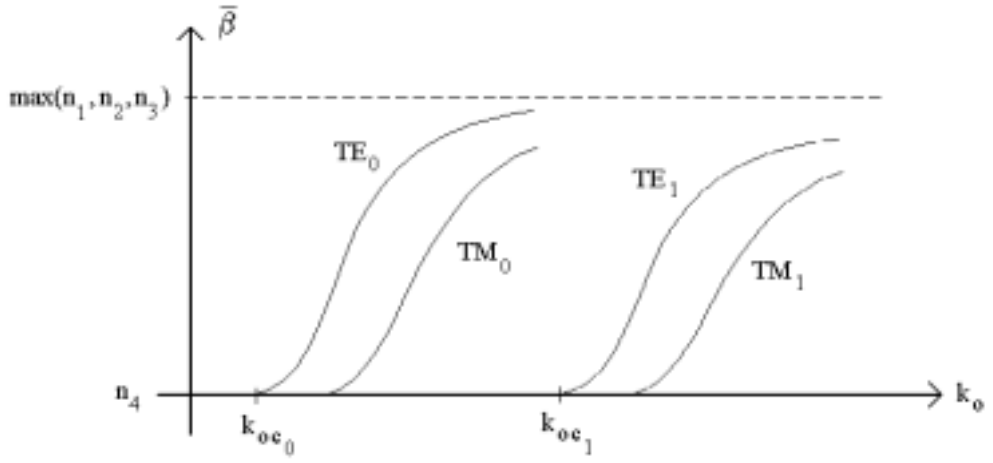

Figure 3-1 Typical dispersion curves for symmetric planar waveguides.

superposition of the modal fields of the identical waveguide without gratings. For example (2.1) is the waveguide without gratings or "unperturbed" waveguide that corresponds to the waveguide with gratings described by $n'(x,z)$ in (3.1). To compute the fields of the perturbed waveguide the fields of the unperturbed waveguide are weighted by coupled functions of z then added as demonstrated in the next section. Then the same transverse modal field distributions exist in the perturbed waveguide as in the unperturbed waveguide, but two or more modes are coupled in the former waveguide. The coupling occurs over a thin slice of spectrum, and within and surrounding this narrow slice of spectrum the gratings are transparent to all the uncoupled modes. Far from this particular slice of spectrum another slice of spectrum may exist over which a different combination of modes are coupled. The slices of spectrum over which coupling occurs -- the wavelengths and modes associated with them -- can be determined using Brillouin diagrams of which an excellent discussion is contained in [6].

This thesis considers only the multiclad symmetric planar waveguide that is given by (2.1). Equation (3.1) represents uniform gratings, the only type considered in this chapter; however, non-uniform gratings are considered in later chapters. It is assumed the waveguide is weakly guiding (defined in Section 2.1.) Figure 3-1 shows typical dispersion curves for symmetric planar waveguides. In this figure $k_o = 2\pi/\lambda_o$, $\bar{\beta} = \beta/k_o$, and k_{oc_i} are the cutoff wavenumbers of the TE_m modes. A future section will prove that no coupling occurs between TE and TM modes, hence we consider them

separately. Furthermore in this thesis we consider coupling between just a single mode propagating in the forward direction and the same mode propagating in the backward direction. This is guaranteed to happen only when $k_o < k_{oc_1}$ (Figure 3-1) and in this case the single mode will be TE_0 or TM_0. In all of the examples that are simulated in this thesis, TE_0 is chosen.

The main result of this chapter will be an expression for reflectivity R, the ratio of the powers of the forward and backward going waves at the input of the section of waveguide containing gratings. It will be assumed $\Lambda_{l1} = \Lambda_{l2} = \Lambda_{l3} = \Lambda_{l4}$ and $\phi_{l1} = \phi_{l2} = \phi_{l3} = \phi_{l4}$ in (3.1b). Also, grating filter design curves produced by plotting R versus normalized wavelength will be presented. In the next chapter the case of $\phi_{l1} \neq \phi_{l2} \neq \phi_{l3} \neq \phi_{l4}$ which has never been presented in the literature to the author's knowledge will be considered.

Although this thesis considers only the planar waveguide geometry which is given by (2.1), most of the results will be independent of the specific geometry as detailed later. Slab.m developed in Chapter 2, a program that computes dispersion curves and field profiles for the multi-clad planar waveguide described by (2.1) and shown in Figure 2-1, will be used. A symmetric multi-clad planar waveguide is chosen as opposed to a single-clad and/or asymmetric waveguide for the following reasons. The difference between the single-clad and multi-clad cases is slight over the single-mode range of wavelengths if $\Lambda_{l1} = \Lambda_{l2} = \Lambda_{l3} = \Lambda_{l4}$ and $\phi_{l1} = \phi_{l2} = \phi_{l3} = \phi_{l4}$. The expression for reflectivity and the governing equations are the same. The exceptions are the expressions for the coupling coefficients, however, no special behavior arises for them as when $\phi_{l1} \neq \phi_{l2} \neq \phi_{l3} \neq \phi_{l4}$ in which case the AC coupling coefficient (yet to be defined) may pass through zero. (Reference [7] describes how an inner cladding layer can reduce the backreflection of narrow-band rejection filters using gratings in a two-mode fiber.) As has already been mentioned the analysis will not be extended to the multi-mode range of wavelengths. However the more general case of $\phi_{l1} \neq \phi_{l2} \neq \phi_{l3} \neq \phi_{l4}$ and non-uniform gratings will be considered in later chapters. For this reason three (six if not considering the symmetry in

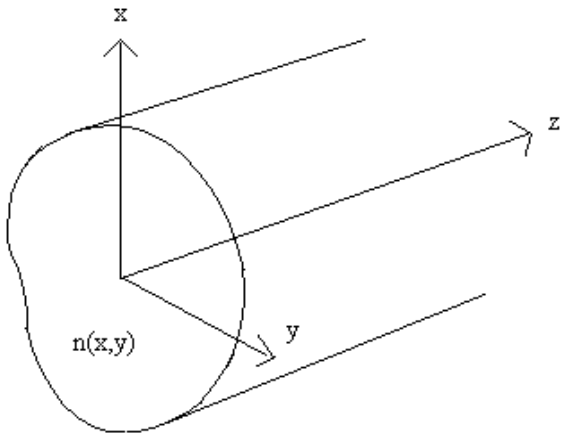

Figure 3-2 Cylindrical Dielectric Waveguide

profile) cladding layers are included. A symmetric planar waveguide is chosen to increase the correspondence with the fiber geometry.

3.2 Coupled Mode Theory

Some background in coupled mode theory is required to solve the specific problem detailed in the introduction to this chapter. A cylindrical dielectric waveguide with an arbitrary cross section is shown in Figure 3-2. The waveguide is assumed translationally invariant, that is, uniform along the z-axis, so $n = n(x, y)$. Of course $\varepsilon = \varepsilon_o n^2(x, y)$. We consider only time harmonic fields which vary with time as $e^{j\omega t}$, ω being the angular frequency. It is assumed that at the operating wavelength M guided modes are supported with the fields of the k-th mode expressed as

$$\mathbf{E}_k(x, y, z) = \mathbf{e}_k(x, y) e^{-j\beta_k z} \qquad (3.3a)$$

$$\mathbf{H}_k(x, y, z) = \mathbf{h}_k(x, y) e^{-j\beta_k z} . \qquad (3.3b)$$

It is the source which determines which modes are excited and how strongly. Thus, neglecting radiation modes, the total fields in the waveguide may be expressed as a superposition of guided modes as

$$\mathbf{E}(x, y, z) = \sum_{k=1}^{M} \psi_k \mathbf{e}_k(x, y) e^{-j\beta_k z} \qquad (3.4a)$$

$$\mathbf{H}(x, y, z) = \sum_{k=1}^{M} \psi_k \mathbf{h}_k(x, y) e^{-j\beta_k z} . \qquad (3.4b)$$

The coefficients ψ_k are constants and are determined by the source conditions.

Now a cylindrical waveguide that is described by $\varepsilon' = \varepsilon_o[n'(x,y)]^2 = \varepsilon_o[n(x,y)+\Delta n(x,y)]^2$ using $n(x,y)$ of the unperturbed structure is considered. According to coupled mode theory, the fields in the perturbed guide may be expressed as a superposition of the modal fields that the unperturbed guide can support at the particular wavelength. The fields in the unperturbed guide are denoted by $\begin{pmatrix}\mathbf{E}\\ \mathbf{H}\end{pmatrix}$ as in (3.5), while the fields in the perturbed guide are denoted by $\begin{pmatrix}\mathbf{E}'\\ \mathbf{H}'\end{pmatrix}$. The orthoganality relationship applies to the transverse fields [6] hence the expansion applies to the transverse components of $\mathbf{E}'$ and $\mathbf{H}'$. Dropping the radiation modes, we write

$$\mathbf{E}_t'(x,y,z) = \sum_{m=1}^{M} \psi_m(z)\,\mathbf{e}_{m_t}(x,y)e^{-j\beta_m z} \qquad (3.5a)$$

$$\mathbf{H}_t'(x,y,z) = \sum_{m=1}^{M} \psi_m(z)\,\mathbf{h}_{m_t}(x,y)e^{-j\beta_m z}\ . \qquad (3.5b)$$

A mode propagating in the positive direction and the same mode propagating in the negative direction have separate m values. When considering the problem described in the introduction to this chapter, it is valid to drop the radiation modes because coupling of the two guided modes (a single mode propagating in the positive direction and the same mode with its direction reversed) with the radiation modes is negligible. The coefficients of expansion $\psi_m(z)$ are no longer constants as they were in (3.4) but evolve along the z-axis. Furthermore, the $\psi_m(z)$ of (3.5) with different values of m do not depend only on the source conditions as did the ψ_m of (3.4) but are coupled. The modes exchange energy due to the waveguide perturbation.

With the transverse components given by (3.5), the axial components are readily determined using the following equations [6]

$$\mathbf{a}_z H_z' = -\frac{1}{j\omega\mu_o}\nabla_t \times \mathbf{E}_t' \qquad (3.6a)$$

$$\mathbf{a}_z E_z' = \frac{1}{j\omega\varepsilon_o n'^2}\nabla_t \times \mathbf{H}_t'\,. \qquad (3.6b)$$

Substitution of (3.5a) into (3.6a) yields

$$\mathbf{a}_z H_z^{'} = -\frac{1}{j\omega\mu_o}\sum_{m=1}^{M}\psi_m(z)\,e^{-j\beta_m z}\left(\nabla_t \times \mathbf{e}_{m_t}\right). \tag{3.7}$$

Since each mode satisfies Maxwell's equations

$$\nabla_t \times \mathbf{e}_{m_t} = -j\omega\mu_o h_{m_z}\mathbf{a}_z \tag{3.8}$$

and substitution of (3.8) into (3.7) yields

$$H_z^{'} = \sum_{m=1}^{M}\psi_m(z)h_{m_z}e^{-j\beta_m z}\ . \tag{3.9}$$

Similarly

$$E_z^{'} = \sum_{m=1}^{M}\psi_m(z)\left(\frac{n}{n'}\right)^2 e_{m_z}e^{-j\beta_m z}\ . \tag{3.10}$$

If $n \approx n'$, that is if $\Delta n(x,y)$ is small then

$$\begin{pmatrix}\mathbf{E}'\\ \mathbf{H}'\end{pmatrix} = \sum_{m=1}^{M}\psi_m(z)\begin{pmatrix}\mathbf{e}_m\\ \mathbf{h}_m\end{pmatrix}e^{-j\beta_m z} \tag{3.11}$$

and it is seen that the expansion extends to the axial components as well.

To solve for the coefficients $\psi_m(z)$ in (3.11), the well-known coupled-mode equations are used. A derivation is not given here, as this is detailed in numerous articles and texts [6] [8] [9] [10] [11]. The coupled-mode equations are

$$\frac{d\psi_k(z)}{dz} = -j\sum_{m=1}^{M}\psi_m(z)e^{j(\beta_k-\beta_m)z}\,C_{km}(z) \tag{3.12a}$$

$$C_{km}(z) = \frac{\omega\varepsilon_o}{4P}\,\mathrm{sgn}(\beta_k)\int_S\left(n'^2 - n^2\right)\mathbf{e}_k^{\,*}\cdot\mathbf{e}_m\,ds \tag{3.12b}$$

where $\Delta\varepsilon = \varepsilon_o\left\{[n'(x,y)]^2 - n^2(x,y)\right\}$ is assumed small relative to $\varepsilon = \varepsilon_o n^2(x,y)$ as explained in the next paragraph. Sgn is the signum function with which most readers will already be familiar

$$\mathrm{sgn}(\beta_k) = \begin{cases}+1, & \beta_k > 0\\ -1, & \beta_k < 0\end{cases}.$$

The integral $\int_S$ is over the entire transverse plane, and P is the power in mode k, that is

$$P = \mathrm{sgn}(\beta_k)\frac{1}{2}\,\mathrm{Re}\left\{\int_S \left(\mathbf{e}_{k_t} \times \mathbf{h}_{k_t}^{\ *}\right)\cdot \mathbf{a}_z\, ds\right\}.$$

If radiation modes are included in (3.5) it becomes

$$\mathbf{E}_t'(x,y,z) = \int_m \psi_m(z)\,\mathbf{e}_{m_t}(x,y)e^{-j\beta_m z} \qquad (3.13a)$$

$$\mathbf{H}_t'(x,y,z) = \int_m \psi_m(z)\,\mathbf{h}_{m_t}(x,y)e^{-j\beta_m z} \qquad (3.13b)$$

where $\int_m$ indicates the summation over all modes. The guided modes are summed up since they are discrete, while the radiation modes are integrated with β_m since they exist over a continuum. Modifications are also required to (3.12) which becomes

$$\mathrm{sgn}(\beta_k)\frac{d\psi_k(z)}{dz} = -j\int_m C_{km}(z)\psi_m(z)e^{j(\beta_k-\beta_m)z} \qquad (3.14a)$$

$$C_{km}(z) = C_{km_t}(z) + C_{km_z}(z) \qquad (3.14b)$$

$$C_{km_t}(z) = \frac{\omega\varepsilon_o}{4}\int_S \left(n'^2 - n^2\right)\mathbf{e}_{k_t}^{\ *}\cdot\mathbf{e}_{m_t}\, ds \qquad (3.14c)$$

$$C_{km_z}(z) = \frac{\omega\varepsilon_o}{4}\int_S \left[\frac{\left(n'^2-n^2\right)n^2}{n^2+\left(n'^2-n^2\right)}\right]\mathbf{e}_{k_z}^{\ *}\cdot\mathbf{e}_{m_z}\, ds\,. \qquad (3.14d)$$

The fields in the perturbed waveguide are described precisely by (3.13) and (3.14) while (3.5) and (3.12) are approximations that apply when

- Coupling of guided modes with radiation modes is negligible
- $\left|\left(n'^2-n^2\right)\right| << n^2$ so the term in brackets in (3.14d) is approximately equal to $\left(n'^2-n^2\right)$.

In (3.14c) and (3.14d) it has been assumed the modes are normalized so that $P=1$ for every mode. By replacing $\sum_m$ in (3.5) and (3.12a) with $\int_m$ we have included the radiation modes in (3.13) and (3.14a), respectively.

By making the two assumptions detailed in the preceding paragraph, that is by using (3.5) or (3.11) and (3.12), the analysis becomes approximate. In this case the accuracy depends on the magnitude of $\Delta\varepsilon_r = n'^2 - n^2$ [6]. The canonical structure must be chosen so that the perturbed waveguide may be described by a $\Delta\varepsilon_r$ as small as possible. Regarding the specific problem under investigation, the waveguide described by (2.1) is an appropriate choice for the canonical waveguide for the perturbed waveguide described by (3.1). However, Δn_{l1}, Δn_{l2}, Δn_{l3}, and Δn_{l4} must be small relative to n_1, n_2, n_3, and n_4.

Whether (3.12b) or (3.14b) through (3.14d) are used for C_{km}, if k corresponds to a TE mode and m to a TM mode or vice versa, $C_{km} = 0$ because $\mathbf{e}_k$ and $\mathbf{e}_m$ are perpendicular to each other. Therefore TE-TM mode coupling does not occur. The coefficients $\psi_m(z)$ for the TE modes are described by (3.12a) or (3.14a) where k and m range over just the TE modes. Likewise, for the TM modes k and m range over just the TM modes.

3.3 Application of Coupled Mode Theory to Uniform Gratings in Multiclad Symmetric Planar Waveguides

Returning to the problem of gratings in multi-clad planar waveguides, all of the results of Section 3.2 apply although the y-dependence is lost everywhere due to the two-dimensional nature of the geometry. As already stated, k_o as determined by the source of excitation is assumed less than k_{oc_1} (See Figure 3-1). TE and TM modes do not couple, therefore k and m in (3.12a) range over just the TE modes or just the TM modes. Selecting either TE_0 or TM_0, if propagation is along the positive z-direction the normalized fields are denoted as

$$\begin{cases} \hat{\mathbf{E}} = \hat{\mathbf{e}}_1(x)e^{-j\beta z} \\ \hat{\mathbf{H}} = \hat{\mathbf{h}}_1(x)e^{-j\beta z} \end{cases}. \tag{3.15}$$

If the mode propagates in the negative-z direction, the normalized fields are given as

$$\begin{cases} \hat{\mathbf{E}}_{-} = \hat{\mathbf{e}}_2(x)e^{j\beta z} = \left[\hat{\mathbf{e}}_{1_t}(x) - \hat{\mathbf{e}}_{1_z}(x)\mathbf{a}_z\right]e^{j\beta z} \\ \hat{\mathbf{H}}_{-} = \hat{\mathbf{h}}_2(x)e^{j\beta z} = \left[-\hat{\mathbf{h}}_{1_t}(x) + \hat{\mathbf{h}}_{1_z}(x)\mathbf{a}_z\right]e^{j\beta z} \end{cases}. \qquad (3.16)$$

Readers not familiar with the notion of normalizing a mode note that either $\{\mathbf{E}, \mathbf{H}\}$ or $\{\mathbf{E}_{-}, \mathbf{H}_{-}\}$ divided by any constant are still solutions to Maxwell's equations. The normalized fields are given by

$$\hat{\mathbf{E}} = \frac{\mathbf{E}}{\sqrt{N_1}}, \quad \hat{\mathbf{H}} = \frac{\mathbf{H}}{\sqrt{N_1}}, \quad \hat{\mathbf{E}}_{-} = \frac{\mathbf{E}_{-}}{\sqrt{N_2}}, \quad \text{and } \hat{\mathbf{H}}_{-} = \frac{\mathbf{H}_{-}}{\sqrt{N_2}}$$

$$\text{where} \quad N_1 = \frac{1}{2}\left|\text{Re}\left\{\int_S \left(\mathbf{e}_{1_t} \times \mathbf{h}_{1_t}^{\ *}\right)\cdot \mathbf{a}_z ds\right\}\right|$$

$$\text{and} \quad N_2 = \frac{1}{2}\left|\text{Re}\left\{\int_S \left(\mathbf{e}_{2_t} \times \mathbf{h}_{2_t}^{\ *}\right)\cdot \mathbf{a}_z ds\right\}\right| = N_1 .$$

Equations (3.15) and (3.16) represent normalized guided mode field solutions for the unperturbed waveguide described by (2.1) when $k_o < k_{oc_1}$. Using (3.11), the fields of the perturbed waveguide described by $n'(x)$, (3.1), are written as

$$\begin{cases} \mathbf{E}' = \psi_1(z)\left[\hat{\mathbf{e}}_1(x)e^{-j\beta z}\right] + \psi_2(z)\left[\hat{\mathbf{e}}_2(x)e^{j\beta z}\right] \\ \mathbf{H}' = \psi_1(z)\left[\hat{\mathbf{h}}_1(x)e^{-j\beta z}\right] + \psi_2(z)\left[\hat{\mathbf{h}}_2(x)e^{j\beta z}\right] \end{cases}. \qquad (3.17)$$

Using (3.12a) yields

$$\frac{d\psi_1}{dz} = -j\left(\psi_1 C_{11} + \psi_2 e^{j2\beta z} C_{12}\right) \qquad (3.18a)$$

$$\frac{d\psi_2}{dz} = -j\left(\psi_2 C_{22} + \psi_1 e^{-j2\beta z} C_{21}\right). \qquad (3.18b)$$

An approximation for $\left(n'^2 - n^2\right)$ will be used in (3.12b). Since

$$\left[n'(x,z)\right]^2 = \left[n(x) + \Delta n(x,z)\right]^2 = n^2(x) + 2n(x)\Delta n(x,z) + \left[\Delta n(x,z)\right]^2$$

from (3.1a), it follows that $n'^2 - n^2 \approx 2n(x)\Delta n(x,z), \quad \Delta n(x,z) << n(x)$. $\overline{\Delta n_{l1}}$ in (3.1b) should be less than n_1 by a factor of at least 20, and likewise for $\overline{\Delta n_{l2}}$ and n_2, etc. Thus,

$$n'^2 - n^2 \approx \begin{cases} 2n_1\overline{\Delta n_{l1}}\left[1+\cos\left(\dfrac{2\pi}{\Lambda_{l1}}z+\phi_{l1}\right)\right], & |x|<a_1 \\ 2n_2\overline{\Delta n_{l2}}\left[1+\cos\left(\dfrac{2\pi}{\Lambda_{l2}}z+\phi_{l2}\right)\right], & a_1<|x|<a_2 \\ 2n_3\overline{\Delta n_{l3}}\left[1+\cos\left(\dfrac{2\pi}{\Lambda_{l3}}z+\phi_{l3}\right)\right], & a_2<|x|<a_3 \\ 2n_4\overline{\Delta n_{l4}}\left[1+\cos\left(\dfrac{2\pi}{\Lambda_{l4}}z+\phi_{l4}\right)\right], & a_3<|x| \end{cases} . \tag{3.19}$$

Substituting (3.19) into (3.12b) and noting that $P=1$ yields

$$C_{11}(z)=\frac{\omega\varepsilon_o}{2}\begin{cases} n_1\overline{\Delta n_{l1}}\left[1+\cos\left(\dfrac{2\pi}{\Lambda_{l1}}z+\phi_{l1}\right)\right]\displaystyle\int_{-a_1}^{a_1}\hat{\mathbf{e}}_1^{\,*}\cdot\hat{\mathbf{e}}_1 dx \\ +2n_2\overline{\Delta n_{l2}}\left[1+\cos\left(\dfrac{2\pi}{\Lambda_{l2}}z+\phi_{l2}\right)\right]\displaystyle\int_{a_1}^{a_2}\hat{\mathbf{e}}_1^{\,*}\cdot\hat{\mathbf{e}}_1 dx \\ +2n_3\overline{\Delta n_{l3}}\left[1+\cos\left(\dfrac{2\pi}{\Lambda_{l3}}z+\phi_{l3}\right)\right]\displaystyle\int_{a_2}^{a_3}\hat{\mathbf{e}}_1^{\,*}\cdot\hat{\mathbf{e}}_1 dx \\ +2n_4\overline{\Delta n_{l4}}\left[1+\cos\left(\dfrac{2\pi}{\Lambda_{l4}}z+\phi_{l4}\right)\right]\displaystyle\int_{a_3}^{\infty}\hat{\mathbf{e}}_1^{\,*}\cdot\hat{\mathbf{e}}_1 dx \end{cases} \tag{3.20}$$

where the symmetry of the waveguide and the resulting symmetry of $\hat{\mathbf{e}}_1(x)$ have been exploited. If unnormalized $\{\mathbf{e}_1,\mathbf{h}_1\}$ were used in place of $\{\hat{\mathbf{e}}_1,\hat{\mathbf{h}}_1\}$ in (3.17), then a factor of $1/\sqrt{N_1}$ would appear in the right-hand-side of (3.20), cancelling the factor of $\sqrt{N_1}$ difference between $\{\mathbf{e}_1,\mathbf{h}_1\}$ and $\{\hat{\mathbf{e}}_1,\hat{\mathbf{h}}_1\}$ in (3.17). Similarly,

$$C_{12}(z)=\text{same as } C_{11}(z)\text{ but with } \hat{\mathbf{e}}_1^{\,*}\cdot\hat{\mathbf{e}}_1 \text{ replaced with } \hat{\mathbf{e}}_1^{\,*}\cdot\hat{\mathbf{e}}_2 . \tag{3.21}$$

If $\{\hat{\mathbf{E}},\hat{\mathbf{H}}\}$ and $\{\hat{\mathbf{E}}_-,\hat{\mathbf{H}}_-\}$ correspond to TE_0 then $\hat{\mathbf{e}}_{1_z}=0$ in (3.16) and $\hat{\mathbf{e}}_1=\hat{\mathbf{e}}_2$. In this case $C_{12}=C_{11}$.

If on the other hand $\{\hat{\mathbf{E}},\hat{\mathbf{H}}\}$ and $\{\hat{\mathbf{E}}_-,\hat{\mathbf{H}}_-\}$ correspond to TM_0 then $\hat{\mathbf{e}}_{1_z}\neq 0$, however since the guide is assumed weakly guiding ($n_1\approx n_2\approx n_3\approx n_4$ to within a few percent) $\hat{e}_{1_z}<<\hat{e}_{1_x}$. It is always possible to take the transverse components of a mode to

be real and the axial components to be imaginary [12]. According to Section 2.2.6, for TM modes $e_z = \text{RHS of (2.3)}$ and $(-1/j\beta)e_x = \text{RHS of (2.4)}$. The program fdist.m returned values of A_1, A_2, A_3, A_4, A_5, and A_6 that were all purely real however we are free to multiply A_1, A_2, A_3, A_4, A_5, and A_6 by j. In doing so we find that e_z and, therefore, $\hat{e}_z$ are purely imaginary and e_x and, therefore, $\hat{e}_x$ are purely real. With this in mind it follows that

$$\hat{\mathbf{e}}_1^{\,*}(x)\cdot\hat{\mathbf{e}}_1(x) = \left|\hat{\mathbf{e}}_1(x)\right|^2 = \left|\hat{\mathbf{e}}_{1_t}\right|^2 + \left|\hat{e}_{1_z}\right|^2 \xrightarrow{TM_0} \left|\hat{e}_{1_x}\right|^2 + \left|\hat{e}_{1_z}\right|^2$$

$$\hat{\mathbf{e}}_1^{\,*}(x)\cdot\hat{\mathbf{e}}_2(x) = \left[\hat{\mathbf{e}}_{1_t} - j\,\mathrm{Im}\{\hat{e}_{1_z}\}\mathbf{a}_z\right]\cdot\left[\hat{\mathbf{e}}_{1_t} - j\,\mathrm{Im}\{\hat{e}_{1_z}\}\mathbf{a}_z\right] = \left|\hat{\mathbf{e}}_{1_t}\right|^2 - \left|\hat{\mathbf{e}}_{1_z}\right|^2 \xrightarrow{TM_0} \left|\hat{e}_{1_x}\right|^2 - \left|\hat{e}_{1_z}\right|^2.$$

Since for any weakly guiding cylindrical waveguide with arbitrary cross-section as in Figure 3-2, the $\hat{e}_z$ component is much smaller than $\hat{\mathbf{e}}_t$, for TM_0 of the multi-clad symmetric planar waveguide under consideration with (e_x, h_y, e_z) $\hat{e}_z$ is much smaller than $\hat{e}_x$. Finally,

$$C_{12} \approx C_{11}$$

whether the single mode propagating in the waveguide is TE_0 or TM_0. (Readers not satisfied that $\hat{e}_z$ is much smaller than $\hat{e}_x$ for TM_0 observe again that according to section 2.2.6 for TM modes $e_z = \text{RHS of (2.3)}$ and $(-1/j\beta)e_x = \text{RHS of (2.4)}$. Therefore $\frac{e_z}{e_x} = \frac{\hat{e}_z}{\hat{e}_x}$ is on the order of $-\frac{1}{j\beta}u_i = -\frac{1}{jk_o\bar{\beta}}k_o\sqrt{\bar{\beta}^2 - n_i^{\,2}}$ which is very small since $n_1 \approx n_2 \approx n_3 \approx n_4 \approx \bar{\beta}$.)

By extension of the above argument

$$C_{21} \approx C_{22} \approx -C_{11} \approx -C_{12}. \qquad (3.22)$$

The fact that $C_{22} = -C_{11}$ is due to the $\mathrm{sgn}(\beta_k)$ term in (3.12b) which equals –1 for a mode propagating in the negative-z direction.

An important assumption is now made, that $\Lambda_{l1} = \Lambda_{l2} = \Lambda_{l3} = \Lambda_{l4} = \Lambda$ and $\phi_{l1} = \phi_{l2} = \phi_{l3} = \phi_{l4} = \phi$. In the next chapter, the situation when this is not the case will be considered. However, for now using (3.22) yields

$$C_{11} = C_o\left[1+\cos\left(\frac{2\pi}{\Lambda}z+\phi\right)\right] \tag{3.23a}$$

$$\text{where } C_o = \frac{\omega\varepsilon_o}{2}\begin{cases} n_1\overline{\Delta n_{l1}}\int_{-a_1}^{a_1}\hat{\mathbf{e}}_1^{\,*}\cdot\hat{\mathbf{e}}_1 dx \;+\; 2n_2\overline{\Delta n_{l2}}\int_{a_1}^{a_2}\hat{\mathbf{e}}_1^{\,*}\cdot\hat{\mathbf{e}}_1 dx \\ +2n_3\overline{\Delta n_{l3}}\int_{a_2}^{a_3}\hat{\mathbf{e}}_1^{\,*}\cdot\hat{\mathbf{e}}_1 dx \;+\; 2n_4\overline{\Delta n_{l4}}\int_{a_3}^{\infty}\hat{\mathbf{e}}_1^{\,*}\cdot\hat{\mathbf{e}}_1 dx. \end{cases} \tag{3.23b}$$

C_o is a constant independent of x, y, or z.

Using (3.23a) and (3.22) in (3.18) yields

$$\frac{d\psi_1}{dz} = -jC_o\left[1+\cos\left(\frac{2\pi}{\Lambda}z+\phi\right)\right]\left[\psi_1+\psi_2 e^{j2\beta z}\right] \tag{3.24a}$$

$$\frac{d\psi_2}{dz} = jC_o\left[1+\cos\left(\frac{2\pi}{\Lambda}z+\phi\right)\right]\left[\psi_2+\psi_1 e^{-j2\beta z}\right]. \tag{3.24b}$$

This pair of coupled differential equations is simplified by operating on each of them as follows:

1. Expanding the right-hand-side after substituting for $\cos\left(\frac{2\pi}{\Lambda}z+\phi\right)$ using the identity

$$\cos\theta = \frac{e^{j\theta}+e^{-j\theta}}{2}. \tag{3.25}$$

2. Neglecting oscillatory terms on the RHS that oscillate rapidly with z relative to $\psi_1(z)$ and $\psi_2(z)$ which vary almost not at all over one grating period. Supposing both the left and right hand sides are integrated these terms contribute little to the RHS integral.

The resulting equations can be written

$$\frac{d\psi_1}{dz} = -jC_o\psi_1 - j\frac{C_o'}{2}\psi_2 e^{j\delta z} \tag{3.26a}$$

$$\frac{d\psi_2}{dz} = jC_o\psi_2 + j\frac{\left(C_o'\right)^*}{2}\psi_1 e^{-j\delta z} \tag{3.26b}$$

$$\text{where } C_o' = C_o e^{-j\phi} \tag{3.27}$$

$$\text{and } \delta = 2\beta - \frac{2\pi}{\Lambda}. \tag{3.28}$$

To determine a complete approximate fields solution for the perturbed waveguide, the coupled pair of differential equations (3.26) are solved. The gratings are assumed to extend over a length L of the guide, from $z = 0$ to $z = L$. At $z = L$ the reflected field ceases to exist, that is $\psi_2(L) = 0$. This boundary condition is used to eliminate one of the two constant coefficients occurring in the expressions for $\psi_1(z)$ and $\psi_2(z)$ resulting from solving (3.26a) and (3.26b). The results are

$$\psi_1(z) = -\frac{j4}{\left(C_o'\right)^*} B e^{\left(SL + j\frac{\delta}{2}z\right)} \left\{ S\cosh[(z-L)S] - j\left(\frac{\delta}{2} + C_o\right)\sinh[(z-L)S] \right\} \tag{3.29a}$$

$$\psi_2(z) = 2B e^{\left(SL - j\frac{\delta}{2}z\right)} \sinh[(z-L)S] \tag{3.29b}$$

$$\text{where } S = \sqrt{\left(\frac{C_o}{2}\right)^2 - C_o(C_o + \delta) - \left(\frac{\delta}{2}\right)^2} = \sqrt{\left(\frac{C_o}{2}\right)^2 - \left(C_o + \frac{\delta}{2}\right)^2} \tag{3.30}$$

and B is an arbitrary constant. The powers of the forward and backward propagating modes are

$$P_1(z) = \frac{\text{sgn}(\beta_1)}{2} \text{Re}\left\{ \int_S \hat{\mathbf{E}}_{1_t} \times \hat{\mathbf{H}}_{1_t}{}^* \cdot \mathbf{a}_z \right\}$$

$$= \frac{\text{sgn}(\beta_1)}{4} \int_S \left(\psi_1{}^*(z) \hat{\mathbf{e}}_{1_t}{}^* e^{j\beta z} \times \psi_1(z) \hat{\mathbf{h}}_{1_t} e^{-j\beta z} + \psi_1(z) \hat{\mathbf{e}}_{1_t} e^{-j\beta z} \times \psi_1{}^*(z) \hat{\mathbf{h}}_{1_t}{}^* e^{j\beta z} \right) \cdot \mathbf{a}_z \, ds \tag{3.31a}$$

where $\int_S$ is over the entire transverse plane. The term $\text{sgn}(\beta_1) = \text{sgn}(\beta) = 1$ multiplier does not matter here but the corresponding multiplier in $P_2(z)$ below serves to make $P_2(z)$ positive, equivalent to multiplying $P_1(z)$ with $\mathbf{a}_z$ inside the integral and $P_2(z)$ with $-\mathbf{a}_z$. $P_1(z)$ is the power in mode 1 flowing in the positive-z direction, $P_2(z)$ the power in mode 2 flowing in the negative-z direction, and both are positive quantities.

$$P_2(z)=\frac{\operatorname{sgn}(\beta_2)}{4}\int_S\left(\psi_2^{\,*}(z)\hat{\mathbf{e}}_{2_t}^{\,*}e^{-j\beta z}\times\psi_2(z)\hat{\mathbf{h}}_{2_t}e^{j\beta z}+\psi_2(z)\hat{\mathbf{e}}_{2_t}e^{j\beta z}\times\psi_2^{\,*}(z)\hat{\mathbf{h}}_{2_t}^{\,*}e^{-j\beta z}\right)\cdot\mathbf{a}_z\,ds \tag{3.31b}$$

where $\operatorname{sgn}(\beta_2)=\operatorname{sgn}(-\beta)=-1$. Since $\{\hat{\mathbf{E}},\hat{\mathbf{H}}\}$ and $\{\hat{\mathbf{E}}_-,\hat{\mathbf{H}}_-\}$ are normalized

$$\frac{\operatorname{sgn}(\beta_k)}{4}\int_S\left(\hat{\mathbf{e}}_{k_t}^{\,*}\times\hat{\mathbf{h}}_{k_t}+\hat{\mathbf{e}}_{k_t}\times\hat{\mathbf{h}}_{k_t}^{\,*}\right)\cdot\mathbf{a}_z\,ds=1\qquad k=1,2 \tag{3.32}$$

Equations (3.31a) and (3.31b) are the powers in the forward and backward propagating modes in the perturbed waveguide while (3.32) indicates that the forward and backward propagating modes in the unperturbed waveguide have been normalized. Using (3.32) in (3.31a) and (3.31b) yields

$$P_1(z)=|\psi_1(z)|^2 \tag{3.33a}$$

$$\text{and } P_2(z)=|\psi_2(z)|^2 \tag{3.33b}$$

respectively. Substituting (3.29a) into (3.33a) and (3.29b) into (3.33b) yields

$$P_1(z)=\begin{cases}\dfrac{16}{C_o^{\,2}}|B|^2e^{2SL}\left\{S^2\cosh^2[(z-L)S]+\left(\dfrac{\delta}{2}+C_o\right)^2\sinh^2[(z-L)S]\right\}, & S\text{ real}\\ \dfrac{16}{C_o^{\,2}}|B|^2\left\{\hat{S}^2\cos^2[(z-L)\hat{S}]+\left(\dfrac{\delta}{2}+C_o\right)^2\sin^2[(z-L)\hat{S}]\right\}, & S\text{ imaginary}\end{cases} \tag{3.34a}$$

and

$$P_2(z)=\begin{cases}4|B|^2e^{2SL}\sinh^2[(z-L)S], & S\text{ real}\\ 4|B|^2\sin^2[(z-L)\hat{S}], & S\text{ imaginary}\end{cases} \tag{3.34b}$$

where

$$\hat{S}=\sqrt{\left(C_o+\frac{\delta}{2}\right)^2-\left(\frac{C_o}{2}\right)^2}=\pm\frac{S}{j}=\operatorname{Im}(S),\qquad S\text{ imaginary}. \tag{3.34c}$$

S and $\hat{S}$ both have sign ambiguity. A positive or negative sign can be placed in front of the radical sign in (3.30) and it makes no difference as long as we use the same definition of S in all expressions containing S. Clearly the sign of $\hat{S}$ makes no difference in the two expressions in which it appears, (3.34b) and (3.35).

Reflectivity R is defined as the ratio of the power in the backward propagating mode to the power in the forward propagating mode at the input to the section of the waveguide containing gratings, that is at $z = 0$. Therefore,

$$R = \frac{P_2(0)}{P_1(0)} = \begin{cases} \dfrac{C_o^{\,2}}{4} \dfrac{\sinh^2(LS)}{\left[S^2 \cosh^2(LS) + \left(\dfrac{\delta}{2} + C_o \right)^2 \sinh^2(LS) \right]}, & S \text{ real} \\ \dfrac{C_o^{\,2}}{4} \dfrac{\sin^2(L\hat{S})}{\left[\hat{S}^2 \cos^2(L\hat{S}) + \left(\dfrac{\delta}{2} + C_o \right)^2 \sin^2(L\hat{S}) \right]}, & S \text{ imaginary.} \end{cases} \tag{3.35}$$

The reflectivity does not depend on the phase ϕ of the gratings.

3.4 Other Geometries

In section 3.2, the unperturbed waveguide was a cylindrical dielectric waveguide with an arbitrary cross-section. In section 3.3, it was a weakly guiding multiclad symmetric planar waveguide, a type of cylindrical waveguide. Also, although the perturbation $\Delta n(x, y)$ was left general in section 3.2, in section 3.3 it was specified by (3.1b). So section 3.3 is not as general as section 3.2. However, the results of section 3.3 are easily extended to weakly-guiding cylindrical dielectric waveguides of arbitrary cross-section that have a perturbation of the same form as in section 3.3. As a reminder, by perturbation we mean $\Delta n(x, y)$ where

$$\varepsilon' = \varepsilon_o [n'(x, y)]^2 = \varepsilon_o [n(x, y) + \Delta n(x, y)]^2 \tag{3.36}$$

describes the perturbed guide using $n(x, y)$ of the unperturbed guide. Specifically, if the perturbation has the form

$$\Delta n(x, y, z) = \overline{\Delta n}(x, y) \left[1 + \cos\left(\frac{2\pi}{\Lambda} z + \phi \right) \right] \tag{3.37}$$

then (3.35) for R still applies. $\overline{\Delta n}(x, y)$ is the "dc" index change spatially averaged over one grating period. For now it is independent of z – the gratings are uniform – so the average might just as well be over the entire length of the gratings. δ is still given by (3.28), S by (3.30), and $\hat{S}$ by (3.34c). However, now C_o is given by

$$C_o = \frac{\omega \varepsilon_o}{2} \iint n(x,y)\overline{\Delta n}(x,y)\hat{\mathbf{e}}_1^{\,*} \cdot \hat{\mathbf{e}}_1 \, ds \qquad (3.38)$$

where $\iint$ is over the entire transverse plane and $\overline{\Delta n}(x,y) = 0$ anywhere that gratings do not exist. $\hat{\mathbf{e}}_1$ is the electric field of either

1. the single guided mode that is supported at the wavelength of excitation or
2. if one TE and one TM mode and no other guided modes are supported, either the TE or the TM mode.

Equation 22 of [1] is equivalent to (3.35) and is for a single-clad step index fiber with gratings in the core of the form of (3.37) with $\overline{\Delta n}(x,y) = \text{constant}$. (Set $v = 1$ in equation 1 of [1].)

3.5 Reflectivity Spectra

Figure 3-3 shows all of the parameters and coefficients used to calculate the reflectivity R given by (3.35). The left-most column contains the input information. $\overline{\Delta n_{l1}}$, $\overline{\Delta n_{l2}}$, $\overline{\Delta n_{l3}}$, and $\overline{\Delta n_{l4}}$ obey (3.2) and could be replaced by α. To the right are variables, each with one or more arrows pointing to them, and each of which, with the exception of β and $\hat{\mathbf{e}}_1$, can be calculated using a single equation appearing in this chapter. Chapter 2 details the computer algorithm used to calculate β and $\hat{\mathbf{e}}_1$. By tracing all of the arrows pointing to a particular variable back to their tails all of the inputs and/or variables used to calculate the particular variable are found. Table 3-1 provides an explanation of the inputs and variables in Figure 3-3.

All of the inputs to the problem are constants. Even λ_o is a constant because it is assumed our phasors have time-dependence of the form $e^{j\omega t}$ where ω is a constant set by the source of excitation. The dependence of R on the dimensions of the waveguide a_1, a_2, and a_3 could be examined but different sets of dimensions correspond to different waveguides. Of more importance is the dependence of R on λ_o. Gratings in waveguides can be used as wavelength filters. All real signals can be expanded into an infinite number of frequency components by taking their Fourier transform. In a bandpass filter configuration, the forward propagating component of $\mathbf{E}'$ where it is

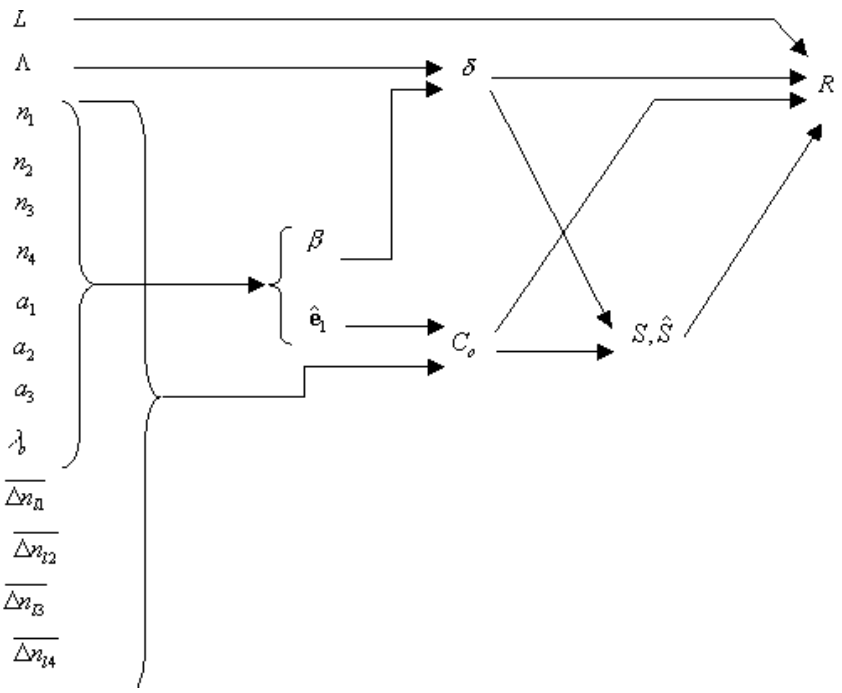

Figure 3-3 Dependence of inputs and variables used to compute reflectivity in (3.35)

Table 3-1 Explanation of inputs in Figure 3-3

L	length of section of waveguide containing gratings
Λ	grating period
n_1	refractive index within $\lvert x\rvert < a_1$
n_2	refractive index within $a_1 < \lvert x\rvert < a_2$
n_3	refractive index within $a_2 < \lvert x\rvert < a_3$
n_4	refractive index within $a_3 < \lvert x\rvert$
a_1	$x = \pm a_1$ marks boundary between core and first cladding
a_2	$x = \pm a_2$ marks boundary between first and second cladding
a_3	$x = \pm a_3$ marks boundary between second and third cladding
λ_o	$2\pi/\omega\sqrt{\mu_o\varepsilon_o}$, wavelength of plane wave with same freq. as the source of excitation
$\overline{\Delta n_{l1}}$	amplitude of gratings within $\lvert x\rvert < a_1$
$\overline{\Delta n_{l2}}$	amplitude of gratings within $a_1 < \lvert x\rvert < a_2$
$\overline{\Delta n_{l3}}$	amplitude of gratings within $a_2 < \lvert x\rvert < a_3$
$\overline{\Delta n_{l4}}$	amplitude of gratings within $a_3 < \lvert x\rvert$

incident on the gratings is the input, and the backward propagating component of $\mathbf{E}'$ where it exits the front end is the output. Using the same input and taking the forward propagating wave after it has exited the gratings as the output results in a bandstop filter. The spectral reflectivity function is described by

$$R(\lambda_o) = \frac{P_2(0)}{P_1(0)} \tag{3.39}$$

while the transmission function is given by

$$\frac{P_1(L)}{P_1(0)} = 1 - R(\lambda_o). \tag{3.40}$$

The validity of (3.40) is demonstrated by finding

$$P_1(0) - P_2(0) = \frac{16}{C_o^{\,2}}|B|^2 e^{2SL}\left\{\frac{C_o^{\,2}}{4}\cosh^2(LS) - \left(\frac{\delta}{2} + C_o\right)^2\right\} - 4|B|^2 e^{2SL}\sinh^2(LS)$$

$$= 4|B|^2 e^{2SL} - \frac{16}{C_o^{\,2}}|B|^2 e^{2SL}\left(\frac{\delta}{2} + C_o\right)^2$$

and

$$P_1(L) = \frac{16}{C_o^{\,2}}|B|^2 e^{2SL} S^2.$$

Then, using (3.30), (3.35a), (3.35b), and the identity $\cosh^2 x - \sinh^2 x = 1$, it follows that

$$P_1(0) - P_2(0) = P_1(L) \tag{3.41}$$

and (3.40) follows from (3.41). Equation (3.41) demonstrates conservation of power.

The peak value of R in a plot of R versus λ_o occurs at the value of λ_o at which the following relation holds

$$\frac{\delta}{2} + C_o = 0$$

$$\frac{2\beta - \dfrac{2\pi}{\Lambda}}{2} + C_o = 0$$

$$\frac{\pi}{\Lambda} = \beta + C_o. \tag{3.42}$$

At this value of λ_o the interaction between the forward and backward propagating waves is the strongest. Referring to this λ_o as λ_{o_D} ("D" for design)

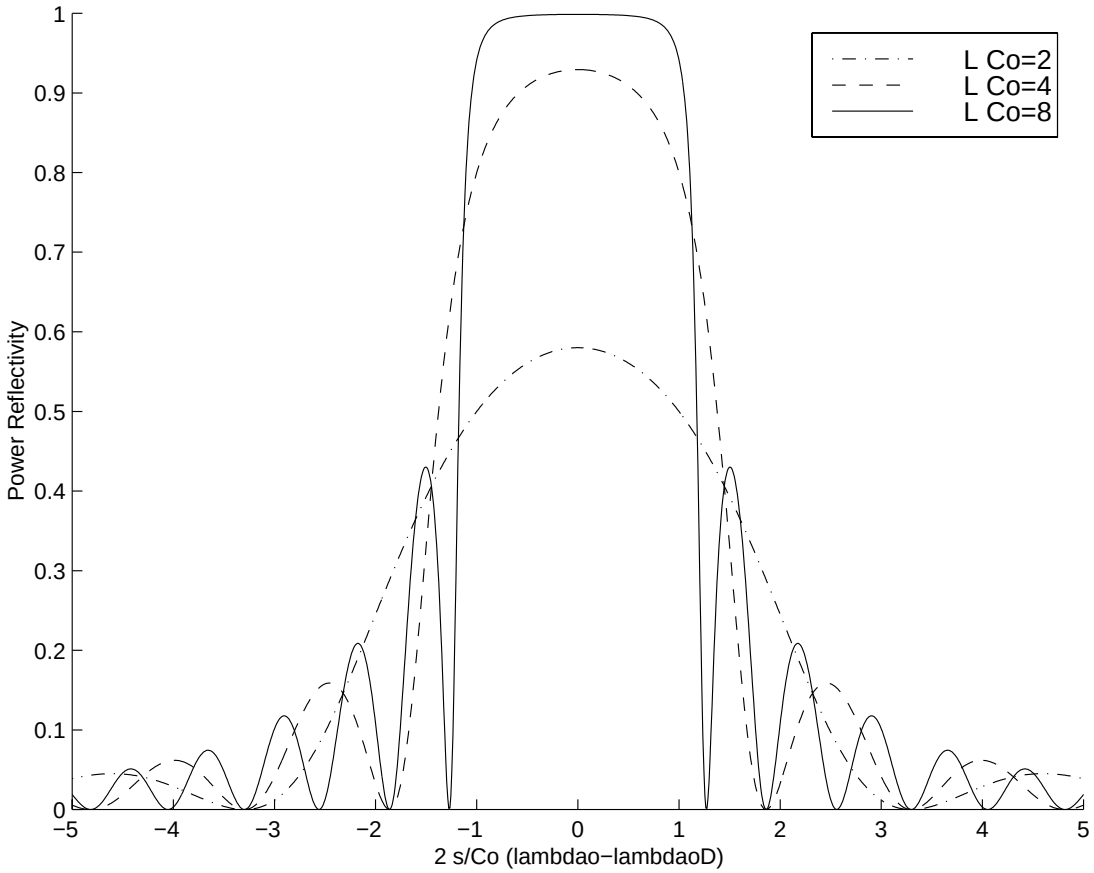

Figure 3-4 Reflection spectra versus normalized wavelength

$$\frac{\pi}{\Lambda} = \beta\left(\lambda_{o_D}\right) + C_o\left(\lambda_{o_D}\right).$$

As will be seen R versus λ_o is almost exactly symmetric about λ_{o_D}. If a certain λ_{o_D} is desired, it is achieved by setting the period of the gratings

$$\Lambda = \frac{\pi}{\beta\left(\lambda_{o_D}\right) + C_o\left(\lambda_{o_D}\right)}. \qquad (3.43)$$

Figure 3-4 is a plot of R versus normalized wavelength for values of $LC_o = 2, 4, \text{and } 8$. The equations used to plot it are derived in appendix C. As detailed there, two sources of error make Figure 3-4 only approximate, but it is very useful for designing uniform gratings. It shows us, for example, how increasing L changes the spectrum, which is not obvious by inspection of (3.35).

In Figure 3-4, C_o is fixed to a constant value, its value at λ_{o_D}, hence its dependence on wavelength is neglected. This is one of the two sources of error although the amount of error introduced is very small because C_o varies by only one or two percent over the range of λ_o over which R is significant. Fixing C_o to a constant value enables one value of the product LC_o to be associated with any R versus λ_o curve.

The second source of error in Figure 3-4 is the use of an approximation to the β versus λ_o dispersion curve. Specifically, it has been approximated as a straight line given by

$$\beta \approx -s\lambda_o + b \qquad \text{(C.4)}$$

where s is the negative of the slope of the exact β versus λ_o curve at λ_o equal to λ_{o_D} or in the vicinity. The range of λ_o over which R is non-negligible is so small that a straight line is an excellent approximation to the β versus λ_o curve. Therefore, it matters almost not at all whether s is set equal to the slope of the actual curve at λ_{o_D} or anywhere else in the non-negligible R range. The value of b affects the derivation in Appendix C although it does not appear anywhere on Figure 3-4 and therefore does not matter to someone using this figure to design uniform gratings. The y-intercept b is set such that whatever the value of s, the straight line approximation (C.4) passes through the point $\left(\lambda_{o_D}, \beta\left(\lambda_{o_D}\right)\right)$ on the exact curve.

Figure 3-4 can be used to answer questions such as the one already posed, how does increasing L change the spectrum? The answer is that if all else remains the same then we advance to LC_o = constant curves with larger values of LC_o. There are, of course, an infinite number of curves between the three actually plotted. The bandwidth decreases and the first sidelobe level increases. If L is increased while the product LC_o is held constant then C_o is decreased – although the normalized bandwidth remains the same the unnormalized bandwidth

$$\text{bandwidth} = 2\left(\lambda_o - \lambda_{o_D}\right) = 2\frac{x \cdot C_o}{2s} = \frac{xC_o}{s} \qquad \text{(3.44)}$$

decreases. In (3.44) x is the positive value of normalized wavelength at which the LC_o = constant curve in question drops below $R = \frac{1}{2}$ or $\frac{1}{10}\ldots$ or some other level depending on the definition of bandwidth being used.

It is seen from (3.44) that the range of un-normalized λ_o over which R is non-negligible is nearly always very small. The three LC_o = constant curves given in Figure 3-4 and any other LC_o = constant curves that might be plotted decay to nearly zero at values of the normalized wavelength of ± 15 or so. Using (3.44), for typical values of C_o and s this corresponds to a very small un-normalized wavelength range. R equals zero everywhere over the single-mode range of λ_o except for within a narrow range surrounding λ_{o_D}. C_o has to be much larger than usual or s much smaller for the un-normalized wavelength range over which R is non-negligible to grow substantial. Very large values of C_o do not occur because $\overline{\Delta n_{l1}}$ through $\overline{\Delta n_{l4}}$ in (3.23b) are never larger than about 10^{-2} [2] because of the limitations of existing fabrication techniques. Anyway, as discussed at the end of section 3.2 assumptions that have been made cause the accuracy of the analysis to depend on the magnitude of $\Delta\varepsilon_r$. Accurate results cannot be expected if too large values of $\overline{\Delta n_{l1}}$ through $\overline{\Delta n_{l4}}$ are used. The slope s might possibly be very small in certain circumstances – if λ_{o_D} is far from cuttoff, for instance. However, in general the analysis is restricted to the range of wavelengths over which only a single TE or a single TM mode is supported -- $k_{oc_0} < k_o < k_{oc_1}$ in Figure 3-2 for symmetric planar waveguides. The dispersion curve probably can't be very flat in this range. Under special circumstances the analysis also extends to multi-mode waveguides, meaning multiple TE modes if TE modes are being considered or multiple TM modes if TM modes are being considered. Brillouin diagrams, for which [6] is an excellent reference, can be used to identify when coupling occurs only between a single mode propagating in the forward and backward directions in a multi-mode guide. In this case s might possibly be very small. Still, in general it is safe to state that the range of un-normalized λ_o over which R is non-negligible is nearly always very small. Therefore

the two approximations that were used to plot Figure 3-4 detailed at the end of Appendix C are safe. Even if λ_{o_D} is far from cuttoff of the single mode under consideration so that the range of λ_o over which R is non-negligible is relatively large the two assumptions are probably still safe. Over this extended λ_o range the β versus λ_o curve will still be nearly a straight line, now almost flat. Also C_o will still not vary much because far from cuttoff $\hat{\mathbf{e}}_1$ evolves more slowly with λ_o.

Figure 3-4 reveals that the product LC_o sets the shape of the spectrum, which can then be contracted or expanded in the x-direction to achieve any desired bandwidth by adjusting C_o and L. This can be the basis of a design methodology. The product LC_o sets the level of the sidelobes.

Figure 3-4 also reveals that any spectrum that can be achieved for one value of λ_{o_D} can be achieved for any other value of λ_{o_D}. In this sense λ_{o_D} doesn't matter. As always λ_{o_D} must be chosen within the range of λ_o over which the analysis is valid – see the middle of the paragraph above the paragraph above this one – but otherwise λ_{o_D} is completely arbitrary. The only way in which Figure 3-4 is impacted by λ_{o_D} is in s, the negative of the slope of the β versus λ_o curve at λ_{o_D}. However, C_o can be adjusted so that the ratio $\frac{s}{C_o}$ is independent of λ_{o_D}. Then by adjusting C_o, then L so that LC_o stays the same, the same spectrum can be achieved at any two different values of λ_{o_D} to within the accuracy of Figure 3-4.

Chapter 4

Gratings In Multilayer Waveguides With a Phase Shift Between Layers

4.1 Description of the Perturbation

An expression for the power reflectivity in the more general case of non-zero shift in the phase of the gratings between layers is found. That is, (3.1b) is still used for $\Delta n(x,z)$, but it is not assumed that $\phi_{l1} = \phi_{l2} = \phi_{l3} = \phi_{l4}$. It is, however, still assumed that $\Lambda_{l1} = \Lambda_{l2} = \Lambda_{l3} = \Lambda_{l4} = \Lambda$. The perturbed refractive index, denoted as $n'(x,z)$, is that given by (3.1a). As discussed in chapter 3, the accuracy of the analysis depends on the magnitude of the perturbation. In this chapter, as in chapter 3, the amplitudes of the gratings in the separate layers, namely $\overline{\Delta n_{l1}}$, $\overline{\Delta n_{l2}}$, $\overline{\Delta n_{l3}}$, and $\overline{\Delta n_{l4}}$ in (3.1b), are constants independent of z, hence the gratings considered are uniform.

4.2 Coupled-Wave Equations

Again, the coupling between a single mode, usually TE_0 or TM_0, propagating in the positive-z direction given by (3.15) and the same mode propagating in the negative-z direction given by (3.16) is considered. The fields of both (3.15) and (3.16) are normalized. Recalling that $C_{21} = C_{22} = -C_{11} = -C_{12}$ (see Section 3.3), the coupled-mode equations (3.18a) and (3.18b) become

$$\frac{d\psi_1}{dz} = -j\left(\psi_1 C_{11} + \psi_2 e^{j2\beta z} C_{11}\right) \qquad (4.1a)$$

$$\frac{d\psi_2}{dz} = j\left(\psi_2 C_{11} + \psi_1 e^{-j2\beta z} C_{11}\right) \qquad (4.1b)$$

where $C_{11}(z)$ is given by (3.20) in which $\Lambda_{l1} = \Lambda_{l2} = \Lambda_{l3} = \Lambda_{l4} = \Lambda$ are used. Expressing the cosine terms in (3.20) as

$$1+\cos\left(\frac{2\pi}{\Lambda}z+\phi_{l1}\right)=1+\frac{e^{j\frac{2\pi}{\Lambda}z}e^{j\phi_{l1}}+e^{-j\frac{2\pi}{\Lambda}z}e^{-j\phi_{l1}}}{2},\qquad |x|<a_1$$

$$1+\cos\left(\frac{2\pi}{\Lambda}z+\phi_{l2}\right)=1+\frac{e^{j\frac{2\pi}{\Lambda}z}e^{j\phi_{l2}}+e^{-j\frac{2\pi}{\Lambda}z}e^{-j\phi_{l2}}}{2},\qquad a_1<|x|<a_2$$

$$\vdots$$

the coefficient C_{11} can be written as

$$C_{11}=C_o+e^{j\frac{2\pi}{\Lambda}z}K+e^{-j\frac{2\pi}{\Lambda}z}K^* \tag{4.2a}$$

where

$$C_o=\frac{\omega\varepsilon_o}{2}\left\{\begin{array}{l} n_1\overline{\Delta n_{l1}}\int_{-a_1}^{a_1}\hat{\mathbf{e}}_1^{\,*}\cdot\hat{\mathbf{e}}_1dx\ +\ 2n_2\overline{\Delta n_{l2}}\int_{a_1}^{a_2}\hat{\mathbf{e}}_1^{\,*}\cdot\hat{\mathbf{e}}_1dx \\ +2n_3\overline{\Delta n_{l3}}\int_{a_2}^{a_3}\hat{\mathbf{e}}_1^{\,*}\cdot\hat{\mathbf{e}}_1dx\ +\ 2n_4\overline{\Delta n_{l4}}\int_{a_3}^{\infty}\hat{\mathbf{e}}_1^{\,*}\cdot\hat{\mathbf{e}}_1dx \end{array}\right\} \tag{4.2b}$$

$$K=\frac{\omega\varepsilon_o}{4}\left\{\begin{array}{l} e^{j\phi_{l1}}n_1\overline{\Delta n_{l1}}\int_{-a_1}^{a_1}\hat{\mathbf{e}}_1^{\,*}\cdot\hat{\mathbf{e}}_1dx\ +\ e^{j\phi_{l2}}2n_2\overline{\Delta n_{l2}}\int_{a_1}^{a_2}\hat{\mathbf{e}}_1^{\,*}\cdot\hat{\mathbf{e}}_1dx \\ +e^{j\phi_{l3}}2n_3\overline{\Delta n_{l3}}\int_{a_2}^{a_3}\hat{\mathbf{e}}_1^{\,*}\cdot\hat{\mathbf{e}}_1dx\ +\ e^{j\phi_{l4}}2n_4\overline{\Delta n_{l4}}\int_{a_3}^{\infty}\hat{\mathbf{e}}_1^{\,*}\cdot\hat{\mathbf{e}}_1dx \end{array}\right\}. \tag{4.2c}$$

Using (4.2a) in (4.1a) and (4.1b) and neglecting rapidly oscillating terms yields

$$\frac{d\psi_1}{dz}=-j\psi_1C_o-j\psi_2e^{j\left(2\beta-\frac{2\pi}{\Lambda}\right)z}K^* \tag{4.3a}$$

$$\frac{d\psi_2}{dz}=j\psi_2C_o+j\psi_1e^{j\left(\frac{2\pi}{\Lambda}-2\beta\right)z}K\,. \tag{4.3b}$$

4.3 Solution for Power Reflectivity

An expression for the power reflectivity is found in Appendix D. The result is

$$R=\left\{\begin{array}{ll} \dfrac{|K|^2\sinh^2(LS)}{S^2\cosh^2(LS)+\left(\dfrac{\delta}{2}+C_o\right)^2\sinh^2(LS)}, & S \text{ real} \\ \dfrac{|K|^2\sin^2(L\hat{S})}{\hat{S}^2\cos^2(L\hat{S})+\left(\dfrac{\delta}{2}+C_o\right)^2\sin^2(L\hat{S})}, & S \text{ imaginary} \end{array}\right. \tag{D.14}$$

where L is the length of the grating and δ, S, and $\hat{S}$ are given by (D.2), (D.6), and (D.12) respectively.

Equation (D.14) for R can be manipulated in the same way that Appendix C manipulated (3.35) for R when the gratings in every layer are in phase. Doing so yields

$$R = \frac{\sinh^2(LS)}{\cosh^2(LS) - \dfrac{(\delta + 2C_o)^2}{4|K|^2}} \tag{4.4}$$

where

$$LS = \sqrt{(L|K|)^2 - (L|K|)^2 \frac{(\delta + 2C_o)^2}{4|K|^2}}\,. \tag{4.5}$$

R given by (D.14) is still almost exactly symmetric about a center wavelength or "design" wavelength λ_{o_D} given by

$$\frac{\delta}{2} + C_o = 0$$

$$\beta(\lambda_{o_D}) - \frac{\pi}{\Lambda} + C_o(\lambda_{o_D}) = 0\,. \tag{4.6}$$

This is precisely the same equation that determined λ_{o_D} before (when the gratings in every layer were in phase.) As before, we solve for Λ using (4.6) in order to set λ_{o_D}. Because (4.6) and the definition of δ are the same as before, and since β can still be approximated using (C.4),

$$\frac{\delta + 2C_o}{|K|} \approx -\frac{2s}{|K|}(\lambda_o - \lambda_{o_D}), \tag{4.7}$$

which is the analogue of (C.7). Substituting (4.7) into (4.4) and (4.5), the same expressions are obtained as when (C.7) is substituted into (C.2) and (C.3) except $2|K|$ replaces C_o everywhere. It is concluded that Figure 3-4 applies to (D.14) as well if we replace every occurrence of C_o in this figure with $2|K|$.

The implication of the preceding paragraph is that any spectrum that can be obtained with a non-zero phase shift between layers can also be obtained with no phase shift. Supposing a design with a non-zero shift between layers is given, a design with no

phase shift having the same reflectivity spectrum is readily obtained. Whatever the value of $2|K|$ for the non-zero phase shift design, C_o for the no phase shift design is set to the same value by adjusting α of (3.2). C_o and $2|K|$ for the non-zero phase shift design are not equal, hence C_o for the no phase shift design does not equal C_o for the non-zero phase shift design. Thus, because (4.6) applies to both types of designs, if we wish to preserve the value of λ_{o_D}, the period of the gratings Λ must be adjusted. The resulting spectra will be nearly identical – not exactly so because of one of the approximations attached to Figure 3-4, that C_o or $2|K|$ is a constant independent of λ_o. In fact, as was stated in chapter 3, C_o varies by 1 or 2 percent over the range of λ_o over which R is non-negligible. The variable $2|K|$ will vary a little more than C_o, perhaps by as much as 4 percent.

Figures 4-1 through 4-4 demonstrate the correctness of the preceding paragraph. Figure 4-1 illustrates the reflectivity spectrum for a waveguide imprinted with gratings having the parameters listed in the figure. Gratings exist only in layers 1 and 3 (corresponding to $|x| < a_1$ and $a_2 < |x| < a_3$) since $n = n_{\mathrm{SiO}_2}$ in the other layers, indicating they are undoped. $\phi_{l3} - \phi_{l1} = 0^\circ$ and $C_o = 1.5749 \times 10^4$. Figure 4-2 illustrates the spectrum for the same waveguide imprinted with the same gratings, except $\phi_{l3} - \phi_{l1} = 180^\circ$. The peak reflectivity is reduced, consistent with Figure 3-4 since $2|K| = 4.4816 \times 10^3$ for the case at hand is smaller than C_o for Figure 4-1. Using the same waveguide and gratings as in Figure 4-2, but increasing α from 0.4 to 1.4057, $2|K|$ increases proportionately so $2|K| = 1.5749 \times 10^4$. C_o increases proportionately as well. Thus, to preserve λ_{o_D}, Λ decreases from 4.4639×10^{-7} m to 4.4389×10^{-7} m according to (4.6), which applies whether or not a phase shift between layers exists. The resulting spectrum is nearly identical to Figure 4-1 as demonstrated by Figure 4-3, a plot of the spectrum in Figure 4-1 minus the spectrum of this, the third case. If α is increased to 1.42, the resulting spectrum is even closer to Figure 4-1 as demonstrated by Figure 4-4, a plot of the spectrum in Figure 4-1 minus the spectrum of this, the forth case. An

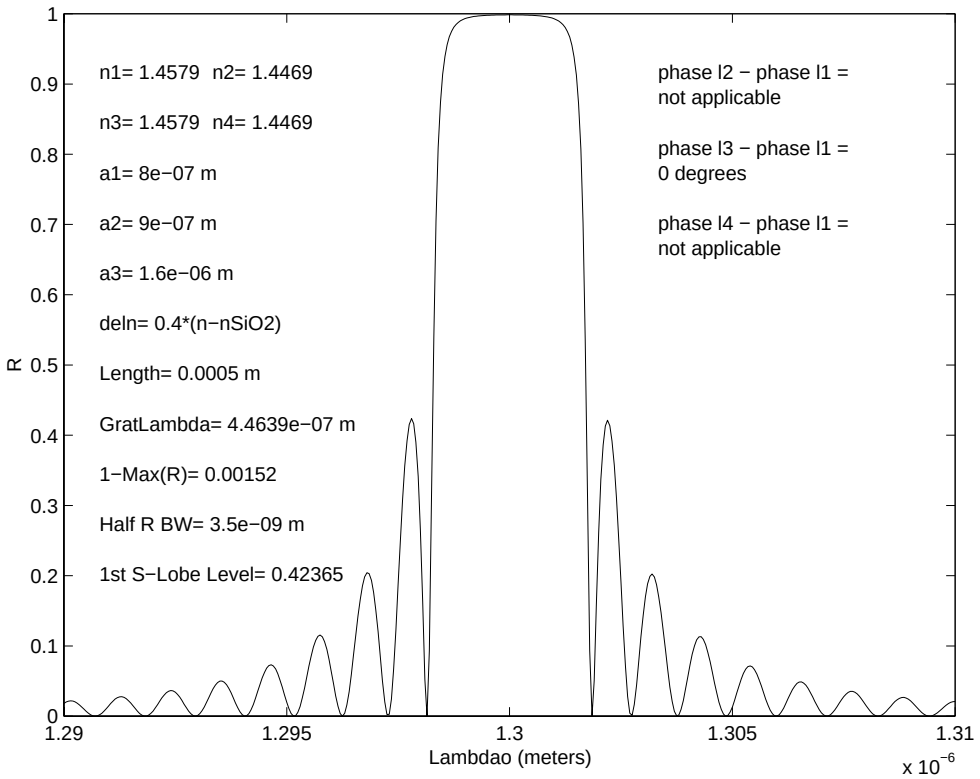

Figure 4-1 Reflectivity for $\alpha = 0.4$ and $\phi_{l3} - \phi_{l1} = 0^{\circ}$

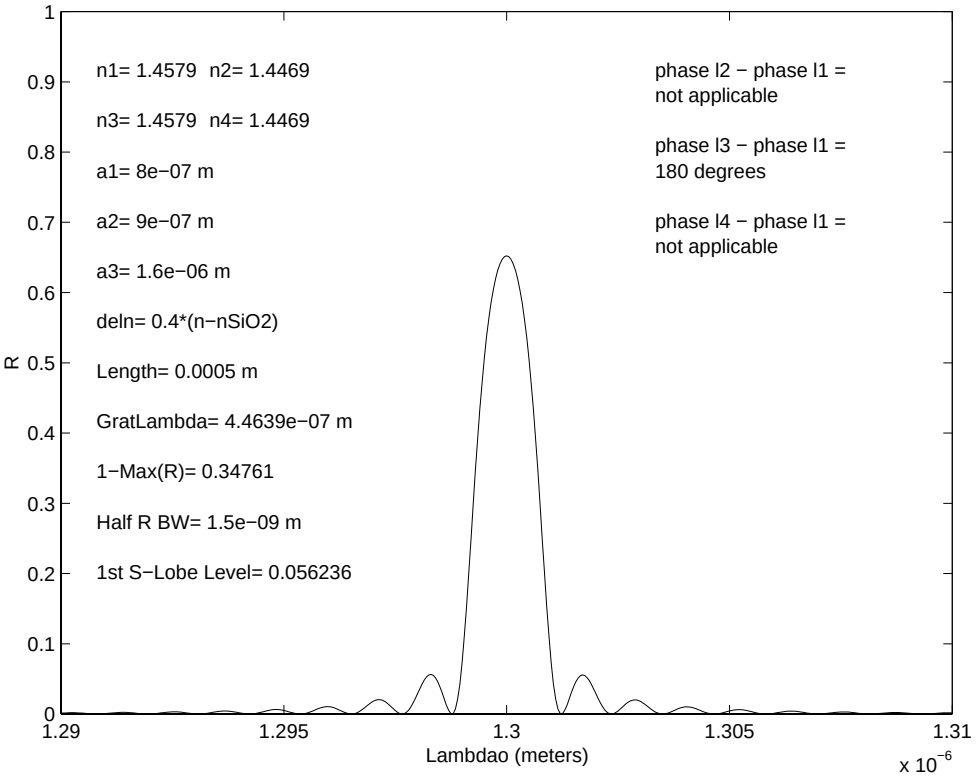

Figure 4-2 Reflectivity for $\alpha = 0.4$ and $\phi_{l3} - \phi_{l1} = 180^{\circ}$

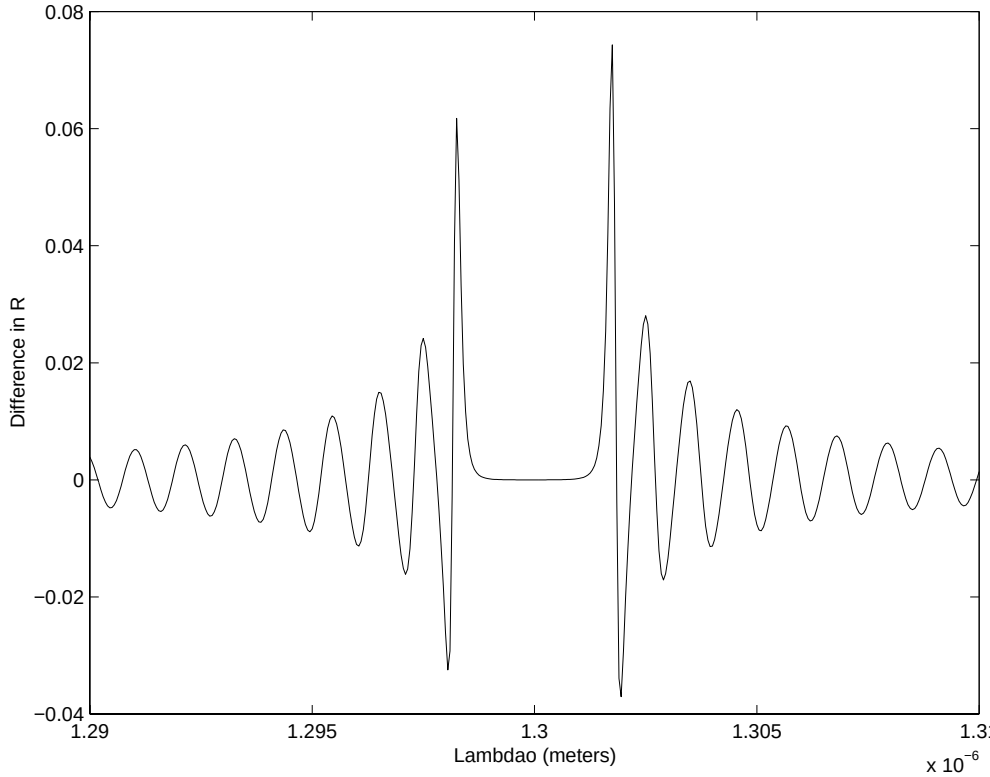

Figure 4-3 Reflectivity in Figure 4-1 minus reflectivity for $\alpha = 1.4057$ and $\phi_{l3} - \phi_{l1} = 180^{\circ}$

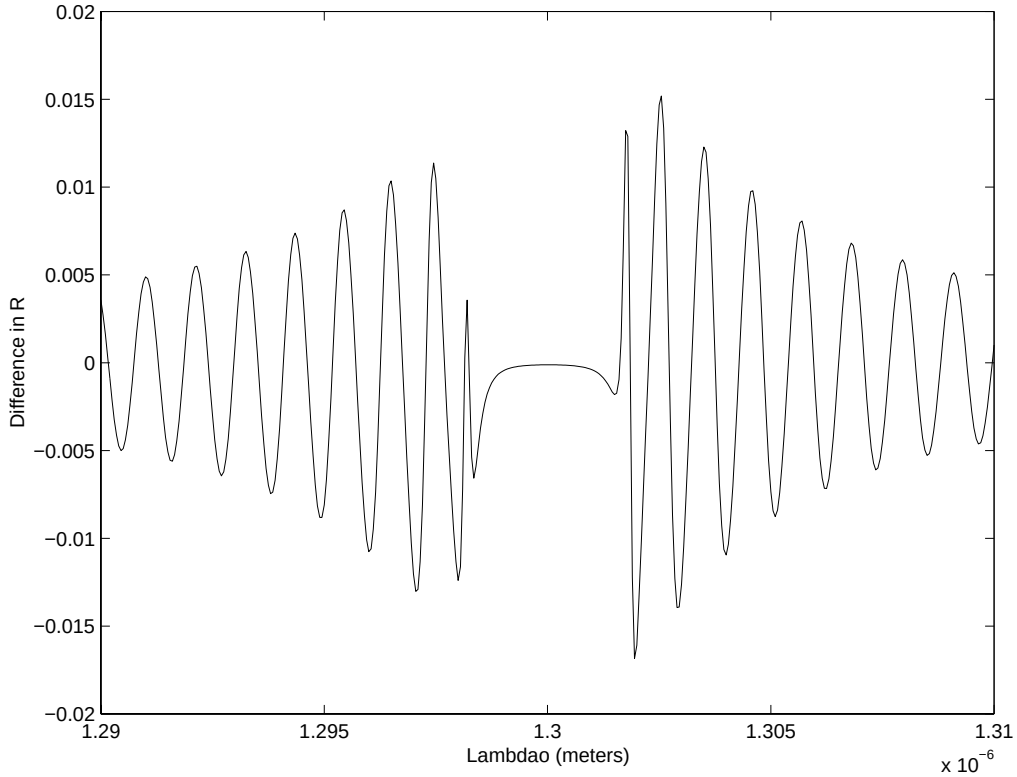

Figure 4-4 Reflectivity in Figure 4-1 minus reflectivity for $\alpha = 1.42$ and $\phi_{l3} - \phi_{l1} = 180^{\circ}$

explanation lies in the slight asymmetry of the spectra caused by the dependence of C_o and $|K|$ on λ_o. Listings of refcoPhv2.m and eysqr.m, the Matlab program and subprogram, respectively, that produced Figures 4-1 through 4-4, are found in Appendix E, Section 1.

Why $2|K|$ varies more than C_o can be understood by considering how the field $\hat{\mathbf{e}}_1(x)$ in (4.2c) and (3.23b) (equivalent to (4.2b)) changes with λ_o. A review of how R was solved facilitates this understanding. First the discrete set of guided modes

$$\mathbf{E}_k(x,y,z) = \mathbf{e}_k(x,y)e^{-j\beta_k z}$$

$$\mathbf{H}_k(x,y,z) = \mathbf{h}_k(x,y)e^{-j\beta_k z}$$

where $k = \{1, 2, \ldots \#\text{ of guided modes}\}$ was computed. This was accomplished in chapter 2. The fields take this form assuming they are time-harmonic with $e^{j\omega t}$ dependence. In chapter 3, the fields described by (3.15) and (3.16), which are assumed to be the only supported guided modes propagating in the forward and backward directions were used to find C_o. C_o was substituted into the coupled wave equations which were solved for $\psi_1(z)$ and $\psi_2(z)$. At each wavelength, the field is normalized, the result of which is that the area under $|\hat{\mathbf{e}}_1(x)|^2$ remains constant. If the area under $|\hat{\mathbf{e}}_1(x)|^2$ within $|x| < a_1$, for instance, increases from one value of λ_o to another, then perhaps the area under $|\hat{\mathbf{e}}_1(x)|^2$ within $a_1 < |x| < a_2$ decreases. If this is the case, and if $(\phi_{l2} - \phi_{l1}) = \pi$, for instance, then K will change by a larger percentage than C_o. If $(\phi_{l2} - \phi_{l1}) = \pi$, the second definite integral in the right-hand side of (4.2c) for K is subtracted from the first. The second definite integral in the right-hand side of (3.23b) for C_o is added to the first, and if the value of the first definite integral is increased and the value of the second is decreased, then the sum will change by a smaller percentage than the difference.

The 2 percent variation in C_o if no phase shift between layers is considered, or the 4 percent variation in $2|K|$ if non-zero phase shift is considered, produces some asymmetry in the spectrum. The spectra in Figure 3-4 appear to be perfectly symmetric but in plotting an exact spectrum that does not ignore the dependence of C_o or $2|K|$ on

λ_o, some insignificant asymmetry results. In summary, it may be generally stated that any spectrum that can be produced with a non-zero phase shift can also be achieved with a high degree of accuracy from a zero phase shift by adjusting α in (3.2). However, there is an exception which is considered next. The parameter α and the dimensions of the waveguide a_1, a_2, and a_3 can be chosen so that $|K|$ passes through zero near or at λ_{o_D}, the wavelength at which (4.6) is satisfied. With or without a phase shift between layers the spectrum is nearly symmetric about λ_{o_D}, and usually the peak value of R occurs at λ_{o_D}. The range of λ_o over which R is non-negligible, that is the passband, is centered on λ_{o_D}. But if $|K| = 0$ at λ_{o_D}, then according to (D.14) the numerator of R equals zero at λ_{o_D}, the wavelength at which the peak of R usually occurs. There is no analogous case to this situation in the old no-phase-shift-between-layers case, because C_o cannot equal zero unless it equals zero everywhere. If $|K| = 0$ exactly at λ_{o_D}, then inspection of (D.14) shows that the denominator of R also equals zero at this λ_o. It turns out that the indeterminate $\frac{0}{0}$ equals zero in the limit as $\lambda_o \to \lambda_{o_D}$. This case of $|K|$ passing through zero at or in the vicinity of λ_{o_D} will be considered more closely in chapter 6.

Chapter 5

Coupled-Wave Equations For Apodized Gratings

5.1 Introduction

The remaining part of this thesis is devoted to the analysis of uniform gratings placed in series and non-uniform gratings. So far, two cases have been examined. The first of these considered a perturbation of the form of (3.1b) with $\Lambda_{l1} = \Lambda_{l2} = \Lambda_{l3} = \Lambda_{l4} = \Lambda$ and $\phi_{l1} = \phi_{l2} = \phi_{l3} = \phi_{l4} = \phi$; namely, a uniform grating with no phase shift between gratings written in separate layers. The second case also involved a uniform grating but allowed phase shifts between gratings written in separate layers; that is, $\phi_{l1}, \phi_{l2}, \phi_{l3}$, and ϕ_{l4} remained distinct. The second problem actually encompasses the first problem since if $\phi_{l1} = \phi_{l2} = \phi_{l3} = \phi_{l4} = \phi$ then K given by (4-2c) reduces to $\left(C_o'\right)^* \Big/ 2$ where C_o' is given by (3.27) ,and the coupled-wave equations (4.3a) and (4.3b) reduce to the coupled-wave equations (3.26a) and (3.26b).

This chapter will consider a more general problem that encompasses both of the problems considered so far. The formulation of the solution will be such that later when gratings placed in series are considered, and when apodized gratings are eventually modeled as many uniform grating elements in series, the mathematics will be tractable. This formulation closely resembles that of [1].

5.2 Coupled-Wave Equations

For apodized gratings, the perturbation is of the form

$$\Delta n(x,z)=\begin{cases}\Delta n_{l1}(z)=\overline{\Delta n_{l1}}\ f(z)\left[1+v\cos\left(\dfrac{2\pi}{\Lambda}z+\phi_{l1}(z)\right)\right], & |x|<a_1\\ \Delta n_{l2}(z)=\overline{\Delta n_{l2}}\ f(z)\left[1+v\cos\left(\dfrac{2\pi}{\Lambda}z+\phi_{l1}(z)+\Delta\phi_{l2}\right)\right], & a_1<|x|<a_2\\ \Delta n_{l3}(z)=\overline{\Delta n_{l3}}\ f(z)\left[1+v\cos\left(\dfrac{2\pi}{\Lambda}z+\phi_{l1}(z)+\Delta\phi_{l3}\right)\right], & a_2<|x|<a_3\\ \Delta n_{l4}(z)=\overline{\Delta n_{l4}}\ f(z)\left[1+v\cos\left(\dfrac{2\pi}{\Lambda}z+\phi_{l1}(z)+\Delta\phi_{l4}\right)\right], & a_3<|x|\end{cases}. \tag{5.1}$$

$f(z)$ is a real apodizing function, hence the gratings are no longer uniform. $f(z)$ varies slowly with z, thus it is nearly constant over one grating period. Although the envelope in layer 1, $\overline{\Delta n_{l1}}\ f(z)$, the envelope in layer 2, $\overline{\Delta n_{l2}}\ f(z)$, and the envelopes in layers 3 and 4 all have the same shape, each is weighted by a different constant. This is because layers in the unperturbed waveguide with a larger refractive index respond more strongly to irradiation, as implied in (3.2). The apodizing function $f(z)$ might be Guassian, for example, since Guassian laser beams are readily available.

Ordinarily, the constant v equals 1, but not if a technique detailed in [1] and at the end of this section is used to adapt a computer program that assumes a perturbation taking the form of (5.1) to the “zero-dc” case. If "1+" is absent from the layers in (5.1), the grating is “zero-dc”.

The phase in each layer varies with z, so the analysis encompasses gratings with a “chirp”. However, the dependence of the phase on z is assumed to be the same in all layers but some constant phase shift might exist between any two layers.

The coupled-mode equations (3.18a) and (3.18b) are quite general enough to apply here. Also, (3.22) is true regardless of the form of the perturbation $\Delta n(x,z)$ provided that the unperturbed waveguide is weakly guiding. Thus, the coupled-wave equations are

$$\frac{d\psi_1}{dz}=-j\left(\psi_1+\psi_2 e^{j2\beta z}\right)C_{11}(z) \tag{5.2a}$$

$$\frac{d\psi_2}{dz}=j\left(\psi_2+\psi_1 e^{-j2\beta z}\right)C_{11}(z) \tag{5.2b}$$

where

$$C_{11}(z)=\frac{\omega\varepsilon_o}{2}\begin{cases} n_1\ \overline{\Delta n_{l1}}\ f(z)\left[1+v\cos\left(\frac{2\pi}{\Lambda}z+\phi_{l1}(z)\right)\right]\int_{-a_1}^{a_1}\hat{\mathbf{e}}_1^{\,*}\cdot\hat{\mathbf{e}}_1 dx \\ +2n_2\ \overline{\Delta n_{l2}}\ f(z)\left[1+v\cos\left(\frac{2\pi}{\Lambda}z+\phi_{l1}(z)+\Delta\phi_{l2}\right)\right]\int_{a_1}^{a_2}\hat{\mathbf{e}}_1^{\,*}\cdot\hat{\mathbf{e}}_1 dx \\ +2n_3\ \overline{\Delta n_{l3}}\ f(z)\left[1+v\cos\left(\frac{2\pi}{\Lambda}z+\phi_{l1}(z)+\Delta\phi_{l3}\right)\right]\int_{a_2}^{a_3}\hat{\mathbf{e}}_1^{\,*}\cdot\hat{\mathbf{e}}_1 dx \\ +2n_4\ \overline{\Delta n_{l4}}\ f(z)\left[1+v\cos\left(\frac{2\pi}{\Lambda}z+\phi_{l1}(z)+\Delta\phi_{l4}\right)\right]\int_{a_3}^{\infty}\hat{\mathbf{e}}_1^{\,*}\cdot\hat{\mathbf{e}}_1 dx \end{cases}. \qquad (5.3)$$

Equation (5.3) for $C_{11}(z)$ is a straightforward extension of equation (3.20).

Expanding the cosine terms in (5.3), $C_{11}(z)$ is expressed as

$$C_{11}(z)=\sigma+Ke^{j\left[\frac{2\pi}{\Lambda}z+\phi_{l1}(z)\right]}+K^*e^{-j\left[\frac{2\pi}{\Lambda}z+\phi_{l1}(z)\right]} \qquad (5.4a)$$

where

$$\sigma=\frac{\omega\,\varepsilon_o}{2}\,f(z)\begin{cases} n_1\,\overline{\Delta n_{l1}}\int_{-a_1}^{a_1}\hat{\mathbf{e}}_1^{\,*}\cdot\hat{\mathbf{e}}_1 dx+2n_2\,\overline{\Delta n_{l2}}\int_{a_1}^{a_2}\hat{\mathbf{e}}_1^{\,*}\cdot\hat{\mathbf{e}}_1 dx \\ +2n_3\,\overline{\Delta n_{l3}}\int_{a_2}^{a_3}\hat{\mathbf{e}}_1^{\,*}\cdot\hat{\mathbf{e}}_1 dx+2n_4\,\overline{\Delta n_{l4}}\int_{a_3}^{\infty}\hat{\mathbf{e}}_1^{\,*}\cdot\hat{\mathbf{e}}_1 dx \end{cases} \qquad (5.4b)$$

and

$$K=\frac{\omega\,\varepsilon_o}{4}\,v\ f(z)\begin{cases} n_1\,\overline{\Delta n_{l1}}\int_{-a_1}^{a_1}\hat{\mathbf{e}}_1^{\,*}\cdot\hat{\mathbf{e}}_1 dx+2n_2\,\overline{\Delta n_{l2}}\,e^{j\Delta\phi_{l2}}\int_{a_1}^{a_2}\hat{\mathbf{e}}_1^{\,*}\cdot\hat{\mathbf{e}}_1 dx \\ +2n_3\,\overline{\Delta n_{l3}}\,e^{j\Delta\phi_{l3}}\int_{a_2}^{a_3}\hat{\mathbf{e}}_1^{\,*}\cdot\hat{\mathbf{e}}_1 dx+2n_4\,\overline{\Delta n_{l4}}\,e^{j\Delta\phi_{l4}}\int_{a_3}^{\infty}\hat{\mathbf{e}}_1^{\,*}\cdot\hat{\mathbf{e}}_1 dx \end{cases}. \qquad (5.4c)$$

Using (5.4a) in (5.2a) and (5.2b), dropping rapidly oscillating terms, and realizing the apodizing function $f(z)$ varies slowly with z, the coupled-wave equations are summarized as

$$\frac{d\psi_1}{dz}=-j\psi_1\sigma-j\psi_2e^{j\left[2\beta z-\frac{2\pi}{\Lambda}z-\phi_{l1}(z)\right]}K^* \qquad (5.5a)$$

$$\frac{d\psi_2}{dz} = j\psi_2\sigma + j\psi_1 e^{j\left[-2\beta z + \frac{2\pi}{\Lambda}z + \phi_{l1}(z)\right]}K\,. \qquad (5.5b)$$

In the zero-"dc" case, all of the equations in this section and the remaining parts of this chapter still apply except: by definition "1+" is removed from the layers in (5.1), σ given by (5.4b) equals zero, and (5.3) obviously doesn't apply. (5.3) is an intermediate result not used by any computer program and is ignored. Reference [1] divides $\overline{\Delta n_{l1}}, \overline{\Delta n_{l2}}, \overline{\Delta n_{l3}}$, and $\overline{\Delta n_{l4}}$ by a huge number and sets v equal to the same huge number to effectively remove the "dc" term from (5.1). This technique reduces the right-hand-side of (5.4b) to practically zero while not altering the value of the right-hand-side of (5.4c), the other equation that depends on $\overline{\Delta n_{l1}}, \overline{\Delta n_{l2}}, \overline{\Delta n_{l3}}$, and $\overline{\Delta n_{l4}}$, since it contains the term v. This technique was successfully employed to adapt a computer program that assumes a perturbation taking the form of (5.1) to the "zero-dc" case. However, writing a switch into the program that sets σ to zero if the grating is "zero-dc" proved just as effective.

5.3 Comparison with Coupled-Wave Equations in [1]

This section introduces an alternate form of the coupled-wave equations. The phasor convention is switched to allow the equations to converge to those in [1]; that is, $e^{-j\omega t}$ time dependence is assumed instead of $e^{j\omega t}$. Therefore, the alternate coupled-mode equations should be equivalent to

$$\frac{d\psi_1}{dz} = j\psi_1\sigma + j\psi_2 e^{-j\left[2\beta z - \frac{2\pi}{\Lambda}z - \phi_{l1}(z)\right]}K \qquad (5.6a)$$

$$\frac{d\psi_2}{dz} = -j\psi_2\sigma - j\psi_1 e^{j\left[2\beta z - \frac{2\pi}{\Lambda}z - \phi_{l1}(z)\right]}K^*, \qquad (5.6b)$$

which are the counterparts of (5.5a) and (5.5b). The definitions of σ and K, given in (5.4b) and (5.4c) respectively, are preserved and it makes no difference whether $\mathbf{e}_1$ under the new or old phasor convention is used as only $|\mathbf{e}_1|$ matters. After switching to the new phasor convention, the right-hand-sides of (5.5a) and (5.5b) are conjugated except for ψ_1 and ψ_2. The solutions for $\psi_1(z)$ and $\psi_2(z)$ should equal the conjugate of what they were before in order for the fields in the perturbed waveguide

$$\mathbf{E} = \sum_{m=1}^{2} \psi_m \hat{\mathbf{e}}_m(x,y) e^{j\beta_m z} e^{-j\omega t}$$

to equal the solution that would have been obtained under the old phasor convention after transforming back into the time domain. Under the new phasor convention, the fields $\hat{\mathbf{e}}_m$ are the conjugates of their old forms.

The coupled-wave equations in [1] are:

$$\frac{dR}{dz} = j\hat{\sigma} R(z) + jK S(z) \tag{5.7a}$$

$$\frac{dS}{dz} = -j\hat{\sigma} S(z) - jK^* R(z) \tag{5.7b}$$

where

$$R(z) \equiv \psi_1(z) e^{j\delta z - j\frac{\phi_{l1}(z)}{2}} \tag{5.8a}$$

$$S(z) \equiv \psi_2(z) e^{-j\delta z + j\frac{\phi_{l1}(z)}{2}} \tag{5.8b}$$

$$\hat{\sigma} \equiv \delta + \sigma - \frac{1}{2}\frac{d\phi_{l1}(z)}{dz} \tag{5.9}$$

and

$$\delta = \beta - \frac{\pi}{\Lambda} \tag{5.10}$$

are equivalent to (5.6a) and (5.6b). This can be demonstrated by substituting (5.8) and (5.9) in (5.7) and arriving back at (5.6a) and (5.6b). Doing so for (5.7a), yields

$$\frac{d}{dz}\left[\psi_1(z) e^{j\delta z - j\frac{\phi_{l1}(z)}{2}}\right] = j\left[\delta + \sigma - \frac{1}{2}\frac{d\phi_{l1}(z)}{dz}\right]\psi_1(z) e^{j\delta z - j\frac{\phi_{l1}(z)}{2}} + jK\psi_2(z) e^{-j\delta z + j\frac{\phi_{l1}(z)}{2}}$$

$$\left\{\left[j\delta - j\frac{1}{2}\frac{d\phi_{l1}(z)}{dz}\right]\psi_1(z) + \frac{d\psi_1(z)}{dz}\right\} e^{j\delta z - j\frac{\phi_{l1}(z)}{2}}$$

$$= j\left[\delta + \sigma - \frac{1}{2}\frac{d\phi_{l1}(z)}{dz}\right]\psi_1(z) e^{j\delta z - j\frac{\phi_{l1}(z)}{2}} + jK\psi_2(z) e^{-j\delta z + j\frac{\phi_{l1}(z)}{2}}$$

$$\frac{d\psi_1(z)}{dz} e^{j\delta z - j\frac{\phi_{l1}(z)}{2}} = j\sigma\psi_1(z) e^{j\delta z - j\frac{\phi_{l1}(z)}{2}} + jK\psi_2(z) e^{-j\delta z + j\frac{\phi_{l1}(z)}{2}}.$$

Dividing both sides by $e^{j\delta z - j\frac{\phi_{l1}(z)}{2}}$ yields (5.6a).

The advantage of (5.7) through (5.10) over (5.6a) and (5.6b) is that for many problems and especially in the next chapter they lead to more tractable solutions for apodized and multi-gratings. In summary this chapter has derived the coupled-wave equations for the perturbation given by (5.1), which includes an apodizing function $f(z)$. This form of perturbation encompasses the other two forms of perturbation that have been seen prior to this chapter because $f(z)$ can equal a constant. The two coupled-wave equations were written using a form similar to previous chapters, then they were re-written in a form that will make the math more tractable in the next chapter than it would otherwise be.

For a given $f(z)$ and $\frac{d\phi_{l1}}{dz}$, equations (5.7a) and (5.7b) can be solved by direct numerical integration. This coupled pair of differential equations has variable coefficients, so an analytical solution usually is not available. The initial conditions for gratings of length L are $R\left(\frac{L}{2}\right)=1$ and $S\left(\frac{L}{2}\right)=0$, and the integration proceeds backward from $z=\frac{L}{2}$ to $z=-\frac{L}{2}$. [1] reports that adaptive-stepsize Runge-Kutta numerical integration works well. This procedure yields $R(z)$ and $S(z)$. The amplitude reflectivity is defined as the quotient $\frac{\psi_2(-L/2)}{\psi_1(-L/2)}$, which can be computed using the quotient

$$\frac{S(-L/2)}{R(-L/2)}=\frac{\psi_2(-L/2)}{\psi_1(-L/2)}e^{j\delta L+j\phi_{l1}\left(-\frac{L}{2}\right)}$$

by dividing out the phase term containing the known quantities $\delta(\lambda_o)$ and $\phi_{l1}(-L/2)$. If the phase of $\frac{\psi_2(-L/2)}{\psi_1(-L/2)}$ is not of interest except to use it to compute the delay time for light reflected off the grating, then the phase term can stay. If θ_1 is the phase of $\frac{\psi_2(-L/2)}{\psi_1(-L/2)}$ then the delay time τ for light reflected off of the grating is

$$\tau=\frac{d\theta_1}{d\omega}=-\frac{\lambda_o^{\,2}}{2\pi c}\frac{d\theta_1}{d\lambda_o}. \qquad (5.11)$$

If θ_2 is the phase of $\frac{S(-L/2)}{R(-L/2)}$, then

$$\theta_2 = \theta_1 + \delta L + \phi_{l1}(-L/2)$$

and

$$\frac{d\theta_2}{d\lambda_o} = \frac{d\theta_1}{d\lambda_o} + \text{constant}$$

since $\delta(\lambda_o)$ is nearly linear. It is seen that θ_2 can be used instead of θ_1 in (5.11) to compute τ if relative delay, not absolute delay, is of interest. Absolute delay depends upon the identification of time zero.

As chapter 3 has already established the power reflection coefficient is defined as

$$R = \left|\frac{\psi_2(-L/2)}{\psi_1(-L/2)}\right|^2 = \left|\frac{S(-L/2)}{R(-L/2)}\right|^2 .$$

Observant readers may have noticed that now the grating extends from $z = -\frac{L}{2}$ to $\frac{L}{2}$ instead of from 0 to L as in previous chapters, but this is of no consequence if the initial conditions are used accordingly -- $S(L/2) = 0$ was used this time instead of $S(L) = 0$ as in chapter 3. Centering the grating on zero is convenient if the apodizing function is centered on zero. A method for finding $R(z)$ and $S(z)$ given any arbitrary $f(z)$ and $\frac{d\phi_{l1}(z)}{dz}$ that is often preferred to the direct integration approach is presented in the next chapter.

Chapter 6

Nonuniform Gratings

6.1 Introduction

Nonuniform gratings can be modeled by dividing the gratings into M uniform sections [1]. A 2x2 matrix is associated with each uniform section, and R_i and S_i are by definition the field amplitudes after traversing the i^{th} section. Beginning with $R_o = R(L/2) = 1$ and $S_o = S(L/2) = 0$, $R(-L/2) = R_M$ and $S(-L/2) = S_M$ are calculated. The matrix $\mathbf{F}_i$ describes propagation through uniform section i according to

$$\begin{bmatrix} R_i \\ S_i \end{bmatrix} = \mathbf{F}_i \begin{bmatrix} R_{i-1} \\ S_{i-1} \end{bmatrix}. \tag{6.1}$$

The matrix $\mathbf{F}_i$ is given by

$$\mathbf{F}_i = \begin{bmatrix} \cosh(\gamma_B \Delta z) - j\frac{\hat{\sigma}}{\gamma_B}\sinh(\gamma_B \Delta z) & -j\frac{K}{\gamma_B}\sinh(\gamma_B \Delta z) \\ j\frac{K^*}{\gamma_B}\sinh(\gamma_B \Delta z) & \cosh(\gamma_B \Delta z) + j\frac{\hat{\sigma}}{\gamma_B}\sinh(\gamma_B \Delta z) \end{bmatrix} \tag{6.2}$$

where $\gamma_B \equiv \sqrt{|K|^2 - \hat{\sigma}^2}$, Δz is the length of the i^{th} section, and K and $\hat{\sigma}$ are the local values in the i^{th} section. For apodized or chirped gratings the constant values σ, K, and $\frac{1}{2}\frac{d\phi_{l1}}{dz}$ assigned to each uniform section are the z-dependent values of $\sigma(z)$, $K(z)$, and $\frac{1}{2}\frac{d\phi_{l1}(z)}{dz}$ evaluated at the center of each section. Once the matrices for the individual sections are known R_M and S_M are found using

$$\begin{bmatrix} R_M \\ S_M \end{bmatrix} = \mathbf{F}\begin{bmatrix} R_o \\ S_o \end{bmatrix}; \qquad \mathbf{F} = \mathbf{F}_M \mathbf{F}_{M-1} \mathbf{F}_{M-2} \ldots \mathbf{F}_i \ldots \mathbf{F}_1 \tag{6.3}$$

with $R_o = 1$ and $S_o = 0$.

One potentially useful nonuniform grating that has been presented in the literature [11] is a so-called "double" grating, consisting of two gratings separated by a nongrating region. In this case the output amplitudes are computed from

$$\begin{bmatrix} R_M \\ S_M \end{bmatrix} = \mathbf{F}_2 \mathbf{F}_{p1} \mathbf{F}_1 \begin{bmatrix} R_o = 1 \\ S_o = 0 \end{bmatrix} \tag{6.4}$$

where $\mathbf{F}_{p1}$ is a phase-shift matrix that models the nongrating region. The definition of $\mathbf{F}_{p1}$ is the subject of section 6.3. One limitation of the matrix approach is that unless it is modified, Λ must be the same for every uniform section. The value of $\frac{d\phi_{l1}}{dz}$, however, can be different for different sections. Accounting for the constant $\frac{d\phi_{l1}}{dz}$ in a uniform section, the period might be considered as $\frac{2\pi}{\frac{2\pi}{\Lambda} + \frac{d\phi_{l1}}{dz}}$. Thus, uniform gratings in series with varying Λ can be analyzed by suitably choosing the values of $\frac{d\phi_{l1}}{dz}$. Equation (6.1) implicitly enforces the continuity of $R(z)$ and $S(z)$ across the interfaces between uniform sections. Thus,

$$R_{i-1} \equiv \psi_1(z) e^{j\delta z - j\frac{\phi_{l1}(z)}{2}}\Big|_{z=\frac{L}{2}-\sum_{m=1}^{i-1}\Delta z_m} \quad \text{and} \quad S_{i-1} \equiv \psi_2(z) e^{-j\delta z + j\frac{\phi_{l1}(z)}{2}}\Big|_{z=\frac{L}{2}-\sum_{m=1}^{i-1}\Delta z_m},$$

which are by definition the output amplitudes of section $i-1$ (the output of a section is on the less positive-z side), are the inputs to section i. $R(z)$ and $S(z)$ are continuous functions of z over all z for which

1) $\psi_1(z)$ and $\psi_2(z)$ are continuous functions of z, which, from the coupled-wave equations, is all z excluding points where $\hat{\sigma}$ or K equals a Dirac delta function. Such a point occurs where $\phi_{l1}(z)$ has a discrete jump.

2) $e^{\pm j\delta z}$ is a continuous function of z. Since $\delta \equiv \beta - \frac{\pi}{\Lambda}$, this is true over all z if every uniform grating has the same Λ. Thus the analysis is limited to this case.

If $\phi_{l1}(z)$ has a discrete jump at $z = \frac{L}{2} - \sum_{m=1}^{i-1} \Delta z_m$ at the boundary between the two uniform gratings then a phase-shift matrix associated with the discrete change in $\phi_{l1}(z)$ must be inserted between $\mathbf{F}_{i-1}$ and $\mathbf{F}_i$ in (6.3).

6.2 Setting the Period of the Gratings

Using the matrix approach introduced in Section 6.1, the reflectivity of a single uniform grating with $\Delta n(x,z)$ given by (5.1) is easily computed. For a uniform grating, in (5.1) $f(z) = 1$ and σ, K, and $\frac{1}{2}\frac{d\phi_{l1}}{dz}$ are constant, and therefore the matrix approach can be used with M in (6.3) equal 1. It follows that

$$\begin{bmatrix} R_1 \\ S_1 \end{bmatrix} = \mathbf{F}_1 \begin{bmatrix} 1 \\ 0 \end{bmatrix}$$

where $\mathbf{F}_1$ is given by (6.2). For the amplitude reflection coefficient it immediately follows that

$$\rho = \frac{S_1}{R_1} = \frac{-K^* \sinh\left(\sqrt{|K|^2 - \hat{\sigma}^2}\, L\right)}{\hat{\sigma}^2 \sinh\left(\sqrt{|K|^2 - \hat{\sigma}^2}\, L\right) + j\sqrt{|K|^2 - \hat{\sigma}^2}\, \cosh\left(\sqrt{K^2 - \hat{\sigma}^2}\, L\right)}$$

where $L = \Delta z$. The expression for the power reflection coefficient is then

$$R = |\rho|^2 = \frac{\sinh^2\left(\sqrt{|K|^2 - \hat{\sigma}^2}\, L\right)}{\cosh^2\left(\sqrt{|K|^2 - \hat{\sigma}^2}\, L\right) - \frac{\hat{\sigma}^2}{|K|^2}},$$

which is equivalent to (D.14) if $\frac{d\phi_{l1}}{dz} = 0$. The peak reflectivity occurs at $\lambda_o = \lambda_{o_D}$ given by

$$\hat{\sigma}(\lambda_{o_D}) = \beta(\lambda_{o_D}) - \frac{\pi}{\Lambda} + \sigma(\lambda_{o_D}) - \frac{1}{2}\frac{d\phi_{l1}(z)}{dz} = 0 \qquad (6.5)$$

which is equivalent to (4.6) if $\frac{d\phi_{l1}}{dz} = 0$. The definition of C_o given by (4.2b) is the same as the definition of σ given by (5.4b). Equation (6.5) can be used to set λ_{o_D} by setting Λ.

6.3 Phase-Shift Matrix

This section derives the phase-shift matrix that models the nongrating region between the two gratings in the double grating. This can be achieved by finding the limit of $\mathbf{F}_i$ given by (6.2) as $\overline{\Delta n_{l1}}, \overline{\Delta n_{l2}}, \overline{\Delta n_{l3}}$, and $\overline{\Delta n_{l4}}$ in (5.1) approach zero. In this case σ and K approach zero, $\hat{\sigma} \to \delta - \frac{1}{2}\frac{d\phi_{l1}(z)}{dz}$, and $\gamma_B \to \pm j\hat{\sigma}$. It follows that

$$\mathbf{F}_{p1} = \begin{bmatrix} e^{-j\left[\left(\delta - \frac{1}{2}\frac{d\phi_{l1}}{dz}\right)\Delta z\right]} & 0 \\ 0 & e^{j\left[\left(\delta - \frac{1}{2}\frac{d\phi_{l1}}{dz}\right)\Delta z\right]} \end{bmatrix}.$$

The derivative $\frac{d\phi_{l1}}{dz}$ equals zero if $\phi_{l1}(z)$ at the input to the nongrating region equals $\phi_{l1}(z)$ at the output. Otherwise the shift in $\phi_{l1}(z)$ can be modeled as occurring at one discrete point at the input or the output or as a constant finite $\frac{d\phi_{l1}(z)}{dz}$ over the length Δz. Either way, the above equation simplifies to

$$\mathbf{F}_{p1} = \begin{bmatrix} e^{-j\delta\Delta z}e^{-j\frac{\Delta\phi_{l1}}{2}} & 0 \\ 0 & e^{j\delta\Delta z}e^{j\frac{\Delta\phi_{l1}}{2}} \end{bmatrix} \qquad (6.6)$$

where $\Delta\phi_{l1}$ is the difference $\phi_{l1}(z)$ at the output of the nongrating region (less positive-z end) minus $\phi_{l1}(z)$ at the input of the nongrating region (more positive-z end).

If Δz equals zero so the two actual gratings in the double grating touch each other then (6.6) reduces to

$$\mathbf{F}_{p1} = \begin{bmatrix} e^{-j\frac{\Delta\phi_{l1}}{2}} & 0 \\ 0 & e^{j\frac{\Delta\phi_{l1}}{2}} \end{bmatrix} \qquad (6.7)$$

which is the same result given by [1]. This case represents a pure discrete phase shift. Equation (6.7) can also be derived by considering that since some finite shift in $\phi_{l1}(z)$ occurs over a vanishingly small distance then $\hat{\sigma}$ equals a Dirac impulse function with weight $\frac{1}{2}\Delta\phi_{l1}$. The σ assigned to the vanishingly short section between the gratings is ambiguous but irrelevant since it cannot be non-negligible compared to the Dirac delta function. It follows that (6.2) simplifies to (6.7).

If $\phi_{l1}(z)$ at the output of the nongrating section equals $\phi_{l1}(z)$ at the input then (6.6) reduces to

$$\mathbf{F}_{p1} = \begin{bmatrix} e^{-j\delta\,\Delta z} & 0 \\ 0 & e^{j\delta\,\Delta z} \end{bmatrix}. \qquad (6.8)$$

This does not match the result in [1] which has β where δ is in (6.8). The two results are definitely not equivalent. As will be seen, if (6.8) is used and Δz is smaller than one wavelength $\frac{2\pi}{\beta(\lambda_{o_D})}$ then the nongrating region has practically no effect. It definitely does have an effect if the equation for $\mathbf{F}_{p1}$ in [1] is used. Later in this chapter, the power reflectivity for a double grating is solved again using two alternate approaches, and the same results are obtained as with the matrix approach if (6.8) is used. As will be discussed later, it is concluded that (6.8) is correct and [1] has a typographical error.

It was stated before that if the nongrating section has non-zero length and non-zero phase shift then the shift in $\phi_{l1}(z)$ can be modeled as occurring at one discrete point at the input or the output. The fact that this is true is demonstrated by noting that $\mathbf{F}_{p1}$ given by (6.7) matrix multiplied by $\mathbf{F}_{p1}$ given by (6.8), or vice versa, equals $\mathbf{F}_{p1}$ given by (6.6).

Another more heuristic method of demonstrating that (6.6) is valid begins by considering the inputs and outputs of the nongrating section as shown in Figure 6-1. Since the nongrating region is assigned a perturbation $\Delta n(x,z) = 0$, in (5.1) $\overline{\Delta n_{l1}} = \overline{\Delta n_{l2}} = \overline{\Delta n_{l3}} = \overline{\Delta n_{l4}} = 0$. Therefore within the nongrating section $\sigma = 0$ and $K = 0$, and the coupled-wave equations (5.9a) and (5.9b) become

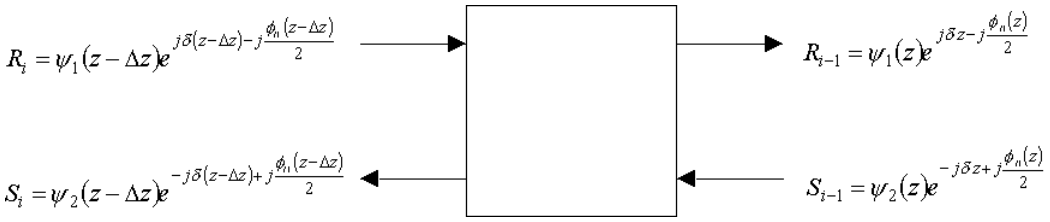

Figure 6-1 Inputs and Outputs to the Non-Grating Section

$$\frac{dR}{dz} = j\left[\delta - \frac{1}{2}\frac{d\phi_{l1}(z)}{dz}\right]R(z)$$

$$\frac{dS}{dz} = -j\left[\delta - \frac{1}{2}\frac{d\phi_{l1}(z)}{dz}\right]S(z),$$

which upon using (5.8a) and (5.8b) can be shown to be equivalent to

$$\left\{\frac{d\psi_1(z)}{dz} + \psi_1(z)\left[j\delta - \frac{j}{2}\frac{d\phi_{l1}(z)}{dz}\right]\right\}e^{j\delta z - j\frac{\phi_{l1}(z)}{2}} = j\left[\delta - \frac{1}{2}\frac{d\phi_{l1}(z)}{dz}\right]\psi_1(z)e^{j\delta z - j\frac{\phi_{l1}(z)}{2}}$$

$$\left\{\frac{d\psi_2(z)}{dz} + \psi_2(z)\left[-j\delta + \frac{j}{2}\frac{d\phi_{l1}(z)}{dz}\right]\right\}e^{-j\delta z + j\frac{\phi_{l1}(z)}{2}} = -j\left[\delta - \frac{1}{2}\frac{d\phi_{l1}(z)}{dz}\right]\psi_2(z)e^{-j\delta z + j\frac{\phi_{l1}(z)}{2}}.$$

Canceling terms in the above results, we obtain

$$\frac{d\psi_1(z)}{dz} = 0 \qquad (6.9a)$$

$$\frac{d\psi_2(z)}{dz} = 0\,. \qquad (6.9b)$$

Therefore, $\psi_1(z)$ and $\psi_2(z)$ are constants in the non-grating section. Referring back to Figure 6-1, since $\psi_1(z-\Delta z) = \psi_1(z)$ and $\psi_2(z-\Delta z) = \psi_2(z)$, equation (6.6) is the obvious form of $\mathbf{F}_{p1}$ where

$$\Delta\phi_{l1}(z) \equiv \phi_{l1}(z-\Delta z) - \phi_{l1}(z).$$

The program that implements the matrix approach described in Sections 6.1 through 6.3, called KNotaGenSampledRev2.m, is listed in Appendix E.

6.4 Reflectivity Spectra of Double Gratings

The parameters and dispersion characteristic of the unperturbed waveguide to be used in the remainder of this chapter are given in Table 6-1 and Figure 6-2. Double gratings with $\Delta z = 0$ for the nongrating section in the middle are considered first. $\mathbf{F}_{p1}$ is given by (6.7). The two uniform gratings are identical, and each is described by the parameters given in Table 6-2. Figure 6-3 shows the power reflectivity versus λ_o for $\Delta\phi_{l1}$, the discrete phase shift occurring at the point where the two gratings touch, ranging from zero to $\frac{7\pi}{2}$. The case of $\Delta\phi_{l1} = 0$ corresponds to a single uniform grating with the

Table 6-1 Waveguide Used Throughout Chapter 6

$n_1 = 1.45785587$
$n_2 = 1.45238317$
$n_3 = n_4 = n_{\mathrm{SiO2}}$ $= 1.44691047$
$a_1 = 4x10^{-7}\ m$
$a_2 = 1.548661x10^{-6}\ m$
$a_3 = 3x10^{-6}\ m$

Table 6-2 Parameters for Grating Sections in Figures 6-3 through 6-8

$\Delta z = 1x10^{-4}$ m
$\frac{d\phi_{l1}(z)}{dz} = 0$
$\alpha = 1.2135$
$\Delta\phi_{l2} = \Delta\phi_{l3} = \Delta\phi_{l4} = 0$
$v = 1$
$f(z) = 1$
$\Lambda = 4.4615x10^{-7}$ m
$\sigma \approx 3.077x10^{4}$

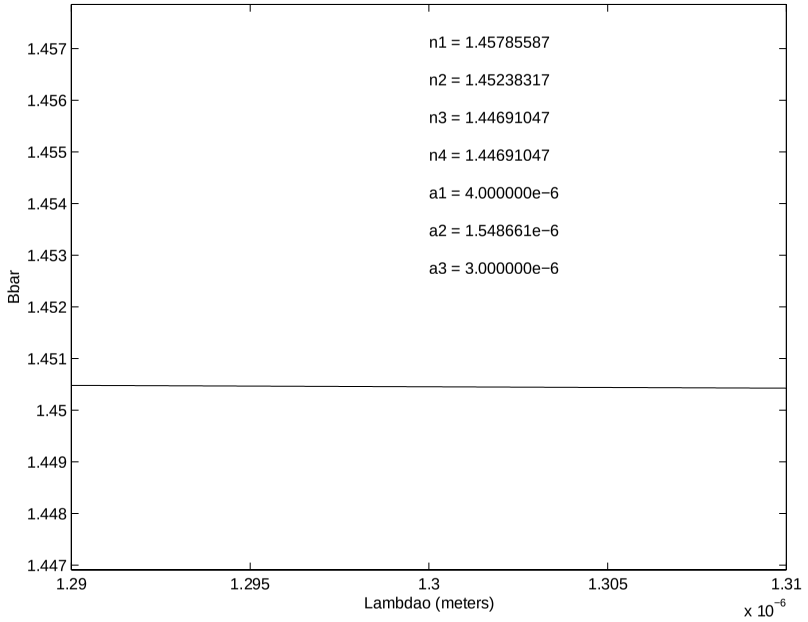

Figure 6-2 Dispersion Curve for the unperturbed waveguide used throughout Chapter 6.

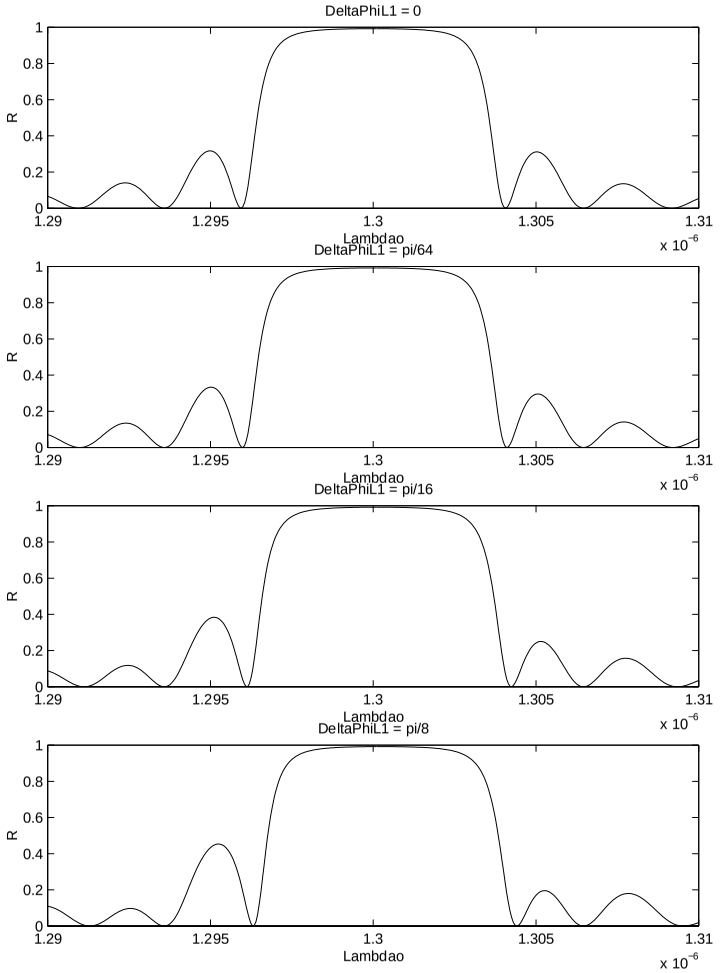

(a)

Figure 6-3 Reflectivity for double grating with $\Delta z = 0$, for $\Delta\phi_{l1}$, the discrete phase shift, ranging from (a) 0 to $\pi/8$ (b) $\pi/4$ to π (c) $5\pi/4$ to 2π (d) $9\pi/4$ to $7\pi/2$

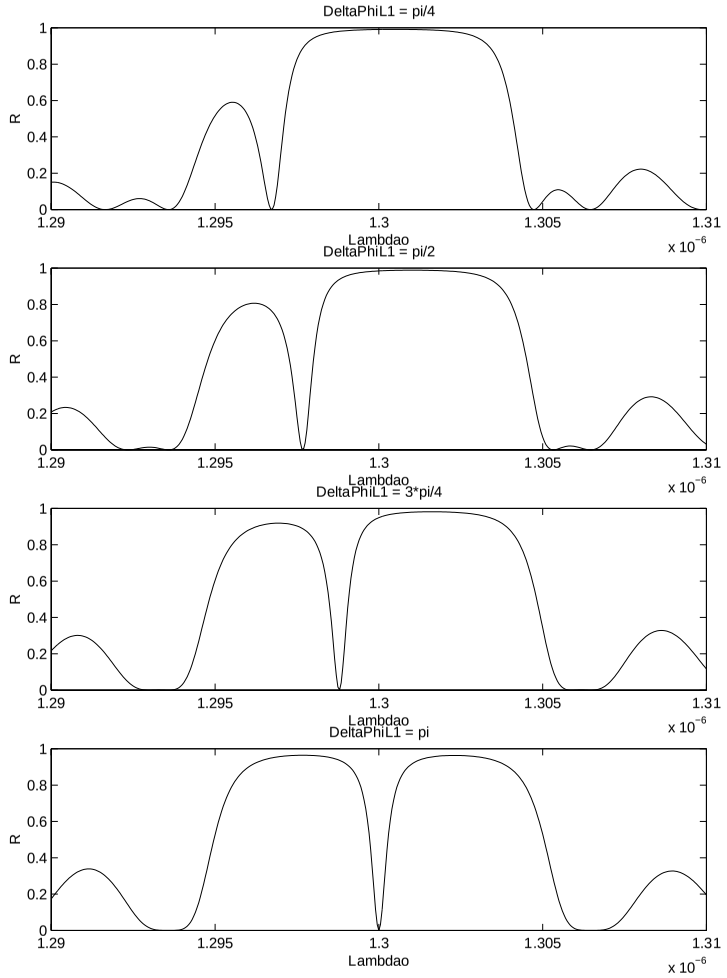

(b)

Figure 6-3 continued

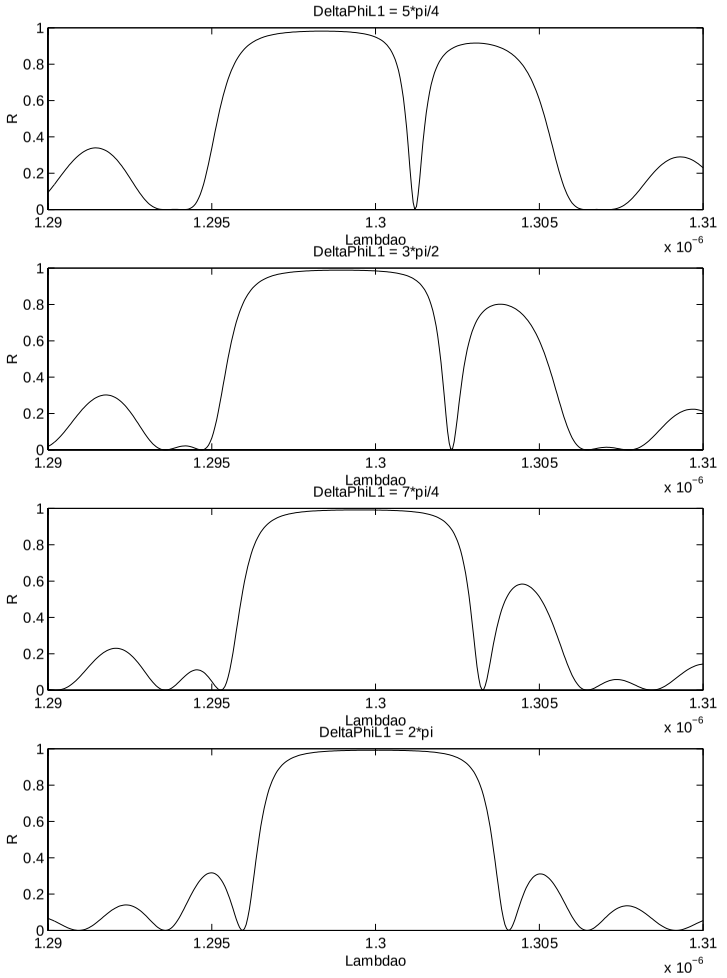

(c)

Figure 6-3 continued

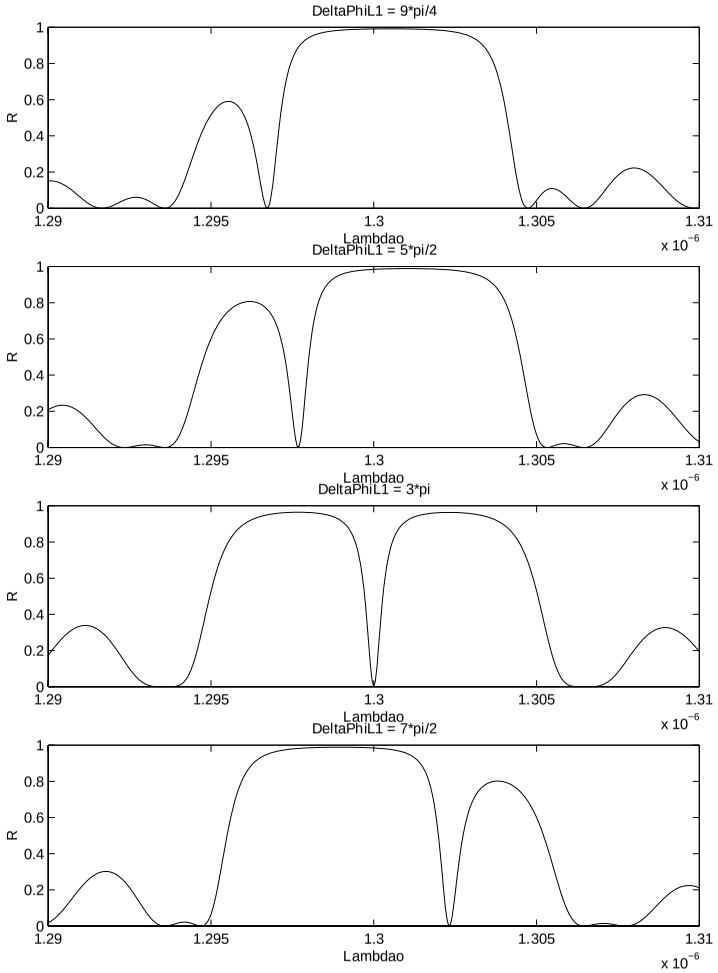

(d)

Figure 6-3 continued

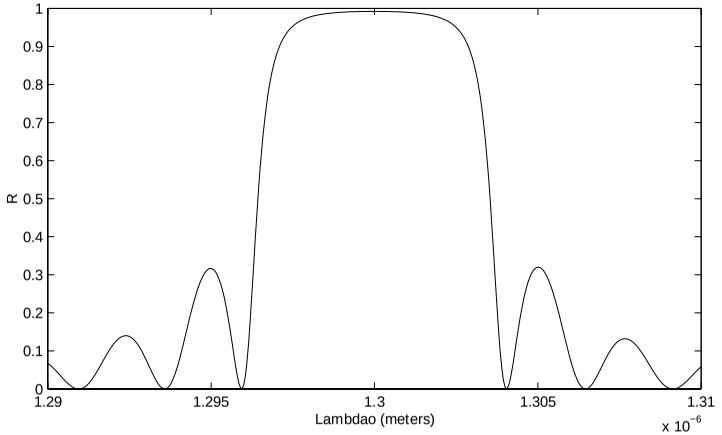

Figure 6-4 Reflectivity for double grating with $\Delta\phi_{l1} = 0$, for Δz, the separation, equal $1/4$ wavelength

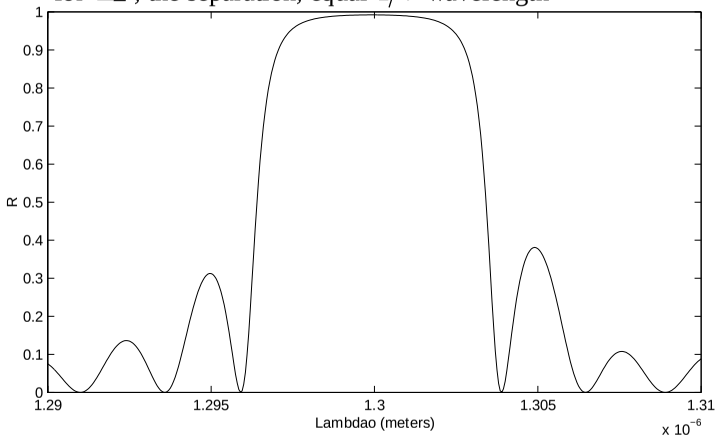

Figure 6-5 Reflectivity for double grating with $\Delta\phi_{l1} = 0$, for Δz, the separation, equal 2 wavelengths

same parameters as in Table 6-2 except that the length of the grating is $\Delta z = 2x10^{-4}$ m. It can be seen that small values of $\Delta\phi_{l1}$ make little difference, as their spectra are not much different than the spectrum for $\Delta\phi_{l1} = 0$. Furthermore, $0 < \Delta\phi_{l1} < \pi$ or $2\pi < \Delta\phi_{l1} < 3\pi$ produces a notch to the left-of-center while $\pi < \Delta\phi_{l1} < 2\pi$ or $3\pi < \Delta\phi_{l1} < 4\pi$ produces a notch to the right-of- center. When $\Delta\phi_{l1}$ is in the range $2\pi < \Delta\phi_{l1} < 4\pi$ it produces the same spectrum as $\Delta\phi_{l1} - 2\pi$. Equation (6.7) makes it obvious that $\Delta\phi_{l1} = 4\pi + x$ produces the same spectrum as $\Delta\phi_{l1} = x$.

Double gratings with $\Delta\phi_{l1} = 0$ are considered next, but the nongrating section has non-zero Δz. This time $\mathbf{F}_{p1}$ for the nongrating section is given by (6.8). The two grating sections still have the parameters given in Table 6-2. Figure 6-4 shows the spectrum when Δz of the nongrating region equals $\frac{1}{4}$ wavelength, that is $\Delta z = \frac{1}{4}\frac{2\pi}{\beta(\lambda_o = 1.3\mu m)}$. Figure 6-5 illustrates the spectrum when Δz of the nongrating region equals 2 wavelengths. Neither of these spectra is noticeably different than the spectrum when the nongrating section $\Delta z = 0$, shown as the top plot in Figure 6-3a. Thus, it is seen that if the non-grating section is not longer than a few wavelengths then the two gratings might as well be touching. To understand this behavior we examine the first plot in Figure 6-6, which is a plot of δ versus λ_o, and the second plot, which is a plot of $\delta\Delta z$ versus λ_o where Δz equals 2 wavelengths, that is, $\Delta z = \frac{4\pi}{\beta(\lambda_o = 1.3\mu\text{m})}$. At no wavelength $|\delta\Delta z|$ exceeds 0.2. The previous paragraph, which examined double gratings with nongrating $\Delta z = 0$, demonstrated that at no λ_o is R sensitive to a small value of $\left|\frac{\Delta\phi_{l1}}{2}\right|$ in (6.7), so now of course no λ_o will be affected by a small value of $|\delta\Delta z|$ in (6.8).

If the phase-shift matrix given in [1] for a nongrating region with non-zero Δz but $\Delta\phi_{l1} = 0$ had been used instead of (6.8), which applies to the same situation, the results would have been different. The two places that δ occurs in (6.8), [1] has β instead. The third plot in Figure 6-6 shows β versus λ_o, and the last shows the quantity

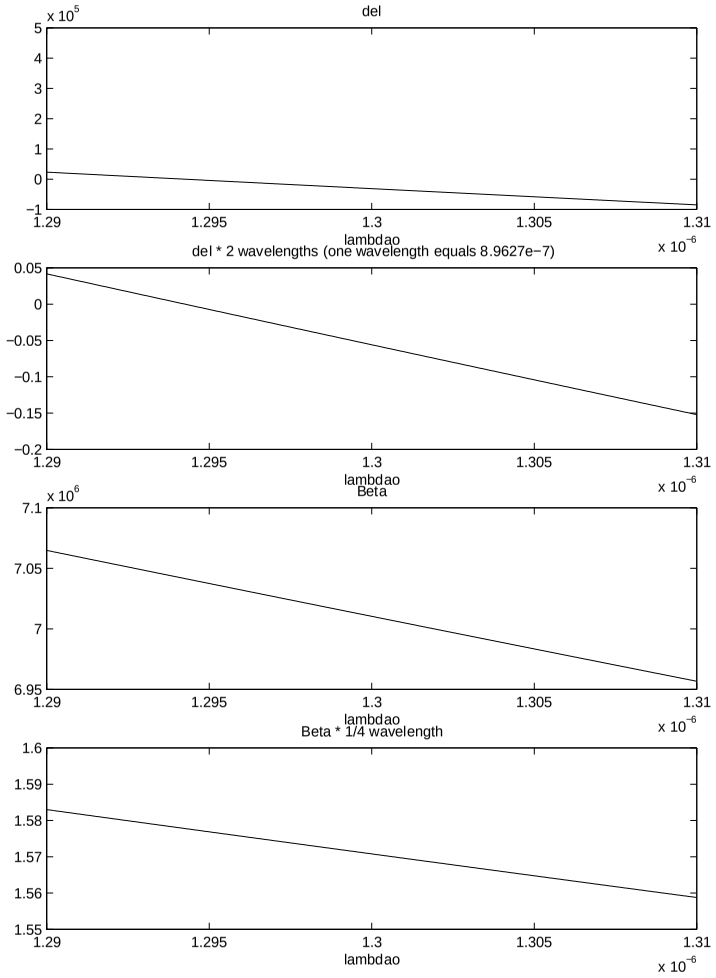

Figure 6-6 Variables influencing behavior of double grating with small separation Δz.

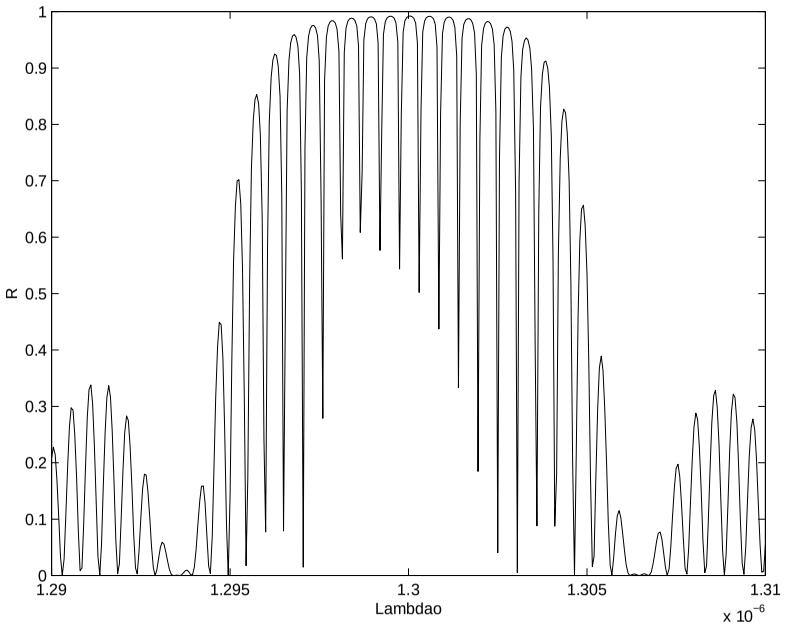

Figure 6-7 Reflectivity for double grating with $\Delta\phi_{l1} = 0$, for Δz, the separation, equal 1×10^{-3} m

$\beta \cdot \frac{1}{4}\text{wavelength} = \beta \frac{1}{4} \frac{2\pi}{\beta(\lambda_o = 1.3\mu\text{m})}$ versus λ_o, which almost has a constant value of $\frac{\pi}{2}$. Therefore, if the phase-shift matrix given in [1] is used when $\Delta z = \frac{1}{4}$ wavelength and $\Delta\phi_{l1} = 0$, the result for the reflectivity spectrum is nearly the same as when $\Delta z = 0$ and $\Delta\phi_{l1} = \pi$, as shown in Figure 6-3b. This spectrum has a null at λ_{o_D}, the center wavelength for the identical uniform gratings in the double grating, given by (4.6) or (6.5). References [11] and [13] report such a null when $\Delta z = \frac{1}{4}$ wavelength, but both references assume a non-zero discrete phase shift accompanying the $\Delta z = \frac{1}{4}$ wavelength separation. Reference [13] indicates that the $\Delta z = \frac{1}{4}$ wavelength separation is responsible for the null. But if [1] has an error and (6.6) is correct, then the null could be viewed as a consequence of the discrete phase shift, not the Δz. In fact, [13] is consistent with the formulation here including (6.6), because it assumes the quarter wavelength separation is achieved by splitting the grating and shifting the pieces. Since $\frac{2\pi}{\beta(\lambda_o)} \approx 2\Lambda$ from (6.5), shifting the pieces by $\frac{1}{4}\frac{2\pi}{\beta(\lambda_o)}$ introduces a $\Delta\phi_{l1} \approx \pi$ discrete phase shift. [11] also assumes that a discrete phase shift accompanies the $\Delta z = \frac{1}{4}$ wavelength separation, but the value of $\Delta\phi_{l1}$ depends on the length of the less-positive-z grating. Thus, the phase-shift matrices given by (6.6) and (6.8) are consistent with [11] and [13], and it is likely that a typographical error has occurred in [1]. To confirm this, the problem has been re-worked using two alternate approaches. The first alternate approach computes the reflectivity R for double gratings, but this time the approach was the same as that used by [11] which is different than the matrix approach used so far in this chapter. The details are given in the next section. For every problem tested, that is in choosing any values for Δz of the nongrating region and $\Delta\phi_{l1}$, the same spectrum as the matrix approach yielded was obtained. The second alternate approach, presented in Section 6.6, also computes R for double gratings. This approach also

reproduces Figures 6-4 through 6-7 exactly. For this reason and because the phase-shift matrices used in this chapter have been derived using two different ways, we believe that they are correct and that [1] has a typographical error.

Double gratings with $\Delta\phi_{l1} = 0$ and nongrating section $\Delta z \neq 0$ are now considered again, but this time much larger values of Δz of the nongrating section are used. $\mathbf{F}_{p1}$ for the nongrating section is given by (6.8). The two grating sections on the ends are still identical, and each still has the parameters given in Table 6-2. Figure 6-7 shows the reflectivity spectrum when the nongrating section $\Delta z = 1x10^{-3}$ m, that is, the separation between the gratings equals ten times the length of each grating. The spectrum has somewhat the same shape as when $\Delta z = 0$ and $\Delta\phi_{l1} = 0$, shown at the top of Figure 6-3a, but has numerous nulls, each of which drops to zero although this does not appear so in the Figure 6-7 because only 400 points are plotted. Insight into the behavior observed is provided by Figure 6-8. The data for the dashed lines was taken from Figure 6-3, plots of the spectra when the nongrating section $\Delta z = 0$ and $\Delta\phi_{l1}$ might not equal zero. For every one of these spectra $\frac{\Delta\phi_{l1}}{2}$ is a constant independent of λ_o, and one point along one of the dashed lines is taken from each spectrum. Where the notch occurs in the spectrum is located and this value of λ_o, together with the value of $\frac{\Delta\phi_{l1}}{2}$ for the spectrum, becomes one point on one of the dashed lines in Figure 6-8. No notch is produced when $\frac{\Delta\phi_{l1}}{2}$ is very small or when it is near π. In light of the correspondence between $\frac{\Delta\phi_{l1}}{2}$ and $\delta\,\Delta z$ in equations (6.7) and (6.8) the expression

$$\mathrm{mod}\left(1x10^{-3}\delta, 2\pi\right)$$

where mod is the modulus versus λ_o has been plotted on the same plot as the dashed lines. δ varies with λ_o and $1x10^{-3}$ m is the value of Δz that was used in Figure 6-7. Where the solid line crosses one of the dashed lines a null is expected in Figure 6-7. This approach successfully predicts the number of nulls in the mail lobe in Figure 6-7, which is 22. By adjusting Δz for the nongrating region and $\Delta\phi_{l1}$ (they can be nonzero

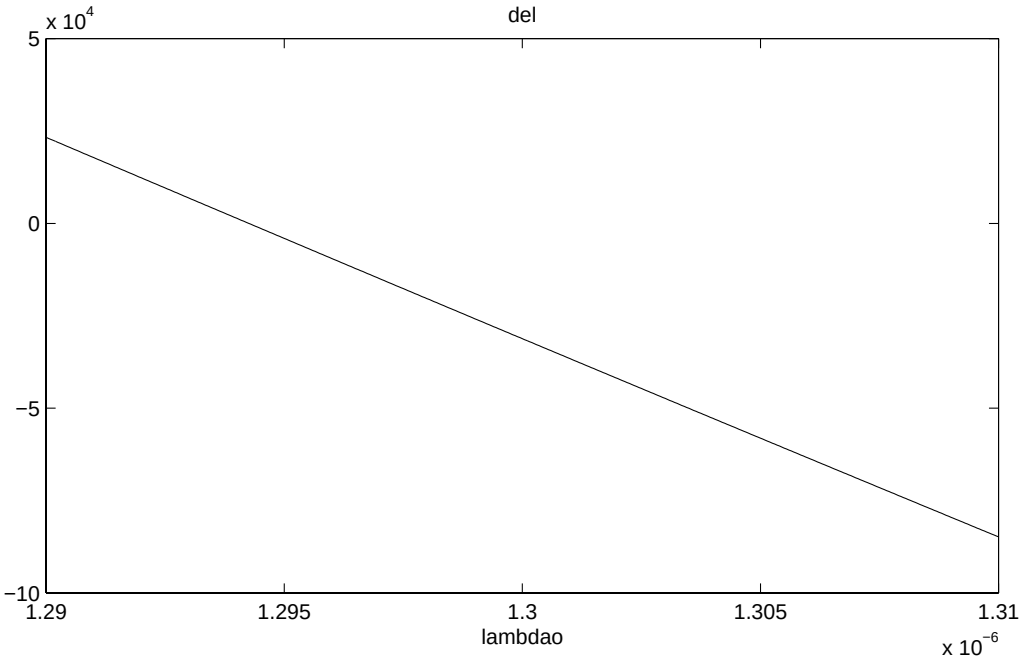

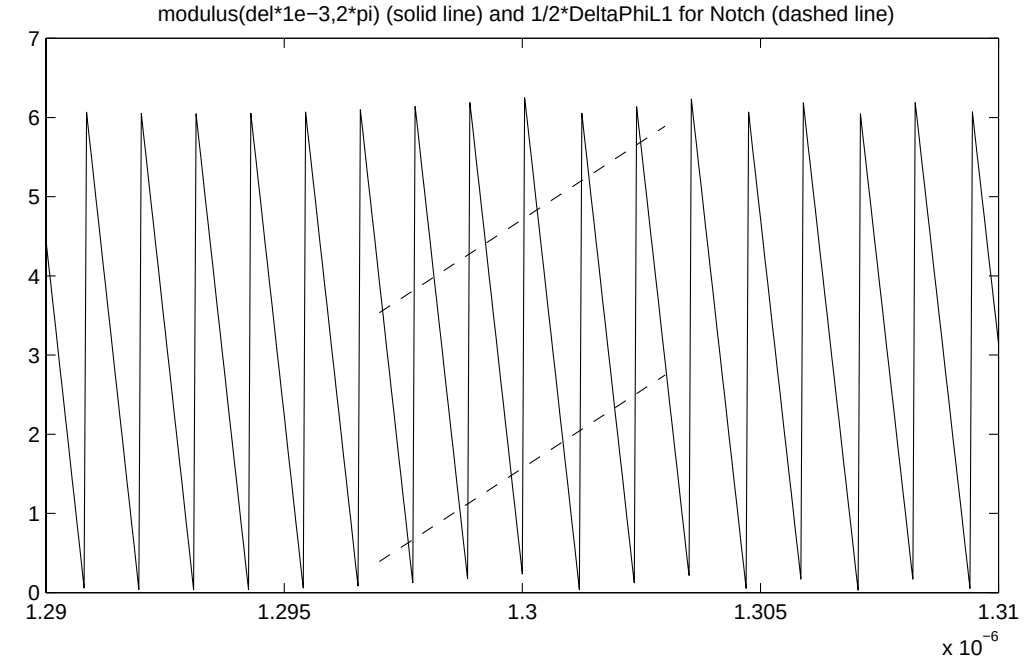

Figure 6-8 Variables influencing nulls in Figure 6-7

simultaneously) the number of notches and their placement can be controlled. Increasing Δz of the nongrating section by a factor of two should increase the number of nulls by a factor of two. It is also worth noting that the behavior in Figure 6-7 is very similar to that of a Fabry-perot interferometer. In fact, the "widely" separated gratings here behave as end reflectors, while the nongrating region is the cavity part in which interference takes place. It is possible the transmission function of this filter could find applications similar to those proposed in [14] and [15] for the spectral reflectivity function of "sampled" gratings, since the functions are similar. The spectral reflectivity function for a typical "sampled" grating is shown in Figure 6-18b. The application proposed in [15] is use as a wavelength reference standard for DWDM systems.

6.5 First Alternate Method of Analyzing Double Gratings

The power reflectivity for double gratings is found using a different method in order to check the results of the previous section. The approach is to write expressions for $\psi_1(z)$ and $\psi_2(z)$, the field amplitudes, in each of the three sections of the double grating and then enforce the boundary conditions, which is the same approach used in [11]. It will be seen that this method produces results that match those presented in the previous section, confirming that the phase-shift matrices used in this chapter are correct and that [1] has a typographical error.

The coupled-mode equations in (3.26) are used. Reverting to these is more convenient than using (5.7) upon which the matrix approach of the last section is based. The notation attached to equations (3.26) is different than for equations (5.7), and one likely source of confusion is that for (3.26) $\delta = 2\beta - \frac{2\pi}{\Lambda}$ whereas for (5.7) the definition $\delta = \beta - \frac{\pi}{\Lambda}$ has been used in [1].

Figure 6-9 shows the geometry of a double grating with l denoting the separation between the gratings and L_1 and L_2 their lengths. Within the grating on the more positive-z end $\psi_1(z)$ and $\psi_2(z)$ are given by equations (3.29a) and (3.29b) because the boundary condition $\psi_2(L_1) = 0$ applies. Thus,

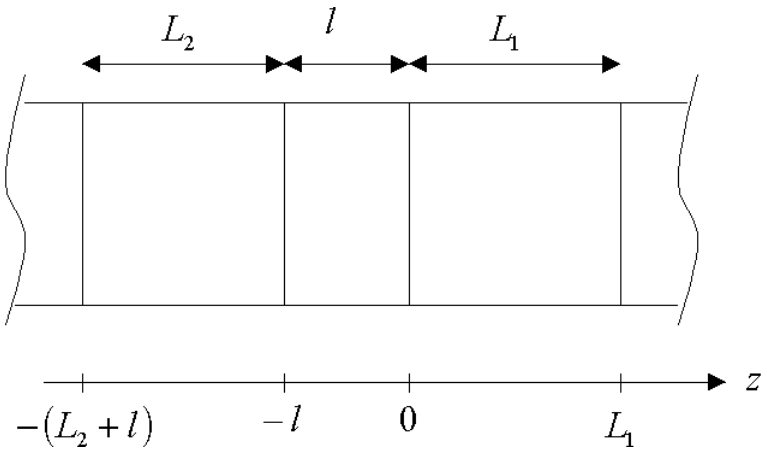

Figure 6-9 Double grating with dimensions labeled using notation of Section 6.5

$$\psi_1(0<z<L_1)=\frac{-j4}{\left(C_{o_1}'\right)^*}B_1 e^{\left(S_1L_1+j\frac{\delta_1}{2}z\right)}\left\{S_1\cosh[(z-L_1)S_1]-j\left(\frac{\delta_1}{2}+C_{o_1}\right)\sinh[(z-L_1)S_1]\right\} \tag{6.10a}$$

$$\psi_2(0<z<L_1)=2B_1 e^{\left(S_1L_1-j\frac{\delta_1}{2}z\right)}\sinh[(z-L_1)S_1] \tag{6.10b}$$

where

$$\delta_1=2\beta-\frac{2\pi}{\Lambda_1} \tag{6.11}$$

$$S_1=\sqrt{\frac{C_{o_1}{}^2}{4}-C_{o_1}\left(C_{o_1}+\delta_1\right)-\left(\frac{\delta_1{}^2}{2}\right)^2} \tag{6.12}$$

$$C_{o_1}{}'=C_{o_1}e^{-j\phi_1} \tag{6.13}$$

and C_{o_1} is given by (3.23b) using the parameters of the grating under consideration. Variables δ_2, S_2, and C_{o_2} which will be used shortly are similarly defined using the parameters of the grating on the negative-z end. For all of the problems solved in Section 6.4 the two gratings are identical but here δ_1, S_1, C_{o_1} and δ_2, S_2, C_{o_2} are kept distinct to preserve generality. When the two gratings are identical except possibly for a phase shift, $C_{o_1}=C_{o_2}$, but $C_{o_1}{}'\neq C_{o_2}{}'$ if a non-zero phase shift exists, that is, if $\phi_1\neq\phi_2$.

Within the nongrating region the coupling coefficient equals zero, so the coupled-mode equations become $\frac{d\psi_1(z)}{dz}=0$ and $\frac{d\psi_2(z)}{dz}=0$. Consequently, the boundary conditions for the grating on the left in Figure 6-9 are

$$\psi_1(-l)=\psi_1(0)=\frac{-j4}{\left(C_{o_1}'\right)^*}B_1e^{S_1L_1}\left\{S_1\cosh(L_1S_1)+j\left(\frac{\delta_1}{2}+C_{o_1}\right)\sinh(L_1S_1)\right\} \tag{6.14a}$$

$$\psi_2(-l)=\psi_2(0)=-2B_1e^{S_1L_1}\sinh(L_1S_1). \tag{6.14b}$$

Within the grating on the left, the field amplitude $\psi_2(z)$ is found by solving equations (3.26) without enforcing the boundary condition $\psi_2(-l)=0$ which does not apply. The result is

$$\psi_2(-L_2-l<z<-l)=e^{-j\frac{\delta_2}{2}z}\left(B_2e^{S_2z}+B_2'e^{-S_2z}\right) \tag{6.15}$$

where B_2 and B_2' are arbitrary constants. Solving (3.26b) for $\psi_1(z)$ yields

$$\psi_1(z)=\frac{-2j}{\left(C_{o_2}'\right)^*}e^{j\delta_2z}\left(\frac{d\psi_2}{dz}-jC_{o_2}\psi_2\right). \tag{6.16}$$

Using (6.15) in (6.16) yields

$$\psi_1(-L_2-l<z<-l)=$$
$$\frac{-2j}{\left(C_{o_2}'\right)^*}e^{j\delta_2z}\left\{\begin{array}{l}B_2e^{S_2z}\left[e^{-j\frac{\delta_2}{2}z}\left(-j\frac{\delta_2}{2}\right)+S_2e^{-j\frac{\delta_2}{2}z}-jC_{o_2}e^{-j\frac{\delta_2}{2}z}\right]\\+B_2'e^{-S_2z}\left[e^{-j\frac{\delta_2}{2}z}\left(-j\frac{\delta_2}{2}\right)-S_2e^{-j\frac{\delta_2}{2}z}-jC_{o_2}e^{-j\frac{\delta_2}{2}z}\right]\end{array}\right\}. \tag{6.17}$$

Enforcing the boundary conditions (6.14a) and (6.14b) yields two equations that can be solved for B_2 and B_2' assuming $B_1=1$. The constant B_1 is related to the power incident on the double grating from $z=-\infty$ and is arbitrary since only the ratio

$$R=\frac{\left|\psi_2(-L_2-l)\right|^2}{\left|\psi_1(-L_2-l)\right|^2} \tag{6.18}$$

is of interest. In matrix form, the two equations are expressed as

$$\begin{bmatrix} N_{11} & N_{12} \\ N_{21} & N_{22} \end{bmatrix} \begin{bmatrix} B_2 \\ B_2' \end{bmatrix} = B_1 \begin{bmatrix} Q_1 \\ Q_2 \end{bmatrix} \tag{6.19a}$$

where

$$N_{11} = \frac{-2j}{\left(C_{o_2}'\right)^*} e^{j\delta_2(-l)} e^{S_2(-l)} \left[e^{-j\frac{\delta_2}{2}(-l)} \left(-j\frac{\delta_2}{2} \right) + S_2 e^{-j\frac{\delta_2}{2}(-l)} - jC_{o_2} e^{-j\frac{\delta_2}{2}(-l)} \right] \tag{6.19b}$$

$$N_{12} = \frac{-2j}{\left(C_{o_2}'\right)^*} e^{j\delta_2(-l)} e^{-S_2(-l)} \left[e^{-j\frac{\delta_2}{2}(-l)} \left(-j\frac{\delta_2}{2} \right) - S_2 e^{-j\frac{\delta_2}{2}(-l)} - jC_{o_2} e^{-j\frac{\delta_2}{2}(-l)} \right] \tag{6.19c}$$

$$N_{21} = e^{-j\frac{\delta_2}{2}(-l)} e^{S_2(-l)} \tag{6.19d}$$

$$N_{22} = e^{-j\frac{\delta_2}{2}(-l)} e^{-S_2(-l)} \tag{6.19e}$$

$$Q_1 = \frac{-j4}{\left(C_{o_1}'\right)^*} e^{S_1 L_1} \left\{ S_1 \cosh(L_1 S_1) + j\left(\frac{\delta_1}{2} + C_{o_1} \right) \sinh(L_1 S_1) \right\} \tag{6.19f}$$

and

$$Q_2 = -2e^{S_1 L_1} \sinh(L_1 S_1). \tag{6.19g}$$

After solving (6.19) for B_2 and B_2', using the inverse of the matrix $\mathbf{N}$ and assuming $B_1 = 1$, they are used in (6.15) and (6.17) to compute R in (6.18). Implementation of this procedure using Matlab yielded exactly the same results as those presented in Section 6.4 in every case, indicating that the phase-shift matrices derived in Section 6.3 are correct. The Matlab program, called DoubleGrat.m, is listed in Appendix E.

Equations (3.26) cannot handle a non-zero phase shift between layers of a grating nor can they handle the cases for $\frac{d\phi_{l1}}{dz} \neq 0$ and $\nu \neq 1$. Another constraint not shared by (5.7) is that the apodizing function $f(z)$ in (5.1) is constrained to equal a constant

independent of z – equations (5.7) can handle the $\Delta n(x,z)$ given by (5.1) while equations (3.26) can only handle the less general $\Delta n(x,z)$ given by (3.1b) with $\Lambda_{l1} = \Lambda_{l2} = \Lambda_{l3} = \Lambda_{l4} = \Lambda$ and $\phi_{l1} = \phi_{l2} = \phi_{l3} = \phi_{l4} = \phi$. However, this is not a problem in the case at hand as uniform gratings are of interest. The problems solved in the last section can be re-worked because the grating described by the parameters given in Table 6-2 including $\frac{d\phi_{l1}(z)}{dz} = 0$, $v = 1$, and $\Delta\phi_{l2} = \Delta\phi_{l3} = \Delta\phi_{l4} = 0$ was used every time, and no other grating was used.

6.6 Second Alternate Method of Analyzing Double Gratings

In this section, the power reflectivity for double gratings is recomputed using a second alternate approach based on the so-called "effective medium picture" presented in [16]. As with the matrix approach, the derivation, which is not provided here, begins with the coupled-wave equations (5.7a) and (5.7b). Hence, the coupling coefficients σ, $\hat{\sigma}$, and K and the detuning δ appear in this approach as well and are defined as before. However, besides their definitions and the computation of the propagation constant β the expressions and computations used by this approach are quite dissimilar from the previous two. The approach in this section is also unlike the other approaches in that it provides physical insight into the qualitative nature of the solutions.

According to the "effective medium picture" presented in [16] a double grating is analogous to the situation illustrated in Figure 6-10. In this figure, a plane wave is incident from $z = -\infty$ upon 5 layers of dielectric. The problem is one-dimensional; each layers occupies all of $z_x < z < z_{x+1}$ extending to $\pm\infty$ in the x and y directions. The first and last layers are semi-infinite in the z direction. The reflection coefficient at the 1-2 interface is easily found using a well-known procedure. The first expression required in the procedure is for the ratio of the electric-field intensities of the positive-travelling wave incident from the left on the interface between regions 4 and 5 and the reflected, negative-travelling wave in region 4

$$r_{54} = \frac{1 - Z_4}{1 + Z_4} \tag{6.20}$$

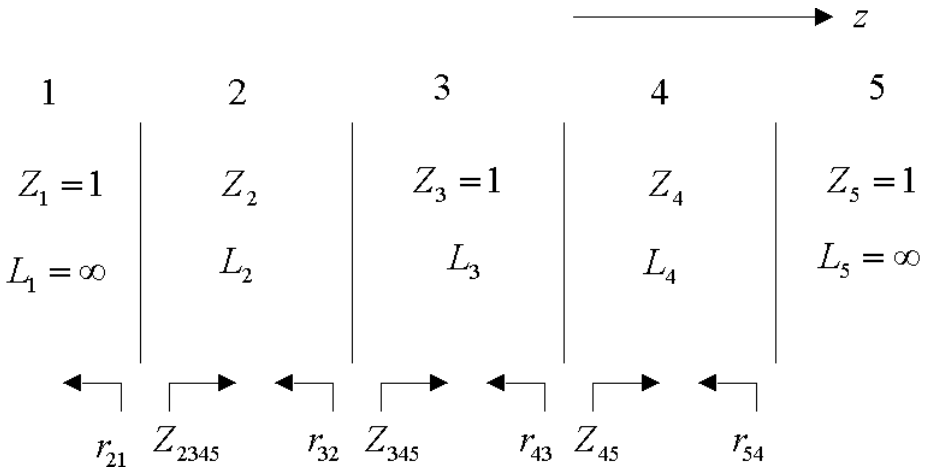

Figure 6-10 Layers of dielectric upon which a plane wave is incident

where Z_4 is the intrinsic impedance of region 4 and region 5 has $Z_5 = 1$. The ratio of the total electric and magnetic field intensities a vanishingly small distance to the right of the 3-4 interface is given by

$$Z_{45} = Z_4 \frac{e^{j\beta_4 L_4} + r_{54} e^{-j\beta_4 L_4}}{e^{j\beta_4 L_4} - r_{54} e^{-j\beta_4 L_4}}. \tag{6.21}$$

The ratio of the electric-field intensities of the positive-travelling wave incident from the left on the interface between regions 3 and 4 and the reflected, negative-travelling wave in region 3 is given by

$$r_{43} = \frac{Z_{45} - 1}{Z_{45} + 1} \tag{6.22}$$

since $Z_3 = 1$. Corresponding variables are defined at the other interfaces as indicated in Figure 6-10:

$$Z_{345} = Z_3 \frac{e^{j\beta_3 L_3} + r_{43} e^{-j\beta_3 L_3}}{e^{j\beta_3 L_3} - r_{43} e^{-j\beta_3 L_3}} \tag{6.23}$$

$$r_{32} = \frac{Z_{345} - Z_2}{Z_{345} + Z_2} \tag{6.24}$$

$$Z_{2345} = Z_2 \frac{e^{j\beta_2 L_2} + r_{32} e^{-j\beta_2 L_2}}{e^{j\beta_2 L_2} - r_{32} e^{-j\beta_2 L_2}} \tag{6.25}$$

$$r = r_{21} = \frac{Z_{2345} - 1}{Z_{2345} + 1}. \tag{6.26}$$

In the analogy drawn between the situation illustrated in Figure 6-10 and a double grating, regions 2 and 4 correspond to the two uniform gratings, and regions 1, 3, and 5 correspond to the nongrating regions. The quantities r and $|r|^2$ for the situation in Figure 6-10 equal the reflectivity and power reflectivity, respectively, for the double grating if

$$Z_4 = \sqrt{\frac{\hat{\sigma}_4 - K_4}{\hat{\sigma}_4 + K_4}} \tag{6.27}$$

where $\hat{\sigma}_4$ and K_4 are the (uniform) coupling coefficients, defined by (5.9), (5.10), (5.4b), and (5.4c), in the more-positive-z uniform grating in the double grating;

$$Z_2 = \sqrt{\frac{\hat{\sigma}_2 - K_2}{\hat{\sigma}_2 + K_2}} \tag{6.28}$$

where $\hat{\sigma}_2$ and K_2 are the (uniform) coupling coefficients in the less-positive-z uniform grating in the double grating;

$$\beta_4 = \sqrt{\hat{\sigma}_4^{\,2} - K_4^{\,2}}\,; \tag{6.29}$$

$$\beta_2 = \sqrt{\hat{\sigma}_2^{\,2} - K_2^{\,2}}\,; \tag{6.30}$$

and

$$\beta_3 L_3 = \delta L_3 + \frac{1}{2}\Delta\phi_{l1} \tag{6.31}$$

where δ is given by (5.10) and $\Delta\phi_{l1}$ is the difference $\phi_{l1}(z)$ at the output of the nongrating region (less positive-z end) minus $\phi_{l1}(z)$ at the input of the nongrating region (more positive-z end). In the case at hand, since $\frac{d\phi_{l1}}{dz} = 0$ in both gratings, $\Delta\phi_{l1}$ is the difference $\phi_{l1}(z)$ throughout the less positive-z end grating minus $\phi_{l1}(z)$ throughtout the more positive-z end grating. As demonstrated by [16], the intrinsic impedance is unity in layers in the plane-wave problem corresponding to nongrating sections in the double grating.

A Matlab program that implements the approach in this section, called EffMedDoubleGrat.m, is listed in Appendix E. For every problem tested, that is in

choosing any values for Δz of the nongrating region and $\Delta\phi_{l1}$, the same spectrum as those yielded by the previous two approaches was obtained. Figures 6-4 through 6-7 were reproduced to a high degree of accuracy.

6.7 Nonzero Phase Shift Between Layers With $|K| = 0$

In this section, once again just a single grating is considered. At the end of Chapter 4 it was stated that any spectrum that can be achieved with a grating that has a nonzero phase shift between layers, meaning at least one of $\phi_{l1}, \phi_{l2}, \phi_{l3}, \text{or} \phi_{l4}$ in Δn given by (3.1b) does not equal the others, can also be achieved with no phase shift. The exception was when $|K|$ passes through zero at some wavelength near λ_{o_D}, the wavelength about which the reflectivity spectrum is centered, given by (4.6). This situation is now examined more closely. Chapter 4 used the original format coupled-wave equations, but now that this topic is being revisited let us switch to using the matrix approach, and therefore inherently the new format coupled-wave equations (5.7a) and (5.7b) are used. (The original format coupled-wave equations are those used exclusively until Section 5.3.) The form of perturbation $\Delta n(x, z)$ used by (5.7a) and (5.7b) is given by (5.1) which is general enough to encompass the $\Delta n(x, z)$ given by (3.1b) for the original format coupled-wave equations. In (5.1) the phase shift between layers is nonzero if $\Delta\phi_{l2}, \Delta\phi_{l3}, \text{or} \Delta\phi_{l4}$ does not equal zero. The variables $\Delta\phi_{l2}, \Delta\phi_{l3}, \text{or} \Delta\phi_{l4}$ represents the phase shifts between gratings in layers 2,3, and 4, respectively, and gratings in layer 1, the core. The variable $\Delta\phi_{l1}$, on the other hand, represents the difference $\phi_{l1}(z)$ at the output of the nongrating region (less positive-z end) minus $\phi_{l1}(z)$ at the input of the nongrating region (more positive-z end).

Once again the grating described by the parameters listed in Table 6-2 is considered, however this time we let $\Delta\phi_{l2} = \pi$. Figure 6-11 is a plot of K versus λ_o. (K is given by (5.4c).) K is purely real in the case at hand and goes through zero at $\lambda_{o_D} = 1.3\mu\text{m}$. The grating in Table 6-2 was specifically tailored for this result. Figure 6-12 is a plot of the field distributions when $\lambda_o = \lambda_{o_D} = 1.3\mu\text{m}$, and it can be seen that

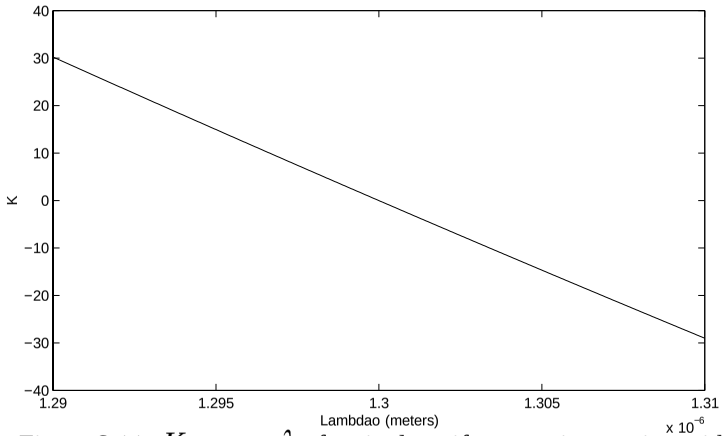

Figure 6-11 K versus λ_o for single uniform grating section with phase shift equal π between layer 2 and the core layer

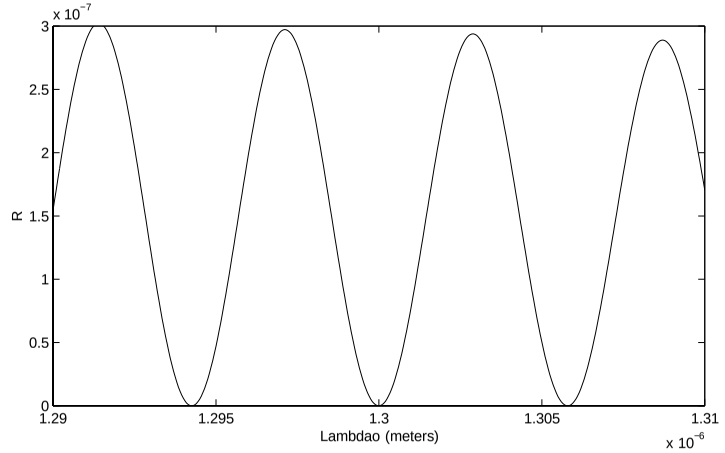

Figure 6-13 Reflectivity for single uniform grating section with $\Delta z = 1 \times 10^{-4}$ m and phase shift equal π between layer 2 and the core layer

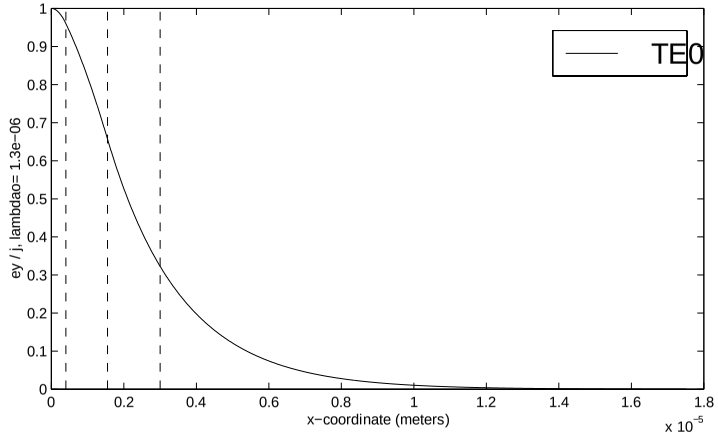

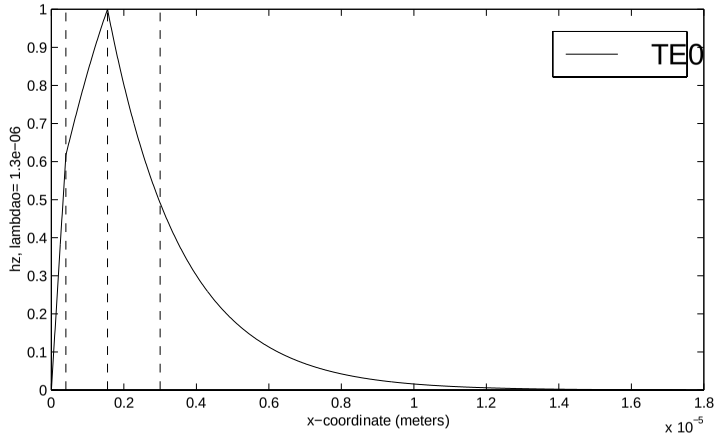

Figure 6-12 Field profiles at $\lambda_o = 1.3 \times 10^{-6}$ m for waveguide described by Table 6-1.

the area under the curve $|e_y|^2$ over $0 < x < a_1$ equals the area under the curve over $a_1 < x < a_2$. This is why K goes through zero at $\lambda_o = 1.3\mu$ m and why it was the dimensions of the waveguide a_1 and a_2 that had to be adjusted to achieve this result. No gratings exist within the layers $a_2 < |x| < a_3$ and $a_4 < |x|$ because the refractive index $n(x)$ in both layers equals the refractive index of pure SiO_2.

Figure 6-13 shows the reflectivity spectrum of this grating with a nonzero phase shift between the core layer and the cladding layer. It was computed using (6.3) with $\mathbf{F} = \mathbf{F}_1$,

$$\begin{bmatrix} R_1 \\ S_1 \end{bmatrix} = \mathbf{F}_1 \begin{bmatrix} 1 \\ 0 \end{bmatrix}. \qquad (6.32)$$

Only one 2x2 matrix is used for $\mathbf{F}$ since only a single uniform section is considered. F_1 was computed using (6.2). The spectrum is shown again in figure 6-14 over a wider range of λ_o. It is nearly sinusoidal but with a small amplitude – on the order of 3×10^{-7}. This spectrum is quite different than the spectra shown in Figure 3-4, which are for gratings with no phase shift between layers. The spectrum in Figure 6-14 has no main lobe, in fact it equals zero at λ_{o_D} where all the spectra in Figure 3-4 have their peak values. Figure 6-14 resembles Figure 3-4 viewed over some range of λ_o far from the main lobe. If anything special can be achieved within a range of λ_o bracketing for example $\lambda_o = 1.3\mu$ m using one or more gratings with a phase shift, with $\lambda_{o_D} = 1.3\mu$ m and K passing through zero near λ_{o_D}, then the same result might be achieved using gratings with no phase shift between layers and λ_{o_D} equal some λ_o far from 1.3μ m.

Insight into the sinusoidal shape of the spectrum depicted in Figure 6-14 may be gained by simplifying the matrix $\mathbf{F}_1$ used to compute this spectrum. $\mathbf{F}_1$ is given by (6.2) which contains the variable $\gamma_B \equiv \sqrt{|K|^2 - \hat{\sigma}^2}$. Figure 6-15a is a plot of $\hat{\sigma}$ and Figure 6-15b is a plot of $\frac{K}{\hat{\sigma}}$ which shows that this ratio is quite small. The point at $\lambda_o = 1.3\mu$ m

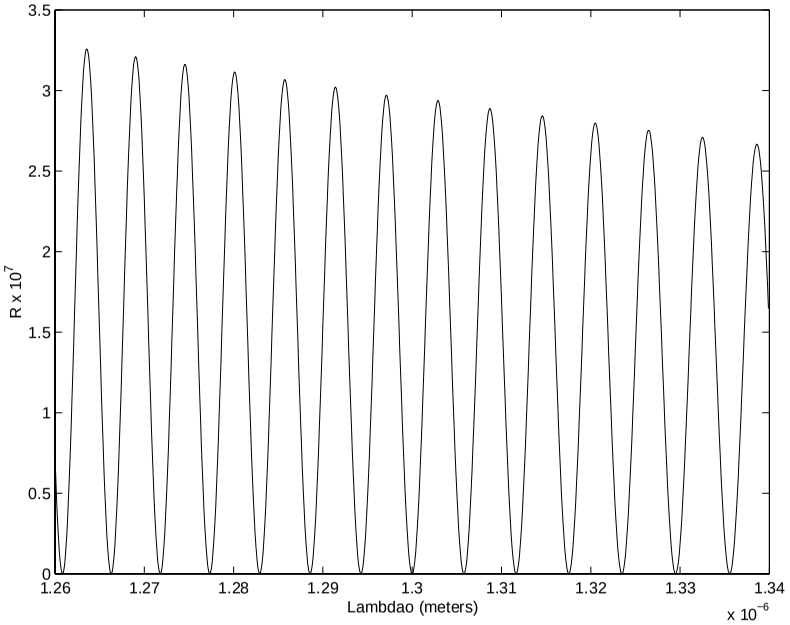

Figure 6-14 Reflectivity in Figure 6-13 viewed over a wider range of free-space wavelength λ_o

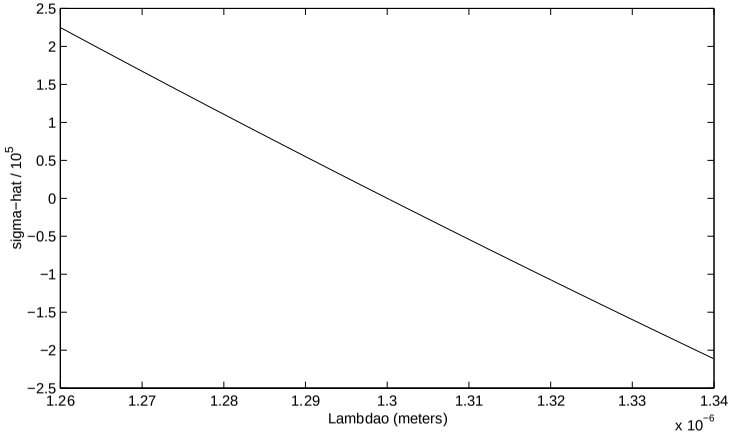

(a)

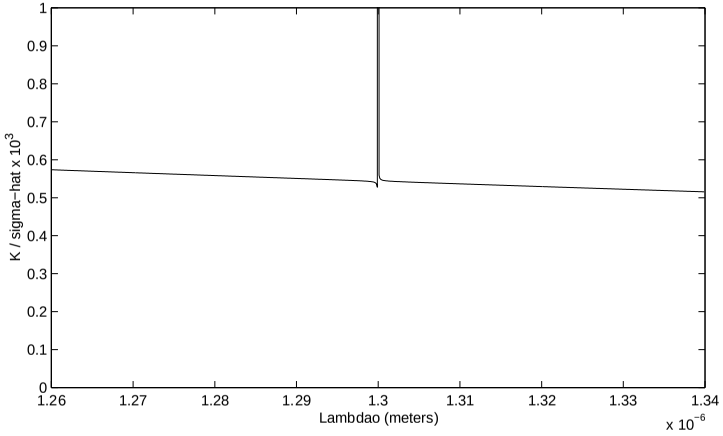

(b)

Figure 6-15 Variables controlling the sinusoidal shape of the spectrum shown in Figure 6-14: (a) $\hat{\sigma}$ (b) $K/\hat{\sigma}$

can be disregarded since the computer attempted to plot $\frac{0}{0}$ there. The relation $|K| << \hat{\sigma}$ applies in general for gratings with a phase shift between layers with K passing through zero. Therefore $\gamma_B \approx \pm j\hat{\sigma}$ and $\mathbf{F}_1$ is approximately given by

$$\mathbf{F}_1 \approx \begin{bmatrix} \cos(\hat{\sigma}\Delta z) - j\sin(\hat{\sigma}\Delta z) & -j\frac{K}{\hat{\sigma}}\sin(\hat{\sigma}\Delta z) \\ j\frac{K^*}{\hat{\sigma}}\sin(\hat{\sigma}\Delta z) & \cos(\hat{\sigma}\Delta z) + j\sin(\hat{\sigma}\Delta z) \end{bmatrix}$$

$$\mathbf{F}_1 \approx \begin{bmatrix} e^{-j\hat{\sigma}\Delta z} & -j\frac{K}{\hat{\sigma}}\sin(\hat{\sigma}\Delta z) \\ j\frac{K^*}{\hat{\sigma}}\sin(\hat{\sigma}\Delta z) & e^{j\hat{\sigma}\Delta z} \end{bmatrix}. \qquad (6.33)$$

Using (6.32) yields

$$R = \frac{|S_1|^2}{|R_1|^2} \approx \frac{|K|^2}{\hat{\sigma}^2}\sin^2(\hat{\sigma}\Delta z). \qquad (6.34)$$

The same result could have been obtained using (D.14). In light of Figure 6-15b the predicted peak level of the spectrum for the example that has been considered throughout this section is approximately $(5.7\times10^{-4})^2 = 3.2\times10^{-7}$, quite close to the actual value in Figure 6-14.

The peak level of the reflectivity spectrum for a single uniform grating with a nonzero phase shift between layers with K passing through zero appears to be always extremely small. The reason, again, is the ratio $\frac{K}{\hat{\sigma}}$ in (6.34) is probably always quite small unless the dispersion curve is much flatter than usual near λ_{o_D} -- β is practically the only non-constant term in $\hat{\sigma}$ since it varies more rapidly with λ_o than σ -- or the slope of K is much larger than usual. K has a large slope if the field profile changes relatively dramatically with λ_o. It seems these two conditions could never occur simultaneously.

Figure 6-16 shows the spectrum of the same single uniform grating used as an example throughout this section, which has the parameters listed in Table 7-2 but with

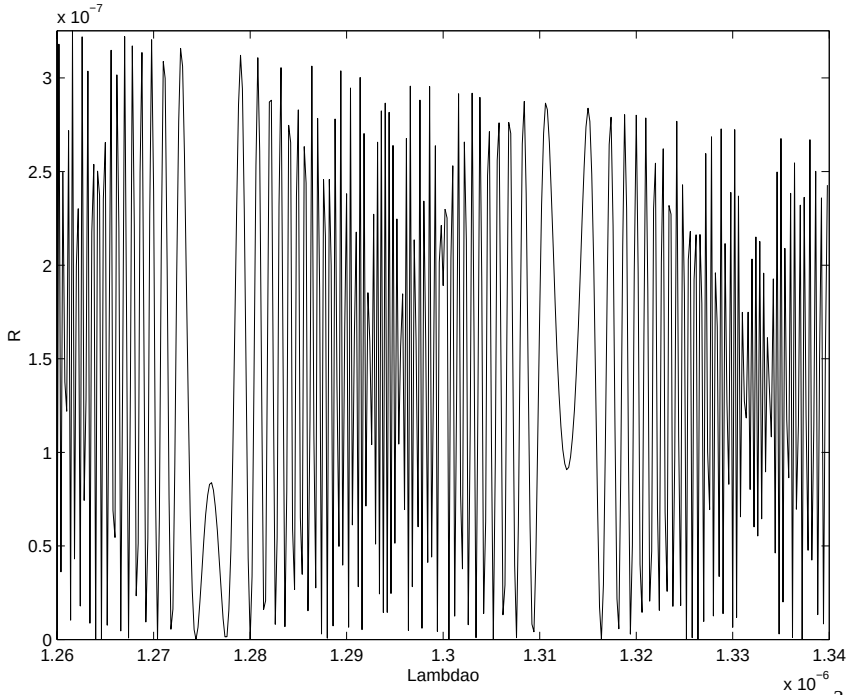

Figure 6-16 Reflectivity for single uniform grating section with $\Delta z = 50 \times 10^{-3}$ m and phase shift equal π between layer 2 and the core layer

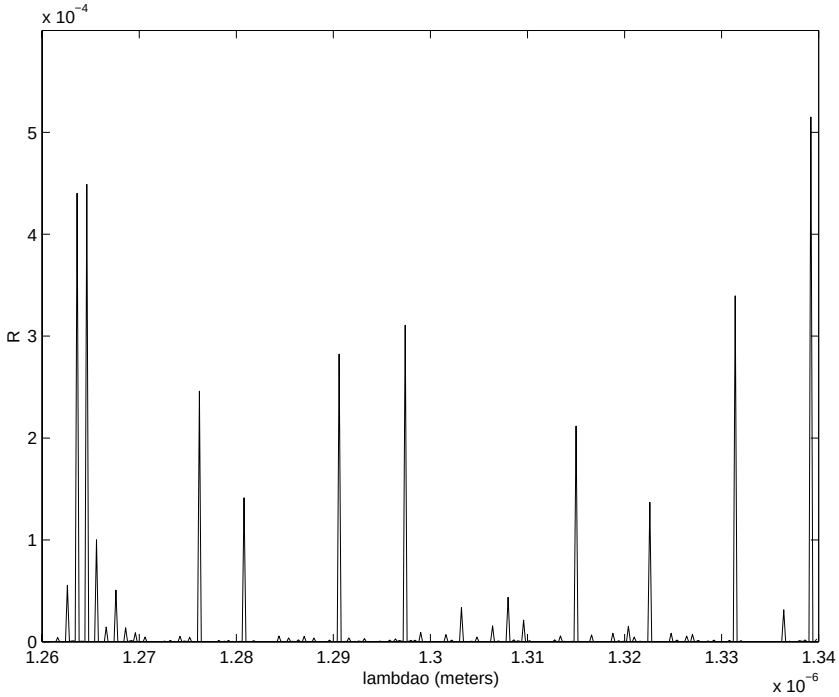

Figure 6-17 Reflectivity for 50 uniform grating sections with $\Delta z = 1 \times 10^{-4}$ m and phase shift between layers equal π, spaced $\Delta z = 1 \times 10^{-3}$ m apart

$\Delta\phi_{l2} = \pi$, except now $\Delta z = 50\times10^{-3}$ m. Predictably, the peak level of the spectrum has not increased. It is unlikely a spectrum with a peak level this low can find any applications. In hopes of "growing" the spectrum, the single grating with a phase shift with $\Delta z = 1\times10^{-4}$ m again was placed in a sampled grating configuration. Fifty gratings are placed in series but each is separated from its neighbor to the left by a nongrating section with $\Delta z = 1\times10^{-3}$ m and is separated from its neighbor to the right by another nongrating section with $\Delta z = 1\times10^{-3}$ m. The analysis uses (6.3) with $M = 50$, the number of actual uniform gratings, but 50 phase shift matrices given by (6.8) are inserted. The result is shown in Figure 6-17. The peak reflection has increased and could possibly be increased further by using more than 50 uniform sections, however this is probably not worth pursuing. Spectra such as Figure 6-17, which resembles a comb filter, can be achieved by using gratings with no phase shift between layers in a sampled grating configuration. Figure 6-18 shows the spectrum when 50 uniform gratings, each described exactly by Table 7-2 so there is no phase shift between layers now, are placed in series. A nongrating section with $\Delta z = 1\times10^{-3}$ m is placed after every uniform grating section, to the less-positive-z side, so there are 50 in all. (The non-grating section after the last uniform grating section, that is on the extreme less-positive-z end, doesn't affect the power reflectivity and could be omitted.) In other words, the situation is the same as for Figure 6-17 but now the gratings have no phase shift between layers. With only 50 sections the peak level in figure 6-18 equals one.

An example of a useful sampled filter is shown in Figures 6-19a and 6-19b. It consists of 50 uniform gratings with the parameters listed in Table 6-3, spaced 1.8 mm apart. Note that they have no phase shift between layers. The unperturbed waveguide is the same as always in this chapter – its parameters are given in Figure 6-2 and Table 6-1. Figure 6-19a uses the same wide range of λ_o as Figures 6-14 through 6-18. Figure 6-19b shows a much narrower range of λ_o centered on $\lambda_o = 1.3\mu$ m, revealing new details. This filter can be used as a comb filter or a wavelength reference standard for dense wavelength-division multiplexed systems. More on sampled gratings can be found in [1], [14], and [15] for more on sampled gratings. [5] describes a fabrication technique for sampled gratings in planar waveguides.

Table 6-3 Parameters for Grating Sections in Figure 6-18

$\Delta z = 200\mu\text{m}$
$\frac{d\phi_{l1}(z)}{dz} = 0$
$\alpha = 0.0369$
$\Delta\phi_{l2} = \Delta\phi_{l3} = \Delta\phi_{l4} = 0$
$v = 1$
$f(z) = 1$
$\Lambda = 4.4807x10^{-7}$ m
$\sigma \approx 944.2$

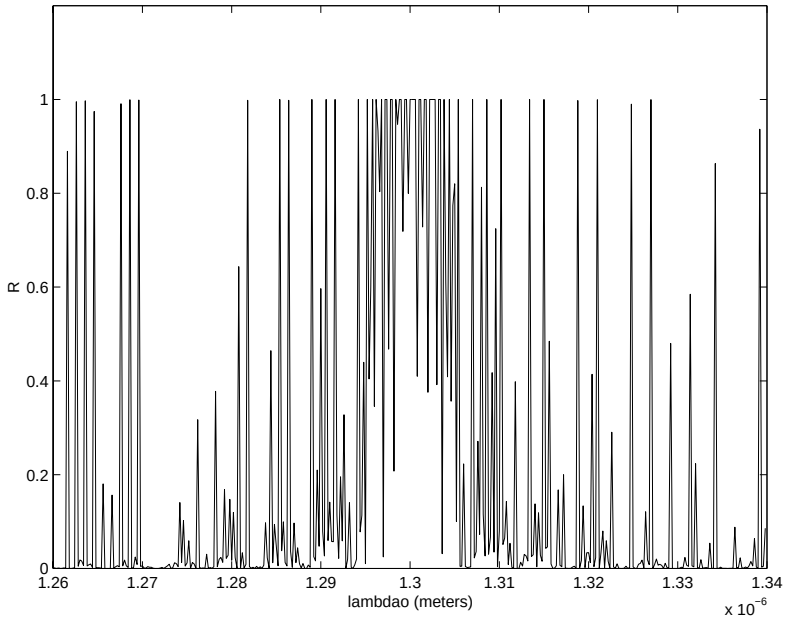

Figure 6-18 Reflectivity for 50 uniform grating sections with $\Delta z = 1\times 10^{-4}$ m and phase shift between layers equal 0, spaced $\Delta z = 1\times 10^{-3}$ m apart

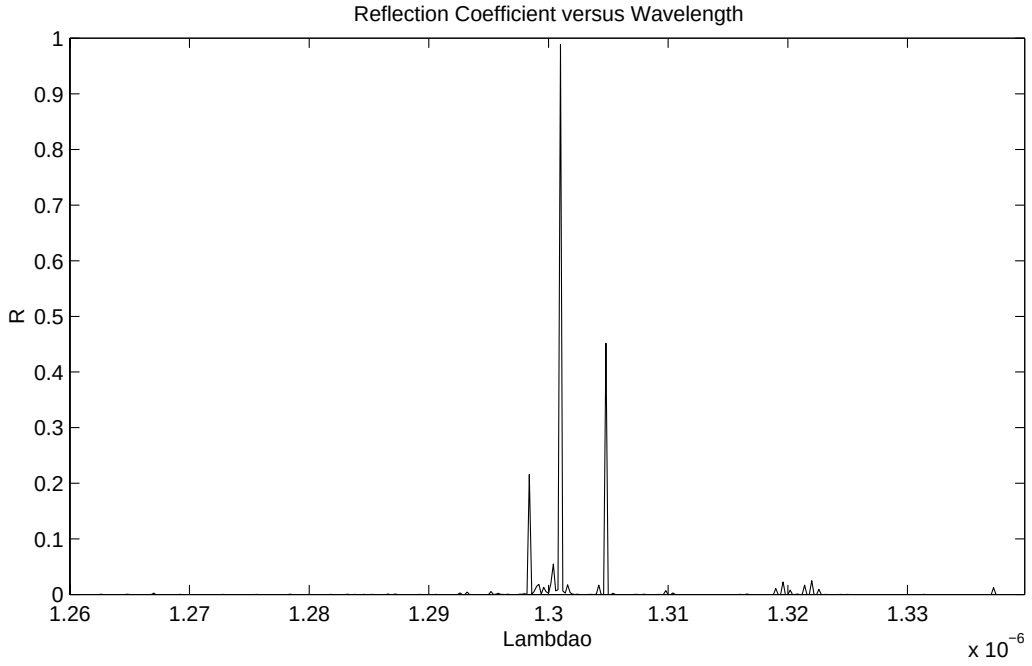

(a)

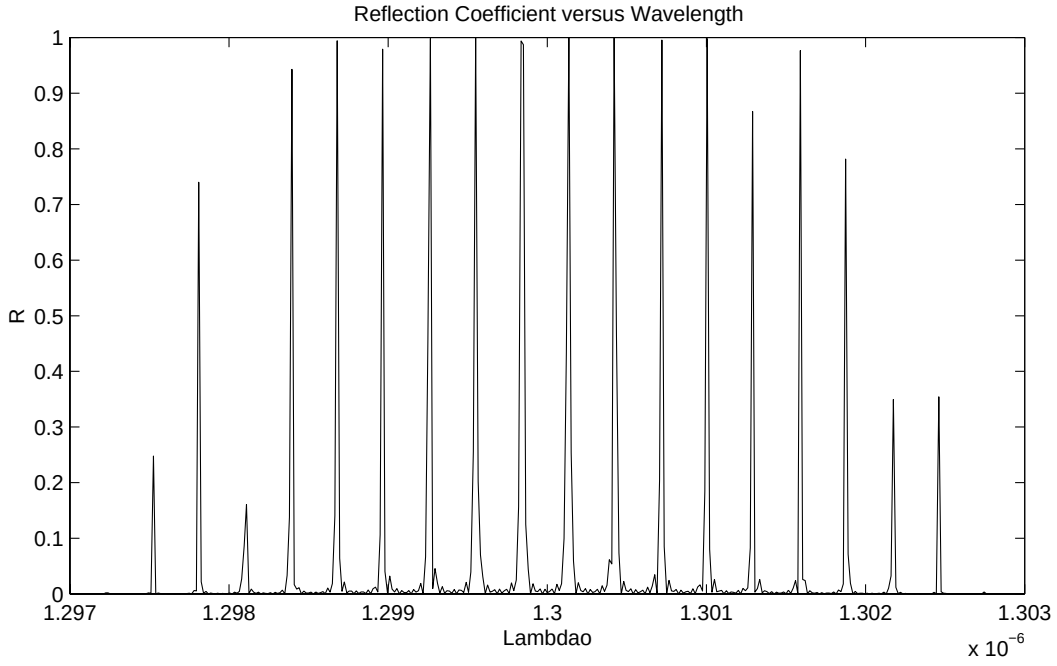

(b)

Figure 6-19 Reflectivity for 50 uniform grating sections described by Table 6-3, spaced $\Delta z = 1.8 \times 10^{-3}$ m apart (a) over the same wide range of λ_o as Figures 6-14 through 6-18 (b) over a narrower range of λ_o

Chapter 7

Gratings in Multilayer Waveguides with Different Layers Apodized by Different Functions

7.1 Introduction

The spectral response characteristics of gratings can be controlled by shaping the profile of the index modulation along the z-axis. This process is called apodization. Gratings are fabricated by illuminating the planar waveguide through the top with two intersecting coherent ultraviolet light beams. They interfere, producing a periodic interference pattern that writes a corresponding periodic grating. The grating is apodized by controlling the irradiation dose spatially. For a planar waveguide described by (2.1), the index perturbation could take the form given in (5.1). Since the ultraviolet light beams would penetrate all layers, the apodizing function $f(z)$ would be the same in every layer and the amplitudes $\overline{\Delta n_{l1}}, \overline{\Delta n_{l2}}, \overline{\Delta n_{l3}}$ and $\overline{\Delta n_{l4}}$ would obey (3.2). Usually, for single or mutli-layer gratings where the perturbation in a layer is as in (5.1), the grating is modeled using a function $f(z)$ for which the peak value is unity. Gratings fabricated using most standard methods are modeled using $v = 1$. Hence, if the peak value of $f(z)$ is unity, the amplitudes $\overline{\Delta n_{l1}}, \overline{\Delta n_{l2}}, \overline{\Delta n_{l3}}$ and $\overline{\Delta n_{l4}}$ represent one half of the peak value of the perturbation $\Delta n(x, z)$ in the respective layers. The function $f(z)$ modeling most gratings is non-negative for all z since the intensity of light is never negative. Gratings fabricated using standard techniques are modeled using $\Delta\phi_{l2} = \Delta\phi_{l3} = \Delta\phi_{l4} = 0$.

Techniques exist for fabricating gratings that can be modeled by (5.1) with "1+" term eliminated from every layer. The gratings that have actually been fabricated, as described in the literature [17] [18], have been photoimprinted in waveguides that are different than (2.1). The form of the gratings in a layer for the class of gratings considered here is as in a layer of (5.1) with "1+" deleted. For these gratings it is said the "dc" index change equals zero. Since gratings of this type are also fabricated by illuminating the waveguide with ultraviolet light beams that penetrate all layers, it is still true that in (5.1) the apodizing function $f(z)$ is the same in every layer and the

amplitudes $\overline{\Delta n_{l1}}, \overline{\Delta n_{l2}}, \overline{\Delta n_{l3}}$ and $\overline{\Delta n_{l4}}$ obey (3.2). Now, if $f(z)$ is negative over some z, it may be replaced by $|f(z)|$ if $\phi_{l1}(z)$ is replaced by $\phi_{l1}(z)+\pi$ for all z over which $f(z)$ is negative. However, as in the non-zero "dc" index change case, $f(z)$ is non-negative for all z unless a special technique is employed in fabricating the grating.

It is not actually possible to fabricate gratings with zero "dc" index change because the intensity of the imprinting light is always non-negative. However, such gratings are still considered for the following reason. It is possible to fabricate gratings for which the "dc" index change is constant in every layer. That is, a grating can actually be fabricated with the perturbation given by (5.1) with "1+" deleted from every layer and with a different constant added to every layer. This involves one of two known techniques as explained in Section 7.5. In layer x, $\Delta n(x,z)$ is given by

$$\Delta n_{lx}(z) = \overline{\Delta n_{lx}}\, f(z) v \cos\left(\frac{2\pi}{\Lambda} z + \phi_{lx}(z)\right) + \Delta n_{lx\,"dc"}$$

where $\Delta n_{lx\,"dc"}$ is a constant $\geq \overline{\Delta n_{lx}} \max\{f(z)\} v$. The constants $\Delta n_{lx\,"dc"}$ obey (3.2) along with the amplitudes $\overline{\Delta n_{lx}}$. The coupled-wave equations (5.5a) and (5.5b) still apply to the zero "dc" and constant "dc" cases as well as the definition of K given by (5.4c). However, the definition of σ given by (5.4b) no longer applies in either case. In the zero "dc" case σ equals zero for all λ_o, while in the constant "dc" case it is easily seen that sigma is given by

$$\sigma = \frac{\omega \varepsilon_o}{2} \left\{ \begin{array}{l} n_1 \Delta n_{l1\,"dc"} \int_{-a_1}^{a_1} \hat{\mathbf{e}}_1^{\,*} \cdot \hat{\mathbf{e}}_1 dx + 2 n_2 \Delta n_{l2\,"dc"} \int_{a_1}^{a_2} \hat{\mathbf{e}}_1^{\,*} \cdot \hat{\mathbf{e}}_1 dx \\ + 2 n_3 \Delta n_{l3\,"dc"} \int_{a_2}^{a_3} \hat{\mathbf{e}}_1^{\,*} \cdot \hat{\mathbf{e}}_1 dx + 2 n_4 \Delta n_{l4\,"dc"} \int_{a_3}^{\infty} \hat{\mathbf{e}}_1^{\,*} \cdot \hat{\mathbf{e}}_1 dx \end{array} \right\}. \qquad (7.1)$$

That is, σ is independent of z. The coupled-mode equations (5.7a) and (5.7b) and (5.8a), (5.8b), (5.9), and (5.10) still apply if the definition of σ is altered according to the situation as described, since they are derived from (5.5a) and (5.5b). When σ is independent of z, the reflectivity spectrum is nearly the same as when σ equals zero, only shifted to lower wavelengths as can be seen by examining (5.9) and (5.10). The z-independent σ typically varies by less than 2% over the range of λ_o for which the

reflectivity is non-negligible and is typically $1/10$ of 1% of the value of β. The shift is such that the β values are reduced by σ, so β plus σ in the constant "dc" case equals β in the zero "dc" case. The field $\hat{\mathbf{e}}_1$ changes little with such a small change in free-space wavelength, so K changes little after the shift.

For perturbations taking the form given in (5.1), the coupled wave equations were presented in chapter 5 and a method for computing the spectra, namely the matrix method, was presented in chapter 6. The coupled wave equations and the technique for computing the spectra are easily extended to the zero "dc" index change case as described in the preceding paragraph.

If the perturbation described by (5.1) is modified by replacing $f(z)$ in layer x with $f_{lx}(z)$ so every layer has a different apodizing function, and by using $\phi_{lx}(z)$ in layers x, $x \neq 1$, instead of $\phi_{l1}(z) + \Delta\phi_{lx}$, the analyses in chapters 5 and 6 does not apply without modifications. In the next section, an analysis of the modified perturbation is presented. As before, the "dc" index change may or may not equal zero.

7.2 Analysis of Perturbation with Different Apodizing Function for Every Layer

To summarize the previous section, this thesis considers four types of nonuniform gratings. The first has the perturbation given by (5.1), and the second has the perturbation given by (5.1) without the "1+" term in the layers. The third has a perturbation that takes the form given by

$$\Delta n(x,z) = \begin{cases} \Delta n_{l1}(z) = \overline{\Delta n_{l1}} f_{l1}(z)\left[1 + v\cos\left(\dfrac{2\pi}{\Lambda} z + \phi_{l1}(z)\right)\right], & |x| < a_1 \\ \Delta n_{l2}(z) = \overline{\Delta n_{l2}} f_{l2}(z)\left[1 + v\cos\left(\dfrac{2\pi}{\Lambda} z + \phi_{l2}(z)\right)\right], & a_1 < |x| < a_2 \\ \Delta n_{l3}(z) = \overline{\Delta n_{l3}} f_{l3}(z)\left[1 + v\cos\left(\dfrac{2\pi}{\Lambda} z + \phi_{l3}(z)\right)\right], & a_2 < |x| < a_3 \\ \Delta n_{l4}(z) = \overline{\Delta n_{l4}} f_{l4}(z)\left[1 + v\cos\left(\dfrac{2\pi}{\Lambda} z + \phi_{l4}(z)\right)\right], & a_3 < |x| < a_4, \end{cases} \tag{7.2}$$

while the fourth has a perturbation that takes the form given by (7.2) without the "1+" term in the layers. Regardless of whether (5.1) or (7.2) applies in the case at hand, it is

said that with or without the "1+" the gratings have a non-zero or zero "dc" index change, respectively.

The rest of this section considers gratings having a perturbation strictly taking the form of (7.2) unless otherwise noted. Equations (5.2a) and (5.2b) still apply where

$$C_{11}(z)=\frac{\omega\varepsilon_o}{2}\left\{\begin{aligned}&n_1\overline{\Delta n_{l1}}\,f_{l1}(z)\left[1+v\cos\left(\frac{2\pi}{\Lambda}z+\phi_{l1}(z)\right)\right]\int_{-a_1}^{a_1}\hat{\mathbf{e}}_1^{\,*}\cdot\hat{\mathbf{e}}_1\,dx\\&+2n_2\overline{\Delta n_{l2}}\,f_{l2}(z)\left[1+v\cos\left(\frac{2\pi}{\Lambda}z+\phi_{l2}(z)\right)\right]\int_{a_1}^{a_2}\hat{\mathbf{e}}_1^{\,*}\cdot\hat{\mathbf{e}}_1\,dx\\&+2n_3\overline{\Delta n_{l3}}\,f_{l3}(z)\left[1+v\cos\left(\frac{2\pi}{\Lambda}z+\phi_{l3}(z)\right)\right]\int_{a_2}^{a_3}\hat{\mathbf{e}}_1^{\,*}\cdot\hat{\mathbf{e}}_1\,dx\\&+2n_4\overline{\Delta n_{l4}}\,f_{l4}(z)\left[1+v\cos\left(\frac{2\pi}{\Lambda}z+\phi_{l4}(z)\right)\right]\int_{a_3}^{\infty}\hat{\mathbf{e}}_1^{\,*}\cdot\hat{\mathbf{e}}_1\,dx\end{aligned}\right\}. \tag{7.3}$$

Using the expansion

$$\cos\left(\frac{2\pi}{\Lambda}z+\phi_{l1}(z)\right)=\frac{e^{j\left(\frac{2\pi}{\Lambda}z+\phi_{l1}(z)\right)}+e^{-j\left(\frac{2\pi}{\Lambda}z+\phi_{l1}(z)\right)}}{2}, \tag{7.4}$$

$C_{11}(z)$ can be written as

$$\begin{aligned}C_{11}(z)=\sigma(z)&+e^{j\frac{2\pi}{\Lambda}z}\left[K_{l1}(z)e^{j\phi_{l1}(z)}+K_{l2}(z)e^{j\phi_{l2}(z)}+K_{l3}(z)e^{j\phi_{l3}(z)}+K_{l4}(z)e^{j\phi_{l4}(z)}\right]\\&+e^{-j\frac{2\pi}{\Lambda}z}\left[K_{l1}(z)e^{-j\phi_{l1}(z)}+K_{l2}(z)e^{-j\phi_{l2}(z)}+K_{l3}(z)e^{-j\phi_{l3}(z)}+K_{l4}(z)e^{-j\phi_{l4}(z)}\right]\end{aligned} \tag{7.5}$$

where

$$K_{l1}(z)=\frac{\omega\varepsilon_o}{4}n_1\,\overline{\Delta n_{l1}}\;f_{l1}(z)v\int_{-a_1}^{a_1}\hat{\mathbf{e}}_1^{\,*}\cdot\hat{\mathbf{e}}_1\,dx \tag{7.6a}$$

$$K_{l2}(z)=\frac{\omega\varepsilon_o}{2}n_2\,\overline{\Delta n_{l2}}\;f_{l2}(z)v\int_{a_1}^{a_2}\hat{\mathbf{e}}_1^{\,*}\cdot\hat{\mathbf{e}}_1\,dx \tag{7.6b}$$

$$K_{l3}(z)=\frac{\omega\varepsilon_o}{2}n_3\,\overline{\Delta n_{l3}}\;f_{l3}(z)v\int_{a_2}^{a_3}\hat{\mathbf{e}}_1^{\,*}\cdot\hat{\mathbf{e}}_1\,dx \tag{7.6c}$$

$$K_{l4}(z)=\frac{\omega\varepsilon_o}{2}n_4\,\overline{\Delta n_{l4}}\;f_{l4}(z)v\int_{a_3}^{\infty}\hat{\mathbf{e}}_1^{\,*}\cdot\hat{\mathbf{e}}_1\,dx \tag{7.6d}$$

and

$$\sigma(z)=\frac{\omega\varepsilon_o}{2}\left[\begin{array}{l} n_1\overline{\Delta n_{l1}}\,f_{l1}(z)\int_{-a_1}^{a_1}\hat{\mathbf{e}}_1^{\,*}\cdot\hat{\mathbf{e}}_1\,dx+2n_2\overline{\Delta n_{l2}}\,f_{l2}(z)\int_{a_1}^{a_2}\hat{\mathbf{e}}_1^{\,*}\cdot\hat{\mathbf{e}}_1\,dx \\ +2n_3\overline{\Delta n_{l3}}\,f_{l3}(z)\int_{a_2}^{a_3}\hat{\mathbf{e}}_1^{\,*}\cdot\hat{\mathbf{e}}_1\,dx+2n_4\overline{\Delta n_{l4}}\,f_{l4}(z)\int_{a_3}^{\infty}\hat{\mathbf{e}}_1^{\,*}\cdot\hat{\mathbf{e}}_1\,dx \end{array}\right] \qquad (7.7)$$

$$=\frac{2}{v}\left[K_{l1}(z)+K_{l2}(z)+K_{l3}(z)+K_{l4}(z)\right].$$

Equation (7.5) is the same as (5.4a) with

$$|K(z)|e^{j\angle K}e^{j\phi_{l1}(z)}\xrightarrow{\text{replaced by}}K_{l1}(z)e^{j\phi_{l1}(z)}+K_{l2}(z)e^{j\phi_{l2}(z)}+K_{l3}(z)e^{j\phi_{l3}(z)}+K_{l4}(z)e^{j\phi_{l4}(z)}$$
$$=K_{SA}(z)=|K_{SA}(z)|e^{j\angle K_{SA}(z)} \qquad (7.8)$$

and with σ newly defined by (7.7). In chapter 5, the variable $\angle K$ is a constant, and the magnitude of K and the real variable σ are proportional to $f(z)$ as is seen by examining (5.4b) and (5.4c). In this section, however, σ is not proportional to $|K_{SA}(z)|$, rather

$$\sigma\geq\frac{2}{v}|K_{SA}(z)|, \qquad (7.9)$$

which will be the basis of behavior that is unique to the gratings under consideration. It is seen that the coupled-mode equations (5.5a) and (5.5b) and, consequently, the coupled-mode equations in the alternate form given by (5.7) through (5.10) and the matrix approach to solving them apply in the case at hand if the substitutions are made:

$$|K(z)|\longrightarrow|K_{SA}(z)| \qquad (7.10a)$$

$$\phi_{l1}(z)+\angle K\longrightarrow\angle K_{SA}(z) \qquad (7.10b)$$

$$\sigma\ \ (5.4b)\longrightarrow\frac{2}{v}\left[K_{l1}(z)+K_{l2}(z)+K_{l3}(z)+K_{l4}(z)\right]. \qquad (7.10c)$$

Furthermore, given a grating design with perturbation described by (5.1), a grating design with perturbation given by (7.2) having nearly the same spectral response is achieved if

$$|K(z)|=|K_{SA}(z)| \qquad (7.11a)$$

and

$$\hat{\sigma}(z)\,(\text{Section 5.3})=\hat{\sigma}(z)\,(\text{Section 7.2})$$

$$\begin{aligned}&\delta+\sigma(z)-\frac{1}{2}\frac{d\phi_{l1}(z)}{dz}\quad\text{(Section 5.3)}\\&=\delta+\frac{2}{v}\left[K_{l1}(z)+K_{l2}(z)+K_{l3}(z)+K_{l4}(z)\right]-\frac{1}{2}\frac{d\angle K_{SA}(z)}{dz}\quad\text{(Section 7.2).}\end{aligned}\tag{7.11b}$$

Exact equality in (7.11) can only be achieved at a single wavelength λ_o since $\sigma(z)$ (Section 5.3), $\frac{2}{v}\left[K_{l1}(z)+K_{l2}(z)+K_{l3}(z)+K_{l4}(z)\right]$, $|K(z)|$ (Section 5.3), $|K_{SA}(z)|$, and $\angle K_{SA}(z)$ vary by up to a few percent over the range of wavelengths of interest.

The components of (7.5) were parsed and paired with the components of (5.4a) to produce (7.10a,b,c). In equation (7.10b), $e^{j\angle K}$, where $\angle K$ = constant, has been lumped with $\phi_{l1}(z)$. However, there is no problem associated with the angle of K according to the following reasoning. If, in equations (5.7a) and (5.7b),

$$|K|e^{j\angle K}\xrightarrow{\text{replace by}}|K|e^{j(\angle K-A)}$$

$$e^{j\phi_{l1}(z)}\xrightarrow{\text{replace by}}e^{j(\phi_{l1}(z)+A)}$$

the angle of K decreases while $\hat{\sigma}$ is unaffected. The solutions to (5.7a) and (5.7b) are unaltered, as seen by inspection of these two equations and (5.8a) and (5.8b), except that the angle of $R(z)$ decreases by $A/2$ and the angle of $S(z)$ increases by $A/2$. Inspection of (6.1) and (6.2) confirms that R(z) and S(z) are unaffected except as noted. It is seen that, using $A=\angle K$, $|K|e^{j\angle K}$ may be substituted with $|K|$ and $e^{j\phi_{l1}(z)}$ with $e^{j(\phi_{l1}(z)+\angle K)}$ in (5.4a) and (5.7a,b) without affecting the solution for power reflectivity or delay time (see Section 5.3.)

Gratings of type 4, using the label given in the first paragraph of this section, are just as easily modeled using the matrix approach as gratings of type 3. As explained above, the matrix approach is extended to type 3 gratings by making the substitutions given by (7.10a), (7.10b), and (7.10c). For type 4 gratings, the same substitutions are made except, instead of (7.10c), σ is replaced with zero.

Fabricating a perturbation taking the form of (7.2) is surely possible in a planar waveguide, that is, in an optical integrated circuit, but might not be possible in a fiber using existing techniques. Some thoughts on fabrication are presented in Section 7.5.

In the next sections, several designs using the old form of perturbation (5.1) are presented, and equivalent designs using the modified perturbation that might be easier to fabricate are proposed and analyzed. The first design using the old perturbation, presented in Section 7.4, has a Guassian apodizing function and zero "dc" index change. To facilitate an understanding of this design, a similar uniform grating and a similar non-zero "dc" grating are examined.

7.3 Setting the Period of an Apodized Grating

For all of the example apodized gratings in this chapter with a perturbation taking the form of (5.1), (6.5) is used to calculate the period of the grating, Λ. For a given value of Λ, the value of λ_o that satisfies (6.5) varies with z. For the bell-shaped, symmetric about $z = 0$, apodizing functions used in this thesis, the reflectivity spectrum is symmetric about a value of λ_o, λ_{o_D}, where the peak value also occurs. λ_{o_D} is determined by solving (6.5) at $z = 0$ for λ_o, for the given value of Λ. This indicates that the center of the grating is strongly reflective at λ_{o_D}. (6.5) is the equation determining the λ_o where the peak reflectivity occurs for a uniform grating. It is easily derived from the expression for the reflectivity of a uniform grating appearing just above (6.5). Modeling the grating by dividing it into M uniform sections as in the matrix approach, when the apodizing function is bell shaped, the center section has its peak at λ_{o_D}. Alternatively, given λ_{o_D}, Λ is found by using $z = 0$ in (6.5). In (6.5), λ_o is set equal to λ_{o_D} and the values of $\sigma(\lambda_{o_D})$ and $\frac{d\phi_{l1}(z)}{dz}$ are evaluated at z=0, that is, at the center of the grating. Λ is then computed. As explained above, if the “dc” index change is zero for the grating, $\sigma = 0$.

For all of the example apodized gratings in this chapter with a perturbation taking the form of (7.2), the same equation, (6.5), is used to calculate the period of the grating, Λ. First, however, the substitutions (7.10b) and (7.10c) are made in (6.5), unless the “dc” index change is zero for the grating, in which case (7.10b) is used but σ equals zero. The derivative of $\angle K_{SA}(z)$ and $\frac{2}{v}\left[K_{l1}(z)+K_{l2}(z)+K_{l3}(z)+K_{l4}(z)\right]$, if applicable,

are evaluated at $z = 0$ and $\lambda_o = \lambda_{o_D}$. With (6.5) satisfied at $z = 0$ at $\lambda_o = \lambda_{o_D}$, the center of the grating is strongly reflective at λ_{o_D}.

7.4 Guassian Apodized Grating with Zero "dc"

The reflectivity spectrum of a uniform grating written in the waveguide described by Table 7-1 is shown in Figure 7-1. All gratings discussed in this chapter will be written in this waveguide. It is impossible to write gratings in layers $a_1 < |x| < a_2$ and $a_3 < |x|$ since $n = n_{\mathrm{SiO2}}$ there. For the uniform grating at hand, $L = 10$ mm and the perturbation is described by (5.1) with $f(z) = 1$, $v = 1$, $\phi_{l1}(z) =$ arbitrary constant, and $\Delta\phi_{l2} = \Delta\phi_{l3} = \Delta\phi_{l4} = 0$. Using the notation of Section 5.2, the "ac" coupling coefficient K equals 2026.8 and the "dc" coupling coefficient σ equals 4053.7 at $\lambda_o = 1.55\,\mu$m. The coupling coefficients vary nearly linearly with λ_o and are 0.09 % larger at $1.551\,\mu$m, the largest wavelength plotted, and 0.09 % smaller at $1.549\,\mu$m, the smallest wavelength in the range of interest. These values of the coupling coefficient are achieved by setting $\alpha = 0.124038352$, producing $\overline{\Delta n_{l1}} = \overline{\Delta n_{l3}} = 0.0013576494$. Since the coupling coefficients are proportional to α, they are easily scaled by multiplying α by a constant. The index perturbation $\Delta n(x, z)$ equals $2\overline{\Delta n_{l1}}$ at the peaks in the layers containing gratings. The largest $\Delta n(x, z)$ that has been achieved in practice is 0.01 [2] [10]. The period of the gratings, Λ, determines λ_{o_D}, the free-space wavelength at which the peak reflectivity occurs and about which the reflectivity spectrum is symmetric,

Table 7-1 Parameters of Waveguide Used Throughout Chapter 7

$n_1 = n_3 = 1.45785587$
$n_2 = n_4 = n_{\mathrm{SiO2}} = 1.44691047$
$a_1 = 9.3233082707 \times 10^{-7}$ m
$a_2 = 1.0488721805 \times 10^{-6}$ m
$a_3 = 1.8646616541 \times 10^{-6}$ m

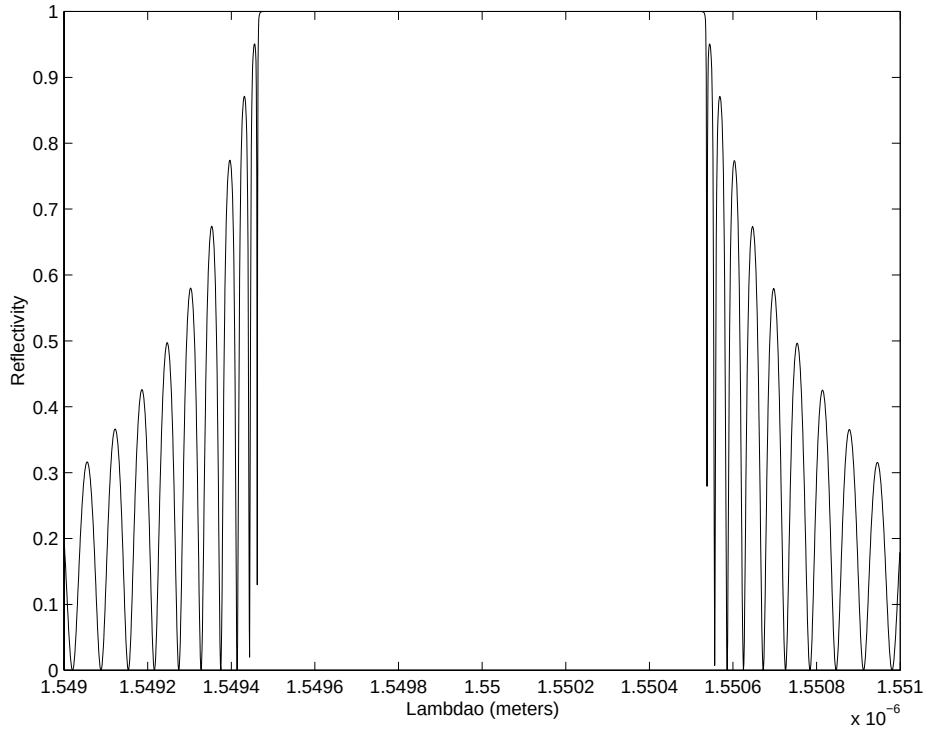

Figure 7-1 Reflectivity spectrum of the uniform grating in Section 7.4

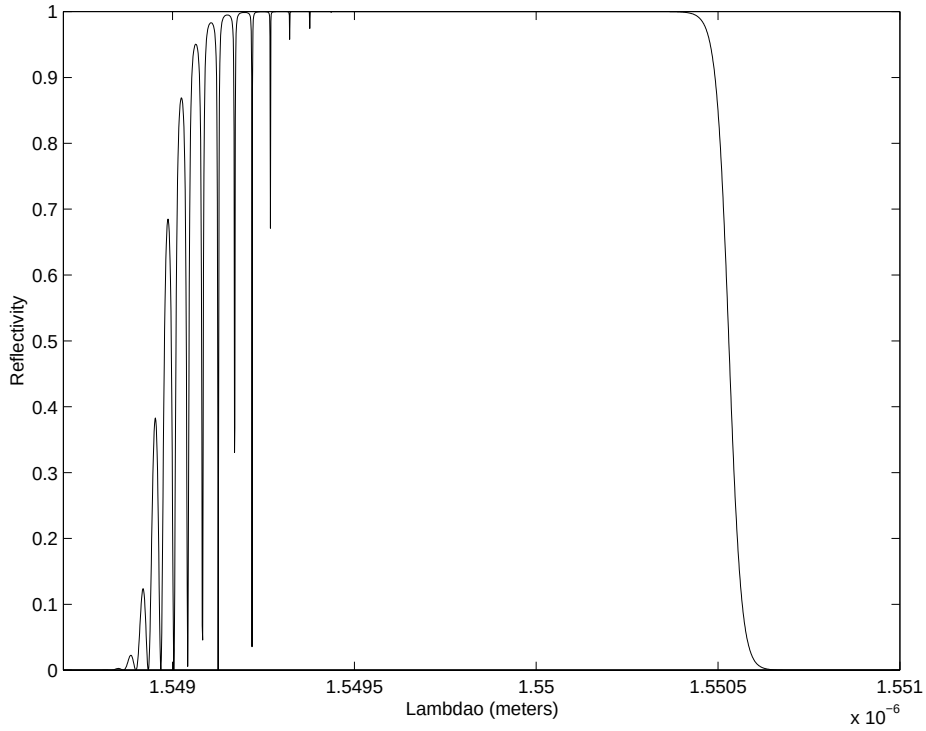

Figure 7-2 Reflectivity spectrum of a Guassian apodized, non-zero “dc” grating

according to equation (4.6) or (6.5) (equivalent since $\frac{d\phi_{l1}}{dz} = 0$ in the case at hand.) In the case at hand, $\Lambda = 5.331\times10^{-7}$ m, resulting in $\lambda_{o_D} = 1.55\,\mu$m.

The sidelobes in the spectrum in Figure 7-1, which are not desirable in applications like wavelength division multiplexing [2], can be suppressed by apodization. Figure 7-2 shows the reflectivity spectrum for a grating that is similar to the one in the preceding paragraph except that it is apodized by a Guassian function. All parameters are the same except: 1) the length $L = 60$ mm and 2) in (5.1) $f(z) = e^{\frac{-4\ln 2 z^2}{\text{FWHM}^2}}$ for $z \in [-L/2, L/2]$ where FWHM $= 10$ mm. FWHM stands for "full width half maximum". The quantities $\overline{\Delta n_{l1}}, \overline{\Delta n_{l2}}, \overline{\Delta n_{l3}}$, and $\overline{\Delta n_{l4}}$ are the same as before since α is the same as before and (3.2) still applies. Therefore, the shape of the profile of the index modulation is the same in every layer, but its weight in a layer depends on the refractive index.

The program used to calculate the spectrum for the grating at hand, as well as the uniform grating in the preceding paragraph, is called apodv2ErgDesGuass.m and is listed in Appendix E. It implements the matrix approach described in Chapter 6, dividing the grating into 200 uniform sections to generate Figure 7-2. This number of sections is sufficient, as a larger number produces the same spectrum to a high degree of accuracy. Of course, one uniform section is sufficient to generate Figure 7-1. The program first calculates Λ, then executes two nested "for" loops. The outer loop fixes λ_o. It then calculates $\max(\sigma)$ and $\max(K)$, using (5.4b) and (5.4c) with $f(z) = 1$, and δ, using (5.10). The inner loop steps through the uniform sections, which are numbered from 1 to 200 with the center of section x at $z = L/2 - x\Delta z + \Delta z/2$ where $\Delta z = L/200$. For each slice it calculates σ and K by multiplying $\max(\sigma)$ and $\max(K)$, respectively, by $f(z)$ evaluated at the center of the slice. Though not necessary in the cases at hand, the program can calculate $\frac{d\phi_{l1}(z)}{dz}$. For the current slice the quantities δ, σ, K, and $\frac{d\phi_{l1}(z)}{dz}$ are used to calculate $\mathbf{F}_i$, which is used to evaluate (6.1).

The period of the Guassian apodized, non-zero "dc" grating is computed as described in Section 7.3. Since $\sigma(\lambda_{o_D})$ at $z = 0$ equals $\sigma(\lambda_{o_D})$ at all z within $[-L/2, L/2]$ for the uniform grating, Λ equals 5.331×10^{-7} m once again.

The spectrum in Figure 7-2 is similar to that in Figure 7-1, except that it has no sidelobes on the long-wavelength side and very different sidelobes on the short wavelength side. The short-wavelength sidelobes arise because (6.5) is satisfied or nearly satisfied at the grating's edges for short wavelengths, indicating strong reflection. That is, (6.5) is nearly satisfied for a range of values of $\lambda_o < \lambda_{o_D}$, which have increased β compared to λ_{o_D}, near the grating's edges where σ is diminished. (6.5) is not satisfied at $z = 0$ for the shorter wavelengths, so at the center they are only weakly reflected. Thus, the edges of the grating act like a Fabry-Perot cavity at short wavelengths [1].

In order to eliminate the sidelobes on the short-wavelength side of the mainlobe, the "dc" index change is set to zero. All other parameters of the Guassian apodized grating remain the same, except $\Lambda = 5.3347\times10^{-7}$ m. All variables have the same values as before except σ, which now equals zero. The resulting spectrum is shown in dB as the solid line in Figure 7-3. This is a useful grating, which might be used in applications like wavelength division multiplexing.

Let us now design a grating with perturbation given by (7.2) having nearly the same spectral response as the solid line in Figure 7-3. Let $v = 1$ and retain "1+" in all the layers; that is, let the "dc" index change not equal zero. This is the easiest form of grating to fabricate as discussed in Section 7.5, although now the two layers containing gratings, layers 1 and 3, must somehow be apodized differently. For the grating with the response given by the solid line in Figure 7-3, at $\lambda_o = \lambda_{o_D}$

$$K(z) = f(z)\max\{K(z)\} = 2026.8e^{-\frac{4\ln 2 z^2}{\mathrm{FWHM}^2}} \quad \text{for } z = [-L/2, L/2]$$

A grating with perturbation given by (7.2) will have the same spectrum if

$$|K_{SA}(z)| = \left|K_{l1}(z)e^{j\phi_{l1}(z)} + K_{l3}(z)e^{j\phi_{l3}(z)}\right| = K(z)$$

$$2(K_{l1}(z) + K_{l3}(z)) = \text{arbitrary constant}$$

$$\angle K_{SA}(z) = 0\,.$$

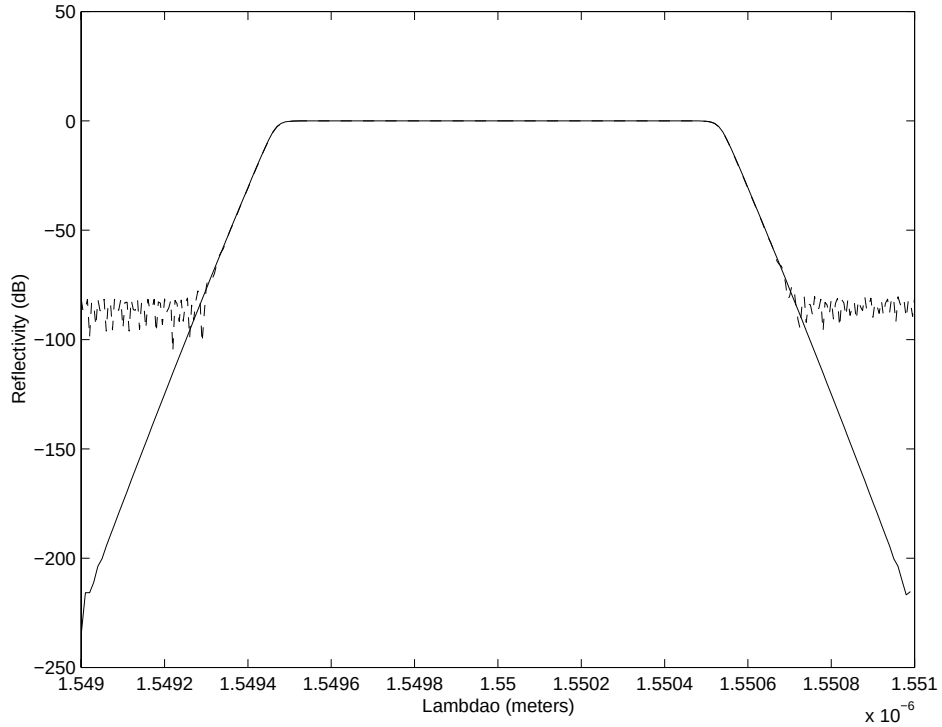

Figure 7-3 Reflectivity spectrum in dB of a Guassian apodized, zero "dc" grating (solid line) and a near equivalent two layer separately apodized grating (dashed line)

That $2\left(K_{l1}(z)+K_{l3}(z)\right)$ can equal a constant and produce the same spectrum as when it equals zero was demonstrated in Section 7.1. Setting $\phi_{l1}(z)=0$ and $\phi_{l3}(z)=\pi$ and insuring that neither $K_{l1}(z)$ nor $K_{l3}(z)$ is negative for any z, so $\Delta n(x,z)$ is not negative yields

$$K_{l1}(z)=\frac{K(z)}{2}+\frac{\max\{K(z)\}}{2}$$

$$K_{l3}(z)=\frac{\max\{K(z)\}}{2}-\frac{K(z)}{2}.$$

These equations can only be satisfied exactly at one value of λ_o; $\lambda_{o_D}=1.55\,\mu\text{m}$ is chosen. Having found $K_{l1}(z)$ and $K_{l3}(z)$, we compute:

$$\overline{\Delta n_{l1}}\,f_{l1}(z)=\frac{K_{l1}(z)}{\frac{\omega\varepsilon_o}{4}n_1\int_{-a_1}^{a_1}\hat{\mathbf{e}}_1^{\,*}\cdot\hat{\mathbf{e}}_1\,dx}$$

$$\overline{\Delta n_{l3}}\, f_{l3}(z) = \frac{K_{l3}(z)}{\frac{\omega\varepsilon_o}{2} n_3 \int_{a_2}^{a_3} \hat{\mathbf{e}}_1^{\,*} \cdot \hat{\mathbf{e}}_1 dx}$$

where we still use $\lambda_o = \lambda_{o_D}$. A program called OneLGuass2TwoLayer.m, listed in Appendix E, performs the conversion to the separately apodized design as discussed. Figure 7-4(a) shows $\Delta n(x,z)$ in layers 1 and 3 (it is the same in both layers) for the zero-"dc" Guassian apodized design which has the spectrum that the separately apodized design attempts to duplicate. The grating period is greatly exaggerated. Figure 7-4(b) shows the perturbation $\Delta n(x,z)$ in layer 1, i.e. for $-a_1 < x < a_1$, for the separately apodized design, and Figure 7-4(c) shows the perturbation in layer 3, i.e. for $a_2 < x < a_3$. The maximum $\Delta n(x,z)$ is less in Figure 7-4(a) than in 7-4(b) or (c). However, it should be considered that zero-"dc" designs are impossible to fabricate, so equivalent constant-"dc" designs are fabricated instead, as discussed in Section 7.1. The maximum $\Delta n(x,z)$ is still less, though not as much so, for the zero-"dc" Guassian design as it is actually implemented compared to the novel separately apodized design.

R for the separately apodized design is shown in dB as the dashed line in Figure 7-3. It nearly exactly coincides with the solid line representing R for the zero-"dc" Guassian apodized design over the wavelength range of significant reflectivity. It is seen that the spectrum for the separately apodized design quite closely duplicates the other. The spectrum for the separately apodized design was computed using a program called apod2LGuass.m, listed in Appendix E. Like apodv2ErgDesGuass.m, it first calculates Λ, then executes two nested "for" loops. As discussed in Section 7.3, 6.5 is used to calculate Λ after substituting $\frac{d\angle K_{SA}(z)}{dz}$ evaluated at $\lambda_o = \lambda_{o_D}$ and $z = 0$, i.e. zero, for $\frac{d\phi_{l1}(z)}{dz}$ and $2\left(K_{l1}\left(z=0,\lambda_{o_D}\right)+K_{l3}\left(z=0,\lambda_{o_D}\right)\right) = 2\max\left\{K\left(\lambda_{o_D}\right)\right\} = 2\times 2026.8$ for σ. The result is $\Lambda = 5.331\times 10^{-7}$ m. The outer loop fixes λ_o and computes $\int_{-a_1}^{a_1} \hat{\mathbf{e}}_1^{\,*} \cdot \hat{\mathbf{e}}_1 dx$, $\int_{a_2}^{a_3} \hat{\mathbf{e}}_1^{\,*} \cdot \hat{\mathbf{e}}_1 dx$, and δ. The inner loop steps through the uniform sections, which are

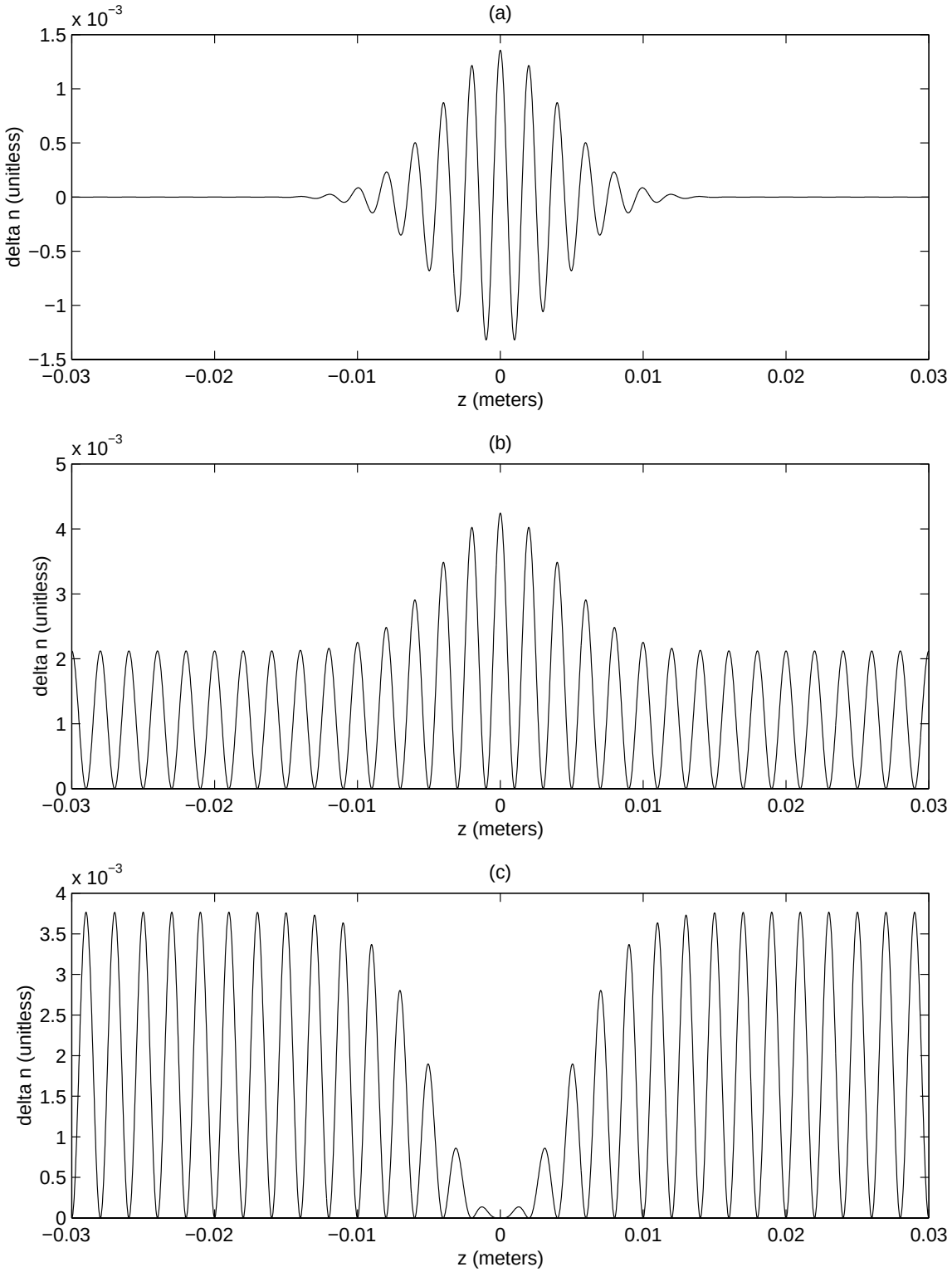

Figure 7-4 Index change (a) in layers 1 and 3 of the Guassian apodized, zero "dc" grating in Section 7-4 and in layers (b) 1 and (c) 3 of the near equivalent separately apodized design.

numbered from 1 to 200 with the center of section x at $z = L/2 - x\Delta z + \Delta z/2$ where $\Delta z = L/200$. For each slice it calculates $K_{l1}(z)$ and $K_{l3}(z)$ using the integrals evaluated by the outer loop and $\overline{\Delta n_{l1}} f_{l1}(z)$ and $\overline{\Delta n_{l3}} f_{l3}(z)$ computed by OneLGuass2TwoLayer.m. The inner loop then calculates σ, $|K_{SA}(z)|$, $\angle K_{SA}(z)$, and $\frac{d\angle K_{SA}(z)}{dz}$. For the current slice the matrix $\mathbf{F}_i$ is computed, which is used to evaluate (6.1).

7.5 Comparison of the Difficulty in Fabricating the Equivalent Designs

This section compares the difficulty in fabricating the two designs in Section 7.4 having nearly the same useful reflectivity spectrum: the conventional zero-"dc" Guassian apodized design and the novel separately apodized design. A variety of methods for grating fabrication have been presented in the literature. One of the earliest is called the transverse holographic technique [2]. Two intersecting coherent UV light beams irradiate the fiber or planar waveguide from the side or top, respectively. An interference pattern is formed. It writes a corresponding periodic grating in germania-doped photosensitive layers of the waveguide. If the UV light beams are nonuniform, apodization is achieved [10] [17]. The induced "ac" index change varies in response to the envelope of the interfering laser beams. This holds for the "dc" change as well [10], so the total index change, as for the light intensity itself, is always non-negative. In other words, the perturbation takes the form of (5.1) with "1+" retained in the layers (so $\Delta n(x,z)$ is always non-negative) and $\Delta\phi_{l2} = \Delta\phi_{l3} = \Delta\phi_{l4} = 0$.

A much simpler method for grating fabrication is called the phase mask technique. A flat slab of silica glass, which is transparent to UV light, is made into a phase mask. Parallel grooves are etched into one of the flat surfaces, forming a one dimensional periodic surface relief structure [2]. The shape of the profile approximates a periodic square wave. The etched surface is placed nearly in contact with the waveguide, with its grooves aligned normal to the waveguide's axis [19]. A UV light beam, which is at normal incidence, passes through the phase mask and is diffracted by the relief structure into the 0, +1, and –1 diffracted orders. However, the amplitude of the surface-relief pattern is chosen to reduce the amount of light in the zero-order to less than 5%

[19]. The +1 and –1 diffracted order beams interfere, producing an interference pattern that photoimprints a grating into the waveguide [2]. The period of the grating is half the period of the phase mask relief pattern, independent of the wavelength of the UV light incident on the mask. The phase mask technique has several advantages over the holographic technique. Alignment of the fiber is easier and the stability requirements on the UV laser beam are reduced [2].

In the phase mask technique, normally the phase mask has constant diffraction efficiency, but the grating can be apodized by varying the exposure time along the length of the grating [17]. This can be achieved through a double exposure [20] [21] or by scanning a writing beam [22]. Apodization can also be achieved by varying the irradiation dose along the length of the grating using a shadow mask [18]. In all of these techniques, a variation in the "dc" index change is induced.

Two methods for photoimprinting gratings with constant "dc" index perturbation have been presented in the literature. The method in [18] uses two exposures, the first of which is made using no phase mask, but a specially designed shadow mask. This first exposure, which is computer controlled, induces a purely "dc" index perturbation tailored to compensate for the variation in the "dc" index induced by the second exposure. In the second exposure, a phase mask and a different shadow mask are used simultaneously to imprint a perturbation with proportional "dc" and "ac" components. The total of the "dc" perturbation induced by the two exposures is uniform. The second method is described in [17]. A phase mask is used, but the groove width and/or depth is varied. This is possible since the phase mask can be manufactured under computer control [19] [23]. The intensity of the ± 1 order diffracted beams, which are responsible for the "ac" component of the induced perturbation and a proportional "dc" component, varies with the groove size. Simultaneously, the intensity of the zero-order transmitted light varies in an inverse fashion, so the total average UV fluence reaching the waveguide is uniform along the grating length [17]. The zero-order transmitted light photoinduces a purely "dc" index perturbation. The sum of the "dc" index changes induced by the 0 and ± 1 diffracted orders is uniform.

We are now prepared to compare the difficulty in fabricating the two designs in Section 7.4, the conventional zero-"dc" Guassian apodized design and the novel

separately apodized design. One of the methods for photoimprinting a constant "dc" index change described in the preceding paragraph can be used to fabricate a grating with virtually the same spectrum as the zero-"dc" Guassian apodized design (see Section 7.1). One of the methods for photoimprinting apodized gratings with varying, proportional, "dc" and "ac" index changes can possibly be used to fabricate the separately apodized design. Somehow, layer one must be apodized using a different function than for layer 3. This is almost certainly possible in a planar waveguide, that is, in an optical integrated circuit.

We are able to propose a fabrication technique for the separately apodized design and provide more of the details if the grating design approach is modified as follows. The "separately apodized" approach can work even if the regions of the waveguide that are separately apodized don't correspond to layers. The regions can correspond to any germanium-doped portions of the transverse cross-section as long as they occur simultaneously over the same range of z. In this case, the coupling coefficient $C_{11}(z)$ is the sum of integrals over the separate regions that are weighted by different functions of z, providing additional degrees of freedom to the design. The regions can be chosen so they correspond to halves of the waveguide separated by a vertical plane directed along the z-axis. More accurately, one region encompasses all $y > 0$, and the ranges of x corresponding to germanium doped layers, and the second region encompasses all $y < 0$, and the same ranges of x. Analyzing the grating might require a fields solution for finite width planar waveguides. A grating similar to the separately apodized design derived in Section 7.4 can then be fabricated as follows. First a phase mask is created with uniform groove size that phase shifts by π radians the gratings in one half of the planar waveguide relative to the other half. Phase masks are fabricated by scanning an ion beam that is focused on the surface of the substrate [17]. The implanted ion dose induces damage in the silica, delineating the groove pattern. After etching the surface in a solution of hydrofluoric acid in water, the groove pattern is uncovered. To phase shift one half of the groove pattern, the ion beam scan could be paused after progressing one half of the distance across the phase mask. The ion beam could then be stepped lengthwise one half of the period of the relief pattern before the scan is continued. Since the duty cycle of the relief pattern in profile is 50% [17], this step size corresponds to the

width of the groove. Using this phase mask, gratings could be fabricated by the following method:

1) One half of the waveguide is masked with an opaque mask.
2) The other half is exposed through the phase mask and a shadow mask that controls the irradiation dose. The photoimprinted gratings have varying, proportional, "ac" and "dc" index changes.
3) The other half of the waveguide is masked with an opaque mask.
4) The half not yet imprinted is exposed through the phase mask and a different shadow mask.

Alternatively, only one exposure would be required if a shadow mask divided into halves with different characteristics were available. Using this method to fabricate the separately apodized grating is almost as attractive as using the method involving a phase mask with variable diffraction efficiency to fabricate a constant-"dc" equivalent to the zero-"dc" Guassian apodized design. The novel method has the advantage of reproducibility, like the method using a phase mask with variable diffraction efficiency. For both methods, the variation of the index change depends on the design of the phase and shadow masks alone, and not, for example, on scanning speed. For photoimprinting a constant-"dc" grating, these two techniques are probably more attractive than the method involving two exposures, since the first exposure requires computer control.

In implementing a design that has a varying "dc" index change, however, the two-exposure method could be used, but not the method using a phase mask with variable diffraction efficiency. The novel method could also be used, since a separately apodized design with non-constant $\frac{2}{v}\left[K_{l1}(z)+K_{l2}(z)+K_{l3}(z)+K_{l4}(z)\right]$ that virtually duplicates the desired spectrum is readily obtained. An example is presented in the next section. A varying "dc" index change can be used to induce a chirp without actually varying the grating period, such as is achieved in the next section. The novel method might have an advantage in reproducibility over the two-exposure method. The novel method might be simpler and quicker as well since it could involve only one exposure and computer control is not required. A disadvantage of the novel method is that, as demonstrated in Section 7.4, a slightly larger index perturbation $\Delta n(x,z)$ is required. If the separately

apodized regions correspond to halves of the waveguide, the $\Delta n(x,z)$ is still larger than for the conventional zero-"dc" Guassian apodized design. Since $\max\{K_{l1}(z)\} = \max\{K(z)\}$ ($K_{r1}(z)$ would be more appropriate notation than $K_{l1}(z)$ since the region no longer corresponds to a layer) and the integral involved in $K_{l1}(z)$ is over half the width of the waveguide instead of the entire width as for $K(z)$, the peak $\Delta n(x,z)$ is twice as large.

Corrugating the boundary between layers of the waveguide produces the same effects as a perturbation of the form of (5.1). It is a form of gratings that predates the discovery of photosensitivity. However, the expressions that arise in calculating the reflectivity using coupled-mode theory are virtually the same as for (5.1). The fabrication technique is ion milling [24] [25], which is not as simple or flexible as techniques based on photosensitivity. For this reason, this type of gratings is obsolete. Apodization, which would entail varying the depth of the surface corrugations, has never been achieved to the knowledge of the author of this thesis. If it were possible, however, the separately-apodized approach could be extended to these gratings. Different boundaries would be apodized differently. A similar arrangement has been proposed in [26], where two surface corrugations are used that are unapodized but have different periods. Thus, we have another fabrication technique for the separately-apodized approach, but it requires control of the depth of the surface corrugations.

7.6 Raised-Cosine Apodized, Zero-"dc", Chirped Grating

Another useful grating design is presented, but for it, the novel fabrication method proposed in the preceding section has clearer advantages over the other suitable methods. The waveguide into which the gratings are imprinted is still given by Table 7-1. The perturbation is described by (5.1) with $v = 1$ and $f(z) = 0.5\left(1 + \cos\left(\frac{\pi z}{\text{FWHM}}\right)\right)$ where $\text{FWHM} = 0.01\,\text{m}$. The length $L = 2 * \text{FWHM} = 0.02\,\text{m}$. The "ac" coupling coefficient K varies with z as $1.0134\times10^{3} f(z)$ at $\lambda_o = 1.55\,\mu\text{m}$. This is achieved by $\alpha = 0.062019176$, resulting in $\overline{\Delta n_{l1}} = \overline{\Delta n_{l3}} = 6.7882\times10^{-4}$ (and $\overline{\Delta n_{l2}} = \overline{\Delta n_{l4}} = 0$.) The

design is zero-"dc", meaning "1+" is deleted from the layers in (5.1). Therefore, $\sigma = 0$. This design is chirped because $\frac{d\lambda_{o_D}}{dz} = -1\,\text{nm/cm}$, where $\frac{d\lambda_{o_D}}{dz}$ is related to $\frac{d\phi_{l1}(z)}{dz}$ by

$$\frac{d\phi_{l1}(z)}{dz} = \frac{-4\pi\,\bar{\beta}\,z}{\lambda_{o_D}{}^2}\frac{d\lambda_{o_D}}{dz}. \qquad (7.12)$$

A derivation of this equation begins by rearranging (6.5) into

$$\lambda_{o_D} = 2\bar{\beta}\left(\frac{1}{\Lambda} + \frac{1}{2\pi}\frac{d\phi_{l1}(z)}{dz}\right)^{-1} \qquad (7.13)$$

and differentiating. $\bar{\beta}\left(\lambda_o = \lambda_{o_D}\right)$ and λ_{o_D} vary with z slightly, but this variation is neglected in (7.12). Using $\bar{\beta}\left(\lambda_o = 1.55\,\mu\text{m}\right)$ and $\lambda_{o_D}\left(z = 0\right) = 1.55\,\mu\text{m}$ results in

$$\frac{d\phi_{l1}(z)}{dz} = 7.59880\times10^5\,z, \qquad z \in \left[-0.01\,\text{m}, 0.01\,\text{m}\right]. \qquad (7.14)$$

An arbitrary constant could be added to the RHS of (7.14), but its effect is removed on setting Λ. $\Delta\phi_{l2} = \Delta\phi_{l3} = \Delta\phi_{l4} = 0$ in (5.1). λ_{o_D} varies with z because it is defined as the λ_o that satisfies (6.5), and this equation has the $z-$dependent quantity $\frac{d\phi_{l1}(z)}{dz}$. The λ_{o_D} for a value of z indicates the λ_o that is strongly reflected at this z. However, we have also used the term λ_{o_D} to refer to the λ_o where the peak reflectivity occurs and about which the spectrum is approximately symmetric. For bell-shaped apodized gratings for which the profile of the index modulation is symmetric about the center of the grating at $z = 0$, the λ_{o_D} in this sense is found by evaluating (6.5) at $z = 0$. We desire the peak reflectivity to occur at $1.55\,\mu\text{m}$, so we use $\lambda_o = 1.55\,\mu\text{m}$ and $z = 0$ in (6.5), obtaining $\Lambda = 5.3347\times10^{-7}$ m.

The spectrum for this design is shown in dB as the solid line in Figure 7-5 (the solid and dashed lines virtually overlap). It was calculated using a program called apodv2ErgDesChirp.m, listed in Appendix E, that is similar in operation to apodv2ErgDesGuass.m. Once again, 200 slices are used. The solid line in Figure 7-6 shows the group delay calculated using (5.11). As discussed at the end of Chapter 5,

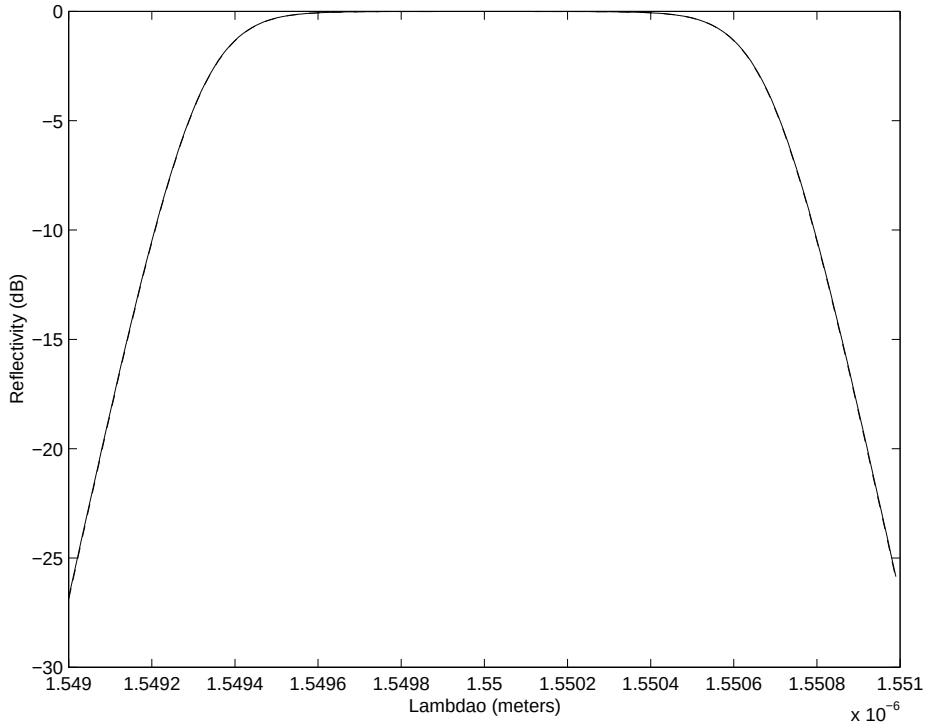

Figure 7-5 Reflectivity in dB of the variable-period chirped grating in Section 7-6 (solid line) and of the near equivalent 4 layer separately apodized design (indistinguishable dashed line)

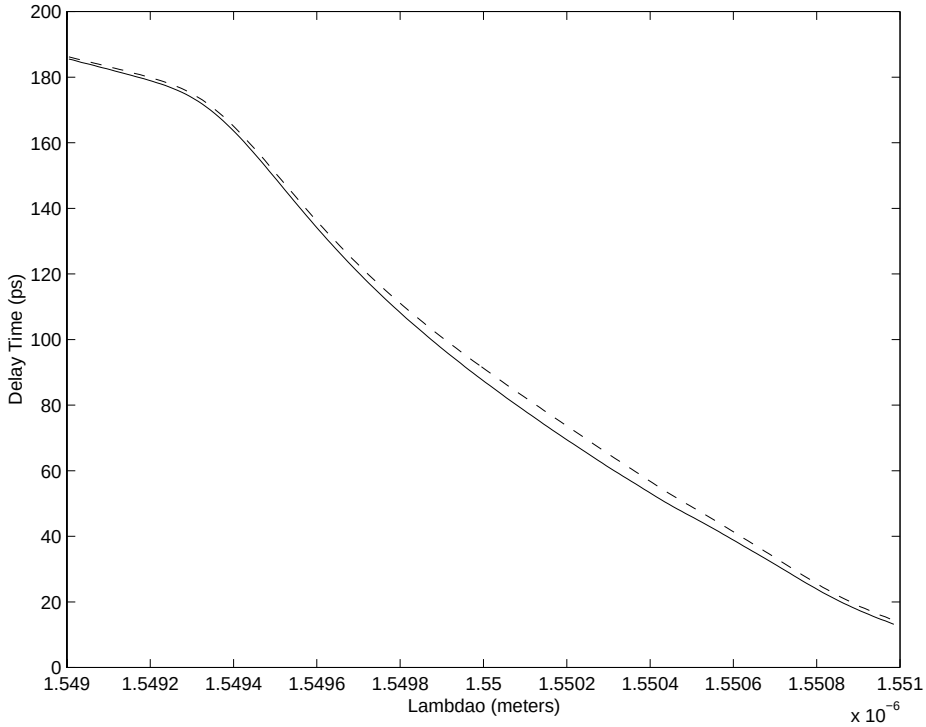

Figure 7-6 Delay time of the variable-period chirped grating in Section 7-6 (solid line) and of the near equivalent 4 layer separately apodized design (dashed line)

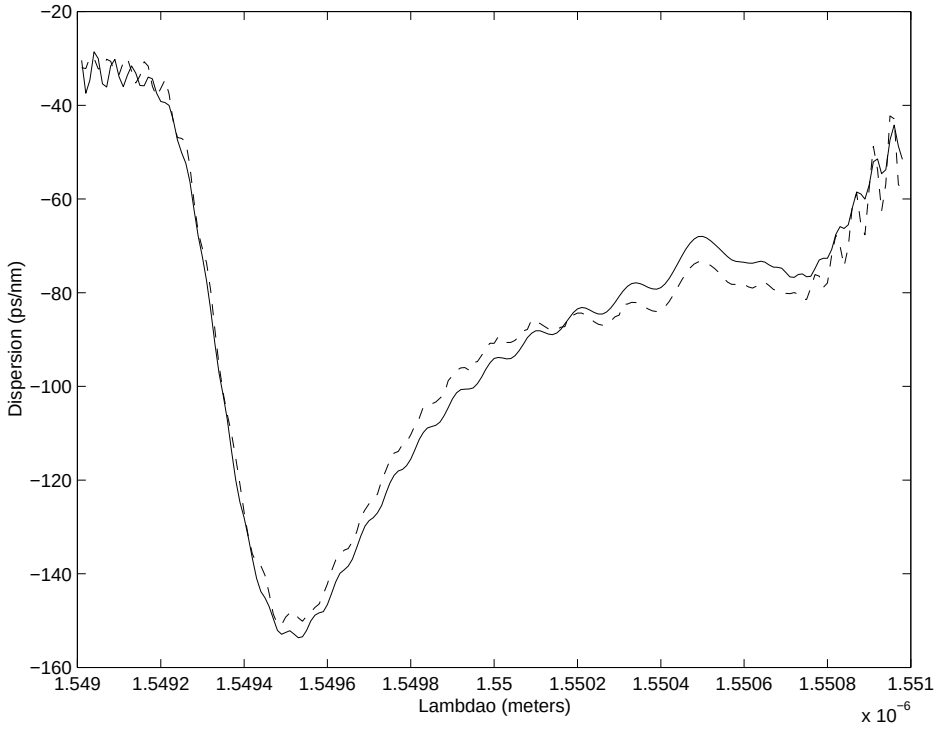

Figure 7-7 Dispersion of the variable-period chirped grating in Section 7-6 (solid line) and of the near equivalent 4 layer separately apodized design (dashed line)

absolute delay is not important, only relative delay matters. The solid line in Figure 7-7 shows the dispersion D calculated from

$$D = \frac{d\tau}{d\lambda_o}. \tag{7.15}$$

The plot is consistent with the parameter $\frac{d\lambda_{o_D}}{dz} = -1\,\text{nm/cm}$ for this grating, which indicates that shorter wavelengths are reflected further into the grating. In this way, the shorter wavelengths are delayed relative to the longer wavelengths. This is a useful dispersion compensator, since longer wavelength light propagating down a fiber is delayed relative to shorter wavelength light.

Virtually the same reflectivity and dispersion can be obtained using a different approach. As noted in [1], the dependence of the coupled-wave equations on $\frac{d\phi_{l1}(z)}{dz}$ isthrough $\hat{\sigma}$ only. Furthermore, $\frac{d\phi_{l1}(z)}{dz}$ can be replaced by a "dc" index variation $\sigma(z)$

with the same functional form without altering the solutions to the coupled-wave equations. It is seen that a dispersion compensating design with virtually the same reflectivity and dispersion as the variable-period design can be achieved without actually varying the grating period. This is the approach used in [27].

Before using this alternate approach we examine whether the required peak index change approaches the limits of available fabrication techniques. Let us consider a constant-period design emulating the chirped grating described in detail at the beginning of this section. All variables are the same except $\frac{d\phi_{l1}(z)}{dz} = 0$,

$$\sigma(z) = -\frac{1}{2} 759{,}880 z + X_1 \quad \text{at } \lambda_o = 1.55\,\mu\text{m} \tag{7.16}$$

where X_1 is an arbitrary constant, and

$$\Delta n(x,z) = \begin{cases} \Delta n_{l1}(z) = \overline{\Delta n_{l1}}\, g(z) + \overline{\Delta n_{l1}}\, f(z) v \cos\left(\frac{2\pi}{\Delta} z + \phi_{l1}(z)\right) & |x| < a_1 \\ \Delta n_{l2}(z) = \overline{\Delta n_{l2}}\, g(z) + \overline{\Delta n_{l2}}\, f(z) v \cos\left(\frac{2\pi}{\Delta} z + \phi_{l1}(z) + \Delta\phi_{l2}\right) & a_1 < |x| < a_2 \\ \Delta n_{l3}(z) = \overline{\Delta n_{l3}}\, g(z) + \overline{\Delta n_{l3}}\, f(z) v \cos\left(\frac{2\pi}{\Delta} z + \phi_{l1}(z) + \Delta\phi_{l3}\right) & a_2 < |x| < a_3 \\ \Delta n_{l4}(z) = \overline{\Delta n_{l4}}\, g(z) + \overline{\Delta n_{l4}}\, f(z) v \cos\left(\frac{2\pi}{\Delta} z + \phi_{l1}(z) + \Delta\phi_{l4}\right). & a_3 < |x| \end{cases} \tag{7.17}$$

The function $g(z)$ is computed below. In the expression for $\sigma(z)$, the constant X_1 is added to the RHS since $\sigma(z)$ is always non-negative, as is the index change. The effect of this constant is removed by adjusting Λ. Equivalence in

$$\sigma(z) = -\frac{1}{2}\frac{d\phi_{l1}(z)}{dz} + X_1 \tag{7.18}$$

is satisfied exactly at only one value of λ_o, namely $\lambda_o = 1.55\,\mu\text{m}$, but near equality is obtained for all λ_o in the range of interest since $\sigma(z)$ varies slowly with λ_o. Using (7.17) it is easily seen that

$$\sigma(z)=\frac{\omega\varepsilon_o}{2}\,g(z)\left\{\begin{array}{l} n_1\overline{\Delta n_{l1}}\int_{-a_1}^{a_1}\hat{\mathbf{e}}_1^{\,*}\cdot\hat{\mathbf{e}}_1 dx+2n_2\overline{\Delta n_{l2}}\int_{a_1}^{a_2}\hat{\mathbf{e}}_1^{\,*}\cdot\hat{\mathbf{e}}_1 dx \\ +2n_3\overline{\Delta n_{l3}}\int_{a_2}^{a_3}\hat{\mathbf{e}}_1^{\,*}\cdot\hat{\mathbf{e}}_1 dx+2n_4\overline{\Delta n_{l4}}\int_{a_3}^{\infty}\hat{\mathbf{e}}_1^{\,*}\cdot\hat{\mathbf{e}}_1 dx \end{array}\right\} \qquad (7.19)$$

$$= 2{,}026.834\,g(z) \quad \text{at } \lambda_o = 1.55\,\mu\text{m} = \lambda_{o\,\text{center}}\,.$$

Letting $v=1$ still, $K(z)$ remains the same. The peak index change in layer x is given by

$$\max\{\Delta n(x,z)\}=\max\left\{\overline{\Delta n_{lx}}\,[g(z)+f(z)]\right\} \qquad (7.20)$$

Using (7.16) in (7.19) yields

$$g(z)=X_2-187.455z\,. \qquad (7.21)$$

The constant X_2 is found by enforcing the requirement $[g(z)-f(z)]>0$, yielding $X_2=1.87455$. Now, solving for $\max\{[g(z)+f(z)]\}$ in (7.20), yields

$$\max\{g(z)+f(z)\}=\max\left\{1.87455-187.455z+\frac{1}{2}\left[1+\cos\left(\frac{\pi z}{0.01}\right)\right]\right\}=3.7491\,. \qquad (7.22)$$

For the variable-period design, which is zero-"dc", the peak index change is given by

$$\max(\Delta n(x,z)) \text{ in layer } x=\overline{\Delta n_{lx}}$$

since $f(z)=|f(z)|$ and $\max\{f(z)\}=1$. However, the design is fabricated by introducing a uniform "dc" index change equal to $\overline{\Delta n_{lx}}\max\{f(z)\}$ in layer x, so the total index change is always non-negative. Therefore, as actually fabricated, the

$$\max(\Delta n(x,z)) \text{ in layer } x=2\,\overline{\Delta n_{lx}}\,.$$

This compares to $3.7491\overline{\Delta n_{lx}}$ for the constant-period design, so its peak index change is not even larger by a factor of two.

Both dispersion compensating designs are acceptable, but let us add to our options by deriving novel "separately apodized" designs using a perturbation taking the form of (7.1). In Section 7.7 we consider which options are easiest to fabricate. The first separately apodized design evolves out of the variable-period chirped design. It requires

four layers; but only two layers in the waveguide used in this chapter will support gratings. Therefore, we modify (7.1), dividing the layers so:

$$K_{l1}(z) = \frac{\omega\varepsilon_o}{4} n_1 \overline{\Delta n_{l1}}\, f_{l1}(z) v \int_{-a_1/2}^{a_1/2} \hat{\mathbf{e}}_1^{\,*} \cdot \hat{\mathbf{e}}_1 dx \tag{7.23a}$$

$$K_{l2}(z) = \frac{\omega\varepsilon_o}{2} n_1 \overline{\Delta n_{l2}}\, f_{l2}(z) v \int_{a_1/2}^{a_1} \hat{\mathbf{e}}_1^{\,*} \cdot \hat{\mathbf{e}}_1 dx \tag{7.23b}$$

$$K_{l3}(z) = \frac{\omega\varepsilon_o}{2} n_3 \overline{\Delta n_{l3}}\, f_{l3}(z) v \int_{a_2}^{\frac{a_2+a_3}{2}} \hat{\mathbf{e}}_1^{\,*} \cdot \hat{\mathbf{e}}_1 dx \tag{7.23c}$$

$$K_{l4}(z) = \frac{\omega\varepsilon_o}{2} n_3 \overline{\Delta n_{l4}}\, f_{l4}(z) v \int_{\frac{a_2+a_3}{2}}^{a_3} \hat{\mathbf{e}}_1^{\,*} \cdot \hat{\mathbf{e}}_1 dx\,. \tag{7.23d}$$

The modified form of (7.1) used for the perturbation is obvious from (7.23). This is the only so-called separately apodized design in this thesis for which the perturbation is not given exactly by (7.1). To achieve virtually the same reflectivity and dispersion as for the variable-period design, we choose:

$$\phi_{l1}(z) = 0 \text{ radians} \tag{7.24a}$$

$$\phi_{l2}(z) = \pi \text{ radians} \tag{7.24b}$$

$$\phi_{l3}(z) = \pi/2 \text{ radians} \tag{7.24c}$$

$$\phi_{l4}(z) = -\pi/2 \text{ radians}\,. \tag{7.24d}$$

Toward satisfying (7.11), we define the variables

$$K_{l1+l2}(z) = \cos\left(\phi_{l1}(z)\right) K(z) \tag{7.25a}$$

$$K_{l3+l4}(z) = \sin\left(\phi_{l1}(z)\right) K(z) \tag{7.25b}$$

where $\phi_{l1}(z)$ and $K(z)$ belong to the variable-period design. $\dfrac{d\phi_{l1}(z)}{dz}$ is known but not $\phi_{l1}(z)$, thus we arbitrarily set $\phi_{l1}(z) = \dfrac{7.59880\times10^5}{2} z^2$ satisfying (7.14). If a constant were added to $\phi_{l1}(z)$, the difference would be felt in calculating Λ, described below (in the term $2\left[\max\left\{\left|K_{l1+l2}(z)\right|\right\} + \max\left\{\left|K_{l3+l4}(z)\right|\right\}\right]$). $K_{l1+l2}(z)$ and $K_{l3+l4}(z)$ themselves could

be implemented in two layers, except that they are not always non-negative, unlike the index change in a layer. Therefore, four layers are required with:

$$K_{l1}(z) = \frac{\max\left\{\left|K_{l1+l2}(z)\right|\right\} + K_{l1+l2}(z)}{2} \tag{7.26a}$$

$$K_{l2}(z) = \frac{\max\left\{\left|K_{l1+l2}(z)\right|\right\} - K_{l1+l2}(z)}{2} \tag{7.26b}$$

$$K_{l3}(z) = \frac{\max\left\{\left|K_{l3+l4}(z)\right|\right\} + K_{l3+l4}(z)}{2} \tag{7.26c}$$

$$K_{l4}(z) = \frac{\max\left\{\left|K_{l3+l4}(z)\right|\right\} - K_{l3+l4}(z)}{2}. \tag{7.26d}$$

The design at hand is assumed non-zero-"dc", unlike the variable period chirped design. In the above four equations, exact equality can only be obtained at one value of λ_o, and $\lambda_o = 1.55\,\mu\text{m}$ is chosen. Therefore, $K(z)$ in equations (7.25) is evaluated at $\lambda_o = 1.55\,\mu\text{m}$ where it equals $1.0134\times10^3\, f(z)$ as stated above. What has been achieved is that the relations (7.11) have been satisfied at $\lambda_o = 1.55\,\mu\text{m}$, and nearly satisfied over the entire range of λ_o of interest. For the separately apodized design, $\sigma(z)$ as defined by (7.7) is independent of z, so the behavior of the variable-period design is mirrored after Λ is adjusted so (7.11) is satisfied.

Using the expressions (7.26), the envelopes of the index change in (7.1) are found according to:

$$\overline{\Delta n_{l1}}\, f_{l1}(z) = \frac{K_{l1}(z)}{\frac{\omega\varepsilon_o}{4} n_1 \int_{-a_1/2}^{a_1/2} \hat{\mathbf{e}}_1^{\,*} \cdot \hat{\mathbf{e}}_1 dx} \tag{7.27a}$$

$$\overline{\Delta n_{l2}}\, f_{l2}(z) = \frac{K_{l2}(z)}{\frac{\omega\varepsilon_o}{2} n_1 \int_{a_1/2}^{a_1} \hat{\mathbf{e}}_1^{\,*} \cdot \hat{\mathbf{e}}_1 dx} \tag{7.27b}$$

$$\overline{\Delta n_{l3}}\, f_{l3}(z) = \frac{K_{l3}(z)}{\frac{\omega\varepsilon_o}{2} n_3 \int_{a_2}^{\frac{a_2+a_3}{2}} \hat{\mathbf{e}}_1^{\,*} \cdot \hat{\mathbf{e}}_1 dx} \tag{7.27c}$$

$$\overline{\Delta n_{l4}}\, f_{l4}(z) = \frac{K_{l4}(z)}{\frac{\omega\varepsilon_o}{2} n_3 \int\limits_{\frac{a_2+a_3}{2}}^{a_3} \hat{\mathbf{e}}_1^{\,*} \cdot \hat{\mathbf{e}}_1 dx} \qquad (7.27d)$$

assuming $v = 1$. $\lambda_o = 1.55\,\mu$m is used again in solving these equations.

A program that performs the conversion as described, called OneLChirp2FourL.m, is listed in Appendix E. The program apodv2ErgDesChirp.m must be run first. This program is similar in its operation to OneLGuass2TwoLayer.m, presented in Section 7.4. Figure 7-8a shows the index perturbation $\Delta n(x,z)$ in layer 1, which is the same as in layer 3, of the original variable-period design. Its variable period is evident. Figures 7-8b-e show the index perturbation $\Delta n(x,z)$ in the layers $0 < |x| < a_1/2$, $a_1/2 < |x| < a_1$, $a_2 < |x| < \frac{a_2 + a_3}{2}$, and $\frac{a_2 + a_3}{2} < |x| < a_3$, respectively, of the separately apodized design. In all layers, the period is independent of z.

The dashed line in Figure 7-5, which virtually overlaps the solid line representing the R for the variable period design, shows R for the separately apodized design in dB. The dashed line in Figure 7-6 shows the group delay for the separately apodized design. The dashed line in Figure 7-7 shows the dispersion for the separately apodized design. In all cases the responses are quite close for all λ_o to the responses for the variable period design. The reflectivity is the same at $\lambda_o = 1.55\,\mu$m, but not the time delay or dispersion because θ_1 in (5.11) is identical at $\lambda_o = 1.55\,\mu$m, but not $\frac{d\theta_1}{d\omega}$. The responses for the separately apodized design were computed using a program called ChirpApod4L.m, listed in Appendix E. This program is very similar to apod2LGuass.m described in Section 7.4. It calculates Λ using (6.5) evaluated at $\lambda_o = 1.55\,\mu$m and $z = 0$. Therefore,

$$\frac{d\left(\angle \left(K_{l1}(z)e^{j0} + K_{l2}(z)e^{j\pi} + K_{l3}(z)e^{j\frac{\pi}{2}} + K_{l4}(z)e^{-j\frac{\pi}{2}} \right) \right)}{dz},$$

which equals zero at $\lambda_o = 1.55\,\mu$m and $z = 0$ as did $\frac{d\phi_{l1}(z)}{dz}$, is substituted for $\frac{d\phi_{l1}(z)}{dz}$.

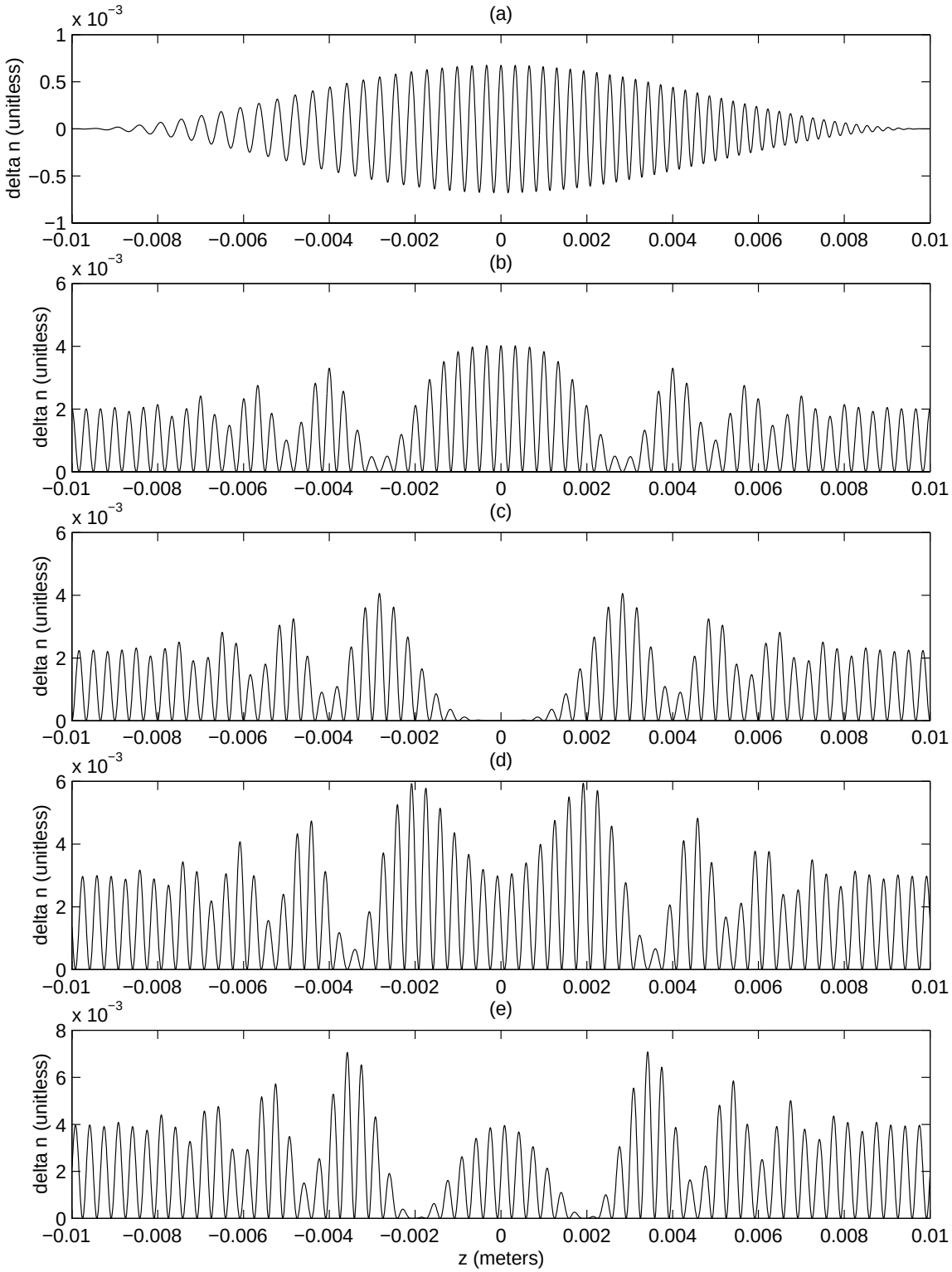

Figure 7-8 Index change (a) in layers 1 and 3 of the variable-period chirped grating in Section 7.6 and in layers (b) $0 < |x| < a_1/2$ (c) $a_1/2 < |x| < a_1$ (d) $a_2 < |x| < \frac{a_2 + a_3}{2}$ and (e) $\frac{a_2 + a_3}{2} < |x| < a_3$ of the near equivalent 4 layer separately apodized design.

The value of $2\left[K_{l1}(z)+K_{l2}(z)+K_{l3}(z)+K_{l4}(z)\right]$ at $\lambda_o = 1.55\,\mu\text{m}$, which equals $2\left[\max\left\{\left|K_{l1+l2}(z)\right|\right\}+\max\left\{\left|K_{l3+l4}(z)\right|\right\}\right]$ evaluated at $\lambda_o = 1.55\,\mu\text{m}$, is substituted for $\sigma(z)$.

The second separately apodized design evolves out of the constant-period design that uses a z-dependent "dc" index change to induce a chirp. This design requires only two layers, so is probably simpler to fabricate than the previous separately apodized design. The layers in which gratings occur are not divided this time, so two "ac"coupling coefficients, $K_{l1}(z)$ and $K_{l3}(z)$, are used, given exactly by (7.6a,c). $K_{l2}(z)$ and $K_{l4}(z)$ equal zero because in these layers the refractive index equals n_{SiO2}, so no gratings occur. (7.1) is used for the form of the perturbation with "$1+$" retained in the layers, i.e. the design is non-zero-"dc", and $v = 1$. We choose

$$\phi_{l1}(z) = 0 \text{ radians} \tag{7.28a}$$

$$\phi_{l3}(z) = \pi \text{ radians} \tag{7.28b}$$

and we require

$$K_{l1}(z)+K_{l3}(z) = Y_1 - \frac{759{,}880}{4}z = Y_1 - \frac{1}{4}\frac{d\phi_{l1}(z)}{dz} \tag{7.29}$$

where Y_1 is an arbitrary constant. $\dfrac{d\phi_{l1}(z)}{dz}$ is for the variable-period design. By enforcing (7.29), the expression substituted for $\sigma(z)$ according to (7.10) when solving the coupling wave equations using the matrix approach is the same function of z as $\dfrac{d\phi_{l1}(z)}{dz}$, except for a constant. Therefore, equation (7.11) is satisfied, because the coupled-wave equations depend on $\dfrac{d\phi_{l1}(z)}{dz}$ only through $\hat{\sigma}(z)$, which contains the term $\sigma(z)$. Examining the form of $\hat{\sigma}(z)$, it is seen the constant in (7.29) does not change the reflectivity spectrum if Λ is adjusted depending on the value of the constant. We also require

$$K_{l1}(z)-K_{l3}(z) = K(z) \tag{7.30}$$

where $K(z)$ is for the variable period design, the same as for the design that uses a z-dependent "dc" index change. $K(z)$ depends on λ_o, as do $K_{l1}(z)$ and $K_{l3}(z)$, so (7.29) and (7.30) can only be satisfied at one value of λ_o. The quantity

$$\angle\left(K_{l1}(z)e^{j\phi_{l1}(z)} + K_{l3}(z)e^{j\phi_{l3}(z)}\right) = \angle\left(K_{l1}(z) - K_{l3}(z)\right)$$

equals zero since $K(z)$ is always positive. At least, this is true at the value of λ_o for which (7.29) and (7.30) are satisfied. Never letting the value of the angle jump to π is the basis of choosing the λ_o for which (7.29) and (7.30) are satisfied as described below.

$K_{l1}(z)$ and $K_{l3}(z)$ are easily solved, yielding

$$K_{l1}(z) = \frac{\overbrace{K - \frac{1}{4}\frac{d\phi_{l1}(z)}{dz}}^{1}}{2} - \min\{1,2\} \qquad (7.31a)$$

$$K_{l3}(z) = \frac{\underbrace{-\frac{1}{4}\frac{d\phi_{l1}(z)}{dz} - K(z)}_{2}}{2} - \min\{1,2\} \qquad (7.31b)$$

where Y_1 was chosen so $K_{l1}(z)$ and $K_{l3}(z)$ are always non-negative (because the index change is always non-negative) and no larger than necessary so the index perturbation $\Delta n(x,z)$ is no larger than necessary. The equations (7.29), (7.30), and (7.31) can only be satisfied exactly at one value of λ_o. Until now, we have always used $\lambda_o = \lambda_{o_D}$, the wavelength about which the reflectivity is symmetric and where the peak occurs. Doing so again, yields

$$\overline{\Delta n_{l1}}\, f_{l1}(z) = \frac{K_{l1}(z)}{\frac{\omega\varepsilon_o}{4} n_1 \int_{-a_1}^{a_1} \hat{\mathbf{e}}_1^{\,*} \cdot \hat{\mathbf{e}}_1 dx} \qquad (7.32a)$$

$$\overline{\Delta n_{l3}}\, f_{l3}(z) = \frac{K_{l3}(z)}{\frac{\omega\varepsilon_o}{2} n_3 \int_{a_2}^{a_3} \hat{\mathbf{e}}_1^{\,*} \cdot \hat{\mathbf{e}}_1 dx} \qquad (7.32b)$$

where $K_{l1}(z)$ and $K_{l3}(z)$ are from (7.31) using $K(z)$ evaluated at $\lambda_o = 1.55\,\mu\text{m}$, and ω and the integrals are evaluated at $\lambda_o = 1.55\,\mu\text{m}$ as well. To find $K_{l1}(z)$ and $K_{l3}(z)$ at

λ_o other than $1.55\,\mu$m, $\overline{\Delta n_{l1}}\, f_{l1}(z)$ and $\overline{\Delta n_{l3}}\, f_{l3}(z)$ solved using the above equations are used in (7.6a) and (7.6c). The factors $\frac{\omega\varepsilon_o}{4} n_1 \int_{-a_1}^{a_1} \hat{\mathbf{e}}_1^{\,*} \cdot \hat{\mathbf{e}}_1 dx$ and $\frac{\omega\varepsilon_o}{2} n_3 \int_{a_2}^{a_3} \hat{\mathbf{e}}_1^{\,*} \cdot \hat{\mathbf{e}}_1 dx$ in (7.6a) and (7.6c), respectively, have different dependence on λ_o. The first factor mentioned drops with increasing λ_o by .21 % over the range of λ_o of interest, while the second factor drops by only .15%. Since the difference $K_{l1}(z) - K_{l3}(z)$ is very small at the edges (i.e. near $z = L/2$ or $-L/2$) as was the bell-shaped $K(z)$, it goes negative for some values of λ_o if (7.29), (7.30), (7.31), and (7.32) are solved at $\lambda_o = 1.55\,\mu$m. The result is that the reflectivity spectrum successfully duplicates that in Figure 7-6, but the delay time, which is shown in Figure 7-9 has large spikes not appearing in the solid line in Figure 7-6. The dispersion shown in Figure 7-10 has large spikes not appearing in the solid line in Figure 7-7.

To solve this problem, (7.29), (7.30), (7.31), and (7.32) are solved at the maximum λ_o in the range of interest, $\lambda_o = 1.551\times10^{-6}$ m. The dashed line in Figure 7-11 shows R in dB for the separately apodized design while the solid line shows R for the variable-period design, the same as the solid line in Figure 7-5. The solid and dashed lines are indistinguishable on this plot. The dashed line in Figure 7-12 shows the delay time for the separately apodized design while the solid line shows the delay time for the variable-period design, the same as the solid line in Figure 7-6. The solid and dashed lines are virtually indistinguishable on this plot. The dashed line in Figure 7-13 shows the dispersion for the separately apodized design while the solid line shows the dispersion for the variable-period design, the same as the solid line in Figure 7-7. All responses are quite close, even closer than for the previous separately apodized design in this section. Figure 7-14a shows the index change, $\Delta n(x,z)$, in layers 1 and 3 of the variable-period design, the same as in Figure 7-8a. Figures 7-14b and 7-14c show the index change in $|x| < a_1$ and $a_2 < |x| < a_3$ for the separately apodized design.

A program that performs the conversion from the design that uses a z-dependent "dc" index change (which is the same as the variable-period design except $\frac{d\phi_{l1}(z)}{dz} = 0$

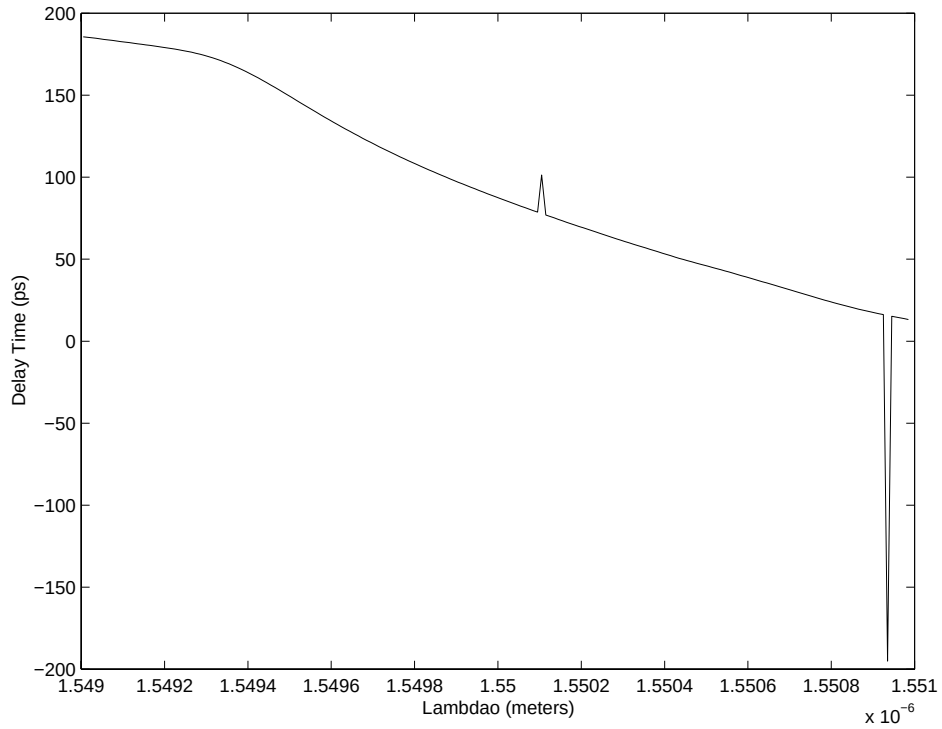

Figure 7-9 Delay time of the two-layer separately apodized grating in Section 7.6 if (7.29), (7.30), (7.31), and (7.32) are solved at $\lambda_o = 1.55\,\mu\text{m}$.

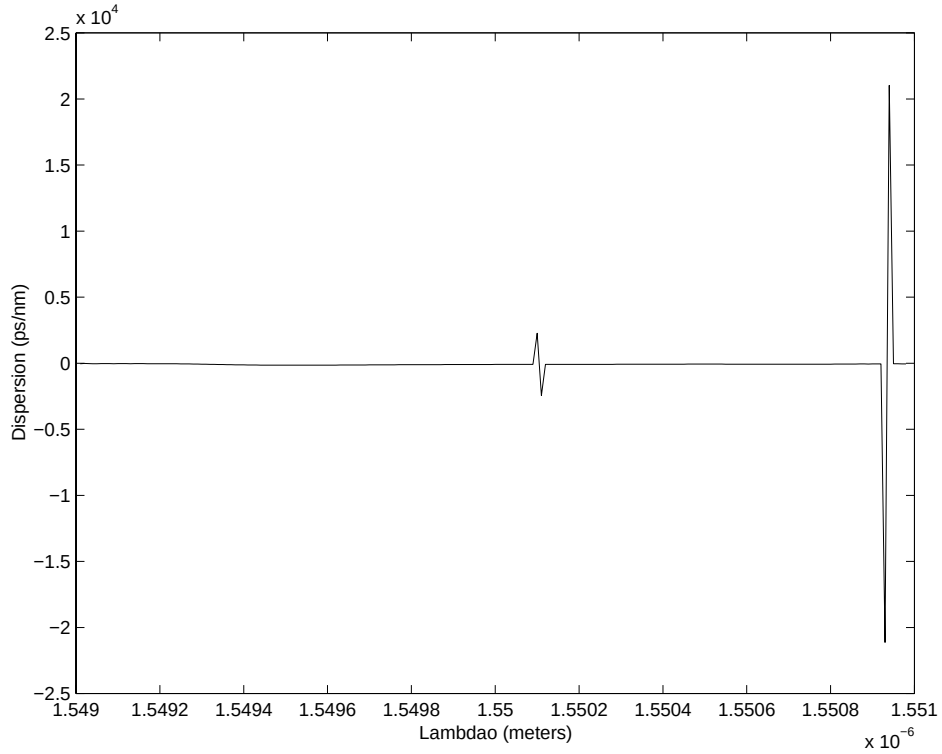

Figure 7-10 Dispersion of the two-layer separately apodized grating in Section 7.6 if (7.29), (7.30), (7.31), and (7.32) are solved at $\lambda_o = 1.55\,\mu\text{m}$.

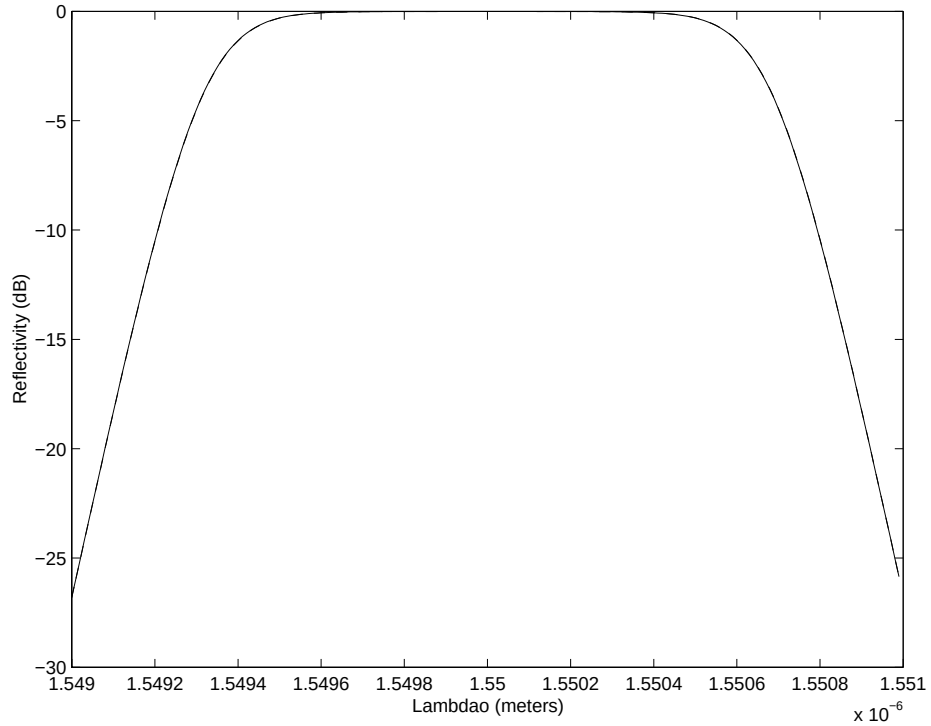

Figure 7-11 Reflectivity in dB of the variable-period chirped grating in Section 7-6 (solid line) and of the near equivalent 2 layer separately apodized design with (7.29), (7.30), (7.31), and (7.32) solved at $\lambda_o = 1.551\ \mu\text{m}$ (indistinguishable dashed line)

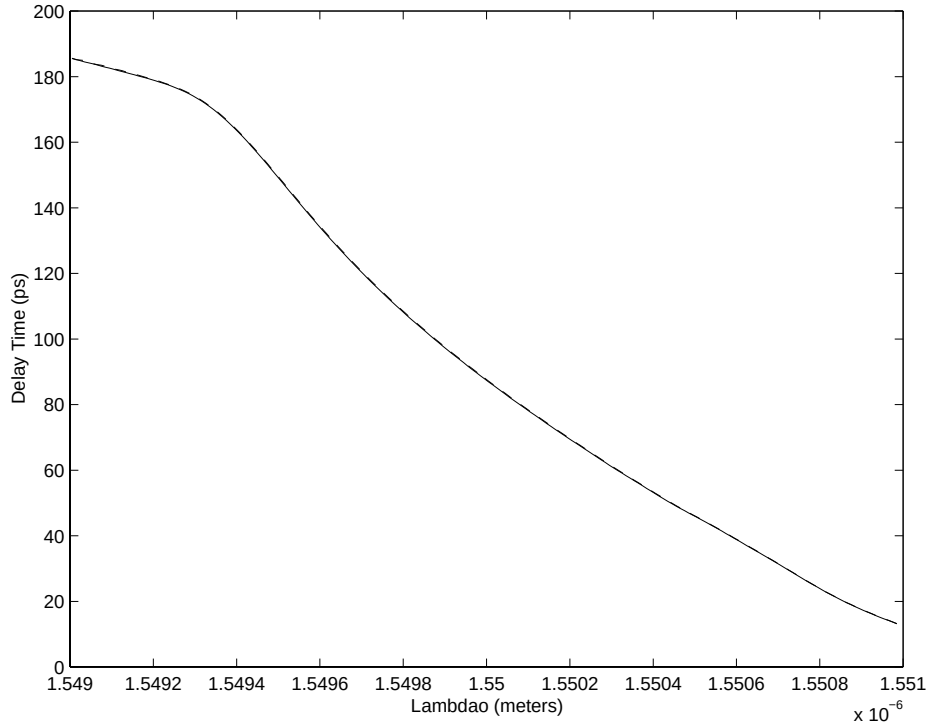

Figure 7-12 Delay time of the variable-period chirped grating in Section 7-6 (solid line) and of the near equivalent 2 layer separately apodized design with (7.29), (7.30), (7.31), and (7.32) solved at $\lambda_o = 1.551\ \mu\text{m}$ (nearly indistinguishable dashed line)

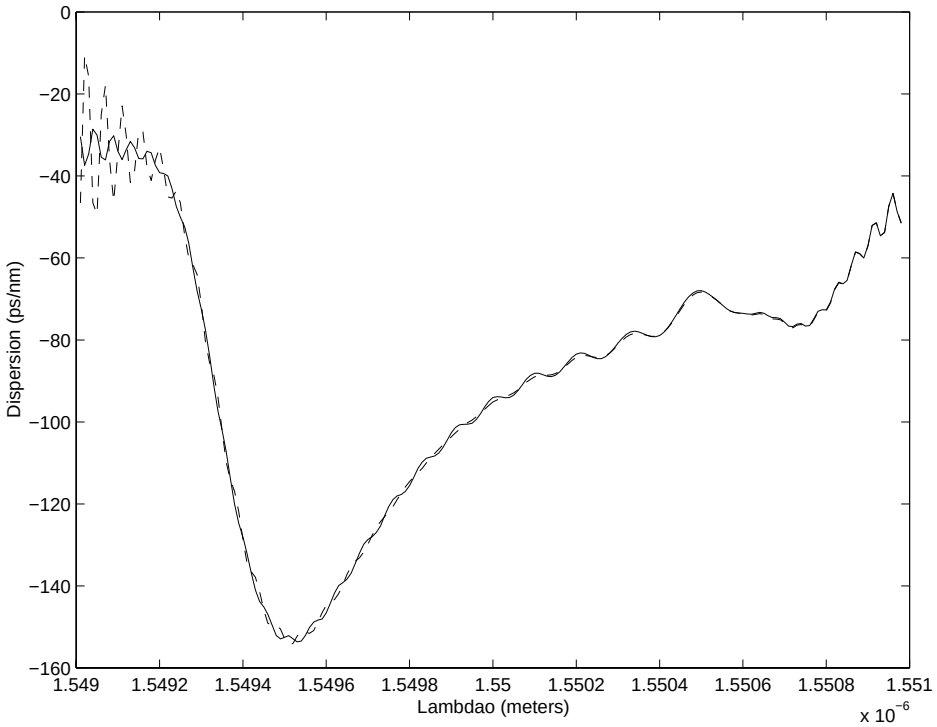

Figure 7-13 Dispersion of the variable-period chirped grating in Section 7-6 (solid line) and of the near equivalent 2 layer separately apodized design with (7.29), (7.30), (7.31), and (7.32) solved at $\lambda_o = 1.551\ \mu\text{m}$ (dashed line)

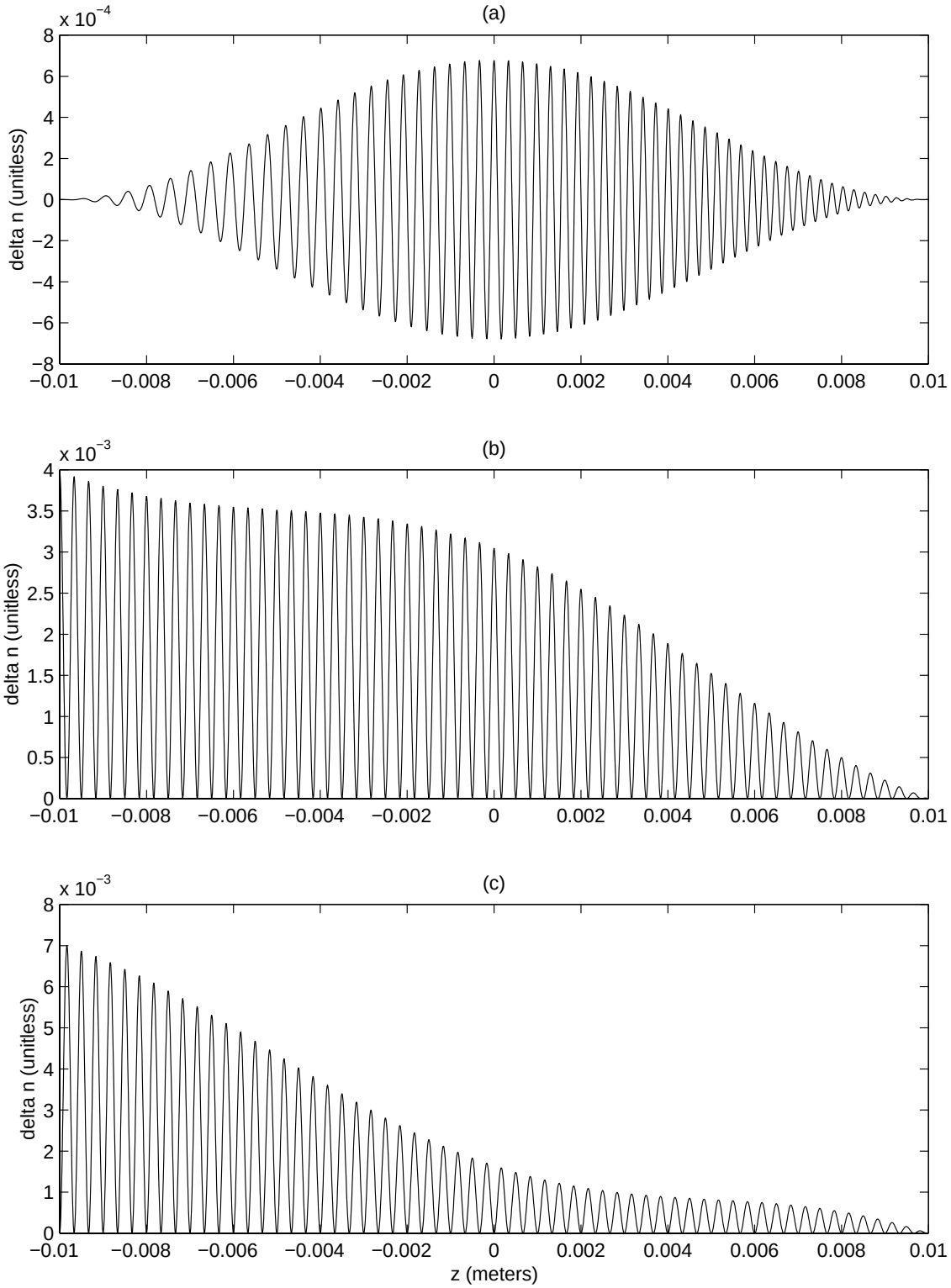

Figure 7-14 Index change (a) in layers 1 and 3 of the variable-period chirped grating in Section 7.6 and in layers (b) 1 and (c) 3 of the near equivalent 2 layer separately apodized design with (7.29), (7.30), (7.31), and (7.32) solved at $\lambda_o = 1.551\ \mu\text{m}$

and $\sigma(z) = \text{non - zero}$), called apod1L2apod2LVarDC.m, is listed in Appendix E. The program apodv2ErgDesChirp.m must be run first. A program that computes the responses for the separately apodized design, called apod2LVarDC.m, is also listed in Appendix E. It computes Λ using equation (6.5) under the conditions described in Section 7.3. The result is:

$$\Lambda = \frac{\pi}{\beta(\lambda_o = 1.55\,\mu\text{m}) - 4\min\{1,2\}} = 5.3312\times10^{-7}\ \text{m}$$

where $\min\{1,2\}$ refers to the terms in (7.31) and is evaluated at $\lambda_o = 1.55\,\mu\text{m}$. The minimum operator refers to variation with z.

7.7 Fabrication of Chirped Gratings

Several fabrication methods for chirped gratings have been presented in the literature. One method depends on curving the fiber in the interference field from the same imprinting arrangement as for uniform gratings [28]. A disadvantage of this method may be that it produces "blazed" gratings that cause radiation loss [29]. The basis of another method is a temperature gradient along the length of the fiber during photoimprinting [30]. Another method depends on varying the "dc" index change to induce a chirp [27]. According to [29], the methods in [30], [27] produce small chirps, and all three methods lack reproducibility. [29] proposes a method that depends on varying the period of the relief structure on the surface of the phase mask. Since the step size of the electron-beam used in fabricating the phase mask is not infinitesimal, the chirp is divided into short sections. In each section, the period is constant, but the next section has a slightly different period. One advantage of this method is reproducibility. A drawback owing to the phase discontinuities at the section boundaries is mentioned in [29], but the details are few. This may be an attractive fabrication method, but so might the method relying on varying the "dc" index change if it were more reproducible. The specific method used to vary the "dc" index change in [27] is not clear. However, the technique in [18] can be used to vary the "dc" index change independently of the "ac" index change to induce a chirp, as suggested in [1]. As demonstrated in Section 7.6, the novel fabrication technique proposed in Section 7.5 is able to vary the "dc" index change. The novel fabrication technique is probably more reproducible than the method in [18], since the

irradiation dose reaching the waveguide depends on the phase mask and shadow masks alone. Furthermore, it may offer an advantage over the technique in [29] if the drawback associated with the phase discontinuities at the section boundaries is significant. It is seen that the novel technique in an induced-chirp application is attractive.

7.8 Broadband Chirped Grating Dispersion Compensators

Fiber transmission systems suffer from dispersion. The route length determines the amount of dispersion [31], expressed in ps/nm. The overall delay per channel equals the dispersion multiplied by the bandwidth per channel. It is necessary to equalize the dispersion in the optical pulses, since it limits the maximum data rate that can be transmitted through the fiber by broadening the pulses so they overlap. Dispersion compensators depend on delaying the long wavelength components of the light pulse relative to the short wavelength components, or vice versa -- the opposite of the fiber's effect. For the dispersion compensator and fiber, alike, the light pulse delay as a function of wavelength is linear, but the slope for the dispersion compensator is the negative of the slope for the fiber.

Using a channel spacing of 100 GHz, as has been proposed for wavelength division multiplexed systems, the requirement for the bandwidth for dispersion compensation increases rapidly [31]. A channelized dispersion compensator, which confines the dispersion to the bandwidth of each channel, is one option. The slope of the delay is constant within, but not between, the channel passbands. A more desirable option is continuous dispersion compensation over a much wider bandwidth range [31], requiring no temperature control. Dispersion compensating fiber is broadband, but its disadvantages include increased nonlinearity, giving rise to four-wave mixing and higher loss [31], besides the fact that some 20 km of fiber might be required.

Increasing the bandwidth of uniform gratings while preserving the peak reflectivity entails increasing the coupling coefficient K and decreasing the length L by the same factor [32]. This is obvious from Figure 3-4, a plot of reflectivity versus normalized wavelength for uniform gratings. After apodization with a bell-shaped function, the main-lobe width for a uniform grating does not substantially change, as noted by comparing Figures 7-1 and 7-3. Therefore, in general, it is possible to extend

the approach to increasing the bandwidth for a uniform grating to apodized gratings. However, applying the approach to chirped gratings, the results are not satisfactory. As an example, let us attempt to increase the bandwidth of the variable-period chirped grating in Section 7.6, which has the responses illustrated by the solid lines in Figures 7-5 through 7-7. The bandwidth is 1.4 nm and the dispersion varies from –70 to –163 ps/nm within the passband. Increasing $K(z)$ by a factor of 3, by increasing α by a factor of 3, and reducing the FWHM and, hence, the length L, by the same factor increases the bandwidth to 1.6 nm, but yields a dispersion that varies from –140 to 160 ps/nm – no longer nearly constant enough for use as a dispersion compensator. That the bandwidth did not increase more is no surprise, since the correspondence between the bandwidth of chirped gratings and similar uniform gratings is less than for non-chirped gratings. A much-preferred approach to increasing the bandwidth of a chirped grating is to increase $\frac{d\lambda_{o_D}}{dz}$. Increasing this parameter for the chirped grating under consideration by a factor of 3 while preserving all the other parameters increases the bandwidth to 3.0 nm. The dispersion ranges from –35 to –31 ps/nm within the passband, which represents less variation than before as a percentage of the average, but the average dispersion, itself, is significantly reduced. The linear dependence of the delay for chirped gratings relies on reflecting long wavelengths near the front while reflecting short wavelengths near the back, or vice versa. Increasing the wavelength of the light reflected near the back increases the bandwidth, but the maximum delay depends on the physical length. Therefore, the bandwidth can be increased by increasing $\frac{d\lambda_{o_D}}{dz}$, but in exchange, the dispersion is reduced.

To increase the bandwidth of a chirped grating while approximately preserving the value of the dispersion, the length is increased while retaining the value of $\frac{d\lambda_{o_D}}{dz}$. Increasing the length of the variable period chirped grating in Section 7.6 by a factor of 3 by increasing the FWHM by the same factor yields the reflectivity spectrum shown in Figure 7-15. The functional form of $\frac{d\phi_{l1}(z)}{dz}$ given by (7.14) is retained, but extended

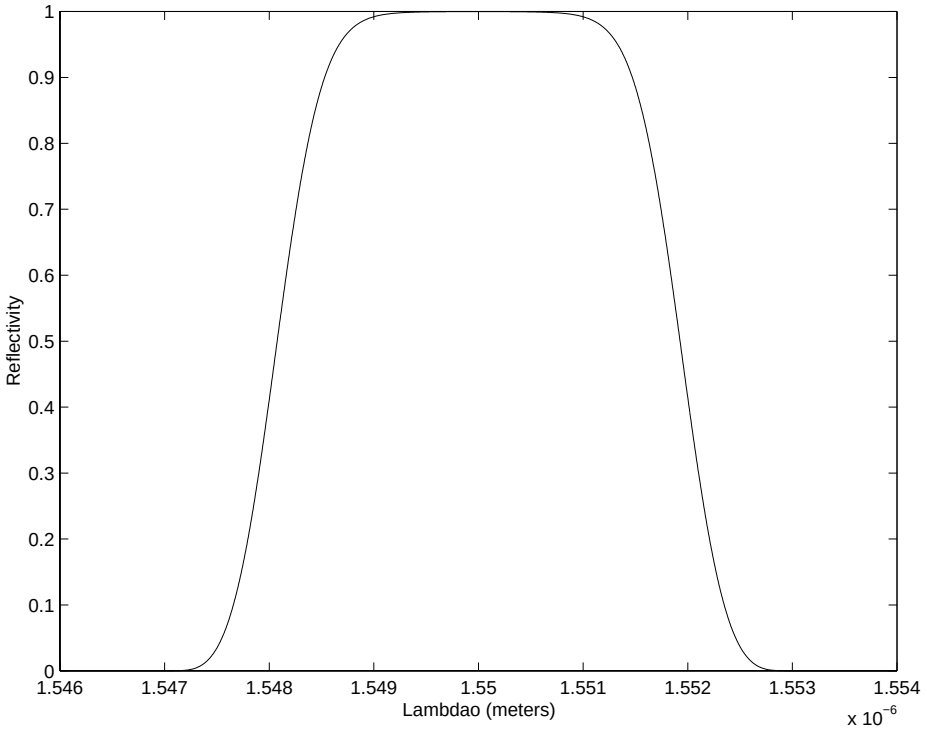

Figure 7-15 Reflectivity of the variable-period chirped grating in Section 7.6 after increasing its length by a factor of 3.

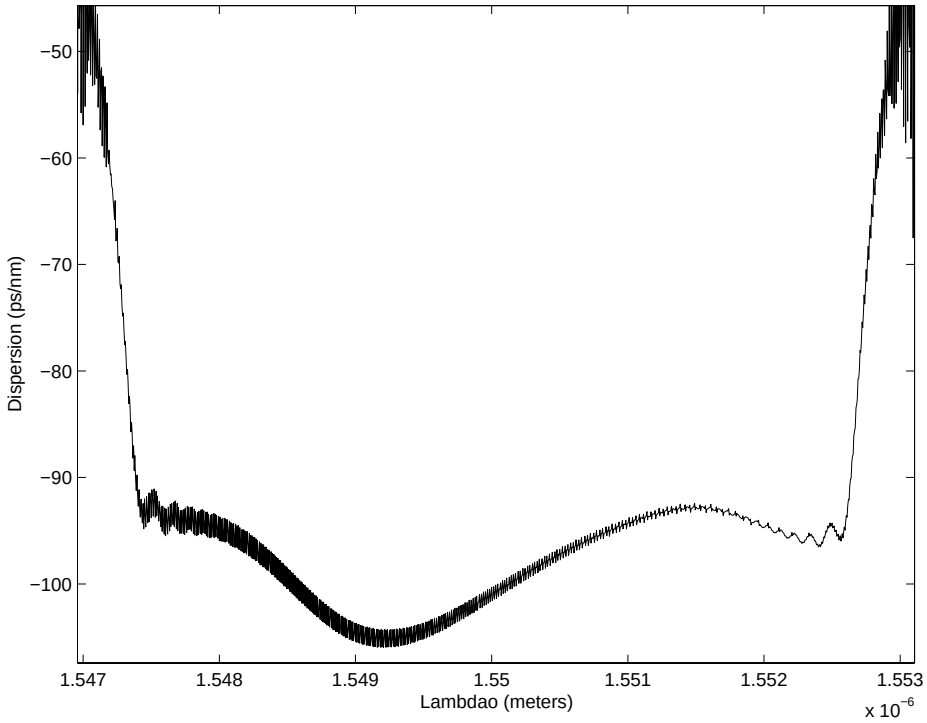

Figure 7-16 Dispersion of the variable-period chirped grating in Section 7.6 after increasing its length by a factor of 3.

over the increased length. The new bandwidth is 3.8 nm, more than twice the previous value. The dispersion, shown in Figure 7-16, varies from –105 to –93 ps/nm within the passband and is flatter than before, though its average value is not significantly reduced. The oscillations in the response, visible as a nonuniform thickness of the line, probably do not actually exist, but are a consequence of using an insufficient number of slices in the computation of the response by the matrix approach. This is in spite of the fact that the number of slices used was increased by a factor of 3 along with the length of the grating, to 600. It is known that linearly chirped gratings have an oscillatory dispersion characteristic if they are unapodized and their bandwidth is small [2] [17] [20] [33] [34]. However, just two points complete one cycle of the oscillations in Figure 7-16, unlike the oscillations in the dispersion characteristic shown as the solid line in Figure 7-7, suggesting a computational limitation.

If $\frac{d\lambda_{o_D}}{dz}$ is a non-zero constant, then the wavelength that is strongly reflected varies linearly with position. A larger $\frac{d\lambda_{o_D}}{dz}$ corresponds to a larger slope of $\frac{d\phi_{l1}(z)}{dz}$ according to (7.12) and produces a smaller dispersion. When the physical distance between the position in the grating reflecting the wavelength λ_{o_1} and the position in the grating reflecting λ_{o_2} decreases, the difference in the delay at the two wavelengths decreases and so does the dispersion. In general, increasing the bandwidth of a chirped grating requires increasing the quantity $\left|\lambda_{o_D}(L/2)-\lambda_{o_D}(-L/2)\right|$. (Increasing α by a factor of 3, and reducing the length L by the same factor was not very successful.) Increasing this quantity means increasing $\left|\left.\frac{d\phi_{l1}(z)}{dz}\right|_{L/2}-\left.\frac{d\phi_{l1}(z)}{dz}\right|_{-L/2}\right|$ if the chirp is accomplished by varying the grating period. It means increasing $\left|\sigma(L/2)-\sigma(-L/2)\right|$ if the chirp is accomplished by linearly varying the "dc" index change. If the excursion of $\frac{d\phi_{l1}(z)}{dz}$ or σ is larger, then the excursion of λ_{o_D} satisfying (6.5) is larger, that is, the bandwidth is larger. Since σ is proportional to the "dc" index change according to

(7.19), the limitation in the maximum index change imposed by available fabrication techniques limits the bandwidth if the chirp is achieved by linearly varying the "dc" index change. The maximum index change required by the two layer separately apodized design that duplicates the responses of the conventional chirped designs is larger than for the conventional design that depends on varying the "dc" index change. Therefore, the maximum bandwidth that can be achieved with this approach is limited as well, and is slightly less than for the conventional design that depends on varying the "dc" index change. There is no limit to the bandwidth possible if the chirp is accomplished by using the four layer separately apodized approach, just as there is no limit to the bandwidth possible if the chirp is accomplished by using the same apodizing function for all layers and varying the period. In these two cases, there is no limit to the magnitude of the quantity $\left|\lambda_{o_D}(L/2)-\lambda_{o_D}(-L/2)\right|$ which determines the bandwidth as explained above.

The length of gratings fabricated using techniques involving a phase mask is limited by the size of the focused spot of the writing beam unless it is scanned [22]. Scanning the beam is possible because, as long as the mask and fiber do not move relative to each other, the phase of the index change induced in the fiber core is determined by the mask regardless of the beam position [22]. If the writing beam is scanned, the length of the phase mask determines the maximum grating length [32] [22]. The longest phase masks reported in the literature to the knowledge of the author of this thesis are 100 mm long [31] [33] [34]. Reference [4] describes the careful attention -- to the calibration of the electron beam scan and correction of scan distortions that are unavoidable in scanning just 2-3 mm -- required to fabricate a 50 mm long phase mask.

Although it is probably possible to fabricate phase masks longer than 100 mm, gratings exceeding this length have been fabricated by concatenating multiple gratings. In [31], a 1.3 m long grating is reported that was fabricated using 13 step-chirped 100 mm long phase masks [29]. The start wavelength of the first phase mask was λ^1_{long} while the end wavelength was λ^1_{short}; the start wavelength of the second phase mask was λ^2_{long} while the end wavelength was λ^2_{short}; etc. Furthermore, $\lambda^1_{\text{long}} > \lambda^1_{\text{short}} > \lambda^2_{\text{long}} > \lambda^2_{\text{short}}$, etc. The first grating was written using the longest wavelength mask, then the fiber was translated at exactly 100 mm and aligned to less than 0.5 mm, then the next phase mask

was used to inscribe the second grating. The next 11 gratings were written sequentially, with no special treatment of the joins other than to ensure that the gap was kept to a minimum [31]. None of the gratings were apodized. λ_{o_D} varies linearly in a linearly-chirped grating, so sequential slices of the reflectivity spectrum correspond to sequential slices of the physical grating. Since the joins between gratings in the super-step-chirped 1.3 m long grating are not perfect, dips appear at the boundaries between gratings in the reflectivity spectrum. This is a disadvantage of the technique, although it is possible to trim the stitch between two gratings by post UV exposure [35], and the imperfect join does not affect the delay characteristic.

Reference [36] describes a fabrication method that, in principle, can write gratings up to 50 cm long without stitching errors. An interferometer or a phase mask produces a UV footprint that writes a short subgrating consisting of a number of grating periods. A feedback controlled linear drive translates the fiber with constant speed relative to the UV fringes, and the position is very accurately tracked by a second interferometer. The position resolution is about 0.3 nm [36]. The position data is used to trigger the UV-laser when the fiber reaches the desired position. Because of its low speed, the position of the fiber within the UV fringe pattern is virtually fixed during the short (10 ns) exposure time. Apodization was accomplished by phase dither, but could also be accomplished by varying the UV laser power for different phase sections [36].

The grating period of each subgrating is constant, therefore this technique cannot write variable-period chirped gratings. However, it might possibly find use in fabricating separately apodized gratings using a technique similar to the one proposed in Section 7.5. Multiple exposures are possible with the fabrication technique in [36] as required by the fabrication technique proposed for separately apodized gratings. This is a possible advantage of the novel separately apodized gratings -- that very long gratings with reflectivity and dispersion characteristics identical to long chirped gratings are possible with no stitching errors. As established above, the bandwidth of a variable-period chirped grating increases with the physical length assuming $\frac{d\lambda_{o_D}}{dz}$ is unchanged, that is, the level of the dispersion is unchanged.

In [36], positioning the uniform-period subgratings so the phase varies quadratically with the position in the grating achieved a chirped grating. The phase, of course, is constant within the subgratings, but each is positioned so its phase equals a quadratic function evaluated at the center of the particular subgrating. Therefore, the phase actually varies with position as a stair-step approximation to a quadratic function. This represents a third method of inducing a chirp without varying the grating period besides varying the "dc" index change and the separately apodized approach. However, it is not clear whether this method can achieve a bandwidth as large as can be achieved by varying the grating period as follows. If the quantity $\left| \left. \frac{d\phi_{l1}(z)}{dz} \right|_{L/2} - \left. \frac{d\phi_{l1}(z)}{dz} \right|_{-L/2} \right|$ is very large then the rate of change of $\phi_{l1}(z)$ is very large at the grating's edges. It may change by more than 2π in the distance between centers of adjoining subgratings, in which case the method described fails. On the other hand, there is no limit to the bandwidth that is possible using the four layer separately apodized approach.

Chapter 8
Conclusions

8.1 Summary of the Work and Results

Gratings in multi-clad, symmetric, planar dielectric waveguides have been investigated. It was assumed the waveguide is weakly-guiding and the coupling occurs between TE_0 propagating in the forward direction and a like, counterpropagating mode. The same coupled-wave equations arise as for gratings photoimprinted in the core of an optical fiber lacking photosensitive cladding layers, except the definitions of the coupling coefficients are modified. Shifting the phase of the index perturbation in one or more layers, so the layers no longer all have the same phase, reduces the "ac" coupling coefficient. However, assuming uniform gratings, non-zero phase-shifted designs usually do not produce reflectivity spectra that cannot be duplicated by non-phase-shifted designs. By decreasing the irradiation dose used in photoimprinting the non-phase-shifted grating, the "ac" coupling coefficient is reduced to the level of the phase-shifted design. This simultaneously reduces the "dc" coupling coefficient to below the level of the phase-shifted design, which would shift the reflectivity spectrum to different wavelengths, except the period of the gratings is readily adjusted, shifting the spectrum back. The analysis, assuming uniform gratings as previously mentioned, was detailed in Chapter 4.

The exception to the rule that phase-shifted gratings produce no spectra that cannot be achieved by non-phase-shifted gratings occurs when the "ac" coupling coefficient passes through zero near the wavelength at which the peak reflectivity normally would occur. In this case, the shape of the reflectivity spectrum is sinusoidal with a null at the wavelength where the "ac" coupling coefficient passes through zero. We derived an estimate of the amplitude of the reflectivity, which is always very small. We also computed the reflectivity when gratings of this type are arranged in a sampled-grating configuration. That is, numerous gratings are arranged sequentially, separated by nongrating regions, so a binary function modulates the index profile. Although the peak reflectivity increased, we found no advantage to phase-shifting the layers in the grating elements in the sampled grating so the "ac" coupling coefficient passes through zero

compared to not phase-shifting the layers so the “ac” coupling coefficient does not pass through zero.

Chapter 5 derived the coupled-wave equations for nonuniform gratings, assuming every layer is apodized by the same function. It was also assumed every layer has the same functional form of the phase, except for a constant phase shift. A constant phase shift between layers reduces K(z) by a constant (independent of z) factor, though K(z) is still proportional to f(z). There is no effect on sigma(z). Thus, responses are possible that are not possible without a phase shift, but no useful application has been found.

The coupled-wave equations in Chapter 5 were converted to an alternate form that leads to solutions that are more tractable. Then, Chapter 6 presented a matrix approach to solving the alternate form of the coupled-wave equations for nonuniform gratings. In the process, it was discovered that a double grating with a long nongrating region – longer than the two gratings by a factor of 10 -- has a transmission function that resembles a comb filter. It might find an application as a wavelength standard in WDM systems as has been proposed for sampled gratings that have a spectral reflectivity function similar to the aforementioned transmission function. A design approach to controlling the number and locations of the peaks in the transmission function was proposed.

Chapter 7 developed the significant useful results of the thesis by demonstrating that apodizing and phase shifting the layers of the grating independently adds more degrees of freedom to the design. The coupled-wave equations for this situation were derived, and the matrix approach was extended to encompass them.

Gratings are apodized by controlling the irradiation dose spatially. Since the light intensity is always non-negative, a “dc” index change is induced along with the “ac” index change, both proportional to the envelope of the interfering UV laser beams. The varying “dc” index change induces a chirp and gives rise to sidelobes on the short wavelength side of the main lobe in the reflectivity spectrum. Eliminating the variation in the “dc” index change yields a reflectivity spectrum that is identical to the zero-“dc” case (after adjusting the period of the gratings) in exchange for requiring a more complicated fabrication technique. A useful zero-“dc” Guassian apodized design that is conventional in the sense that all the layers are apodized by the same function was presented, and its reflectivity spectrum was computed using the matrix approach. A two-

layer, separately-apodized design was proposed and analyzed which duplicates the reflectivity response of the zero-"dc" Guassian apodized grating. However, the "dc" index change in the layers of the separately-apodized design varies in proportion to the "ac" index change, enhancing the prospects of fabricating it using a relatively simple, reproducible technique.

A technique was proposed for fabricating the two-layer, separately apodized design. It relies on fabricating a phase mask by stepping the ion beam lengthwise one half of the period of the relief pattern after it has scanned half of the distance across the mask. Then, half of the planar waveguide is masked with an opaque mask while the other half is exposed through the phase mask and a shadow mask. Next, the other half of the waveguide is masked with an opaque mask and the half not yet imprinted is exposed through the phase mask and a different shadow mask. The separately-apodized regions correspond to halves of the waveguide, but the analysis and design approach for separately-apodized layers are readily extended to this case. Other fabrication techniques are available that fabricate zero-"dc", apodized gratings that in some respects are simpler than the novel fabrication technique. However, for chirped gratings the novel fabrication technique has clearer advantages over the available fabrication techniques.

Two more grating designs were presented that are conventional in the sense that all the layers are apodized and chirped by the same function. In the context of a conventional, non-separately apodized grating, "chirping" means linearly varying either the derivative of the phase or the "dc" index change with position. The first is zero-"dc" and raised-cosine apodized with a variable period yielding a relatively flat dispersion characteristic. Thus, this grating is suitable for use as a dispersion compensator. The derivative of the phase is a linear function of position. The second has the same parameters, except the derivative of the phase is zero and the "dc" index change no longer is zero, but has a linear dependence on position as did the derivative of the phase previously. The reflectivity, group delay, and dispersion responses for the two conventional grating designs are virtually identical. Next, a 4 layer separately apodized design was proposed and analyzed that yields virtually identical reflectivity, group delay, and dispersion responses as the two conventional designs. Increasing the bandwidth of a conventional chirped grating requires increasing the chirp, that is, increasing the

difference in the grating period, if the chirp is achieved by varying the grating period, or the "dc" index change, if the chirp is achieved by varying the "dc" index change, at one end of the grating compared to the other. There is a limit to the bandwidth that can be achieved using conventional gratings that depend on varying the "dc" index change because of the limits on the maximum index change imposed by available fabrication techniques. There is no limit on the bandwidth that can be achieved using conventional gratings that depend on varying the grating period, nor is there a limit using the 4 layer separately apodized approach as long as arbitrarily complex apodizing functions are possible. Next, a 2 layer separately apodized design was proposed and analyzed that evolves out of the variable-"dc" conventional design. It achieves the identical reflectivity, group delay, and dispersion responses as the other chirped designs. Since it has half the layers, it is simpler to fabricate than the 4 layer design. It requires a slightly larger maximum index change than the variable-"dc" conventional design. As with the variable-"dc" design, the maximum possible bandwidth is not as large as for the variable-period conventional design and the 4 layer separately apodized design because of the limits on the maximum index change imposed by available fabrication techniques.

The novel fabrication technique can be extended to the 4 layer separately apodized design. The phase mask and waveguide are divided into quarters instead of halves.

A significant advantage of both the 2 layer and 4 layer separately apodized designs that yield the same responses as conventional chirped designs is that the "dc" index-change in the layers varies in proportion to the "ac" index change. That is, the form of the index change is (1+cos( )) as opposed to just cos( ), which is the form induced by the simplest fabrication techniques. Furthermore, the period of both separately apodized chirped grating designs is constant, yet they can achieve identical dispersion responses as variable-period conventional designs. These considerations enhance the prospects of fabricating the novel separately apodized designs using a relatively simple, reproducible technique. Varying the "dc" index change, but not in proportion to the "ac" index change, requires a second, computer controlled exposure. Holding the "dc" index change constant requires the same technique or a phase mask that has a variable groove shape and hence is more difficult to fabricate. Varying the grating

period harms the prospects of increasing the bandwidth as follows. Increasing the bandwidth of conventional and separately-apodized chirped gratings while preserving the level of the dispersion depends on increasing the physical length. The fabrication method detailed in [32] can produce very long gratings with no stitching errors, however it cannot vary the grating period. Thus, it cannot fabricate a variable-period chirped grating, but possibly can fabricate the separately-apodized designs that yield the identical dispersion response.

8.2 Suggestions of Future Work

The ability to fabricate the novel separately-apodized gratings proposed is an important issue. The theoretical development of the proposed fabrication technique is not complete. For instance, the expressions for the coupling-coefficients remain to be written. They require double integrals, since the separately-apodized regions no longer correspond to layers in the waveguide. A properly equipped research lab can attempt to fabricate a separately-apodized grating in a planar waveguide using the proposed method. If successful, the characteristics of the gratings can be measured and compared to theory. Devising a method for fabricating a separately-apodized optical fiber would be a breakthrough for the concept.

Appendix A

Basic Theory of Field Solutions in Multiclad Symmetric Planar Waveguides

This appendix covers the basic knowledge of planar waveguides required for an understanding of Chapter 2. A more thorough treatment is available in numerous texts, but the material presented here suffices.

A.1 Vector Helmholtz Equations

The geometry of the problem under investigation is detailed in Section 2.1. As discussed in Section 2.2, a set of fields in the waveguide having the separable form of (2.2a) and (2.2b) which satisfy Maxwell's equations, carry the electromagnetic energy along the z-direction, and exponentially decay to zero as x approaches positive or negative infinity is called a guided mode. In order to solve for the guided modes, the well-known vector Helmholtz equations are solved in each layer of the waveguide, then the boundary conditions for the tangential components of the $\mathbf{E}$ and $\mathbf{H}$ fields are imposed. The vector Helmholtz equations are easy to obtain and this may be accomplished using Maxwell's equations in phasor form. In a source-free, linear, isotropic region they are

$$\nabla \times \mathbf{E} = -j\omega\mu\mathbf{H}, \tag{A.1}$$

$$\nabla \times \mathbf{H} = j\omega\varepsilon\mathbf{E}, \tag{A.2}$$

$$\nabla \cdot \mathbf{D} = 0, \tag{A.3}$$

$$\nabla \cdot \mathbf{B} = 0. \tag{A.4}$$

The first two of these are the curl equations and constitute two equations for two unknowns, $\mathbf{E}$ and $\mathbf{H}$. As such, they can be solved for either $\mathbf{E}$ or $\mathbf{H}$. Taking the curl of (A.1) and using (A.2) gives

$$\nabla \times \nabla \times \mathbf{E} = -j\omega\mu\left(\nabla \times \mathbf{H}\right) = \omega^2\mu\varepsilon\mathbf{E}$$

assuming $\mu =$ constant. Simplifying by using the vector identity

$$\nabla \times \nabla \times \mathbf{A} = \nabla\left(\nabla \cdot \mathbf{A}\right) - \nabla^2\mathbf{A}, \tag{A.5}$$

the result, using (A.3) and assuming $n =$ constant so

$$\nabla\left(\nabla\cdot\frac{\mathbf{D}}{\varepsilon_o n^2}\right)=\frac{1}{\varepsilon_o n^2}\nabla(\nabla\cdot\mathbf{D})$$

is

$$\nabla^2\mathbf{E}+\omega^2\mu\varepsilon\,\mathbf{E}=0, \qquad \text{(A.6)}$$

which is the vector Helmholtz equation for $\mathbf{E}$. In an identical manner the vector Helmholtz equation for $\mathbf{H}$ can be derived:

$$\nabla^2\mathbf{H}+\omega^2\mu\varepsilon\,\mathbf{H}=0. \qquad \text{(A.7)}$$

The constant $k\equiv\omega\sqrt{\mu\varepsilon}$ is called the wavenumber of the medium. It has already been established that $\mu=\mu_o$ for the problem under investigation. (A.6) and (A.7) are rewritten as

$$\nabla^2\mathbf{E}+k_o{}^2n^2\mathbf{E}=0, \qquad \text{(A.8)}$$

$$\nabla^2\mathbf{H}+k_o{}^2n^2\mathbf{H}=0, \qquad \text{(A.9)}$$

where $k_o=\omega\sqrt{\mu_o\varepsilon_o}$ is the free-space wavenumber and $n=\sqrt{\varepsilon_r}$ has already been defined. Noting the $e^{-j\beta z}$ z-dependence which has been assumed, the Laplacian operator is decomposed as

$$\nabla^2=\frac{\partial^2}{\partial x^2}+\frac{\partial^2}{\partial y^2}+\frac{\partial^2}{\partial z^2}=\frac{\partial^2}{\partial x^2}+\frac{\partial^2}{\partial y^2}+(-j\beta)^2=\nabla_t{}^2+(-j\beta)^2$$

where "t" stands for transverse. It is recognized that $\frac{\partial}{\partial y}=\frac{\partial^2}{\partial y^2}=0$ for the particular problem under investigation since the slab guide extends to $\pm\infty$ along the y-axis. Then $\nabla_t{}^2=\frac{\partial^2}{\partial x^2}$ and (A.8) and (A.9) become

$$\frac{\partial^2\mathbf{E}}{\partial x^2}+\left(k_o{}^2n^2-\beta^2\right)\mathbf{E}=0, \qquad \text{(A.10)}$$

$$\frac{\partial^2\mathbf{H}}{\partial x^2}+\left(k_o{}^2n^2-\beta^2\right)\mathbf{H}=0. \qquad \text{(A.11)}$$

Dividing both sides of (A.10) and (A.11) by $e^{-j\beta z}$ gives

$$\frac{\partial^2\mathbf{e}}{\partial x^2}+\left(k_o{}^2n^2-\beta^2\right)\mathbf{e}=0, \qquad \text{(A.12)}$$

$$\frac{\partial^2 \mathbf{h}}{\partial x^2} + \left(k_o{}^2 n^2 - \beta^2\right)\mathbf{h} = 0. \qquad \text{(A.13)}$$

A.2 Solving for the Transverse Field Components $\mathbf{e}_t$ and $\mathbf{h}_t$ in Terms of e_z and h_z

Each of (A.12) and (A.13) may be split into three scalar equations. It is not necessary to solve all six equations – if the longitudinal components e_z and h_z are known the transverse components are readily determined. To show this vector equations (A.1) and (A.2) are rewritten noting the $e^{-j\beta z}$ z-dependence which has been assumed and noting $\mu = \mu_o$. The result is

$$\mathbf{a}_x\left[\frac{\partial E_z}{\partial y} + j\beta E_y\right] + \mathbf{a}_y\left[-j\beta E_x - \frac{\partial E_z}{\partial x}\right] + \mathbf{a}_z\left[\frac{\partial E_y}{\partial x} - \frac{\partial E_x}{\partial y}\right] = -j\omega\mu_o \mathbf{H}, \qquad \text{(A.14)}$$

$$\mathbf{a}_x\left[\frac{\partial H_z}{\partial y} + j\beta H_y\right] + \mathbf{a}_y\left[-j\beta H_x - \frac{\partial H_z}{\partial x}\right] + \mathbf{a}_z\left[\frac{\partial H_y}{\partial x} - \frac{\partial H_x}{\partial y}\right] = j\omega\varepsilon_o n^2 \mathbf{E}. \qquad \text{(A.15)}$$

E_y is found in terms of the longitudinal fields by substituting the x-component of (A.14) into the y-component of (A.15) yielding

$$j\omega\varepsilon_o n^2 E_y = -\frac{\partial H_z}{\partial x} + \frac{j\beta}{j\omega\mu_o}\left[\frac{\partial E_z}{\partial y} + j\beta E_y\right].$$

Multiplying both sides by $j\omega\mu_o$ and using the relation

$$k_o{}^2 = \omega^2 \mu_o \varepsilon_o$$

yields

$$\left(\beta^2 - k_o{}^2 n^2\right)E_y = j\beta\frac{\partial E_z}{\partial y} - j\omega\mu_o\frac{\partial H_z}{\partial x}$$

$$E_y = \frac{j}{T}\left[\omega\mu_o\frac{\partial H_z}{\partial x} - \beta\frac{\partial E_z}{\partial y}\right] \qquad \text{(A.16)}$$

where $T = k_o{}^2 n^2 - \beta^2$.

Dividing both sides of (A.16) by $e^{-j\beta z}$ yields

$$e_y = \frac{j}{T}\left[\omega\mu_o \frac{\partial h_z}{\partial x} - \beta \frac{\partial e_z}{\partial y}\right]. \qquad \text{(A.17)}$$

A similar procedure with the other components gives

$$e_x = -\frac{j}{T}\left[\omega\mu_o \frac{\partial h_z}{\partial y} + \beta \frac{\partial e_z}{\partial x}\right], \qquad \text{(A.18)}$$

$$h_y = -\frac{j}{T}\left[\beta \frac{\partial h_z}{\partial y} + \omega\varepsilon_o n^2 \frac{\partial e_z}{\partial x}\right], \qquad \text{(A.19)}$$

$$h_x = -\frac{j}{T}\left[\beta \frac{\partial h_z}{\partial x} - \omega\varepsilon_o n^2 \frac{\partial e_z}{\partial y}\right]. \qquad \text{(A.20)}$$

$T = k_o{}^2 n^2 - \beta^2$ throughout (A.17-A.20). The only assumptions in deriving (A.17-A.20) were the assumptions attached to (A.1) and (A.2), $\mu = \mu_o$, and $e^{-j\beta z}$ z-dependence. ε has the most general form $\varepsilon = \varepsilon_o n^2(x, y, z)$, though $e^{-j\beta z}$ z-dependence is necessarily a bad assumption unless $n = n(x, y)$. This is in contrast with (A.12) and (A.13) for which the derivation included the assumptions attached to (A.1) and (A.2), $\mu = \mu_o$, $e^{-j\beta z}$ z-dependence, $n =$ constant, and $\frac{\partial}{\partial y} = \frac{\partial^2}{\partial y^2} = 0$.

All of the assumptions in the preceding paragraph are valid for the problem under investigation for which n is piecewise constant. As has already been mentioned, (A.12) and (A.13) will be solved in each layer of the slab guide separately, then the continuity of the tangential $\mathbf{E}$ and $\mathbf{H}$ fields will be enforced.

$\frac{\partial}{\partial y} = \frac{\partial^2}{\partial y^2} = 0$ applies to the problem under investigation because the slab guide extends to $\pm\infty$ along the y-axis. Simplifying (A.17) through (A.20) by taking advantage of this fact yields the expressions

$$e_y = \frac{j\omega\mu_o}{T}\frac{dh_z}{dx}, \qquad \text{(A.21)}$$

$$e_x = -\frac{j\beta}{T}\frac{de_z}{dx}, \qquad \text{(A.22)}$$

$$h_y = -\frac{j\omega\varepsilon_o n^2}{T}\frac{de_z}{dx}, \qquad \text{(A.23)}$$

$$h_x = -\frac{j\beta}{T}\frac{dh_z}{dx}. \qquad \text{(A.24)}$$

A.3 Dividing the Fields Into Two Groups: TE and TM Modes

Examining (A.21) through (A.24) reveals that the fields can be divided into two groups: one group with (h_z, e_y, h_x) and another with (e_z, h_y, e_x). The two groups are, in fact, independent field solutions. The field solutions involving (h_z, e_y, h_x) are characterized by $e_z = 0$, that is the electric field, e_y here, lies in a plane transverse to the direction of propagation, the z-direction. For this reason the solutions with only (h_z, e_y, h_x) are referred to as TE (Transverse Electric) modes. By the same token the solutions with only (e_z, h_y, e_x) are called TM (Transverse Magnetic) modes, because h_y lies in the transverse plane.

A.4 Determining the Field Solutions for the TE Guided Modes

A.4.1 TE Modes

The remainder of this appendix sets up Section 2.3 which determines the field solutions for the TE guided modes. To begin, (A.13) is written for h_z

$$\frac{\partial^2 h_z}{\partial x^2} + \left(k_o{}^2 n^2 - \beta^2\right)h_z = 0, \quad n = \begin{cases} n_1, & 0 < x < a_1 \\ n_2, & a_1 < x < a_2 \\ n_3, & a_2 < x < a_3 \\ n_4, & a_3 < x \end{cases} \qquad \text{(A.25)}$$

It is not necessary to include $x < 0$ because the slab guide is symmetric, hence after determining the field solutions for $x > 0$ the field solutions for $x < 0$ can be written by inspection. The same propagation constant has been used in (A.25) for all regions. This must be the case to achieve phase matching at the $x = a_1, a_2,$ and a_3 interfaces for all values of z.

Let us introduce the variables

$$u_1 = k_o\sqrt{\left|n_1^{\,2} - \overline{\beta}^{\,2}\right|} \tag{A.26a}$$

$$u_2 = k_o\sqrt{\left|n_2^{\,2} - \overline{\beta}^{\,2}\right|} \tag{A.26b}$$

$$u_3 = k_o\sqrt{\left|n_3^{\,2} - \overline{\beta}^{\,2}\right|} \tag{A.26c}$$

$$u_4 = k_o\sqrt{\left|n_4^{\,2} - \overline{\beta}^{\,2}\right|} \tag{A.26d}$$

where $\overline{\beta} = \dfrac{\beta}{k_o}$ is called normalized propagation constant.

A.4.2 Even and Odd TE Modes

For $0 < x < a_1$ three solutions to (A.25) are possible

$$h_z(x < a_1) = \begin{cases} A_1 \sin u_1 x + A_2 \cos u_1 x & \text{if } n_1 > \overline{\beta} \\ A_1 \sinh u_1 x + A_2 \cosh u_1 x & \text{if } n_1 < \overline{\beta} \end{cases} \tag{A.27a}$$

$$h_z(x < a_1) = \begin{cases} A_1 \sin u_1 x & \text{if } n_1 > \overline{\beta} \\ A_1 \sinh u_1 x & \text{if } n_1 < \overline{\beta} \end{cases} \tag{A.27b}$$

and

$$h_z(x < a_1) = \begin{cases} A_1 \cos u_1 x & \text{if } n_1 > \overline{\beta} \\ A_1 \cosh u_1 x & \text{if } n_1 < \overline{\beta}\,. \end{cases} \tag{A.27c}$$

At this stage in the analysis the propagation constant is unknown. Absolute value signs are not required in the statements in (A.27) "if $n_1 > \overline{\beta}$" and "if $n_1 < \overline{\beta}$" because n_1 is defined positive and only positive $\overline{\beta}$ are considered. Once we have solved the modal fields for $\overline{\beta} > 0$, the modal fields for $\overline{\beta} < 0$, which represents propagation in the negative-z direction, may be written by making the following transformations

$$\mathbf{e}_t \to \mathbf{e}_t, \qquad \beta \to -\beta$$
$$\mathbf{h}_t \to -\mathbf{h}_t, \qquad h_z \to h_z\,.$$

The question is which of these three forms are sufficient for expressing the field in the core region? (A.27a) is the most general and undoubtedly poses no difficulty. The forms of (A.27b) and (A.27c) do not always work, however. In an asymmetric waveguide the form of (A.27b) alone or (A.27c) alone will not work because the boundary conditions

cannot be satisfied. In the symmetric case, as in the present problem, either (A.27b) or (A.27c) is sufficient for expressing the field in the core region.

When h_z in the core region has the form given by (A.27b) the transverse components, which are responsible for the flow of power, are even functions of x. The corresponding modes are referred to as even TE modes. On the other hand when (A.27c) is used for h_z the modes turn out to be odd TE modes. Which even TE modes and which odd TE modes propagate and how strongly depends upon the excitation of the waveguide.

A.4.3 Axial Component of the TE Modes in the Last Layer of Cladding

Now to assert a well-known fact regarding dielectric waveguides. For guided modes, $\overline{\beta} > n_4$ always and $\overline{\beta} < n_4$ is not possible. A heuristic proof is given in Section 2.3.8. Then "if" statements as in (A.27a,b,c) are not required when writing the field in the last layer. It might be supposed that the correct expression is

$$h_z(x > a_3) = B_1 \sinh u_4 x + B_2 \cosh u_4 x \qquad \text{(A.28)}$$

but this is not accurate. This is seen by rewriting (A.28) using the relations

$$\sinh x = \frac{e^x - e^{-w}}{2},$$

$$\cosh x = \frac{e^x + e^{-x}}{2},$$

to obtain

$$h_z(x > a_3) = B_1' e^{-u_4 x} + B_2' e^{u_4 x}. \qquad \text{(A.29)}$$

Now a requirement which has not yet been considered which pertains only to the semi-infinite (in x as well as infinite in y and z) last layer of cladding is enforced. The field must remain bounded when $x \to \infty$. Hence the term $B_2' e^{u_4 x}$ must be discarded since u_4 is taken to be positive. If u_4 were taken to be negative then $B_1' e^{-u_4 x}$ would be discarded instead, and everywhere u_4 appears in Chapter 2 it would have no minus sign in front of it. Thus equivalence with the expressions obtained by taking u_4 to be positive would be achieved.

Appendix B

Description of the Matlab Program Slab.m

In this appendix, further details are provided for the Matlab program slab.m first introduced in Section 2.3.4. Section B.1 discusses the operation of slab.m and the functions is calls, while Section B.2 discusses selecting $\Delta_{\bar{\beta}}$ and Δ_{λ_o} to avoid slab.m overlooking some or all of a mode's dispersion curve or getting stuck in an infinite loop. Finally, in Section B.3 listings of slab.m, the functions it calls, and fdist.m, the other program introduced in Section 2.3.4, are provided.

B.1 Details of Operation

As was stated in Section 2.3.4, Slab.m calls several original (not built into Matlab) Matlab functions. Two of these are described, then more details are provided for slab.m itself.

The function called UevalM.m calculates $u_1, u_2, u_3,$ and u_4 and the matrix $\mathbf{M}_{i\,j}$ given $\bar{\beta}$ and λ_o as inputs. This of course requires the values of $n_1, n_2, n_3,$ and n_4 and also $a_1, a_2,$ and a_3 which are available to UevalM.m as global variables.

As was stated in Section 2.3.4, when λ_o is fixed at some value then $\left|\mathbf{M}_{i\,j}\right| = f(\bar{\beta})$, that is, a function of $\bar{\beta}$. The original Matlab function bisection.m uses the "bisection" or "interval halving" algorithm for finding the roots of $f(\bar{\beta})$ which works as follows. If the product $\left(f(\bar{\beta})_{\bar{\beta}=a}\right)\left(f(\bar{\beta})_{\bar{\beta}=b}\right)$ is negative then $f(\bar{\beta})$ must have at least one root in the interval (a,b). If $|b-a|$ is set small enough then it is nearly certain that when the aforementioned product is negative only one root is bracketed. (See the upcoming section on the program's weaknesses.) In this case let $m = \dfrac{(a+b)}{2}$. It follows that either $f(a)f(m) < 0$ in which case a root is contained in (a,m), which becomes the current interval, or $f(m)f(b) < 0$ in which case a root is contained in (m,b), which becomes the current interval. This process is repeated until the current interval is smaller than a

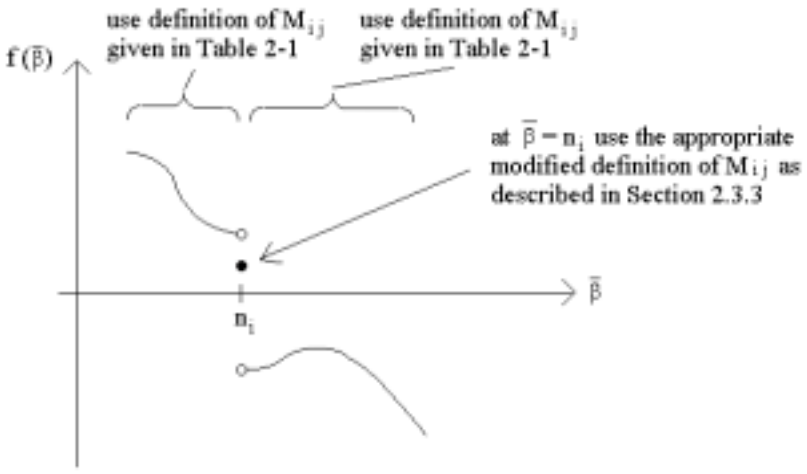

Figure B-1 Example of discontinuity at n_i

designated tolerance. One snag is that $f(\bar{\beta})$ is discontinuous at $\bar{\beta} = n_i, i = 1,2,3,$ and 4 because of the "if" statements used in the definition of $\mathbf{M}_{ij}$ given in Table 2-1. $f(\bar{\beta})$ may be positive on one side of the discontinuity and negative on the other. If so then if (a,b) encloses n_i the product $f(a)f(b)$ will be less than zero if no roots are enclosed in (a,b) and greater than zero if one root is enclosed – exactly the opposite of the correct signals. Of course $f(\bar{\beta})$ has some value at $\bar{\beta} = n_i$, i.e. at the discontinuity, which is potentially equal to zero. See Figure B-1. To determine this value use the appropriate modified definition of $\mathbf{M}_{ij}$ as described in Section 2.3.3. As described in the next paragraphs, slab.m avoids calculating $f(\bar{\beta})\big|_{\bar{\beta}=n_i}$ in order to keep the program simple and also has a method of untangling the crossed signals involving the product $f(a)f(b)$ described above.

Now additional details are provided for slab.m itself. To begin with the program searches for just the $\bar{\beta}$ for the even modes. Thus every time $\mathbf{M}_{ij}$ is calculated the first elements of the first and fourth rows of $\mathbf{M}_{ij}$ have sine and cosine forms respectively as shown in Table 2-1. After slab.m runs all the way through to its end it repeats itself, this time for odd modes.

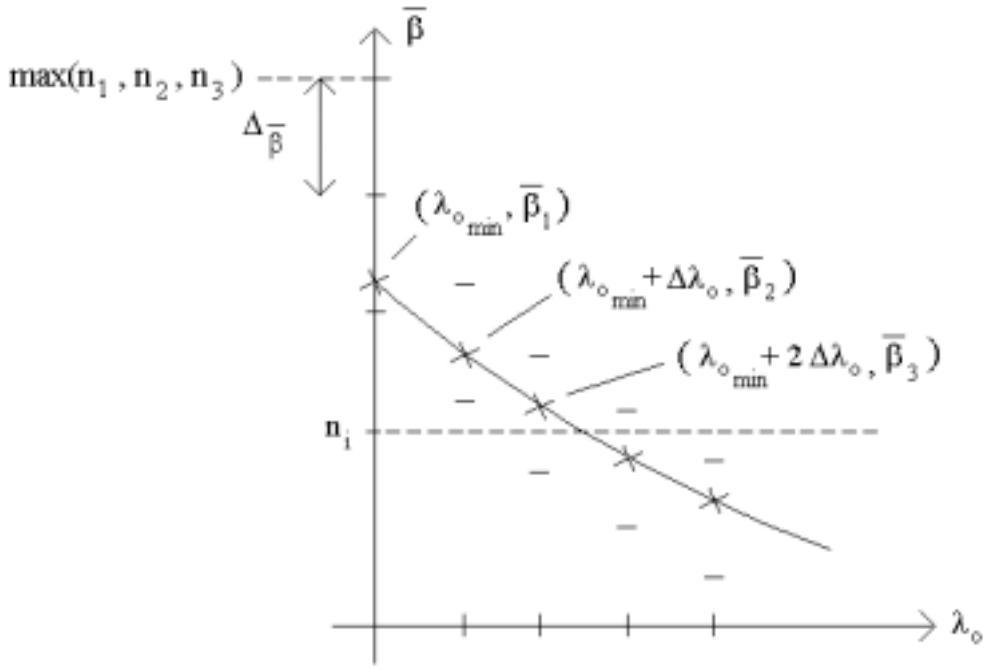

Figure B-2 Root finding technique for plotting dispersion curve

Slab.m searches for the roots of $f(\bar{\beta})$ for all $\lambda_{o\,\min} < \lambda_o < \lambda_{o\,\max}$ in the fashion illustrated in Figure B-2. Recall that it is known in advance that no roots exist outside of $n_4 < \bar{\beta} < \max(n_1, n_2, n_3)$. Slab.m first determines whether the product $f\left(\max(n_1, n_2, n_3) - n\Delta_{\bar{\beta}}\right) f\left(\max(n_1, n_2, n_3) - (n+1)\Delta_{\bar{\beta}}\right)$, $n = 1$, is negative. $f(\cdot)$ is evaluated by calling the function detM.m which in turn calls the function UevalM.m. If the product is not negative with $n = 1$ it evaluates with $n = 2,3,$ etc. until it finds an interval containing a root. It then sends the endpoints of this interval to bisection.m and receives back the value of the enclosed root to within the designated tolerance. This root is labelled $\bar{\beta}_1$ in Figure B-2.

Slab.m next sets λ_o to $\lambda_{o\,\min} + \Delta\lambda_o$ and evaluates the product $f(\bar{\beta}_1) f\left(\bar{\beta}_1 - \Delta_{\bar{\beta}}\right)$. At $\lambda_o = \lambda_{o\,\min} + \Delta\lambda_o$ a root should lie just below where the root was located at $\lambda_{o\,\min}$, so $\bar{\beta}_1$ is the initial value of the search. Unless one of the indices is enclosed in the interval $\left(\bar{\beta}_1, \bar{\beta}_1 + \Delta_{\bar{\beta}}\right)$ the product is negative and the endpoints of the interval are subsequently

sent to bisection.m which locates the enclosed root. This assumes we have not set $\Delta\lambda_o$ too large or $\Delta\overline{\beta}$ too small relative to the slope of the curve.

Next λ_o is set equal to $\lambda_{o\min} + 2\Delta\lambda_o$ and the endpoints of the search interval are set equal to $\overline{\beta}_2$ and $\overline{\beta}_2 - \Delta_{\overline{\beta}}$. Suppose one of the indices n_i is enclosed as shown in Figure B-2. Slab.m evaluates the product $f\left(\overline{\beta}_2\right) f\left(\overline{\beta}_2 - \Delta_{\overline{\beta}}\right)$, notes that it is positive, and concludes that one of the refractive indices n_i is enclosed, call it n_i, then evaluates the product $f\left(\overline{\beta}_2\right) f\left(n_i + \dfrac{\Delta_{\overline{\beta}}}{1x10^{10}}\right)$. Continuing to speak of the example curve shown in Figure B-2, since the root at $\lambda_{o\min} + 2\Delta\lambda_o$ lies just above n_i, the product is negative. Slab.m concludes that the root lies within $\left(\overline{\beta}_2, n_i + \dfrac{\Delta_{\overline{\beta}}}{1x10^{10}}\right)$, i.e. lies above n_i, and sends these endpoints to bisection.m which returns the enclosed root.

Next λ_o is set equal to $\lambda_{o\min} + 3\Delta\lambda_o$ and the endpoints of the search interval are set equal to $\overline{\beta}_3$ and $\overline{\beta}_3 - \Delta_{\overline{\beta}}$. Slab.m evaluates the product $f\left(\overline{\beta}_3\right) f\left(\overline{\beta}_3 - \Delta_{\overline{\beta}}\right)$, finds that it is positive and concludes that one of the refractive indices is enclosed. It then determines which refractive index is the one, which we know is the same n_i though the program doesn't at first, then evaluates the product $f\left(\overline{\beta}_3\right) f\left(n_i + \dfrac{\Delta_{\overline{\beta}}}{1x10^{10}}\right)$. For the curve shown in Figure B-2 the product is positive since the root lies below n_i. After slab.m discovers this it sends the endpoints $\left(n_i - \dfrac{\Delta_{\overline{\beta}}}{1x10^{10}}, n_i - \dfrac{\Delta_{\overline{\beta}}}{1x10^{10}} - \Delta_{\overline{\beta}}\right)$ to bisection.m which locates the enclosed root which we are certain is present unless we have chosen Δ_{λ_o} too large or $\Delta_{\overline{\beta}}$ too small relative to the slope of the curve.

Slab.m then returns to the vertical line $\lambda_o = \lambda_{o\min}$ to the bottom endpoint of the search interval inside of which the first root was found. It searches downward again until it finds the next root, then uses the same procedure as before to find all the roots at

$\lambda_{o\min} + n\Delta_{\lambda_o}$, $n = 1,2,3...$, $\lambda_o < \lambda_{o\max}$ lying on this the second curve. Afterwards it returns to $\lambda_o = \lambda_{o\min}$ to the bottom of the last interval and searches downward once again. Eventually the vertical line $\lambda_o = \lambda_{o\min}$ is searched interval by interval down to $\bar{\beta} = n_4 + \frac{\Delta_{\bar{\beta}}}{1x10^4}$, then the search has encompassed $\max(n_1, n_2, n_3) - \Delta_{\bar{\beta}} \le \bar{\beta} \le n_4 + \frac{\Delta_{\bar{\beta}}}{1x10^4}$ and is complete.

The program repeats itself, this time searching for the $\bar{\beta}$ for the odd modes. Then the dispersion curves are plotted, the even modes with a solid line and the odd modes with a dotted line.

B.2 Selecting $\Delta_{\bar{\beta}}$ and Δ_{λ_o} for Correct Operation of Slab.m

A few pathological problems may cause slab.m to overlook some or all of a mode's dispersion curve or get stuck in an infinite loop. In general this only occurs when the choices of $\Delta_{\bar{\beta}}$ and Δ_{λ_o} used are wrong for the particular problem. By tweaking these variables or the initial values of the first search intervals $\max[n_1, n_2, n_3] - \Delta_{\bar{\beta}}$ and $\lambda_{o\min} + \Delta_{\lambda_o}$ the program can be made to run normally. Use the following guidelines.

- An infinite loop results when $\Delta_{\bar{\beta}}$ is not large enough relative to Δ_{λ_o} and the slopes of the dispersion curves.
- Do not enter n1, n2, n3, and n4 with any two indices spaced closer than $\Delta_{\bar{\beta}}$ unless they are equal.
- An infinite loop results when one of the $\bar{\beta}$ at one of the λ_o computed lies within $\frac{\Delta_{\bar{\beta}}}{1x10^{10}}$ of one of the indices – an extremely unlikely occurrence.
- An infinite loop is possible if two even mode or two odd mode curves pass within $\Delta_{\bar{\beta}}$ of each other.
- In searching for the initial values of the curves, that is the $\bar{\beta}$ at $\lambda_{o\min}$, if one of the values of $\bar{\beta}$ falls close to one of the indices and we are not lucky then that $\bar{\beta}$ and its entire curve will not be discovered.

B.3 Program Listings

Listings of slab.m, the functions it calls, and fdist.m, the other program introduced in Section 2.3.4, follow. See Section 2.3.4 for a description of fdist.m.

slab.m

```
clear all; %close all;

global n1 n2 n3 n4
global a1 a2 a3

%inputs%%%%%%
% WARNING: do not enter n1..n4 that are spaced closer together than delta
% Other possible pitfall for program: if Bbar at one of the lambdao computed
% lies within delta/1e10 of one of the indices.

nSiO2=1.44691047; % at lambdao=1.3 um
n1=1.5;
n2=1.49;
n3=1.485;
n4=1.48;
a1=1e-6;
a2=5e-6;
a3=7e-6;
minLambdao = 1.0e-6;
maxLambdao = 1.4e-6;
accuracy=1e-10;
%%%%%%%%%%%%


delta=(max([n1 n2 n3 n4])-n4)/50
delLambdao=(maxLambdao-minLambdao)/(400)
N=[n1 n2 n3 n4]; % list n4 last, list in order for refco.m

for toggleNum=1:2
if toggleNum==1 toggle='eve'
else toggle='odd'
end; % if toggleNum

aBbar=max([n1 n2 n3 n4])-delta;
aDetM=detM(aBbar,minLambdao,toggle);
count=0;
while aBbar>(n4+delta/1e4)
   bBbar=aBbar-delta;
   if bBbar<n4
      bBbar=n4+delta/1e4;
   end; % if bBbar
   bDetM=detM(bBbar,minLambdao,toggle);
   if aDetM*bDetM<0 & sum((aBbar*ones(1,3)-[n1 n2 n3]).*(bBbar*ones(1,3)-[n1 n2
n3])<0)==0
      count=count+1
      Bbar(1,count,toggleNum)=Bisection('detM',aBbar,bBbar,minLambdao,toggle,accuracy);
      lambdao=minLambdao;
      index=1;
      flag=0;
      while lambdao<=maxLambdao-delLambdao
         if flag<1
            lambdao=lambdao+delLambdao;
            index=index+1;
            initial=Bbar(index-1,count,toggleNum);
         end; % if flag<
         final=initial-delta;
         if final<=n4
            final=n4+delta/1e10;
         end; % if final
         if detM(initial,lambdao,toggle)*detM(final,lambdao,toggle)<0
```

```
Bbar(index,count,toggleNum)=Bisection('detM',initial,final,lambdao,toggle,accuracy);
            flag=0;
         else
            if final==n4 +delta/1e10
               lambdao=maxLambdao;
            end; % if ifnal=n4
            for j=1:length(N)-1
               if (initial-N(j))*(final-N(j))<0
                  if detM(initial,lambdao,toggle)*detM(N(j)+delta/1e10,lambdao,toggle)<0

Bbar(index,count,toggleNum)=Bisection('detM',initial,N(j)+delta/1e10,...
                     lambdao,toggle,accuracy);
                  else
                     initial=N(j)-delta/1e10;
                     flag=1;
                  end; % if detM
               end; % if (initial
            end; % for j=
         end; % if detM
      end; % while lambdao
   end; % if aDetM
aBbar=bBbar;
aDetM=bDetM;
end; % while aBbar

end; % for toggleNum

lambdao=minLambdao:delLambdao:minLambdao+delLambdao*(length(Bbar)-1);
axis([min(lambdao) max(lambdao) n4 max(N)]);
plot(lambdao,Bbar(:,:,1)); hold on;
if length(size(Bbar))==3
   plot(lambdao,Bbar(:,:,2),'--');
end
if n2==n3 & n3==n4
   title(['n1= ',num2str(n1,6),', n2= ',num2str(n2,6),', n3= ',num2str(n3,6),', n4= ',...
   num2str(n4,6),', a1= ',num2str(a1),'m  (a2, a3 are irrelevant)']);
else
   title(['n1= ',num2str(n1,6),', n2= ',num2str(n2,6),', n3= ',num2str(n3,6),', n4= ',...
   num2str(n4,6),', a1= ',num2str(a1),'m, a2= ',num2str(a2),'m, a3= ',num2str(a3),'m']);
end; % if a2==a3
xlabel('Lambdao (meters)');
ylabel('Bbar');
axis([min(lambdao) max(lambdao) n4 max(N)]);
```

UevalM.m

```
function[M,U] = UevalM(Bbar,lambdao,toggle);

global n1 n2 n3 n4
global a1 a2 a3
ko=2*pi/lambdao;

if sum(Bbar*ones(1,4)==[n1 n2 n3 n4]) >= 1 disp ('pWarning: Bbar equal n1,.. or n4');
end; % if sum

u1=ko*sqrt(abs(n1^2-Bbar^2));
u2=ko*sqrt(abs(n2^2-Bbar^2));
u3=ko*sqrt(abs(n3^2-Bbar^2));
% u4=ko*sqrt(Bbar^2-n4^2); % doesn't matter whether use this line or next
u4=ko*sqrt(abs(n4^2-Bbar^2));
U=[u1 u2 u3 u4];

if n1>Bbar
   if toggle=='eve'
      M(1,1)=sin(u1*a1);
   else M(1,1)=cos(u1*a1);
   end; % if toggle
else
   if toggle=='eve'
      M(1,1)=sinh(u1*a1);
```

```
   else M(1,1)=cosh(u1*a1);
   end; % if toggle
end; % if n1>

if n2>Bbar
   M(1,2)=-sin(u2*a1);
   M(1,3)=-cos(u2*a1);
   M(2,2)=sin(u2*a2);
   M(2,3)=cos(u2*a2);
else
   M(1,2)=-sinh(u2*a1);
   M(1,3)=-cosh(u2*a1);
   M(2,2)=sinh(u2*a2);
   M(2,3)=cosh(u2*a2);
end; % if n2>

M(1,4:6)=0;
M(2,1)=0;

if n3>Bbar
   M(2,4)=-sin(u3*a2);
   M(2,5)=-cos(u3*a2);
   M(3,4)=sin(u3*a3);
   M(3,5)=cos(u3*a3);
else
   M(2,4)=-sinh(u3*a2);
   M(2,5)=-cosh(u3*a2);
   M(3,4)=sinh(u3*a3);
   M(3,5)=cosh(u3*a3);
end; % if n3>

M(2,6)=0;
M(3,1:3)=0;
M(3,6)=-exp(-u4*a3);

if n1>Bbar
   if toggle=='eve'
      M(4,1)=a1*u2*cos(u1*a1);
   else M(4,1)=-a1*u2*sin(u1*a1);
   end; % if toggle
else
   if toggle=='eve'
      M(4,1)=-a1*u2*cosh(u1*a1);
   else M(4,1)=-a1*u2*sinh(u1*a1);
   end; % if toggle
end; % if n1>

if n2>Bbar
   M(4,2)=-a1*u1*cos(u2*a1);
   M(4,3)=a1*u1*sin(u2*a1);
   M(5,2)=a2*u3*cos(u2*a2);
   M(5,3)=-a2*u3*sin(u2*a2);
else
   M(4,2)=a1*u1*cosh(u2*a1);
   M(4,3)=a1*u1*sinh(u2*a1);
   M(5,2)=-a2*u3*cosh(u2*a2);
   M(5,3)=-a2*u3*sinh(u2*a2);
end; % if n2>

M(4,4:6)=0;
M(5,1)=0;

if n3>Bbar
   M(5,4)=-a2*u2*cos(u3*a2);
   M(5,5)=a2*u2*sin(u3*a2);
   M(6,4)=a3*u4*cos(u3*a3);
   M(6,5)=-a3*u4*sin(u3*a3);
else
   M(5,4)=a2*u2*cosh(u3*a2);
   M(5,5)=a2*u2*sinh(u3*a2);
   M(6,4)=-a3*u4*cosh(u3*a3);
```

```
   M(6,5)=-a3*u4*sinh(u3*a3);
end; % if n3>

M(5,6)=0;
M(6,1:3)=0;
M(6,6)=-a3*u3*exp(-u4*a3);
```

Bisection.m

```
function root = Bisection(fname,a,b,lambdao,toggle,accuracy);

fa=feval(fname,a,lambdao,toggle);
fb=feval(fname,b,lambdao,toggle);
while abs(a-b) > accuracy+eps*max(abs(a),abs(b))
   mid=(a+b)/2;
   fmid=feval(fname,mid,lambdao,toggle);
   if fa*fmid<=0
      % There is a root in [a,mid].
      b=mid;
      %fb=fmid;
   else
      % There is a root in [mid,b].
      a=mid;
      fa=fmid;
   end
end
root=(a+b)/2;
```

detM.m

```
function [detM] = detM(Bbar,lambdao,toggle);
M=UevalM(Bbar,lambdao,toggle);
detM=det(M);
```

fdist.m

```
% Run slab.m first.

% Plot the field distribution for one pair of (lambdao,Bbar) on the curve
% generated by slab.m .  First find A given A(1)=1.
%inputs%%%%%%
j=201;
toggleNum=1; % 1=even, 2=odd
if toggleNum==1 toggle='eve'; else toggle='odd'; end;
count=1;
%%%%%%%%%%%%

lambdao=minLambdao+delLambdao*(j-1);
BbarP=Bbar(j,count,toggleNum);

[M,U]=UevalM(BbarP,lambdao,toggle);
Mpeice2=M(1:5,2:6);
Mpeice1=M(1:5,1);
A(1)=1;
A(2:6)=inv(Mpeice2)*(-1)*Mpeice1*A(1);

% Compute ey/(j*omega*uo);
delx=(a3+(a3-a2)*5)/1000;

x=0:delx:a1;
x=x';
if n1>BbarP
   if toggle=='eve'
      ey=A(1)*cos(U(1)*x)/U(1);
      hz=A(1)*sin(U(1)*x);
   else
      ey=-A(1)*sin(U(1)*x)/U(1);
      hz=A(1)*cos(U(1)*x);
   end; % if toggle
else
   if toggle=='eve'
```

```
      ey=A(1)*cosh(U(1)*x)/-U(1);
      hz=A(1)*sinh(U(1)*x);
   else
      ey=A(1)*sinh(U(1)*x)/-U(1);
      hz=A(1)*cosh(U(1)*x);
   end; % if toggle
end; % if n1>

x=x(length(x))+delx:delx:a2;
x=x';
if n2>BbarP
   ey=[ey; (A(2)*cos(U(2)*x)-A(3)*sin(U(2)*x))/U(2)];
   hz=[hz; A(2)*sin(U(2)*x)+A(3)*cos(U(2)*x)];
else
   ey=[ey; (A(2)*cosh(U(2)*x)+A(3)*sinh(U(2)*x))/-U(2)];
   hz=[hz; A(2)*sinh(U(2)*x)+A(3)*cosh(U(2)*x)];
end; % if n2>

x=x(length(x))+delx:delx:a3;
x=x';
if n3>BbarP
   ey=[ey; (A(4)*cos(U(3)*x)-A(5)*sin(U(3)*x))/U(3)];
   hz=[hz; A(4)*sin(U(3)*x)+A(5)*cos(U(3)*x)];
else
   ey=[ey; (A(4)*cosh(U(3)*x)+A(5)*sinh(U(3)*x))/-U(3)];
   hz=[hz; A(4)*sinh(U(3)*x)+A(5)*cosh(U(3)*x)];
end; % if n3>

x=x(length(x))+delx:delx:a3+(a3-a2)*10;
x=x';
ey=[ey; A(6)*exp(-U(4)*x)/U(4)];
hz=[hz; A(6)*exp(-U(4)*x)];

figure; orient tall;
subplot(2,1,1);
plot(0:delx:a3+(a3-a2)*10,ey/max(abs(ey)));
title(['ey / j, lambdao= ',num2str(lambdao)]);
legend(['TE',num2str(toggleNum-1+(count-1)*2)]);
V=axis;
text(V(1)+(V(2)-V(1))*1/2,V(3)+(V(4)-V(3))/6,['Bbar= ',num2str(BbarP),', n1= ',...
num2str(n1),', n2= ',num2str(n2),', n3= ',num2str(n3)]);
text(V(1)+(V(2)-V(1))*1/2,V(3)+(V(4)-V(3))/10,['n4= ',num2str(n4),', a1= ',...
num2str(a1),', a2= ',num2str(a2),', a3= ',num2str(a3)]);
line('linestyle','--','xdata',[a1 a1],'ydata',[V(3) V(4)]);
line('linestyle','--','xdata',[a2 a2],'ydata',[V(3) V(4)]);
line('linestyle','--','xdata',[a3 a3],'ydata',[V(3) V(4)]);

subplot(2,1,2);
plot(0:delx:a3+(a3-a2)*10,hz/max(abs(hz)));
title(['hz, lambdao= ',num2str(lambdao)]);
legend(['TE',num2str(toggleNum-1+(count-1)*2)]);
V=axis;
text(V(1)+(V(2)-V(1))*1/2,V(3)+(V(4)-V(3))/6,['Bbar= ',num2str(BbarP),', n1= ',...
num2str(n1),', n2= ',num2str(n2),', n3= ',num2str(n3)]);
text(V(1)+(V(2)-V(1))*1/2,V(3)+(V(4)-V(3))/10,['n4= ',num2str(n4),', a1= ',...
num2str(a1),', a2= ',num2str(a2),', a3= ',num2str(a3)]);
line('linestyle','--','xdata',[a1 a1],'ydata',[V(3) V(4)]);
line('linestyle','--','xdata',[a2 a2],'ydata',[V(3) V(4)]);
line('linestyle','--','xdata',[a3 a3],'ydata',[V(3) V(4)]);
```

Appendix C

Explanation of Figure 3-4

First, realizing that (3.35) does not have to be piecewise defined, either expression can be used whether S is real or imaginary. They are equivalent because of the identities

$$\sinh(jx) = j\sin x$$
$$\cosh(jx) = \cos x$$
$$\sin(jx) = j\sinh x$$
$$\cos(jx) = \cosh x\,.$$

The only advantage of using the expression labeled "S real" when S is real and the other when S is imaginary is all terms will be real and a computer used to evaluate the expression does not have to be able to find sinh, cosh, sin, or cos of an imaginary quantity. The expression labeled "S real" will be rearranged into a form that lends itself to plotting Figure 3-4. The rearranged version also will be valid whether S is real or imaginary. Since, using (3.30),

$$S^2 = -\frac{3}{4}C_o{}^2 - C_o\delta - \frac{\delta^2}{4}$$

and

$$\left(\frac{\delta}{2} + C_o\right)^2 + S^2 = \frac{\delta^2}{4} + \delta C_o + C_o{}^2 + S^2 = \frac{C_o{}^2}{4}$$

using the identity

$$\cosh^2 x - \sinh^2 x = 1 \qquad \text{(C.1)}$$

yields

$$R = \frac{\sinh^2(LS)}{\cosh^2(LS) - \dfrac{(\delta + 2C_o)^2}{C_o{}^2}}\,. \qquad \text{(C.2)}$$

Expanding LS yields

$$LS = \sqrt{\frac{(LC_o)^2}{4} - \frac{(LC_o)^2}{4}\frac{(\delta + 2C_o)^2}{C_o{}^2}}\,. \qquad \text{(C.3)}$$

It is seen that R depends on just (LC_o) and $\frac{(\delta + 2C_o)}{C_o}$.

Because the range of λ_o over which R is non-negligible is very small except possibly under unusual circumstances as explained in section 3.5, β can be approximated as

$$\beta \approx -s\lambda_o + b \qquad \text{(C.4)}$$

where s is positive. Using the definition of δ

$$\delta = 2\beta - \frac{2\pi}{\Lambda} \qquad (3.28)$$

and substituting in (C.4) it follows that

$$\frac{\delta + 2C_o}{C_o} \approx \frac{-2s\lambda_o + 2b - \frac{2\pi}{\Lambda} + 2C_o(\lambda_o)}{C_o(\lambda_o)}. \qquad \text{(C.5)}$$

Equation (C.5) will be simplified in three steps. First it is noted that C_o varies by only 1 or 2 percent over the range of λ_o over which R is non-negligible. $C_o(\lambda_o)$ in (C.5) is replaced with its value at λ_{o_D}, introducing a small amount of error. Next, using (3.43) yields

$$\beta(\lambda_{o_D}) = -s\lambda_{o_D} + b = \frac{\pi}{\Lambda} - C_o(\lambda_{o_D})$$

and solving for b yields

$$b = \frac{\pi}{\Lambda} - C_o(\lambda_{o_D}) + s\lambda_{o_D}. \qquad \text{(C.6)}$$

The value of s could be the value of the slope of the exact β versus λ_o curve at λ_{o_D} or anywhere in the vicinity – it matters little. Lastly (C.6) is substituted into (C.5) yielding

$$\frac{\delta + 2C_o}{C_o} \approx -\frac{2s}{C_o}(\lambda_o - \lambda_{o_D}). \qquad \text{(C.7)}$$

The RHS of (C.7) can be interpreted as normalized wavelength. Figure 3-4 is a plot of R versus this normalized wavelength using (C.2) and (C.3). Two sources of error are present:

1. C_o is set equal to $C_o(\lambda_{o_D})$, a constant independent of λ_o. Without this approximation a single value of LC_o cannot be associated with any R versus λ_o curve.
2. The β versus λ_o curve is approximated as a straight line given by (C.4) over the range of λ_o over which R is non-negligible.

Appendix D

Solution for the Power Reflectivity for Non-Zero Phase Shift Grating Layers

Differentiating (4.3a), yields

$$\frac{d^2\psi_1}{dz^2} = -jC_o\frac{d\psi_1}{dz} - jK^* e^{j\delta z}\left(\frac{d\psi_2}{dz} + j\delta\psi_2\right) \tag{D.1}$$

where

$$\delta = 2\beta - \frac{2\pi}{\Lambda} \tag{D.2}$$

as in Chapter 3.

Substituting for $\frac{d\psi_2}{dz}$ from (4.3b) yields

$$\frac{d^2\psi_1}{dz^2} = -jC_o\frac{d\psi_1}{dz} - jK^* e^{j\delta z}\left(jK\psi_1 e^{-j\delta z} + j(C_o+\delta)\psi_2\right). \tag{D.3}$$

Now, substituting for ψ_2 from (4.3a) results in

$$\frac{d^2\psi_1}{dz^2} = \frac{d\psi_1}{dz}\,j\delta + \psi_1\left[K^*K - (C_o+\delta)C_o\right] \tag{D.4}$$

which has the solution

$$\psi_1(z) = e^{j\frac{\delta}{2}z}\left(B_1 e^{zS} + B_1' e^{-zS}\right). \tag{D.5}$$

In (D.5), B_1 and B_1' are arbitrary constants and

$$S = \sqrt{|K|^2 - \left(\frac{\delta}{2} + C_o\right)^2}\ . \tag{D.6}$$

$\psi_2(z)$ is solved in an identical manner. The result is

$$\psi_2(z) = e^{-j\frac{\delta}{2}z}\left(B_2 e^{zS} + B_2' e^{-zS}\right) \tag{D.7}$$

where B_2 and $B_2^{'}$ are two new arbitrary constants. It is assumed that the section of the waveguide containing gratings extends from $z = 0$ to $z = L$. Enforcing the boundary condition $\psi_2(L) = 0$, yields

$$B_2^{'} = -B_2 e^{2SL}. \tag{D.8}$$

Therefore,

$$\psi_2(z) = 2B_2\, e^{\left(SL - j\frac{\delta}{2}z\right)} \sinh[(z-L)S]. \tag{D.9}$$

Using (D.9) in (4.3b), the solution for $\psi_1(z)$ is obtained as

$$\psi_1(z) = \frac{-j2}{K} B_2 e^{\left(SL + j\frac{\delta}{2}z\right)} \left\{ S\cosh[(z-L)S] - j\left(\frac{\delta}{2} + C_o\right)\sinh[(z-L)S] \right\}. \tag{D.10}$$

Now, the expressions for $\psi_1(z)$ and $\psi_2(z)$ contain only one arbitrary constant B_2 which depends on $\psi_1(0)$, the strength of the wave travelling in the positive-z direction incident at $z = 0$.

To solve for the power reflectivity, first the power of the positive-travelling wave within the grating is found. The result is

$$P_1(z) = \begin{cases} \dfrac{4}{|K|^2}|B_2|^2 e^{2SL}\left\{ S^2\cosh^2[(z-L)S] + \left(\dfrac{\delta}{2} + C_o\right)^2 \sinh^2[(z-L)S] \right\}, & S \text{ real} \\ \dfrac{4}{|K|^2}|B_2|^2 \left\{ \hat{S}^2\cos^2[(z-L)\hat{S}] + \left(\dfrac{\delta}{2} + C_o\right)^2 \sin^2[(z-L)\hat{S}] \right\}, & S \text{ imaginary} \end{cases}$$

(D.11)

where

$$\hat{S} = \sqrt{\left(\frac{\delta}{2} + C_o\right)^2 - |K|^2}. \tag{D.12}$$

The power of the negative-travelling wave within the grating is given by

$$P_2(z) = \begin{cases} 4|B_2|^2 e^{2SL}\sinh^2[(z-L)S], & S \text{ real} \\ 4|B_2|^2 \sin^2[(z-L)\hat{S}], & S \text{ imaginary} \end{cases}. \tag{D.13}$$

Dividing (D.13) by (D.11), the power reflectivity is given by

$$R = \frac{P_2(0)}{P_1(0)} = \begin{cases} \dfrac{|K|^2 \sinh^2(LS)}{S^2 \cosh^2(LS) + \left(\dfrac{\delta}{2} + C_o\right)^2 \sinh^2(LS)}, & S \text{ real} \\ \dfrac{|K|^2 \sin^2(L\hat{S})}{\hat{S}^2 \cos^2(L\hat{S}) + \left(\dfrac{\delta}{2} + C_o\right)^2 \sin^2(L\hat{S})}, & S \text{ imaginary} \end{cases} . \qquad \text{(D.14)}$$

Appendix E

Matlab Program Listings

This appendix contains listings of the Matlab programs that produced the plots in Chapters 4 through 7. Detailed descriptions are not provided for them as were for slab.m and its subprograms in Appendix B. The listings themselves contain some comments, but not so that the programs will be easily understood without substantial self-study. A detailed understanding of these programs should not be required to understand the results and methods in this thesis. Program listings are provided for readers trying to reproduce some plots or who find the description of an algorithm in one chapter inadequate on some point.

E.1 Chapter 4

The program RefcoPhv2.m and its subprogram eysqr.m produced Figures 4-1 through 4-4.

RefcoPhv2.m

```
% Run slab.m first.

%inputs%%%%%%
alpha=0.4;
delnL1=alpha*(N(1)-nSiO2); % must be <= .1 N(1)
delnL2=alpha*(N(2)-nSiO2); % must be <= .1 N(2)
delnL3=alpha*(N(3)-nSiO2); % must be <= .1 N(3), zero is ok
delnL4=alpha*(N(4)-nSiO2); % must be <= .1 N(4), zero is ok
CenterLambdao=1.3e-6;
L=.0005; % length in meters

pl2mpl1 = 0*pi/180;
pl3mpl1 = 0*pi/180;
pl4mpl1 = 0*pi/180;

v=1;

%%%%%%%%%%%%

a=[0 a1 a2 a3];
toggleNum=1; % 1=even
toggle='eve';
count=1;

S=size(Bbar);
if length(S)>2
   disp('Waveguide is not single mode!');
end; % if length


% next block calculates GratLambda which determines CenterLambdao

Centerindex=1+round( (CenterLambdao-minLambdao)/delLambdao );
ActualCenterL=minLambdao+delLambdao*(Centerindex-1);
j=Centerindex;
```

```
lambdao=minLambdao+delLambdao*(j-1);
BbarP=Bbar(j,count,toggleNum);

[M,U]=UevalM(BbarP,lambdao,toggle);
Mpeice2=M(1:5,2:6);
Mpeice1=M(1:5,1);
A(1)=1;
A(2:6)=inv(Mpeice2)*(-1)*Mpeice1*A(1);

P=2*.5*BbarP/377*quad8('eysqr',0,10*a3,[],[],A,U,BbarP,lambdao);
A=A/sqrt(P);

Co=2*.5*2*pi/lambdao/377* ( N(1)*delnL1*quad8('eysqr',a(1),a(2),[],[],A,U,BbarP,lambdao)
                ...
+ N(2)*delnL2*quad8('eysqr',a(2),a(3),[],[],A,U,BbarP,lambdao) ...
+ N(3)*delnL3*quad8('eysqr',a(3),a(4),[],[],A,U,BbarP,lambdao) ...
+ N(4)*delnL4*quad8('eysqr',a(4),10*a(4),[],[],A,U,BbarP,lambdao) );

GratLambda=pi/( Bbar(Centerindex,1,1)*2*pi/ActualCenterL + Co);

if pl3mpl1 == 180*pi/180
   K = 2*pi/lambdao/377 /2 * v * ( ...
   N(1)*delnL1*quad8('eysqr',a(1),a(2),[],[],A,U,BbarP,lambdao) ...
   + exp(-sqrt(-1)*pl2mpl1) *
               N(2)*delnL2*quad8('eysqr',a(2),a(3),[],[],A,U,BbarP,lambdao) ...
   + -1 * N(3)*delnL3*quad8('eysqr',a(3),a(4),[],[],A,U,BbarP,lambdao) ...
   + exp(-sqrt(-1)*pl4mpl1) *
               N(4)*delnL4*quad8('eysqr',a(4),10*a(4),[],[],A,U,BbarP,lambdao) )
else
   K = 2*pi/lambdao/377 /2 * v * ( ...
   N(1)*delnL1*quad8('eysqr',a(1),a(2),[],[],A,U,BbarP,lambdao) ...
   + exp(-sqrt(-1)*pl2mpl1) *
               N(2)*delnL2*quad8('eysqr',a(2),a(3),[],[],A,U,BbarP,lambdao) ...
   + exp(-sqrt(-1)*pl3mpl1) *
               N(3)*delnL3*quad8('eysqr',a(3),a(4),[],[],A,U,BbarP,lambdao) ...
   + exp(-sqrt(-1)*pl4mpl1) *
               N(4)*delnL4*quad8('eysqr',a(4),10*a(4),[],[],A,U,BbarP,lambdao) )
end;

%% end of block


for j=1:S(1)

   lambdao=minLambdao+delLambdao*(j-1);
   BbarP=Bbar(j,count,toggleNum);

   [M,U]=UevalM(BbarP,lambdao,toggle);
   Mpeice2=M(1:5,2:6);
   Mpeice1=M(1:5,1);
   A(1)=1;
   A(2:6)=inv(Mpeice2)*(-1)*Mpeice1*A(1);

   P=2*.5*BbarP/377*quad8('eysqr',0,10*a3,[],[],A,U,BbarP,lambdao);
   A=A/sqrt(P);

   Co=2*.5*2*pi/lambdao/377* (
               N(1)*delnL1*quad8('eysqr',a(1),a(2),[],[],A,U,BbarP,lambdao) ...
   + N(2)*delnL2*quad8('eysqr',a(2),a(3),[],[],A,U,BbarP,lambdao) ...
   + N(3)*delnL3*quad8('eysqr',a(3),a(4),[],[],A,U,BbarP,lambdao) ...
   + N(4)*delnL4*quad8('eysqr',a(4),10*a(4),[],[],A,U,BbarP,lambdao) );

   CoTrack(j) = Co;

   % omega*epsilo = 2*pi/lambdao/377

   if pl3mpl1 == 180*pi/180
      K = 2*pi/lambdao/377 /2 * v * ( ...
      N(1)*delnL1*quad8('eysqr',a(1),a(2),[],[],A,U,BbarP,lambdao) ...
```

```
      + exp(-sqrt(-1)*pl2mpl1) *
               N(2)*delnL2*quad8('eysqr',a(2),a(3),[],[],A,U,BbarP,lambdao) ...
      + -1 * N(3)*delnL3*quad8('eysqr',a(3),a(4),[],[],A,U,BbarP,lambdao) ...
      + exp(-sqrt(-1)*pl4mpl1) *
               N(4)*delnL4*quad8('eysqr',a(4),10*a(4),[],[],A,U,BbarP,lambdao) );
   else
      K = 2*pi/lambdao/377 /2 * v * ( ...
      N(1)*delnL1*quad8('eysqr',a(1),a(2),[],[],A,U,BbarP,lambdao) ...
      + exp(-sqrt(-1)*pl2mpl1) *
               N(2)*delnL2*quad8('eysqr',a(2),a(3),[],[],A,U,BbarP,lambdao) ...
      + exp(-sqrt(-1)*pl3mpl1) *
               N(3)*delnL3*quad8('eysqr',a(3),a(4),[],[],A,U,BbarP,lambdao) ...
      + exp(-sqrt(-1)*pl4mpl1) *
               N(4)*delnL4*quad8('eysqr',a(4),10*a(4),[],[],A,U,BbarP,lambdao) );
   end;

   Ktrack(j) = K;

   del=2*BbarP*2*pi/lambdao-2*pi/GratLambda;

   term = (abs(K))^2 - Co*(Co+del) - del^2/4;

   if term>=0
      S=sqrt(term);
      R(j) = (abs(K))^2 * (sinh(L*S))^2 / (S^2*(cosh(L*S))^2 + (del/2+Co)^2*(sinh(L*S))^2
               );
   else
      S=sqrt(-term);
      R(j) = (abs(K))^2 * (sin(L*S))^2 / (S^2*(cos(L*S))^2 + (del/2+Co)^2*(sin(L*S))^2 );
   end; % if term>=

end; % for j=1:S(1)

lambdao=minLambdao+delLambdao*((1:j)-1);
plot(lambdao,R);
title('Reflection Coefficient versus Wavelength');
xlabel('Lambdao'); ylabel('R');
axis([minLambdao max(lambdao) 0 1]);
V=axis;

vertfrac=1/14;
vertstart=1/12;
vf=vertfrac; vs=vertstart;
text(V(1)+(V(2)-V(1))*1/25,V(3)+(V(4)-V(3))*(1-vs),['n1= ',num2str(n1,5)]);
text(V(1)+(V(2)-V(1))*1/6,V(3)+(V(4)-V(3))*(1-vs),['n2= ',num2str(n2,5)]);
text(V(1)+(V(2)-V(1))*1/25,V(3)+(V(4)-V(3))*(1-vs-vf),['n3= ',num2str(n3,5)]);
text(V(1)+(V(2)-V(1))*1/6,V(3)+(V(4)-V(3))*(1-vs-vf),['n4= ',num2str(n4,5)]);
text(V(1)+(V(2)-V(1))*1/25,V(3)+(V(4)-V(3))*(1-vs-2*vf),['a1= ',num2str(a1),' m']);
if n2==n3 & n3==n4
   text(V(1)+(V(2)-V(1))*1/25,V(3)+(V(4)-V(3))*(1-vs-3*vf),['a2= irrelevant']);
   text(V(1)+(V(2)-V(1))*1/25,V(3)+(V(4)-V(3))*(1-vs-4*vf),['a3= irrelevant']);
else
   text(V(1)+(V(2)-V(1))*1/25,V(3)+(V(4)-V(3))*(1-vs-3*vf),['a2= ',num2str(a2),' m']);
   text(V(1)+(V(2)-V(1))*1/25,V(3)+(V(4)-V(3))*(1-vs-4*vf),['a3= ',num2str(a3),' m']);
end; % if n2==
text(V(1)+(V(2)-V(1))*1/25,V(3)+(V(4)-V(3))*(1-vs-5*vf),['deln= ',num2str(alpha), ...
'*(n-nSiO2)']);
text(V(1)+(V(2)-V(1))*1/25,V(3)+(V(4)-V(3))*(1-vs-6*vf),['Length= ',num2str(L),' m']);
text(V(1)+(V(2)-V(1))*1/25,V(3)+(V(4)-V(3))*(1-vs-7*vf),['GratLambda=
               ',num2str(GratLambda),' m']);

      zMaxR=max(R);
      dummy=R-zMaxR/2; dummy=dummy+abs(dummy);
      mloop=1;
      while dummy(Centerindex+mloop)>0
         mloop=mloop+1;
      end; % while dummy(
      nloop=1;
      while dummy(Centerindex-nloop)>0
         nloop=nloop+1;
      end; % while nloop
```

```
      zHalfRBW=delLambdao*(mloop+nloop);
      zGratLambda=GratLambda;
      mloop=1;
      while R(Centerindex+mloop)<R(Centerindex+mloop-1)
         mloop=mloop+1;
      end; % while mloop
      nloop=1;
      while R(Centerindex-nloop)<R(Centerindex-nloop+1)
         nloop=nloop+1;
      end; % while nloop
      zSLlevel=max(R.*[ones(1,Centerindex-nloop) zeros(1,mloop+nloop-2+1) ...
      ones(1,length(R)-Centerindex-mloop+1)]);

text(V(1)+(V(2)-V(1))*1/25,V(3)+(V(4)-V(3))*(1-vs-8*vf),['1-Max(R)= ',num2str(1-zMaxR)]);
text(V(1)+(V(2)-V(1))*1/25,V(3)+(V(4)-V(3))*(1-vs-9*vf),['Half R BW=
               ',num2str(zHalfRBW,7),' m']);
text(V(1)+(V(2)-V(1))*1/25,V(3)+(V(4)-V(3))*(1-vs-10*vf),['1st S-Lobe Level=
               ',num2str(zSLlevel)]);

text(V(1)+(V(2)-V(1))*2/3,V(3)+(V(4)-V(3))*(1-vs-0*vf),['phase l2 - phase l1 = ']);
if delnL2~=0
   text(V(1)+(V(2)-V(1))*2/3,V(3)+(V(4)-V(3))*(1-vs-.5*vf),[num2str(pl2mpl1*180/pi),'
               degrees']);
else
   text(V(1)+(V(2)-V(1))*2/3,V(3)+(V(4)-V(3))*(1-vs-.5*vf),['not applicable']);
end; % if delnL2
text(V(1)+(V(2)-V(1))*2/3,V(3)+(V(4)-V(3))*(1-vs-1.5*vf),['phase l3 - phase l1 = ']);
text(V(1)+(V(2)-V(1))*2/3,V(3)+(V(4)-V(3))*(1-vs-2*vf),[num2str(pl3mpl1*180/pi),'
               degrees']);
text(V(1)+(V(2)-V(1))*2/3,V(3)+(V(4)-V(3))*(1-vs-3*vf),['phase l4 - phase l1 = ']);
if delnL4~=0
   text(V(1)+(V(2)-V(1))*2/3,V(3)+(V(4)-V(3))*(1-vs-3.5*vf),[num2str(pl4mpl1*180/pi),'
               degrees']);
else
   text(V(1)+(V(2)-V(1))*2/3,V(3)+(V(4)-V(3))*(1-vs-3.5*vf),['not applicable']);
end; % if delnL4
```

eysqr.m

```
function [eysqr] = eysqr(xvector,A,U,BbarP,lambdao)

global n1 n2 n3 n4 a1 a2 a3

% Compute ey/(j*omega*uo) first

for i=1:length(xvector);
   x=xvector(i);

   if x<0 disp('error: function ey input argument x <0');
   end; % if x<

   if x<=a1
      if n1>BbarP
            ey=A(1)*cos(U(1)*x)/U(1);
      else
            ey=A(1)*cosh(U(1)*x)/-U(1);
      end; % if n1>

   elseif x<=a2
      if n2>BbarP
         ey=(A(2)*cos(U(2)*x)-A(3)*sin(U(2)*x))/U(2);
      else
         ey=(A(2)*cosh(U(2)*x)+A(3)*sinh(U(2)*x))/-U(2);
      end; % if n2>

   elseif x<=a3
      if n3>BbarP
         ey=(A(4)*cos(U(3)*x)-A(5)*sin(U(3)*x))/U(3);
      else
         ey=(A(4)*cosh(U(3)*x)+A(5)*sinh(U(3)*x))/-U(3);
      end; % if n3>
```

```
   else
      ey=A(6)*exp(-U(4)*x)/U(4);

   end; % if x<=a1

   ey=2*pi*377/lambdao*ey; % This is Im(ey)

   eysqr(i)=ey^2;

end; % for i=
```

E.2 Chapter 6

The following programs were used in Chapter 6 to plot the reflectivity for double gratings and sampled gratings using the matrix approach (KNotaGenSampledRev2.m), and to plot the reflectivity of double gratings using the approach that writes expressions for the field amplitudes and enforces the boundary conditions (DoubleGrat.m) and the effective medium approach (EffMedDoubleGrat.m).

KNotaGenSampledRev2.m

```
% Run slab.m first.

%inputs%%%%%%%%%%%%%%%%%%%%%%%%%%%%%%%%%%%%%%%%%%%%%%%%%%%%%%%%
alpha=1.2135;
% I changed my mind about using L1 as variable.  Now L1=1, L2=2 etc. is fixed.
delnL1=alpha*(N(1)-nSiO2); % must be <= .1 N(1)
delnL2=alpha*(N(2)-nSiO2); % must be <= .1 N(2)
delnL3=alpha*(N(3)-nSiO2); % must be <= .1 N(2)
delnL4=alpha*(N(4)-nSiO2); % must be <= .1 N(4), zero is ok

% Comment applies if apodized:
% Now these deln are the peak values of the "dc" effective index changes (dc nonzero)
% in other words, they are the peak values of delnbar
% simulate pi/4, pi/8 etc. phase shift between double gratings

CenterLambdao=1.3e-6;

NumGrat = 3;

AllSameDeltaz = 1;
if AllSameDeltaz == 1
   deltaz = 1e-4*ones(NumGrat,1);
end

AllSameV = 1;
if AllSameV == 1
   v = 1 * ones(NumGrat,1);
end

AllSamePL = 1;
if AllSamePL == 1;

   pl2mpl1 = 0*pi/180 * ones(NumGrat,1);
   pl3mpl1 = 0*pi/180 * ones(NumGrat,1);
   pl4mpl1 = 0*pi/180 * ones(NumGrat,1);
end;

%%%%%%%%%%%%%%%% insert special arrangement
if AllSamePL == 0

% for now let phiL1 be the same in every section
```

```
   pl2mpl1(1:2:NumGrat) = 180*pi/180;
   pl3mpl1(1:2:NumGrat) = 0;
   pl4mpl1(1:2:NumGrat) = 0;

   pl2mpl1(2:2:NumGrat) = 180*pi/180;
   pl3mpl1(2:2:NumGrat) = 0;
   pl4mpl1(2:2:NumGrat) = 0;
end;

a=[0 a1 a2 a3];
toggleNum=1; % 1=even
toggle='eve';
count=1;

S=size(Bbar);
if length(S)>2
   disp('Waveguide is not single mode!');
end; % if length


% next block calculates GratLambda which determines CenterLambdao

Centerindex=1+round( (CenterLambdao-minLambdao)/delLambdao );
ActualCenterL=minLambdao+delLambdao*(Centerindex-1);
j=Centerindex;

lambdao=minLambdao+delLambdao*(j-1);
BbarP=Bbar(j,count,toggleNum);

%%%%%%%%%%%%%%%%%%%%%%%%%%%%%%%%%%%%%%%%%%%%%%%%%%%%%%% one more input section
% indicate which sections will be replaced by grating-free slices
GratingFree = [2:2:100]; % ascending order!!!
% array of same length as GratingFree
   deltazFree =  2 * ones(length(GratingFree),1) * ( 2*pi / (2*pi/lambdao*BbarP) );
   %deltazFree = 1.8e-3 * ones(length(GratingFree),1);
   %deltazFree = 1e-3;
GratingFree = [GratingFree 0]; % so doesn't try to look up 1st element in 0 length array


%%%%%%%%%%%%%%%% insert special arrangement
if AllSameDeltaz == 0
   deltaz(1:2:NumGrat) = .1e-3;
   %deltaz(2:2:NumGrat) = 2*pi / (2*pi/lambdao*BbarP) * 1/8;
   deltaz(2:2:NumGrat) = 6.28e-5;
end;

[M,U]=UevalM(BbarP,lambdao,toggle);
Mpeice2=M(1:5,2:6);
Mpeice1=M(1:5,1);
A(1)=1;
A(2:6)=inv(Mpeice2)*(-1)*Mpeice1*A(1);

P=2*.5*BbarP/377*quad8('eysqr',0,10*a3,[],[],A,U,BbarP,lambdao);
A=A/sqrt(P);

%%%%%%%% change the following if zero-dc
Co=2*.5*2*pi/lambdao/377* ( N(1)*delnL1*quad8('eysqr',a(1),a(2),[],[],A,U,BbarP,lambdao)
...
+ N(2)*delnL2*quad8('eysqr',a(2),a(3),[],[],A,U,BbarP,lambdao) ...
+ N(3)*delnL3*quad8('eysqr',a(3),a(4),[],[],A,U,BbarP,lambdao) ...
+ N(4)*delnL4*quad8('eysqr',a(4),10*a(4),[],[],A,U,BbarP,lambdao) );

GratLambda=pi/( Bbar(Centerindex,1,1)*2*pi/ActualCenterL + Co);



KTrack = [];

for j=1:S(1)
j
```

```
   lambdao=minLambdao+delLambdao*(j-1);
   BbarP=Bbar(j,count,toggleNum);

   [M,U]=UevalM(BbarP,lambdao,toggle);
   Mpeice2=M(1:5,2:6);
   Mpeice1=M(1:5,1);
   A(1)=1;
   A(2:6)=inv(Mpeice2)*(-1)*Mpeice1*A(1);
   P=2*.5*BbarP/377*quad8('eysqr',0,10*a3,[],[],A,U,BbarP,lambdao);
   A=A/sqrt(P);


      % change if want to handle apodized as well, move within m= loop
       Co=2*.5*2*pi/lambdao/377* (
N(1)*delnL1*quad8('eysqr',a(1),a(2),[],[],A,U,BbarP,lambdao) ...
      + N(2)*delnL2*quad8('eysqr',a(2),a(3),[],[],A,U,BbarP,lambdao) ...
      + N(3)*delnL3*quad8('eysqr',a(3),a(4),[],[],A,U,BbarP,lambdao) ...
      + N(4)*delnL4*quad8('eysqr',a(4),10*a(4),[],[],A,U,BbarP,lambdao) );

   RoverS = [1; 0];
   GratingFreeCopy = GratingFree;
   deltazFreeCopy = deltazFree;

   for m=1:NumGrat

      if GratingFreeCopy(1) == m
         GratingFreeCopy = GratingFreeCopy(2:length(GratingFreeCopy));
         %phi = 4*pi*BbarP/lambdao*deltazFreeCopy(1);

         del = BbarP*2*pi/lambdao - pi/GratLambda;
         phi = 2 * del * deltazFreeCopy(1);
         %% ONE OR OTHER -- 2nd chance to supercede
         %phi = pi/8;
         % OR if discrete phase shift exists as well as nonzero deltaz
         phi = phi + 0 * ( deltaz(1)+deltazFreeCopy(1) ) * 2*pi/GratLambda;
         deltazFreeCopy = deltazFreeCopy(2:length(deltazFreeCopy));
         F = [  exp(-i*phi/2) 0; 0 exp(i*phi/2) ];

      else

         % change if want to handle apodized as well
         % change if could have 180 shift in other layers besides 2nd
         if pl2mpl1(m) == 180*pi/180
            K = 2*pi/lambdao/377 /2 * v(m) * ( ...
            N(1)*delnL1*quad8('eysqr',a(1),a(2),[],[],A,U,BbarP,lambdao) ...
            + -1 * N(2)*delnL2*quad8('eysqr',a(2),a(3),[],[],A,U,BbarP,lambdao) ...
            + exp(-sqrt(-1)*pl3mpl1(m)) *
N(3)*delnL3*quad8('eysqr',a(3),a(4),[],[],A,U,BbarP,lambdao) ...
            + exp(-sqrt(-1)*pl4mpl1(m)) *
N(4)*delnL4*quad8('eysqr',a(4),10*a(4),[],[],A,U,BbarP,lambdao) );
         else
            K = 2*pi/lambdao/377 /2 * v(m) * ( ...
            N(1)*delnL1*quad8('eysqr',a(1),a(2),[],[],A,U,BbarP,lambdao) ...
            + exp(-sqrt(-1)*pl2mpl1(m)) *
N(2)*delnL2*quad8('eysqr',a(2),a(3),[],[],A,U,BbarP,lambdao) ...
            + exp(-sqrt(-1)*pl3mpl1(m)) *
N(3)*delnL3*quad8('eysqr',a(3),a(4),[],[],A,U,BbarP,lambdao) ...
            + exp(-sqrt(-1)*pl4mpl1(m)) *
N(4)*delnL4*quad8('eysqr',a(4),10*a(4),[],[],A,U,BbarP,lambdao) );
         end;
         KTrack(j,m) = K;

         del = BbarP*2*pi/lambdao - pi/GratLambda;
         delTrack(j) = del;

         sigmahat = del + Co;
         sigmaHatTrack(j,m) = sigmahat;

         gamma = sqrt( (abs(K))^2 - sigmahat^2) ;
```

```
        F = [ cosh(gamma*deltaz(m)) - i*sigmahat/gamma*sinh(gamma*deltaz(m)) ...
              -i*K/gamma*sinh(gamma*deltaz(m));
              i*conj(K)/gamma*sinh(gamma*deltaz(m)) ...
              cosh(gamma*deltaz(m)) + i*sigmahat/gamma*sinh(gamma*deltaz(m)) ];
      end; % if GratingFree(1) ==

   RoverS = F * RoverS;
   end; % for m=
R(j) = ( abs( RoverS(2)/RoverS(1) ) )^2;

end; % for j=1:S(1)


lambdao=minLambdao+delLambdao*((1:j)-1);
%figure;
plot(lambdao,R);
title('Reflection Coefficient versus Wavelength');
xlabel('Lambdao'); ylabel('R');
axis([minLambdao max(lambdao) 0 1]);
V=axis;

%vertfrac=1/14;
%vertstart=1/12;
%vf=vertfrac; vs=vertstart;
%text(V(1)+(V(2)-V(1))*1/25,V(3)+(V(4)-V(3))*(1-vs),['n1= ',num2str(n1,5)]);
%text(V(1)+(V(2)-V(1))*1/6,V(3)+(V(4)-V(3))*(1-vs),['n2= ',num2str(n2,5)]);
%text(V(1)+(V(2)-V(1))*1/25,V(3)+(V(4)-V(3))*(1-vs-vf),['n3= ',num2str(n3,5)]);
%text(V(1)+(V(2)-V(1))*1/6,V(3)+(V(4)-V(3))*(1-vs-vf),['n4= ',num2str(n4,5)]);
%text(V(1)+(V(2)-V(1))*1/25,V(3)+(V(4)-V(3))*(1-vs-2*vf),['a1= ',num2str(a1),' m']);
%if n2==n3 & n3==n4
%   text(V(1)+(V(2)-V(1))*1/25,V(3)+(V(4)-V(3))*(1-vs-3*vf),['a2= irrelevant']);
%   text(V(1)+(V(2)-V(1))*1/25,V(3)+(V(4)-V(3))*(1-vs-4*vf),['a3= irrelevant']);
%else
%   text(V(1)+(V(2)-V(1))*1/25,V(3)+(V(4)-V(3))*(1-vs-3*vf),['a2= ',num2str(a2),' m']);
%   text(V(1)+(V(2)-V(1))*1/25,V(3)+(V(4)-V(3))*(1-vs-4*vf),['a3= ',num2str(a3),' m']);
%end; % if n2==
```

DoubleGrat.m

```
% Run slab.m first.

%inputs%%%%%%
alpha(1)=1.2135;
alpha(3)=1.2135;
phi(1) = 0;
phi(3) = 0;
% I changed my mind about using L1 as variable.  Now L1=1, L2=2 etc. is fixed.

L(1) = .1e-3;
L(3) = .1e-3;

CenterLambdao=1.3e-6;

%%%%%%%%%%%%


a=[0 a1 a2 a3];
toggleNum=1; % 1=even
toggle='eve';
count=1;

S=size(Bbar);
if length(S)>2
   disp('Waveguide is not single mode!');
end; % if length


% next block calculated GratLambda which determines CenterLambdao

Centerindex=1+round( (CenterLambdao-minLambdao)/delLambdao );
ActualCenterL=minLambdao+delLambdao*(Centerindex-1);
```

```
j=Centerindex;

lambdao=minLambdao+delLambdao*(j-1);
BbarP=Bbar(j,count,toggleNum);

[M,U]=UevalM(BbarP,lambdao,toggle);
Mpeice2=M(1:5,2:6);
Mpeice1=M(1:5,1);
A(1)=1;
A(2:6)=inv(Mpeice2)*(-1)*Mpeice1*A(1);

P=2*.5*BbarP/377*quad8('eysqr',0,10*a3,[],[],A,U,BbarP,lambdao);
A=A/sqrt(P);

%%%%%%%%%%%%%%%%%%%%%%%%%%%%
%L(2) = 2*pi / (BbarP*2*pi/lambdao) * 0/16;
L(2) = 1e-3;

% Grating 1

   delnL1=alpha(1)*(N(1)-nSiO2); % must be <= .1 N(1)
   delnL2=alpha(1)*(N(2)-nSiO2); % must be <= .1 N(2)
   delnL3=alpha(1)*(N(3)-nSiO2); % must be <= .1 N(3), zero is ok
   delnL4=alpha(1)*(N(4)-nSiO2); % must be <= .1 N(4), zero is ok

   Co=2*.5*2*pi/lambdao/377* (
N(1)*delnL1*quad8('eysqr',a(1),a(2),[],[],A,U,BbarP,lambdao) ...
   + N(2)*delnL2*quad8('eysqr',a(2),a(3),[],[],A,U,BbarP,lambdao) ...
   + N(3)*delnL3*quad8('eysqr',a(3),a(4),[],[],A,U,BbarP,lambdao) ...
   + N(4)*delnL4*quad8('eysqr',a(4),10*a(4),[],[],A,U,BbarP,lambdao) );

   GratLambda(1)=pi/( Bbar(Centerindex,1,1)*2*pi/ActualCenterL + Co);

% Grating 3 -- unless alpha(3) = alpha(1) GratLambda(1) != GratLambda(3)
%% before can use this block need to use del(1) and del(2)

%   delnL1=alpha(3)*(N(1)-nSiO2); % must be <= .1 N(1)
%   delnL2=alpha(3)*(N(2)-nSiO2); % must be <= .1 N(2)
%   delnL3=alpha(3)*(N(3)-nSiO2); % must be <= .1 N(3), zero is ok
%   delnL4=alpha(3)*(N(4)-nSiO2); % must be <= .1 N(4), zero is ok

%   Co=2*.5*2*pi/lambdao/377* (
N(1)*delnL1*quad8('eysqr',a(1),a(2),[],[],A,U,BbarP,lambdao) ...
%   + N(2)*delnL2*quad8('eysqr',a(2),a(3),[],[],A,U,BbarP,lambdao) ...
%   + N(3)*delnL3*quad8('eysqr',a(3),a(4),[],[],A,U,BbarP,lambdao) ...
%   + N(4)*delnL4*quad8('eysqr',a(4),10*a(4),[],[],A,U,BbarP,lambdao) )

%   GratLambda(3)=pi/( Bbar(Centerindex,1,1)*2*pi/ActualCenterL + Co);

%% end of block


for j=1:S(1)

   lambdao=minLambdao+delLambdao*(j-1);
   BbarP=Bbar(j,count,toggleNum);

   [M,U]=UevalM(BbarP,lambdao,toggle);
   Mpeice2=M(1:5,2:6);
   Mpeice1=M(1:5,1);
   A(1)=1;
   A(2:6)=inv(Mpeice2)*(-1)*Mpeice1*A(1);

   P=2*.5*BbarP/377*quad8('eysqr',0,10*a3,[],[],A,U,BbarP,lambdao);
   A=A/sqrt(P);

   del=2*BbarP*2*pi/lambdao-2*pi/GratLambda(1);


   % Number 1 grating first
```

```
      delnL1=alpha(1)*(N(1)-nSiO2); % must be <= .1 N(1)
      delnL2=alpha(1)*(N(2)-nSiO2); % must be <= .1 N(2)
      delnL3=alpha(1)*(N(3)-nSiO2); % must be <= .1 N(3), zero is ok
      delnL4=alpha(1)*(N(4)-nSiO2); % must be <= .1 N(4), zero is ok

      Co=2*.5*2*pi/lambdao/377* (
N(1)*delnL1*quad8('eysqr',a(1),a(2),[],[],A,U,BbarP,lambdao) ...
      + N(2)*delnL2*quad8('eysqr',a(2),a(3),[],[],A,U,BbarP,lambdao) ...
      + N(3)*delnL3*quad8('eysqr',a(3),a(4),[],[],A,U,BbarP,lambdao) ...
      + N(4)*delnL4*quad8('eysqr',a(4),10*a(4),[],[],A,U,BbarP,lambdao) );

      S = sqrt( Co^2/4 - Co*(Co+del) - (del/2)^2 );

      RHS(1,1) = -sqrt(-1)*4/ conj(Co*exp(-sqrt(-1)*phi(1))) *exp(S*L(1)) ...
               *( S*cosh(L(1)*S) + sqrt(-1)*(del/2+Co)*sinh(L(1)*S) );
      RHS(2,1) = -2*exp(S*L(1))*sinh(L(1)*S);

      %RpreInterm(j) = abs( RHS(2,1)^2 / RHS(1,1)^2 );
      RpreInterm(j) = ( abs(RHS(2,1))/abs(RHS(1,1)) )^2;


   % Number 3 grating

      delnL1=alpha(3)*(N(1)-nSiO2); % must be <= .1 N(1)
      delnL2=alpha(3)*(N(2)-nSiO2); % must be <= .1 N(2)
      delnL3=alpha(3)*(N(3)-nSiO2); % must be <= .1 N(3), zero is ok
      delnL4=alpha(3)*(N(4)-nSiO2); % must be <= .1 N(4), zero is ok

      Co=2*.5*2*pi/lambdao/377* (
N(1)*delnL1*quad8('eysqr',a(1),a(2),[],[],A,U,BbarP,lambdao) ...
      + N(2)*delnL2*quad8('eysqr',a(2),a(3),[],[],A,U,BbarP,lambdao) ...
      + N(3)*delnL3*quad8('eysqr',a(3),a(4),[],[],A,U,BbarP,lambdao) ...
      + N(4)*delnL4*quad8('eysqr',a(4),10*a(4),[],[],A,U,BbarP,lambdao) );

      S = sqrt( Co^2/4 - Co*(Co+del) - (del/2)^2 );

      LHS(1,1) = -2*sqrt(-1) / conj(Co*exp(-sqrt(-1)*phi(3))) *exp(sqrt(-1)*del*-L(2))
...
                *exp(S*-L(2)) *( ...
                (exp(-sqrt(-1)*del/2*-L(2))*-sqrt(-1)*del/2) ...
                + S*exp(-sqrt(-1)*del/2*-L(2)) - sqrt(-1)*Co*exp(-sqrt(-1)*del/2*-L(2))
);

      LHS(1,2) = -2*sqrt(-1) / conj(Co*exp(-sqrt(-1)*phi(3))) *exp(sqrt(-1)*del*-L(2))
...
                *exp(-S*-L(2)) *( ...
                (exp(-sqrt(-1)*del/2*-L(2))*-sqrt(-1)*del/2) ...
                - S*exp(-sqrt(-1)*del/2*-L(2)) - sqrt(-1)*Co*exp(-sqrt(-1)*del/2*-L(2))
);
      LHS(2,1) = exp(-sqrt(-1)*del/2*-L(2)) * exp(S*-L(2));
      LHS(2,2) = exp(-sqrt(-1)*del/2*-L(2)) * exp(-S*-L(2));


%   Bfour = det([RHS(1,1) LHS(1,2) ; RHS(2,1) LHS(2,2)])/det(LHS);
%   BfourPrime = det([LHS(1,1) RHS(1,1) ; LHS(2,1) RHS(2,1)])/det(LHS);
   [dummy] = inv(LHS)*RHS;
   Bfour = dummy(1);
   BfourPrime = dummy(2);

z = -L(2);
Psi1 = -2*sqrt(-1) / conj(Co*exp(-sqrt(-1)*phi(3))) *exp(sqrt(-1)*del*z) * ...
       ( Bfour *exp(S*z) *( exp(-sqrt(-1)*del/2*z)*-sqrt(-1)*del/2 + S*exp(-sqrt(-
1)*del/2*z) ...
                          -sqrt(-1)*Co*exp(-sqrt(-1)*del/2*z) ) ...
        +BfourPrime*exp(-S*z) *( exp(-sqrt(-1)*del/2*z)*-sqrt(-1)*del/2 - S*exp(-sqrt(-
1)*del/2*z) ...
                          -sqrt(-1)*Co*exp(-sqrt(-1)*del/2*z) ) );
Psi2 = exp(-sqrt(-1)*del/2*z) * (Bfour*exp(S*z) + BfourPrime*exp(-S*z));

%Rinterm(j) = abs( Psi2^2 / Psi1^2 );
Rinterm(j) = ( abs(Psi2)/abs(Psi1) )^2;
```

```
z = -L(3)-L(2);
Psi1 = -2*sqrt(-1) / conj(Co*exp(-sqrt(-1)*phi(3))) *exp(sqrt(-1)*del*z) * ...
       ( Bfour *exp(S*z) *( exp(-sqrt(-1)*del/2*z)*-sqrt(-1)*del/2 + S*exp(-sqrt(-
1)*del/2*z) ...
                           -sqrt(-1)*Co*exp(-sqrt(-1)*del/2*z) ) ...
        +BfourPrime*exp(-S*z) *( exp(-sqrt(-1)*del/2*z)*-sqrt(-1)*del/2 - S*exp(-sqrt(-
1)*del/2*z) ...
                           -sqrt(-1)*Co*exp(-sqrt(-1)*del/2*z) ) );
Psi2 = exp(-sqrt(-1)*del/2*z) * (Bfour*exp(S*z) + BfourPrime*exp(-S*z));

%R(j) = abs( Psi2^2 / Psi1^2 );
R(j) = ( abs(Psi2)/abs(Psi1) )^2;


end; % for j=1:S(1)


lambdao=minLambdao+delLambdao*((1:j)-1);
plot(lambdao,R);
title('Reflection Coefficient versus Wavelength');
xlabel('Lambdao'); ylabel('R');
%axis([minLambdao max(lambdao) 0 1]);
V=axis;

vertfrac=1/14;
vertstart=1/12;
vf=vertfrac; vs=vertstart;
text(V(1)+(V(2)-V(1))*1/25,V(3)+(V(4)-V(3))*(1-vs),['n1= ',num2str(n1,5)]);
text(V(1)+(V(2)-V(1))*1/6,V(3)+(V(4)-V(3))*(1-vs),['n2= ',num2str(n2,5)]);
text(V(1)+(V(2)-V(1))*1/25,V(3)+(V(4)-V(3))*(1-vs-vf),['n3= ',num2str(n3,5)]);
text(V(1)+(V(2)-V(1))*1/6,V(3)+(V(4)-V(3))*(1-vs-vf),['n4= ',num2str(n4,5)]);
text(V(1)+(V(2)-V(1))*1/25,V(3)+(V(4)-V(3))*(1-vs-2*vf),['a1= ',num2str(a1),' m']);
if n2==n3 & n3==n4
   text(V(1)+(V(2)-V(1))*1/25,V(3)+(V(4)-V(3))*(1-vs-3*vf),['a2= irrelevant']);
   text(V(1)+(V(2)-V(1))*1/25,V(3)+(V(4)-V(3))*(1-vs-4*vf),['a3= irrelevant']);
else
   text(V(1)+(V(2)-V(1))*1/25,V(3)+(V(4)-V(3))*(1-vs-3*vf),['a2= ',num2str(a2),' m']);
   text(V(1)+(V(2)-V(1))*1/25,V(3)+(V(4)-V(3))*(1-vs-4*vf),['a3= ',num2str(a3),' m']);
end; % if n2==
text(V(1)+(V(2)-V(1))*1/25,V(3)+(V(4)-V(3))*(1-vs-5*vf),['deln= ',num2str(alpha), ...
'*(n-nSiO2)']);
text(V(1)+(V(2)-V(1))*1/25,V(3)+(V(4)-V(3))*(1-vs-6*vf),['Length= ',num2str(L),' m']);
text(V(1)+(V(2)-V(1))*1/25,V(3)+(V(4)-V(3))*(1-vs-7*vf),['GratLambda=
',num2str(GratLambda),' m']);
```

EffMedDoubleGrat.m

```
% Run slab.m first.

%inputs%%%%%%
alpha=1.2135;

% I changed my mind about using L1 as variable.  Now L1=1, L2=2 etc. is fixed.
delnL1=alpha*(N(1)-nSiO2); % must be <= .1 N(1)
delnL2=alpha*(N(2)-nSiO2); % must be <= .1 N(2)
delnL3=alpha*(N(3)-nSiO2); % must be <= .1 N(3), zero is ok
delnL4=alpha*(N(4)-nSiO2); % must be <= .1 N(4), zero is ok
% Now these deln are the peak values of the "dc" effective index changes (dc nonzero)
% in other words, they are the peak values of delnbar

L2=1e-4;
% L3 = see below;
L4=1e-4;

pl2mpl1 = 0;
pl3mpl1 = 0;
pl4mpl1 = 0;

CenterLambdao=1.3e-6;
```

```
v = 1;

%%%%%%%%%%%%

a=[0 a1 a2 a3];
toggleNum=1; % 1=even
toggle='eve';
count=1;

S=size(Bbar);
if length(S)>2
   disp('Waveguide is not single mode!');
end; % if length


% next block calculates GratLambda which determines CenterLambdao

Centerindex=1+round( (CenterLambdao-minLambdao)/delLambdao );
ActualCenterL=minLambdao+delLambdao*(Centerindex-1);
j=Centerindex;

lambdao=minLambdao+delLambdao*(j-1);
BbarP=Bbar(j,count,toggleNum);

%%%%%%%%%%%%%
% L3 =  1/4 * 2*pi / ( BbarP*2*pi/CenterLambdao );
L3 = 1e-3;
%%%%%%%%%%%%%

[M,U]=UevalM(BbarP,lambdao,toggle);
Mpeice2=M(1:5,2:6);
Mpeice1=M(1:5,1);
A(1)=1;
A(2:6)=inv(Mpeice2)*(-1)*Mpeice1*A(1);

P=2*.5*BbarP/377*quad8('eysqr',0,10*a3,[],[],A,U,BbarP,lambdao);
A=A/sqrt(P);

Co=2*.5*2*pi/lambdao/377* ( N(1)*delnL1*quad8('eysqr',a(1),a(2),[],[],A,U,BbarP,lambdao)
...
+ N(2)*delnL2*quad8('eysqr',a(2),a(3),[],[],A,U,BbarP,lambdao) ...
+ N(3)*delnL3*quad8('eysqr',a(3),a(4),[],[],A,U,BbarP,lambdao) ...
+ N(4)*delnL4*quad8('eysqr',a(4),10*a(4),[],[],A,U,BbarP,lambdao) );

GratLambda=pi/( Bbar(Centerindex,1,1)*2*pi/ActualCenterL + Co);

%% end of block


for j=1:S(1)

   lambdao=minLambdao+delLambdao*(j-1);
   BbarP=Bbar(j,count,toggleNum);

   [M,U]=UevalM(BbarP,lambdao,toggle);
   Mpeice2=M(1:5,2:6);
   Mpeice1=M(1:5,1);
   A(1)=1;
   A(2:6)=inv(Mpeice2)*(-1)*Mpeice1*A(1);

   P=2*.5*BbarP/377*quad8('eysqr',0,10*a3,[],[],A,U,BbarP,lambdao);
   A=A/sqrt(P);

   sigma=2*.5*2*pi/lambdao/377* (
N(1)*delnL1*quad8('eysqr',a(1),a(2),[],[],A,U,BbarP,lambdao) ...
   + N(2)*delnL2*quad8('eysqr',a(2),a(3),[],[],A,U,BbarP,lambdao) ...
   + N(3)*delnL3*quad8('eysqr',a(3),a(4),[],[],A,U,BbarP,lambdao) ...
   + N(4)*delnL4*quad8('eysqr',a(4),10*a(4),[],[],A,U,BbarP,lambdao) );
```

```
   K = v/2 * 2*.5*2*pi/lambdao/377* (
N(1)*delnL1*quad8('eysqr',a(1),a(2),[],[],A,U,BbarP,lambdao) ...
   + N(2)*delnL2*exp(sqrt(-1)*pl2mpl1)*quad8('eysqr',a(2),a(3),[],[],A,U,BbarP,lambdao)
...
   + N(3)*delnL3*exp(sqrt(-1)*pl3mpl1)*quad8('eysqr',a(3),a(4),[],[],A,U,BbarP,lambdao)
...
   + N(4)*delnL4*exp(sqrt(-
1)*pl4mpl1)*quad8('eysqr',a(4),10*a(4),[],[],A,U,BbarP,lambdao) );


   delE = BbarP*2*pi/lambdao-pi/GratLambda;

   derLambdaoD = -1 * 1e-9/1e-2;
   derphi = 0;
   sigmahat = delE + sigma -.5*derphi;

   Z4 = sqrt( (sigmahat-K)/(sigmahat+K) );
   Z2 = Z4;
   Z3 = 1;
   Beta4 = sqrt( sigmahat^2 - K^2 );
   Beta2 = Beta4;
   Beta3 = delE;

   r54 = (1-Z4)/(1+Z4);

   Z45 = Z4*( exp(i*Beta4*L4) + r54*exp(-i*Beta4*L4) ) / ...
            ( exp(i*Beta4*L4) - r54*exp(-i*Beta4*L4) );

   r43 = (Z45-1)/(Z45+1);

   Z345 = Z3*( exp(i*Beta3*L3) + r43*exp(-i*Beta3*L3) ) / ...
             ( exp(i*Beta3*L3) - r43*exp(-i*Beta3*L3) );

   r32 = (Z345-Z2)/(Z345+Z2);

   Z2345 = Z2*( exp(i*Beta2*L2) + r32*exp(-i*Beta2*L2) ) / ...
              ( exp(i*Beta2*L2) - r32*exp(-i*Beta2*L2) );

   r21 = (Z2345-1)/(Z2345+1);

   R(j) = ( abs(r21) )^2;
   PhaseRho1(j) = angle( r21 );

end; % for j=1:S(1)


lambdao=minLambdao+delLambdao*((1:j)-1);
PhaseRho1 = unwrap(PhaseRho1);
temp1 = [ lambdao(1:length(lambdao)-1); lambdao(2:length(lambdao)) ];
temp2 = [ -1*PhaseRho1(1:length(PhaseRho1)-1); PhaseRho1(2:length(PhaseRho1)) ];
for index=1:length(temp1)
   lambdaoDT(index) = sum( temp1(:,index) )/2;
   DelayTime(index) = -1*lambdaoDT(index)^2 / (2*pi*3e8) * sum( temp2(:,index)
)/delLambdao;
end; % for index=

temp1 = [ lambdaoDT(1:length(lambdaoDT)-1); lambdaoDT(2:length(lambdaoDT)) ];
temp2 = [ -1*DelayTime(1:length(DelayTime)-1); DelayTime(2:length(DelayTime)) ];
for index=1:length(temp1)
   lambdaoDis(index) = sum( temp1(:,index) )/2;
   Dispersion(index) = sum( temp2(:,index) ) / delLambdao;
end; % for index=


plot(lambdao,R);
title('Reflection Coefficient versus Wavelength');
xlabel('Lambdao'); ylabel('R');
axis([minLambdao max(lambdao) 0 1]);
V=axis;

vertfrac=1/14;
```

```
vertstart=1/12;
vf=vertfrac; vs=vertstart;
text(V(1)+(V(2)-V(1))*1/25,V(3)+(V(4)-V(3))*(1-vs),['n1= ',num2str(n1,5)]);
text(V(1)+(V(2)-V(1))*1/6,V(3)+(V(4)-V(3))*(1-vs),['n2= ',num2str(n2,5)]);
text(V(1)+(V(2)-V(1))*1/25,V(3)+(V(4)-V(3))*(1-vs-vf),['n3= ',num2str(n3,5)]);
text(V(1)+(V(2)-V(1))*1/6,V(3)+(V(4)-V(3))*(1-vs-vf),['n4= ',num2str(n4,5)]);
text(V(1)+(V(2)-V(1))*1/25,V(3)+(V(4)-V(3))*(1-vs-2*vf),['a1= ',num2str(a1),' m']);
if n2==n3 & n3==n4
   text(V(1)+(V(2)-V(1))*1/25,V(3)+(V(4)-V(3))*(1-vs-3*vf),['a2= irrelevant']);
   text(V(1)+(V(2)-V(1))*1/25,V(3)+(V(4)-V(3))*(1-vs-4*vf),['a3= irrelevant']);
else
   text(V(1)+(V(2)-V(1))*1/25,V(3)+(V(4)-V(3))*(1-vs-3*vf),['a2= ',num2str(a2),' m']);
   text(V(1)+(V(2)-V(1))*1/25,V(3)+(V(4)-V(3))*(1-vs-4*vf),['a3= ',num2str(a3),' m']);
end; % if n2==

text(V(1)+(V(2)-V(1))*1/25,V(3)+(V(4)-V(3))*(1-vs-6*vf),['GratLambda=
',num2str(GratLambda),' m']);

      zMaxR=max(R);
      dummy=R-zMaxR/2; dummy=dummy+abs(dummy);
      mloop=1;
      while dummy(Centerindex+mloop)>0
         mloop=mloop+1;
      end; % while dummy(
      nloop=1;
      while dummy(Centerindex-nloop)>0
         nloop=nloop+1;
      end; % while nloop
      zHalfRBW=delLambdao*(mloop+nloop);
%%    zGratLambda=GratLambda;
%     mloop=1;
%     while R(Centerindex+mloop)<R(Centerindex+mloop-1)
%        mloop=mloop+1;
%     end; % while mloop
%     nloop=1;
%     while R(Centerindex-nloop)<R(Centerindex-nloop+1)
%        nloop=nloop+1;
%     end; % while nloop
%     zSLlevel=max(R.*[ones(1,Centerindex-nloop) zeros(1,mloop+nloop-2+1) ...
%     ones(1,length(R)-Centerindex-mloop+1)]);

text(V(1)+(V(2)-V(1))*1/25,V(3)+(V(4)-V(3))*(1-vs-7*vf),['Measurements:']);
text(V(1)+(V(2)-V(1))*1/25,V(3)+(V(4)-V(3))*(1-vs-8*vf),['1-Max(R)= ',num2str(1-zMaxR)]);
text(V(1)+(V(2)-V(1))*1/25,V(3)+(V(4)-V(3))*(1-vs-9*vf),['Half R BW=
',num2str(zHalfRBW,7),' m']);
%%text(V(1)+(V(2)-V(1))*1/25,V(3)+(V(4)-V(3))*(1-vs-10*vf),['1st S-Lobe Level=
',num2str(zSLlevel)]);

text(V(1)+(V(2)-V(1))*2/3,V(3)+(V(4)-V(3))*(1-vs),['Double Grating']);
text(V(1)+(V(2)-V(1))*2/3,V(3)+(V(4)-V(3))*(1-vs-1*vf),['Both Gratings Identical,']);


text(V(1)+(V(2)-V(1))*2/3,V(3)+(V(4)-V(3))*(1-vs-2*vf),['except L2=',num2str(L2),',
L4=',num2str(L4)]);
text(V(1)+(V(2)-V(1))*2/3,V(3)+(V(4)-V(3))*(1-vs-3*vf),['Dist. between =L3
=',num2str(L3)]);

text(V(1)+(V(2)-V(1))*2/3,V(3)+(V(4)-V(3))*(1-vs-5*vf),['delnbar= ',num2str(alpha),'*(n-
nSiO2)']);

text(V(1)+(V(2)-V(1))*2/3,V(3)+(V(4)-V(3))*(1-vs-6*vf),['"dc" index change = nonzero']);
text(V(1)+(V(2)-V(1))*2/3,V(3)+(V(4)-V(3))*(1-vs-7*vf),['v= ',num2str(v)]);
```

E.3 Chapter 7

The following programs were used in Chapter 7 to plot the reflectivity, group delay, and dispersion responses of the conventional designs, perform the conversion to

the separately-apodized designs, and plot the responses for them. The specific purpose of each program is detailed in Chapter 7.

apodv2ErgDesGuass.m

```
% Run slab.m first.

%inputs%%%%%%
alpha = 2*.062019176;

% I changed my mind about using L1 as variable.  Now L1=1, L2=2 etc. is fixed.
delnL1=alpha*(N(1)-nSiO2); % must be <= .1 N(1)
delnL2=alpha*(N(2)-nSiO2); % must be <= .1 N(2)
delnL3=alpha*(N(3)-nSiO2); % must be <= .1 N(3), zero is ok
delnL4=alpha*(N(4)-nSiO2); % must be <= .1 N(4), zero is ok
% Now these deln are the peak values of the "dc" effective index changes (dc nonzero)
% in other words, they are the peak values of delnbar

pl2mpl1 = 0;
pl3mpl1 = 0;
pl4mpl1 = 0;

CenterLambdao=1.55e-6;

toggleProf=1; % 1=Guassian, 2=Raised Cosine
if toggleProf==1
   FWHM=.010;
   L=6*FWHM; % Length in meters
else
if toggleProf==2
   FWHM=.01;
   L=2*FWHM;
else
   L=.010;
end; % if toggleProf==2
end; % if toggleProf==1

% Set ZeroDC=1 if want "dc" index change = 0
ZeroDC=1;

v = 1;
LargeNum=1e9;
if ZeroDC==1
   v=v*LargeNum;
end; % if ZeroDC

%%%%%%%%%%%%


a=[0 a1 a2 a3];
toggleNum=1; % 1=even
toggle='eve';
count=1;

S=size(Bbar);
if length(S)>2
   disp('Waveguide is not single mode!');
end; % if length


% next block calculates GratLambda which determines CenterLambdao

Centerindex=1+round( (CenterLambdao-minLambdao)/delLambdao );
ActualCenterL=minLambdao+delLambdao*(Centerindex-1);
j=Centerindex;

lambdao=minLambdao+delLambdao*(j-1);
BbarP=Bbar(j,count,toggleNum);
```

```
[M,U]=UevalM(BbarP,lambdao,toggle);
Mpeice2=M(1:5,2:6);
Mpeice1=M(1:5,1);
A(1)=1;
A(2:6)=inv(Mpeice2)*(-1)*Mpeice1*A(1);

P=2*.5*BbarP/377*quad8('eysqr',0,10*a3,[],[],A,U,BbarP,lambdao);
A=A/sqrt(P);

% Co = sigma
Co=2*.5*2*pi/lambdao/377* ( N(1)*delnL1*quad8('eysqr',a(1),a(2),[],[],A,U,BbarP,lambdao)
...
+ N(2)*delnL2*quad8('eysqr',a(2),a(3),[],[],A,U,BbarP,lambdao) ...
+ N(3)*delnL3*quad8('eysqr',a(3),a(4),[],[],A,U,BbarP,lambdao) ...
+ N(4)*delnL4*quad8('eysqr',a(4),10*a(4),[],[],A,U,BbarP,lambdao) );

GratLambda=pi/( Bbar(Centerindex,1,1)*2*pi/ActualCenterL + Co);
if ZeroDC==1
   GratLambda = pi/( Bbar(Centerindex,1,1)*2*pi/ActualCenterL );
end; % if ZeroDC==1;

%% end of block

test = v * 2 * ( N(1)*delnL1*quad8('eysqr',a(1),a(2),[],[],A,U,BbarP,lambdao) ...
          + N(2)*delnL2*exp(sqrt(-
1)*pl2mpl1)*quad8('eysqr',a(2),a(3),[],[],A,U,BbarP,lambdao) ...
          + N(3)*delnL3*exp(sqrt(-
1)*pl3mpl1)*quad8('eysqr',a(3),a(4),[],[],A,U,BbarP,lambdao) ...
          + N(4)*delnL4*exp(sqrt(-
1)*pl4mpl1)*quad8('eysqr',a(4),10*a(4),[],[],A,U,BbarP,lambdao) )
if ZeroDC==1
   test = test/LargeNum
end; % if ZeroDC==1
% want test = 2*0.377 to match Erdogan's example of a Guassian grating



for j=1:S(1)

   j

   lambdao=minLambdao+delLambdao*(j-1);
   BbarP=Bbar(j,count,toggleNum);

   [M,U]=UevalM(BbarP,lambdao,toggle);
   Mpeice2=M(1:5,2:6);
   Mpeice1=M(1:5,1);
   A(1)=1;
   A(2:6)=inv(Mpeice2)*(-1)*Mpeice1*A(1);

   P=2*.5*BbarP/377*quad8('eysqr',0,10*a3,[],[],A,U,BbarP,lambdao);
   A=A/sqrt(P);

   maxsigma=2*.5*2*pi/lambdao/377* (
N(1)*delnL1*quad8('eysqr',a(1),a(2),[],[],A,U,BbarP,lambdao) ...
   + N(2)*delnL2*quad8('eysqr',a(2),a(3),[],[],A,U,BbarP,lambdao) ...
   + N(3)*delnL3*quad8('eysqr',a(3),a(4),[],[],A,U,BbarP,lambdao) ...
   + N(4)*delnL4*quad8('eysqr',a(4),10*a(4),[],[],A,U,BbarP,lambdao) );
   maxsigmaTrack(j) = maxsigma;

   if ZeroDC==1
      maxsigma = maxsigma/LargeNum;
   end; % if ZeroDC

   maxK = v/2 * 2*.5*2*pi/lambdao/377* (
N(1)*delnL1*quad8('eysqr',a(1),a(2),[],[],A,U,BbarP,lambdao) ...
   + N(2)*delnL2*exp(sqrt(-1)*pl2mpl1)*quad8('eysqr',a(2),a(3),[],[],A,U,BbarP,lambdao)
...
   + N(3)*delnL3*exp(sqrt(-1)*pl3mpl1)*quad8('eysqr',a(3),a(4),[],[],A,U,BbarP,lambdao)
...
```

```
   + N(4)*delnL4*exp(sqrt(-
1)*pl4mpl1)*quad8('eysqr',a(4),10*a(4),[],[],A,U,BbarP,lambdao) );
   maxKTrack(j) = maxK;

   if ZeroDC==1
      maxK = maxK/LargeNum;
   end; % if ZeroDC

   delE = BbarP*2*pi/lambdao-pi/GratLambda;

   maxSlice=200;

   deltaz=L/maxSlice;
   if deltaz<10*GratLambda
      disp('Error: decrease maxSlice !!!');
   end; % if deltaz

   RoverS = [1; 0];

   for Slice=1:maxSlice

      % Guassian profile
      if toggleProf==1
         term = exp( -4 * log(2) * (L/2 -Slice*deltaz +deltaz/2)^2 / FWHM^2 );
      else
      % Raised-Cosine Profile
      if toggleProf==2
         term = .5 * ( 1+cos(pi* (L/2 -Slice*deltaz +deltaz/2) / FWHM ));
      else
         term = 1;
      end; % if toggleProj==2
      end; % if toggleProf==1

      sigma = maxsigma * term;
      K = maxK * term;
      derLambdaoD = 0;
      derphi = -4*pi*Bbar(Centerindex,count,toggleNum)* (L/2 -Slice*deltaz +deltaz/2) /
(CenterLambdao^2) * derLambdaoD;
      sigmahat = delE + sigma -.5*derphi;

      gamma = sqrt( (abs(K))^2 - sigmahat^2);
      F = [ cosh(gamma*deltaz) - i*sigmahat/gamma*sinh(gamma*deltaz) ...
            -i*K/gamma*sinh(gamma*deltaz);
            i*conj(K)/gamma*sinh(gamma*deltaz) ...
            cosh(gamma*deltaz) + i*sigmahat/gamma*sinh(gamma*deltaz) ];
      RoverS = F*RoverS;
   end; % for Slice=

R(j) = ( abs( RoverS(2)/RoverS(1) ) )^2;
PhaseRho1(j) = angle( RoverS(2)/RoverS(1) );
PhaseRho1Pre(j) = PhaseRho1(j);
PhaseRho2(j) = angle( RoverS(2)/RoverS(1) ) - (-2*delE*L/2);

end; % for j=1:S(1)


lambdao=minLambdao+delLambdao*((1:j)-1);
PhaseRho1 = unwrap(PhaseRho1);
temp1 = [ lambdao(1:length(lambdao)-1); lambdao(2:length(lambdao)) ];
temp2 = [ -1*PhaseRho1(1:length(PhaseRho1)-1); PhaseRho1(2:length(PhaseRho1)) ];
for index=1:length(temp1)
   lambdaoDT(index) = sum( temp1(:,index) )/2;
   DelayTime(index) = -1*lambdaoDT(index)^2 / (2*pi*3e8) * sum( temp2(:,index)
)/delLambdao;
end; % for index=

temp1 = [ lambdaoDT(1:length(lambdaoDT)-1); lambdaoDT(2:length(lambdaoDT)) ];
temp2 = [ -1*DelayTime(1:length(DelayTime)-1); DelayTime(2:length(DelayTime)) ];
for index=1:length(temp1)
   lambdaoDis(index) = sum( temp1(:,index) )/2;
   Dispersion(index) = sum( temp2(:,index) ) / delLambdao;
```

```
end; % for index=


plot(lambdao,R);
title('Reflection Coefficient versus Wavelength');
xlabel('Lambdao'); ylabel('R');
axis([minLambdao max(lambdao) 0 1]);
V=axis;

vertfrac=1/14;
vertstart=1/12;
vf=vertfrac; vs=vertstart;
text(V(1)+(V(2)-V(1))*1/25,V(3)+(V(4)-V(3))*(1-vs),['n1= ',num2str(n1,5)]);
text(V(1)+(V(2)-V(1))*1/6,V(3)+(V(4)-V(3))*(1-vs),['n2= ',num2str(n2,5)]);
text(V(1)+(V(2)-V(1))*1/25,V(3)+(V(4)-V(3))*(1-vs-vf),['n3= ',num2str(n3,5)]);
text(V(1)+(V(2)-V(1))*1/6,V(3)+(V(4)-V(3))*(1-vs-vf),['n4= ',num2str(n4,5)]);
text(V(1)+(V(2)-V(1))*1/25,V(3)+(V(4)-V(3))*(1-vs-2*vf),['a1= ',num2str(a1),' m']);
if n2==n3 & n3==n4
   text(V(1)+(V(2)-V(1))*1/25,V(3)+(V(4)-V(3))*(1-vs-3*vf),['a2= irrelevant']);
   text(V(1)+(V(2)-V(1))*1/25,V(3)+(V(4)-V(3))*(1-vs-4*vf),['a3= irrelevant']);
else
   text(V(1)+(V(2)-V(1))*1/25,V(3)+(V(4)-V(3))*(1-vs-3*vf),['a2= ',num2str(a2),' m']);
   text(V(1)+(V(2)-V(1))*1/25,V(3)+(V(4)-V(3))*(1-vs-4*vf),['a3= ',num2str(a3),' m']);
end; % if n2==

text(V(1)+(V(2)-V(1))*1/25,V(3)+(V(4)-V(3))*(1-vs-5*vf),['Length= ',num2str(L),' m']);
text(V(1)+(V(2)-V(1))*1/25,V(3)+(V(4)-V(3))*(1-vs-6*vf),['GratLambda=
',num2str(GratLambda),' m']);

      zMaxR=max(R);
      dummy=R-zMaxR/2; dummy=dummy+abs(dummy);
      mloop=1;
      while dummy(Centerindex+mloop)>0
         mloop=mloop+1;
      end; % while dummy(
      nloop=1;
      while dummy(Centerindex-nloop)>0
         nloop=nloop+1;
      end; % while nloop
      zHalfRBW=delLambdao*(mloop+nloop);
%%    zGratLambda=GratLambda;
%     mloop=1;
%     while R(Centerindex+mloop)<R(Centerindex+mloop-1)
%        mloop=mloop+1;
%     end; % while mloop
%     nloop=1;
%     while R(Centerindex-nloop)<R(Centerindex-nloop+1)
%        nloop=nloop+1;
%     end; % while nloop
%     zSLlevel=max(R.*[ones(1,Centerindex-nloop) zeros(1,mloop+nloop-2+1) ...
%     ones(1,length(R)-Centerindex-mloop+1)]);

text(V(1)+(V(2)-V(1))*1/25,V(3)+(V(4)-V(3))*(1-vs-7*vf),['Measurements:']);
text(V(1)+(V(2)-V(1))*1/25,V(3)+(V(4)-V(3))*(1-vs-8*vf),['1-Max(R)= ',num2str(1-zMaxR)]);
text(V(1)+(V(2)-V(1))*1/25,V(3)+(V(4)-V(3))*(1-vs-9*vf),['Half R BW=
',num2str(zHalfRBW,7),' m']);
%%text(V(1)+(V(2)-V(1))*1/25,V(3)+(V(4)-V(3))*(1-vs-10*vf),['1st S-Lobe Level=
',num2str(zSLlevel)]);

text(V(1)+(V(2)-V(1))*2/3,V(3)+(V(4)-V(3))*(1-vs),['# Slices = ',num2str(maxSlice)]);


if toggleProf==1
   text(V(1)+(V(2)-V(1))*2/3,V(3)+(V(4)-V(3))*(1-vs-2*vf),['Profile is Guassian-->']);
   text(V(1)+(V(2)-V(1))*2/3,V(3)+(V(4)-V(3))*(1-vs-3*vf),['delnbar=
',num2str(alpha),'*(n-nSiO2) *']);
   text(V(1)+(V(2)-V(1))*2/3,V(3)+(V(4)-V(3))*(1-vs-3.5*vf),['   exp ( -4 ln2 z^2 /
FWHM^2 )']);
   text(V(1)+(V(2)-V(1))*2/3,V(3)+(V(4)-V(3))*(1-vs-4*vf),['z= -L/2 to L/2']);
   text(V(1)+(V(2)-V(1))*2/3,V(3)+(V(4)-V(3))*(1-vs-5*vf),['FWHM= ',num2str(FWHM),' m']);
else
```

```
if toggleProf==2
   text(V(1)+(V(2)-V(1))*2/3,V(3)+(V(4)-V(3))*(1-vs-2*vf),['Profile is Raised Cosine--
>']);
   text(V(1)+(V(2)-V(1))*2/3,V(3)+(V(4)-V(3))*(1-vs-3*vf),['delnbar=
',num2str(alpha),'*(n-nSiO2) *']);
   text(V(1)+(V(2)-V(1))*2/3,V(3)+(V(4)-V(3))*(1-vs-3.5*vf),['   0.5*(1+cos( pi*z/FWHM )
']);
   text(V(1)+(V(2)-V(1))*2/3,V(3)+(V(4)-V(3))*(1-vs-4*vf),['z= -L/2 to L/2']);
   text(V(1)+(V(2)-V(1))*2/3,V(3)+(V(4)-V(3))*(1-vs-5*vf),['FWHM= ',num2str(FWHM),' m']);
else
   text(V(1)+(V(2)-V(1))*2/3,V(3)+(V(4)-V(3))*(1-vs-2*vf),['Profile is Uniform']);
   text(V(1)+(V(2)-V(1))*2/3,V(3)+(V(4)-V(3))*(1-vs-3*vf),['delnbar=
',num2str(alpha),'*(n-nSiO2)']);
end; % if toggleProj==2
end; % if toggleProf==1

if ZeroDC==1
   text(V(1)+(V(2)-V(1))*2/3,V(3)+(V(4)-V(3))*(1-vs-6*vf),['"dc" index change = zero']);
   text(V(1)+(V(2)-V(1))*2/3,V(3)+(V(4)-V(3))*(1-vs-7*vf),['v= ',num2str(v/LargeNum)]);
else
   text(V(1)+(V(2)-V(1))*2/3,V(3)+(V(4)-V(3))*(1-vs-6*vf),['"dc" index change =
nonzero']);
   text(V(1)+(V(2)-V(1))*2/3,V(3)+(V(4)-V(3))*(1-vs-7*vf),['v= ',num2str(v)]);
end; % if ZeroDC



%%%save Refcorun4 zMaxR zHalfRBW zGratLambda zSLlevel ActualCenterL L alpha...
%%%n1 n2 n3 n4 a1
```

OneLGuass2TwoLayer.m

```
% original design is Ergodan's example of a Guassian apod. grating, fig. 11
% run apodv2ErgDes.m first

% profile of single apodizing function of original design is zero-dc
% profiles of both apodizing functions of new design are non-zero dc

%%%%%%%%%%

   j = Centerindex;
   lambdao=minLambdao+delLambdao*(j-1);
   BbarP=Bbar(j,count,toggleNum);

   [M,U]=UevalM(BbarP,lambdao,toggle);
   Mpeice2=M(1:5,2:6);
   Mpeice1=M(1:5,1);
   A(1)=1;
   A(2:6)=inv(Mpeice2)*(-1)*Mpeice1*A(1);

   P=2*.5*BbarP/377*quad8('eysqr',0,10*a3,[],[],A,U,BbarP,lambdao);
   A=A/sqrt(P);

   maxsigma=2*.5*2*pi/lambdao/377* (
N(1)*delnL1*quad8('eysqr',a(1),a(2),[],[],A,U,BbarP,lambdao) ...
   + N(2)*delnL2*quad8('eysqr',a(2),a(3),[],[],A,U,BbarP,lambdao) ...
   + N(3)*delnL3*quad8('eysqr',a(3),a(4),[],[],A,U,BbarP,lambdao) ...
   + N(4)*delnL4*quad8('eysqr',a(4),10*a(4),[],[],A,U,BbarP,lambdao) );

   if ZeroDC==1
      maxsigma = maxsigma/LargeNum;
   end; % if ZeroDC

   maxK = v/2 * 2*.5*2*pi/lambdao/377* (
N(1)*delnL1*quad8('eysqr',a(1),a(2),[],[],A,U,BbarP,lambdao) ...
   + N(2)*delnL2*exp(sqrt(-1)*pl2mpl1)*quad8('eysqr',a(2),a(3),[],[],A,U,BbarP,lambdao)
...
   + N(3)*delnL3*exp(sqrt(-1)*pl3mpl1)*quad8('eysqr',a(3),a(4),[],[],A,U,BbarP,lambdao)
...
```

```
   + N(4)*delnL4*exp(sqrt(-
1)*pl4mpl1)*quad8('eysqr',a(4),10*a(4),[],[],A,U,BbarP,lambdao) );

   % omega = 2*pi*f = 2*pi*c / lambdao;
   PerturbL1divisor = 2*pi / lambdao /377 /4 * 2 * ...
                      N(1)*quad8('eysqr',a(1),a(2),[],[],A,U,BbarP,lambdao);
   PerturbL3divisor = 2*pi / lambdao /377 /2 * ...
                      N(3)*quad8('eysqr',a(3),a(4),[],[],A,U,BbarP,lambdao);

   if ZeroDC==1
      maxK = maxK/LargeNum;
   end; % if ZeroDC

%%%%%%%%%%

maxSlice4plotting = 200;
deltaz=L/maxSlice4plotting;

for Slice=1:maxSlice4plotting

   % Guassian profile
   if toggleProf==1
      term = exp( -4 * log(2) * (L/2 -Slice*deltaz +deltaz/2)^2 / FWHM^2 );
      termTrack(Slice) = term;
   else
   % Raised-Cosine Profile
   if toggleProf==2
      term = .5 * ( 1+cos(pi* (L/2 -Slice*deltaz +deltaz/2) / FWHM ));
      termTrack(Slice) = term;
   else
      term = 1;
   end; % if toggleProj==2
   end; % if toggleProf==1

%   sigma = maxsigma * term;
   K = maxK * term;
   KTrack(Slice) = K;

   BbarP=Bbar(Centerindex,count,toggleNum);
   derLambdaoD = 0;
   Phi(Slice) = .5 * -4*pi*Bbar(Centerindex,count,toggleNum)* (L/2 -Slice*deltaz
+deltaz/2)^2 / ...
         (CenterLambdao^2) * derLambdaoD;

   z(Slice) = (L/2 -Slice*deltaz +deltaz/2);

   % assume PhiL1(z)=0, PhiL3(z)=pi;
   Kl1(Slice) = (maxK + K) / 2;
   Kl3(Slice) = (maxK - K) / 2;

   % find delnL1bar * fL1 * v for layers
   PerturbL1(Slice) = Kl1(Slice) / PerturbL1divisor;
   PerturbL3(Slice) = Kl3(Slice) / PerturbL3divisor;

end; % for Slice=

   figure;
   plot(z,KTrack);

   figure; subplot(3,1,2);
   plot( z,PerturbL1.* ( ones(1,length(z)) + cos( 2*pi/ (L/30) * z + 0 ) ) );
%   title('Perturbation within layer 1 (gratings exist in layers 1 and 3)');
   title('(a)');
   xlabel('z (meters)');
   ylabel('delta n (unitless)');

   subplot(3,1,3);
   % v=1
   plot( z,PerturbL3.*( ones(1,length(z)) + cos( 2*pi/ (L/30) * z + pi) ) );
%   title('Perturbation within layer 3');
   title('(b)');
```

```
   xlabel('z (meters)');
   ylabel('delta n (unitless)');

   subplot(3,1,1);
   plot( z,delnL1*termTrack.* cos( 2*pi/ (L/30) * z + Phi ) );
%   title('Perturbation within layers 1 and 3 for original design');
   title('(c)');
   xlabel('z (meters)');
   ylabel('delta n (unitless)');
```

apod2LGuass.m

```
% first run apodv2ErgDes.m, then apod1L2apod2L.m

% sigma = constant = 2*maxK (calculated by 1LGuass2TwoLayer.m)
GratLambda=pi/( Bbar(Centerindex,1,1)*2*pi/ActualCenterL + 2*maxK);

for j=1:S(1)

   lambdao=minLambdao+delLambdao*(j-1);
   BbarP=Bbar(j,count,toggleNum);

   [M,U]=UevalM(BbarP,lambdao,toggle);
   Mpeice2=M(1:5,2:6);
   Mpeice1=M(1:5,1);
   A(1)=1;
   A(2:6)=inv(Mpeice2)*(-1)*Mpeice1*A(1);

   P=2*.5*BbarP/377*quad8('eysqr',0,10*a3,[],[],A,U,BbarP,lambdao);
   A=A/sqrt(P);

   % omega = 2*pi*c/lambdao
   Kl1ReadyMult = 2*pi/lambdao /377 /2 *
N(1)*quad8('eysqr',a(1),a(2),[],[],A,U,BbarP,lambdao);
   Kl3ReadyMult = 2*pi/lambdao /377 /2 *
N(3)*quad8('eysqr',a(3),a(4),[],[],A,U,BbarP,lambdao);

   PhiL1 = 0;
   PhiL3 = pi;

   delE = BbarP*2*pi/lambdao-pi/GratLambda;

   maxSlice = maxSlice4plotting;

   deltaz=L/maxSlice;
   if deltaz<10*GratLambda
      disp('Error: decrease maxSlice !!!');
   end; % if deltaz

   RoverS = [1; 0];

   for Slice=1:maxSlice

      Kl1 = Kl1ReadyMult * PerturbL1(Slice);
      Kl3 = Kl3ReadyMult * PerturbL3(Slice);

      ZeroDC4MultLayer = 0;
      if ZeroDC4MultLayer~=1
         v=1;
         sigma = 2 /v * (Kl1 + Kl3);
      else
         sigma = 0;
      end; % if ZeroDC4MultLayer

      Ksa = Kl1*exp(i*PhiL1) + Kl3*exp(i*PhiL3);
      K = abs(Ksa);
      Phi(Slice) = angle(Ksa);

   end; % for Slice=

   Phi = unwrap(Phi);
```

```
   Phi = fliplr( Phi ); % Slices were ordered from L/2 to -L/2
   derPhiTemp1 = diff(Phi) / deltaz;
   derPhiTemp2 = interp( derPhiTemp1, 2);
   derPhiTemp3 = derPhiTemp2( 2:2:length(derPhiTemp2) );
   derAtNegLDiv2 = interp( fliplr(derPhiTemp1), 2 );
   derAtNegLDiv2 = derAtNegLDiv2( length(derAtNegLDiv2) );
   derPhi = [ derAtNegLDiv2 derPhiTemp3 ];
   derPhi = fliplr(derPhi); % Slices are again ordered from L/2 to -L/2
   if j==1
      derPhiTrack = derPhi;
   end;

   % check
   if length(derPhi) ~= maxSlice
      disp('Error: length(derPhi) ~= maxSlice');
   end;

   RoverS = [1; 0];
   for Slice=1:maxSlice

      Kl1 = Kl1ReadyMult * PerturbL1(Slice);
      Kl3 = Kl3ReadyMult * PerturbL3(Slice);

      ZeroDC4MultLayer = 0;
      if ZeroDC4MultLayer~=1
         v=1;
         sigma = 2 /v * (Kl1 + Kl3);
      else
         sigma = 0;
      end; % if ZeroDC4MultLayer

      Ksa = Kl1*exp(i*PhiL1) + Kl3*exp(i*PhiL3);
      K = abs(Ksa);
      if j==1
         KTrack(Slice) = K;
      end; % if j==1

      sigmahat = delE + sigma -.5*derPhi(Slice);

      gamma = sqrt( (abs(K))^2 - sigmahat^2);
      F = [ cosh(gamma*deltaz) - i*sigmahat/gamma*sinh(gamma*deltaz) ...
            -i*K/gamma*sinh(gamma*deltaz);
            i*conj(K)/gamma*sinh(gamma*deltaz) ...
            cosh(gamma*deltaz) + i*sigmahat/gamma*sinh(gamma*deltaz) ];
      RoverS = F*RoverS;
   end; % for Slice=

R(j) = ( abs( RoverS(2)/RoverS(1) ) )^2;
PhaseRho1(j) = angle( RoverS(2)/RoverS(1) );
PhaseRho2(j) = angle( RoverS(2)/RoverS(1) ) - (-2*delE*L/2);

end; % for j=1:S(1)



lambdao=minLambdao+delLambdao*((1:j)-1);
PhaseRho1 = unwrap(PhaseRho1);
temp1 = [ lambdao(1:length(lambdao)-1); lambdao(2:length(lambdao)) ];
temp2 = [ -1*PhaseRho1(1:length(PhaseRho1)-1); PhaseRho1(2:length(PhaseRho1)) ];
for index=1:length(temp1)
   lambdaoDT(index) = sum( temp1(:,index) )/2;
   DelayTime(index) = -1*lambdaoDT(index)^2 / (2*pi*3e8) * sum( temp2(:,index)
)/delLambdao;
end; % for index=

temp1 = [ lambdaoDT(1:length(lambdaoDT)-1); lambdaoDT(2:length(lambdaoDT)) ];
temp2 = [ -1*DelayTime(1:length(DelayTime)-1); DelayTime(2:length(DelayTime)) ];
for index=1:length(temp1)
   lambdaoDis(index) = sum( temp1(:,index) )/2;
   Dispersion(index) = sum( temp2(:,index) ) / delLambdao;
end; % for index=
```

```
plot(lambdao,R);
title('Reflection Coefficient versus Wavelength');
xlabel('Lambdao'); ylabel('R');
axis([minLambdao max(lambdao) 0 1]);
V=axis;

vertfrac=1/14;
vertstart=1/12;
vf=vertfrac; vs=vertstart;
text(V(1)+(V(2)-V(1))*1/25,V(3)+(V(4)-V(3))*(1-vs),['n1= ',num2str(n1,5)]);
text(V(1)+(V(2)-V(1))*1/6,V(3)+(V(4)-V(3))*(1-vs),['n2= ',num2str(n2,5)]);
text(V(1)+(V(2)-V(1))*1/25,V(3)+(V(4)-V(3))*(1-vs-vf),['n3= ',num2str(n3,5)]);
text(V(1)+(V(2)-V(1))*1/6,V(3)+(V(4)-V(3))*(1-vs-vf),['n4= ',num2str(n4,5)]);
text(V(1)+(V(2)-V(1))*1/25,V(3)+(V(4)-V(3))*(1-vs-2*vf),['a1= ',num2str(a1),' m']);
if n2==n3 & n3==n4
   text(V(1)+(V(2)-V(1))*1/25,V(3)+(V(4)-V(3))*(1-vs-3*vf),['a2= irrelevant']);
   text(V(1)+(V(2)-V(1))*1/25,V(3)+(V(4)-V(3))*(1-vs-4*vf),['a3= irrelevant']);
else
   text(V(1)+(V(2)-V(1))*1/25,V(3)+(V(4)-V(3))*(1-vs-3*vf),['a2= ',num2str(a2),' m']);
   text(V(1)+(V(2)-V(1))*1/25,V(3)+(V(4)-V(3))*(1-vs-4*vf),['a3= ',num2str(a3),' m']);
end; % if n2==

text(V(1)+(V(2)-V(1))*1/25,V(3)+(V(4)-V(3))*(1-vs-5*vf),['Length= ',num2str(L),' m']);
text(V(1)+(V(2)-V(1))*1/25,V(3)+(V(4)-V(3))*(1-vs-6*vf),['GratLambda=
',num2str(GratLambda),' m']);

      zMaxR=max(R);
      dummy=R-zMaxR/2; dummy=dummy+abs(dummy);
      mloop=1;
      while dummy(Centerindex+mloop)>0
         mloop=mloop+1;
      end; % while dummy(
      nloop=1;
      while dummy(Centerindex-nloop)>0
         nloop=nloop+1;
      end; % while nloop
      zHalfRBW=delLambdao*(mloop+nloop);
%%    zGratLambda=GratLambda;
%     mloop=1;
%     while R(Centerindex+mloop)<R(Centerindex+mloop-1)
%        mloop=mloop+1;
%     end; % while mloop
%     nloop=1;
%     while R(Centerindex-nloop)<R(Centerindex-nloop+1)
%        nloop=nloop+1;
%     end; % while nloop
%     zSLlevel=max(R.*[ones(1,Centerindex-nloop) zeros(1,mloop+nloop-2+1) ...
%     ones(1,length(R)-Centerindex-mloop+1)]);

text(V(1)+(V(2)-V(1))*1/25,V(3)+(V(4)-V(3))*(1-vs-7*vf),['Measurements:']);
text(V(1)+(V(2)-V(1))*1/25,V(3)+(V(4)-V(3))*(1-vs-8*vf),['1-Max(R)= ',num2str(1-zMaxR)]);
text(V(1)+(V(2)-V(1))*1/25,V(3)+(V(4)-V(3))*(1-vs-9*vf),['Half R BW=
',num2str(zHalfRBW,7),' m']);
%%text(V(1)+(V(2)-V(1))*1/25,V(3)+(V(4)-V(3))*(1-vs-10*vf),['1st S-Lobe Level=
',num2str(zSLlevel)]);

text(V(1)+(V(2)-V(1))*2/3,V(3)+(V(4)-V(3))*(1-vs),['# Slices = ',num2str(maxSlice)]);


%if toggleProf==1
%   text(V(1)+(V(2)-V(1))*2/3,V(3)+(V(4)-V(3))*(1-vs-2*vf),['Profile is Guassian-->']);
%   text(V(1)+(V(2)-V(1))*2/3,V(3)+(V(4)-V(3))*(1-vs-3*vf),['delnbar=
',num2str(alpha),'*(n-nSiO2) *']);
%   text(V(1)+(V(2)-V(1))*2/3,V(3)+(V(4)-V(3))*(1-vs-3.5*vf),['   exp ( -4 ln2 z^2 /
FWHM^2 )']);
   text(V(1)+(V(2)-V(1))*2/3,V(3)+(V(4)-V(3))*(1-vs-4*vf),['z= -L/2 to L/2']);
%   text(V(1)+(V(2)-V(1))*2/3,V(3)+(V(4)-V(3))*(1-vs-5*vf),['FWHM= ',num2str(FWHM),'
m']);
%else
```

```
%if toggleProf==2
%   text(V(1)+(V(2)-V(1))*2/3,V(3)+(V(4)-V(3))*(1-vs-2*vf),['Profile is Raised Cosine--
>']);
%   text(V(1)+(V(2)-V(1))*2/3,V(3)+(V(4)-V(3))*(1-vs-3*vf),['delnbar=
',num2str(alpha),'*(n-nSiO2) *']);
%   text(V(1)+(V(2)-V(1))*2/3,V(3)+(V(4)-V(3))*(1-vs-3.5*vf),['   0.5*(1+cos( pi*z/FWHM )
']);
%   text(V(1)+(V(2)-V(1))*2/3,V(3)+(V(4)-V(3))*(1-vs-4*vf),['z= -L/2 to L/2']);
%   text(V(1)+(V(2)-V(1))*2/3,V(3)+(V(4)-V(3))*(1-vs-5*vf),['FWHM= ',num2str(FWHM),'
m']);
%else
%   text(V(1)+(V(2)-V(1))*2/3,V(3)+(V(4)-V(3))*(1-vs-2*vf),['Profile is Uniform']);
%   text(V(1)+(V(2)-V(1))*2/3,V(3)+(V(4)-V(3))*(1-vs-3*vf),['delnbar=
',num2str(alpha),'*(n-nSiO2)']);
%end; % if toggleProj==2
%end; % if toggleProf==1

%if ZeroDC==1
%   text(V(1)+(V(2)-V(1))*2/3,V(3)+(V(4)-V(3))*(1-vs-6*vf),['"dc" index change = zero']);
%   text(V(1)+(V(2)-V(1))*2/3,V(3)+(V(4)-V(3))*(1-vs-7*vf),['v= ',num2str(v/LargeNum)]);
%else
%   text(V(1)+(V(2)-V(1))*2/3,V(3)+(V(4)-V(3))*(1-vs-6*vf),['"dc" index change =
nonzero']);
%   text(V(1)+(V(2)-V(1))*2/3,V(3)+(V(4)-V(3))*(1-vs-7*vf),['v= ',num2str(v)]);
%end; % if ZeroDC



%%%save Refcorun4 zMaxR zHalfRBW zGratLambda zSLlevel ActualCenterL L alpha...
%%%n1 n2 n3 n4 a1
```

apodv2ErgDesChirp.m

```
% Run slab.m first.

%inputs%%%%%%
alpha=.062019176;

% I changed my mind about using L1 as variable.  Now L1=1, L2=2 etc. is fixed.
delnL1=alpha*(N(1)-nSiO2); % must be <= .1 N(1)
delnL2=alpha*(N(2)-nSiO2); % must be <= .1 N(2)
delnL3=alpha*(N(3)-nSiO2); % must be <= .1 N(3), zero is ok
delnL4=alpha*(N(4)-nSiO2); % must be <= .1 N(4), zero is ok
% Now these deln are the peak values of the "dc" effective index changes (dc nonzero)
% in other words, they are the peak values of delnbar

pl2mpl1 = 0;
pl3mpl1 = 0;
pl4mpl1 = 0;

CenterLambdao=1.55e-6;

toggleProf=2; % 1=Guassian, 2=Raised Cosine
if toggleProf==1
   FWHM=5e-3/3;
   L=3*FWHM; % Length in meters
else
if toggleProf==2
   FWHM=.01;
   L=2*FWHM;
else
   L=5e-3;
end; % if toggleProf==2
end; % if toggleProf==1

% Set ZeroDC=1 if want "dc" index change = 0
ZeroDC=1;

v = 1;
LargeNum=1e9;
```

```
if ZeroDC==1
   v=v*LargeNum;
end; % if ZeroDC

%%%%%%%%%%%%


a=[0 a1 a2 a3];
toggleNum=1; % 1=even
toggle='eve';
count=1;

S=size(Bbar);
if length(S)>2
   disp('Waveguide is not single mode!');
end; % if length


% next block calculates GratLambda which determines CenterLambdao

Centerindex=1+round( (CenterLambdao-minLambdao)/delLambdao );
ActualCenterL=minLambdao+delLambdao*(Centerindex-1);
j=Centerindex;

lambdao=minLambdao+delLambdao*(j-1);
BbarP=Bbar(j,count,toggleNum);

[M,U]=UevalM(BbarP,lambdao,toggle);
Mpeice2=M(1:5,2:6);
Mpeice1=M(1:5,1);
A(1)=1;
A(2:6)=inv(Mpeice2)*(-1)*Mpeice1*A(1);

P=2*.5*BbarP/377*quad8('eysqr',0,10*a3,[],[],A,U,BbarP,lambdao);
A=A/sqrt(P);

Co=2*.5*2*pi/lambdao/377* ( N(1)*delnL1*quad8('eysqr',a(1),a(2),[],[],A,U,BbarP,lambdao)
...
+ N(2)*delnL2*quad8('eysqr',a(2),a(3),[],[],A,U,BbarP,lambdao) ...
+ N(3)*delnL3*quad8('eysqr',a(3),a(4),[],[],A,U,BbarP,lambdao) ...
+ N(4)*delnL4*quad8('eysqr',a(4),10*a(4),[],[],A,U,BbarP,lambdao) );

GratLambda=pi/( Bbar(Centerindex,1,1)*2*pi/ActualCenterL + Co);
if ZeroDC==1
   GratLambda = pi/( Bbar(Centerindex,1,1)*2*pi/ActualCenterL );
end; % if ZeroDC==1;

%% end of block

test = v * 2 * ( N(1)*delnL1*quad8('eysqr',a(1),a(2),[],[],A,U,BbarP,lambdao) ...
          + N(2)*delnL2*exp(sqrt(-
1)*pl2mpl1)*quad8('eysqr',a(2),a(3),[],[],A,U,BbarP,lambdao) ...
          + N(3)*delnL3*exp(sqrt(-
1)*pl3mpl1)*quad8('eysqr',a(3),a(4),[],[],A,U,BbarP,lambdao) ...
          + N(4)*delnL4*exp(sqrt(-
1)*pl4mpl1)*quad8('eysqr',a(4),10*a(4),[],[],A,U,BbarP,lambdao) )
if ZeroDC==1
   test = test/LargeNum
end; % if ZeroDC==1
% want test = 0.377 to match Erdogan's example of a chirped grating



for j=1:S(1)

   lambdao=minLambdao+delLambdao*(j-1);
   BbarP=Bbar(j,count,toggleNum);

   [M,U]=UevalM(BbarP,lambdao,toggle);
   Mpeice2=M(1:5,2:6);
   Mpeice1=M(1:5,1);
```

```
   A(1)=1;
   A(2:6)=inv(Mpeice2)*(-1)*Mpeice1*A(1);

   P=2*.5*BbarP/377*quad8('eysqr',0,10*a3,[],[],A,U,BbarP,lambdao);
   A=A/sqrt(P);

   maxsigma=2*.5*2*pi/lambdao/377* (
N(1)*delnL1*quad8('eysqr',a(1),a(2),[],[],A,U,BbarP,lambdao) ...
   + N(2)*delnL2*quad8('eysqr',a(2),a(3),[],[],A,U,BbarP,lambdao) ...
   + N(3)*delnL3*quad8('eysqr',a(3),a(4),[],[],A,U,BbarP,lambdao) ...
   + N(4)*delnL4*quad8('eysqr',a(4),10*a(4),[],[],A,U,BbarP,lambdao) );

   if ZeroDC==1
      maxsigma = maxsigma/LargeNum;
   end; % if ZeroDC

   maxK = v/2 * 2*.5*2*pi/lambdao/377* (
N(1)*delnL1*quad8('eysqr',a(1),a(2),[],[],A,U,BbarP,lambdao) ...
   + N(2)*delnL2*exp(sqrt(-1)*pl2mpl1)*quad8('eysqr',a(2),a(3),[],[],A,U,BbarP,lambdao)
...
   + N(3)*delnL3*exp(sqrt(-1)*pl3mpl1)*quad8('eysqr',a(3),a(4),[],[],A,U,BbarP,lambdao)
...
   + N(4)*delnL4*exp(sqrt(-
1)*pl4mpl1)*quad8('eysqr',a(4),10*a(4),[],[],A,U,BbarP,lambdao) );

   if ZeroDC==1
      maxK = maxK/LargeNum;
   end; % if ZeroDC

   delE = BbarP*2*pi/lambdao-pi/GratLambda;

   maxSlice=200;

   deltaz=L/maxSlice;
   if deltaz<10*GratLambda
      disp('Error: decrease maxSlice !!!');
   end; % if deltaz

   RoverS = [1; 0];

   for Slice=1:maxSlice

      % Guassian profile
      if toggleProf==1
         term = exp( -4 * log(2) * (L/2 -Slice*deltaz +deltaz/2)^2 / FWHM^2 );
      else
      % Raised-Cosine Profile
      if toggleProf==2
         term = .5 * ( 1+cos(pi* (L/2 -Slice*deltaz +deltaz/2) / FWHM ));
      else
         term = 1;
      end; % if toggleProj==2
      end; % if toggleProf==1

      sigma = maxsigma * term;
      K = maxK * term;
      derLambdaoD = -1 * 1e-9/1e-2;
      derphi = -4*pi*Bbar(Centerindex,count,toggleNum)* (L/2 -Slice*deltaz +deltaz/2) /
(CenterLambdao^2) * derLambdaoD;
      sigmahat = delE + sigma -.5*derphi;

      gamma = sqrt( (abs(K))^2 - sigmahat^2);
      F = [ cosh(gamma*deltaz) - i*sigmahat/gamma*sinh(gamma*deltaz) ...
            -i*K/gamma*sinh(gamma*deltaz);
            i*conj(K)/gamma*sinh(gamma*deltaz) ...
            cosh(gamma*deltaz) + i*sigmahat/gamma*sinh(gamma*deltaz) ];
      RoverS = F*RoverS;
   end; % for Slice=

R(j) = ( abs( RoverS(2)/RoverS(1) ) )^2;
PhaseRho1(j) = angle( RoverS(2)/RoverS(1) );
```

```
PhaseRho2(j) = angle( RoverS(2)/RoverS(1) ) - (-2*delE*L/2);

end; % for j=1:S(1)


lambdao=minLambdao+delLambdao*((1:j)-1);
PhaseRho1 = unwrap(PhaseRho1);
temp1 = [ lambdao(1:length(lambdao)-1); lambdao(2:length(lambdao)) ];
temp2 = [ -1*PhaseRho1(1:length(PhaseRho1)-1); PhaseRho1(2:length(PhaseRho1)) ];
for index=1:length(temp1)
   lambdaoDT(index) = sum( temp1(:,index) )/2;
   DelayTime(index) = -1*lambdaoDT(index)^2 / (2*pi*3e8) * sum( temp2(:,index)
)/delLambdao;
end; % for index=

temp1 = [ lambdaoDT(1:length(lambdaoDT)-1); lambdaoDT(2:length(lambdaoDT)) ];
temp2 = [ -1*DelayTime(1:length(DelayTime)-1); DelayTime(2:length(DelayTime)) ];
for index=1:length(temp1)
   lambdaoDis(index) = sum( temp1(:,index) )/2;
   Dispersion(index) = sum( temp2(:,index) ) / delLambdao;
end; % for index=


plot(lambdao,R);
title('Reflection Coefficient versus Wavelength');
xlabel('Lambdao'); ylabel('R');
axis([minLambdao max(lambdao) 0 1]);
V=axis;

vertfrac=1/14;
vertstart=1/12;
vf=vertfrac; vs=vertstart;
text(V(1)+(V(2)-V(1))*1/25,V(3)+(V(4)-V(3))*(1-vs),['n1= ',num2str(n1,5)]);
text(V(1)+(V(2)-V(1))*1/6,V(3)+(V(4)-V(3))*(1-vs),['n2= ',num2str(n2,5)]);
text(V(1)+(V(2)-V(1))*1/25,V(3)+(V(4)-V(3))*(1-vs-vf),['n3= ',num2str(n3,5)]);
text(V(1)+(V(2)-V(1))*1/6,V(3)+(V(4)-V(3))*(1-vs-vf),['n4= ',num2str(n4,5)]);
text(V(1)+(V(2)-V(1))*1/25,V(3)+(V(4)-V(3))*(1-vs-2*vf),['a1= ',num2str(a1),' m']);
if n2==n3 & n3==n4
   text(V(1)+(V(2)-V(1))*1/25,V(3)+(V(4)-V(3))*(1-vs-3*vf),['a2= irrelevant']);
   text(V(1)+(V(2)-V(1))*1/25,V(3)+(V(4)-V(3))*(1-vs-4*vf),['a3= irrelevant']);
else
   text(V(1)+(V(2)-V(1))*1/25,V(3)+(V(4)-V(3))*(1-vs-3*vf),['a2= ',num2str(a2),' m']);
   text(V(1)+(V(2)-V(1))*1/25,V(3)+(V(4)-V(3))*(1-vs-4*vf),['a3= ',num2str(a3),' m']);
end; % if n2==

text(V(1)+(V(2)-V(1))*1/25,V(3)+(V(4)-V(3))*(1-vs-5*vf),['Length= ',num2str(L),' m']);
text(V(1)+(V(2)-V(1))*1/25,V(3)+(V(4)-V(3))*(1-vs-6*vf),['GratLambda=
',num2str(GratLambda),' m']);

      zMaxR=max(R);
      dummy=R-zMaxR/2; dummy=dummy+abs(dummy);
      mloop=1;
      while dummy(Centerindex+mloop)>0
         mloop=mloop+1;
      end; % while dummy(
      nloop=1;
      while dummy(Centerindex-nloop)>0
         nloop=nloop+1;
      end; % while nloop
      zHalfRBW=delLambdao*(mloop+nloop);
%%    zGratLambda=GratLambda;
%     mloop=1;
%     while R(Centerindex+mloop)<R(Centerindex+mloop-1)
%        mloop=mloop+1;
%     end; % while mloop
%     nloop=1;
%     while R(Centerindex-nloop)<R(Centerindex-nloop+1)
%        nloop=nloop+1;
%     end; % while nloop
%     zSLlevel=max(R.*[ones(1,Centerindex-nloop) zeros(1,mloop+nloop-2+1) ...
%     ones(1,length(R)-Centerindex-mloop+1)]);
```

```
text(V(1)+(V(2)-V(1))*1/25,V(3)+(V(4)-V(3))*(1-vs-7*vf),['Measurements:']);
text(V(1)+(V(2)-V(1))*1/25,V(3)+(V(4)-V(3))*(1-vs-8*vf),['1-Max(R)= ',num2str(1-zMaxR)]);
text(V(1)+(V(2)-V(1))*1/25,V(3)+(V(4)-V(3))*(1-vs-9*vf),['Half R BW=
',num2str(zHalfRBW,7),' m']);
%%text(V(1)+(V(2)-V(1))*1/25,V(3)+(V(4)-V(3))*(1-vs-10*vf),['1st S-Lobe Level=
',num2str(zSLlevel)]);

text(V(1)+(V(2)-V(1))*2/3,V(3)+(V(4)-V(3))*(1-vs),['# Slices = ',num2str(maxSlice)]);


if toggleProf==1
   text(V(1)+(V(2)-V(1))*2/3,V(3)+(V(4)-V(3))*(1-vs-2*vf),['Profile is Guassian-->']);
   text(V(1)+(V(2)-V(1))*2/3,V(3)+(V(4)-V(3))*(1-vs-3*vf),['delnbar=
',num2str(alpha),'*(n-nSiO2) *']);
   text(V(1)+(V(2)-V(1))*2/3,V(3)+(V(4)-V(3))*(1-vs-3.5*vf),['   exp ( -4 ln2 z^2 /
FWHM^2 )']);
   text(V(1)+(V(2)-V(1))*2/3,V(3)+(V(4)-V(3))*(1-vs-4*vf),['z= -L/2 to L/2']);
   text(V(1)+(V(2)-V(1))*2/3,V(3)+(V(4)-V(3))*(1-vs-5*vf),['FWHM= ',num2str(FWHM),' m']);
else
if toggleProf==2
   text(V(1)+(V(2)-V(1))*2/3,V(3)+(V(4)-V(3))*(1-vs-2*vf),['Profile is Raised Cosine--
>']);
   text(V(1)+(V(2)-V(1))*2/3,V(3)+(V(4)-V(3))*(1-vs-3*vf),['delnbar=
',num2str(alpha),'*(n-nSiO2) *']);
   text(V(1)+(V(2)-V(1))*2/3,V(3)+(V(4)-V(3))*(1-vs-3.5*vf),['   0.5*(1+cos( pi*z/FWHM )
']);
   text(V(1)+(V(2)-V(1))*2/3,V(3)+(V(4)-V(3))*(1-vs-4*vf),['z= -L/2 to L/2']);
   text(V(1)+(V(2)-V(1))*2/3,V(3)+(V(4)-V(3))*(1-vs-5*vf),['FWHM= ',num2str(FWHM),' m']);
else
   text(V(1)+(V(2)-V(1))*2/3,V(3)+(V(4)-V(3))*(1-vs-2*vf),['Profile is Uniform']);
   text(V(1)+(V(2)-V(1))*2/3,V(3)+(V(4)-V(3))*(1-vs-3*vf),['delnbar=
',num2str(alpha),'*(n-nSiO2)']);
end; % if toggleProj==2
end; % if toggleProf==1

if ZeroDC==1
   text(V(1)+(V(2)-V(1))*2/3,V(3)+(V(4)-V(3))*(1-vs-6*vf),['"dc" index change = zero']);
   text(V(1)+(V(2)-V(1))*2/3,V(3)+(V(4)-V(3))*(1-vs-7*vf),['v= ',num2str(v/LargeNum)]);
else
   text(V(1)+(V(2)-V(1))*2/3,V(3)+(V(4)-V(3))*(1-vs-6*vf),['"dc" index change =
nonzero']);
   text(V(1)+(V(2)-V(1))*2/3,V(3)+(V(4)-V(3))*(1-vs-7*vf),['v= ',num2str(v)]);
end; % if ZeroDC




%%%save Refcorun4 zMaxR zHalfRBW zGratLambda zSLlevel ActualCenterL L alpha...
%%%n1 n2 n3 n4 a1
```

OneLChirp2FourL.m

```
% original design is Ergodan's example of a chirped grating
% run apodv2ErgDes.m first

% profile of single apodizing function of original design is zero-dc
% as well as both apodizing functions of new design

%%%%%%%%%%

   j = Centerindex;
   lambdao=minLambdao+delLambdao*(j-1);
   BbarP=Bbar(j,count,toggleNum);

   [M,U]=UevalM(BbarP,lambdao,toggle);
   Mpeice2=M(1:5,2:6);
   Mpeice1=M(1:5,1);
   A(1)=1;
   A(2:6)=inv(Mpeice2)*(-1)*Mpeice1*A(1);
```

```
   P=2*.5*BbarP/377*quad8('eysqr',0,10*a3,[],[],A,U,BbarP,lambdao);
   A=A/sqrt(P);

   maxsigma=2*.5*2*pi/lambdao/377* (
N(1)*delnL1*quad8('eysqr',a(1),a(2),[],[],A,U,BbarP,lambdao) ...
   + N(2)*delnL2*quad8('eysqr',a(2),a(3),[],[],A,U,BbarP,lambdao) ...
   + N(3)*delnL3*quad8('eysqr',a(3),a(4),[],[],A,U,BbarP,lambdao) ...
   + N(4)*delnL4*quad8('eysqr',a(4),10*a(4),[],[],A,U,BbarP,lambdao) );

   if ZeroDC==1
      maxsigma = maxsigma/LargeNum;
   end; % if ZeroDC

   maxK = v/2 * 2*.5*2*pi/lambdao/377* (
N(1)*delnL1*quad8('eysqr',a(1),a(2),[],[],A,U,BbarP,lambdao) ...
   + N(2)*delnL2*exp(sqrt(-1)*pl2mpl1)*quad8('eysqr',a(2),a(3),[],[],A,U,BbarP,lambdao)
...
   + N(3)*delnL3*exp(sqrt(-1)*pl3mpl1)*quad8('eysqr',a(3),a(4),[],[],A,U,BbarP,lambdao)
...
   + N(4)*delnL4*exp(sqrt(-
1)*pl4mpl1)*quad8('eysqr',a(4),10*a(4),[],[],A,U,BbarP,lambdao) );

   % omega = 2*pi*f = 2*pi*c / lambdao;
   PerturbL1divisor = 2*pi / lambdao /377 /4 * 2 * ...
                      N(1)*quad8('eysqr',a(1),a(2)/2,[],[],A,U,BbarP,lambdao);
   PerturbL2divisor = 2*pi / lambdao /377 /2 * ...
                      N(1)*quad8('eysqr',a(2)/2,a(2),[],[],A,U,BbarP,lambdao);
   PerturbL3divisor = 2*pi / lambdao /377 /2 * ...
                      N(3)*quad8('eysqr',a(3), (a(3)+a(4))/2 ,[],[],A,U,BbarP,lambdao);
   PerturbL4divisor = 2*pi / lambdao /377 /2 * ...
                      N(3)*quad8('eysqr', (a(3)+a(4))/2 ,a(4),[],[],A,U,BbarP,lambdao);

   if ZeroDC==1
      maxK = maxK/LargeNum;
   end; % if ZeroDC

%%%%%%%%%%

maxSlice4plotting = 200;
deltaz=L/maxSlice4plotting;

for Slice=1:maxSlice4plotting

   % Guassian profile
   if toggleProf==1
      term = exp( -4 * log(2) * (L/2 -Slice*deltaz +deltaz/2)^2 / FWHM^2 );
   else
   % Raised-Cosine Profile
   if toggleProf==2
      term = .5 * ( 1+cos(pi* (L/2 -Slice*deltaz +deltaz/2) / FWHM ));
      termTrack(Slice) = term;
   else
      term = 1;
   end; % if toggleProj==2
   end; % if toggleProf==1

%   sigma = maxsigma * term;
   K = maxK * term;

   BbarP=Bbar(Centerindex,count,toggleNum);
   derLambdaoD = -1 * 1e-9/1e-2;
   Phi(Slice) = .5 * -4*pi*Bbar(Centerindex,count,toggleNum)* (L/2 -Slice*deltaz
+deltaz/2)^2 / ...
         (CenterLambdao^2) * derLambdaoD;

   z(Slice) = (L/2 -Slice*deltaz +deltaz/2);

   % assume PhiL1(z)=0, PhiL3(z)=pi/2
   Kl1andl2(Slice) = cos(Phi(Slice)) * K;
   Kl3andl4(Slice) = sin(Phi(Slice)) * K;
```

```
end; % for Slice=

for Slice=1:maxSlice4plotting

   Kl1(Slice) = ( max(abs(Kl1andl2)) + Kl1andl2(Slice) ) /2;
   Kl2(Slice) = ( max(abs(Kl1andl2)) - Kl1andl2(Slice) ) /2;
   Kl3(Slice) = ( max(abs(Kl3andl4)) + Kl3andl4(Slice) ) /2;
   Kl4(Slice) = ( max(abs(Kl3andl4)) - Kl3andl4(Slice) ) /2;

   % find delnL1bar * fL1 * v for layers

   PerturbL1(Slice) = Kl1(Slice) / PerturbL1divisor;
   PerturbL2(Slice) = Kl2(Slice) / PerturbL2divisor;
   PerturbL3(Slice) = Kl3(Slice) / PerturbL3divisor;
   PerturbL4(Slice) = Kl4(Slice) / PerturbL4divisor;

end; % for Slice=


   figure; subplot(5,1,1);
   plot( z,delnL1*termTrack.*cos( 2*pi/ (L/60) * z + Phi ) );
%   title('Variation of the index change for original design');
   title('(a)');
   xlabel('z (meters)');
   ylabel('delta n (unitless)');

   subplot(5,1,2);
   plot( z,PerturbL1.*( ones(1,length(z)) + cos( 2*pi/ (L/60) * z + 0 ) ) );
%   title('Perturbation within abs(x)<a1/2');
   title('(b)');
   xlabel('z (meters)');
   ylabel('delta n (unitless)');

   subplot(5,1,3);
   plot( z,PerturbL2.*( ones(1,length(z)) + cos( 2*pi/ (L/60) * z + pi ) ) );
%   title('Perturbation within a1/2<abs(x)<a1');
   title('(c)');
   xlabel('z (meters)');
   ylabel('delta n (unitless)');

   subplot(5,1,4);
   plot( z,PerturbL3.*( ones(1,length(z)) + cos( 2*pi/ (L/60) * z + pi/2 ) ) );
%   title('Perturbation within a2<abs(x)<(a2+a3)/2');
   title('(d)');
   xlabel('z (meters)');
   ylabel('delta n (unitless)');

   subplot(5,1,5);
   plot( z,PerturbL4.*( ones(1,length(z)) + cos( 2*pi/ (L/60) * z + 3*pi/2 ) ) );
%   title('Perturbation within (a2+a3)/2<abs(x)<a3');
   title('(e)');
   xlabel('z (meters)');
   ylabel('delta n (unitless)');
```

ChirpApod4L.m

```
% first run apodv2ErgDesChirp.m, then OneLChirp2FourL.m

% sigmaAtCenterLambdao is independent of z;
sigmaAtCenterLambdao = 2*( max(abs(Kl1andl2)) + max(abs(Kl3andl4)) );
GratLambda=pi/( Bbar(Centerindex,1,1)*2*pi/ActualCenterL + sigmaAtCenterLambdao);

for j=1:S(1)

   lambdao=minLambdao+delLambdao*(j-1);
   BbarP=Bbar(j,count,toggleNum);

   [M,U]=UevalM(BbarP,lambdao,toggle);
   Mpeice2=M(1:5,2:6);
   Mpeice1=M(1:5,1);
   A(1)=1;
```

```
A(2:6)=inv(Mpeice2)*(-1)*Mpeice1*A(1);

P=2*.5*BbarP/377*quad8('eysqr',0,10*a3,[],[],A,U,BbarP,lambdao);
A=A/sqrt(P);

% omega = 2*pi*c/lambdao

Kl1ReadyMult = 2*pi / lambdao /377 /4 * 2 * ...
               N(1)*quad8('eysqr',a(1),a(2)/2,[],[],A,U,BbarP,lambdao);
Kl2ReadyMult = 2*pi / lambdao /377 /2 * ...
               N(1)*quad8('eysqr',a(2)/2,a(2),[],[],A,U,BbarP,lambdao);
Kl3ReadyMult = 2*pi / lambdao /377 /2 * ...
               N(3)*quad8('eysqr',a(3), (a(3)+a(4))/2 ,[],[],A,U,BbarP,lambdao);
Kl4ReadyMult = 2*pi / lambdao /377 /2 * ...
               N(3)*quad8('eysqr', (a(3)+a(4))/2 ,a(4),[],[],A,U,BbarP,lambdao);

PhiL1 = 0;
PhiL2 = pi;
PhiL3 = pi/2;
PhiL4 = -pi/2;

delE = BbarP*2*pi/lambdao-pi/GratLambda;

maxSlice = maxSlice4plotting;

deltaz=L/maxSlice;
if deltaz<10*GratLambda
   disp('Error: decrease maxSlice !!!');
end; % if deltaz

RoverS = [1; 0];

for Slice=1:maxSlice

   Kl1 = Kl1ReadyMult * PerturbL1(Slice);
   Kl2 = Kl2ReadyMult * PerturbL2(Slice);
   Kl3 = Kl3ReadyMult * PerturbL3(Slice);
   Kl4 = Kl4ReadyMult * PerturbL4(Slice);

   ZeroDC4MultLayer = 0;
   if ZeroDC4MultLayer~=1
      v=1;
      sigma = 2 /v * (Kl1 + Kl2 + Kl3 + Kl4);
   else
      sigma = 0;
   end; % if ZeroDC4MultLayer

   Ksa = Kl1*exp(i*PhiL1) + Kl2*exp(i*PhiL2) + Kl3*exp(i*PhiL3) + Kl4*exp(i*PhiL4);
   K = abs(Ksa);
   Phi(Slice) = angle(Ksa);

end; % for Slice=

Phi = unwrap(Phi);
Phi = fliplr( Phi ); % Slices were ordered from L/2 to -L/2
derPhiTemp1 = diff(Phi) / deltaz;
derPhiTemp2 = interp( derPhiTemp1, 2);
derPhiTemp3 = derPhiTemp2( 2:2:length(derPhiTemp2) );
derAtNegLDiv2 = interp( fliplr(derPhiTemp1), 2 );
derAtNegLDiv2 = derAtNegLDiv2( length(derAtNegLDiv2) );
derPhi = [ derAtNegLDiv2 derPhiTemp3 ];
derPhi = fliplr(derPhi); % Slices are again ordered from L/2 to -L/2
if j==1
   derPhiTrack = derPhi;
end;

% check
if length(derPhi) ~= maxSlice
   disp('Error: length(derPhi) ~= maxSlice');
end;
```

```
   RoverS = [1; 0];
   for Slice=1:maxSlice

      Kl1 = Kl1ReadyMult * PerturbL1(Slice);
      Kl2 = Kl2ReadyMult * PerturbL2(Slice);
      Kl3 = Kl3ReadyMult * PerturbL3(Slice);
      Kl4 = Kl4ReadyMult * PerturbL4(Slice);

      ZeroDC4MultLayer = 0;
      if ZeroDC4MultLayer~=1
         v=1;
         sigma = 2 /v * (Kl1 + Kl2 + Kl3 + Kl4);
      else
         sigma = 0;
      end; % if ZeroDC4MultLayer

      Ksa = Kl1*exp(i*PhiL1) + Kl2*exp(i*PhiL2) + Kl3*exp(i*PhiL3) + Kl4*exp(i*PhiL4);
      K = abs(Ksa);
      if j==1
         KTrack(Slice) = K;
      end; % if j==1

      sigmahat = delE + sigma -.5*derPhi(Slice);

      gamma = sqrt( (abs(K))^2 - sigmahat^2);
      F = [ cosh(gamma*deltaz) - i*sigmahat/gamma*sinh(gamma*deltaz) ...
            -i*K/gamma*sinh(gamma*deltaz);
            i*conj(K)/gamma*sinh(gamma*deltaz) ...
            cosh(gamma*deltaz) + i*sigmahat/gamma*sinh(gamma*deltaz) ];
      RoverS = F*RoverS;
   end; % for Slice=

R(j) = ( abs( RoverS(2)/RoverS(1) ) )^2;
PhaseRho1(j) = angle( RoverS(2)/RoverS(1) );
PhaseRho2(j) = angle( RoverS(2)/RoverS(1) ) - (-2*delE*L/2);

end; % for j=1:S(1)



lambdao=minLambdao+delLambdao*((1:j)-1);
PhaseRho1 = unwrap(PhaseRho1);
temp1 = [ lambdao(1:length(lambdao)-1); lambdao(2:length(lambdao)) ];
temp2 = [ -1*PhaseRho1(1:length(PhaseRho1)-1); PhaseRho1(2:length(PhaseRho1)) ];
for index=1:length(temp1)
   lambdaoDT(index) = sum( temp1(:,index) )/2;
   DelayTime(index) = -1*lambdaoDT(index)^2 / (2*pi*3e8) * sum( temp2(:,index)
)/delLambdao;
end; % for index=

temp1 = [ lambdaoDT(1:length(lambdaoDT)-1); lambdaoDT(2:length(lambdaoDT)) ];
temp2 = [ -1*DelayTime(1:length(DelayTime)-1); DelayTime(2:length(DelayTime)) ];
for index=1:length(temp1)
   lambdaoDis(index) = sum( temp1(:,index) )/2;
   Dispersion(index) = sum( temp2(:,index) ) / delLambdao;
end; % for index=


plot(lambdao,R);
title('Reflection Coefficient versus Wavelength');
xlabel('Lambdao'); ylabel('R');
axis([minLambdao max(lambdao) 0 1]);
V=axis;

vertfrac=1/14;
vertstart=1/12;
vf=vertfrac; vs=vertstart;
text(V(1)+(V(2)-V(1))*1/25,V(3)+(V(4)-V(3))*(1-vs),['n1= ',num2str(n1,5)]);
text(V(1)+(V(2)-V(1))*1/6,V(3)+(V(4)-V(3))*(1-vs),['n2= ',num2str(n2,5)]);
text(V(1)+(V(2)-V(1))*1/25,V(3)+(V(4)-V(3))*(1-vs-vf),['n3= ',num2str(n3,5)]);
text(V(1)+(V(2)-V(1))*1/6,V(3)+(V(4)-V(3))*(1-vs-vf),['n4= ',num2str(n4,5)]);
```

```
text(V(1)+(V(2)-V(1))*1/25,V(3)+(V(4)-V(3))*(1-vs-2*vf),['a1= ',num2str(a1),' m']);
if n2==n3 & n3==n4
   text(V(1)+(V(2)-V(1))*1/25,V(3)+(V(4)-V(3))*(1-vs-3*vf),['a2= irrelevant']);
   text(V(1)+(V(2)-V(1))*1/25,V(3)+(V(4)-V(3))*(1-vs-4*vf),['a3= irrelevant']);
else
   text(V(1)+(V(2)-V(1))*1/25,V(3)+(V(4)-V(3))*(1-vs-3*vf),['a2= ',num2str(a2),' m']);
   text(V(1)+(V(2)-V(1))*1/25,V(3)+(V(4)-V(3))*(1-vs-4*vf),['a3= ',num2str(a3),' m']);
end; % if n2==

text(V(1)+(V(2)-V(1))*1/25,V(3)+(V(4)-V(3))*(1-vs-5*vf),['Length= ',num2str(L),' m']);
text(V(1)+(V(2)-V(1))*1/25,V(3)+(V(4)-V(3))*(1-vs-6*vf),['GratLambda=
',num2str(GratLambda),' m']);

      zMaxR=max(R);
      dummy=R-zMaxR/2; dummy=dummy+abs(dummy);
      mloop=1;
      while dummy(Centerindex+mloop)>0
         mloop=mloop+1;
      end; % while dummy(
      nloop=1;
      while dummy(Centerindex-nloop)>0
         nloop=nloop+1;
      end; % while nloop
      zHalfRBW=delLambdao*(mloop+nloop);
%%    zGratLambda=GratLambda;
%     mloop=1;
%     while R(Centerindex+mloop)<R(Centerindex+mloop-1)
%        mloop=mloop+1;
%     end; % while mloop
%     nloop=1;
%     while R(Centerindex-nloop)<R(Centerindex-nloop+1)
%        nloop=nloop+1;
%     end; % while nloop
%     zSLlevel=max(R.*[ones(1,Centerindex-nloop) zeros(1,mloop+nloop-2+1) ...
%     ones(1,length(R)-Centerindex-mloop+1)]);

text(V(1)+(V(2)-V(1))*1/25,V(3)+(V(4)-V(3))*(1-vs-7*vf),['Measurements:']);
text(V(1)+(V(2)-V(1))*1/25,V(3)+(V(4)-V(3))*(1-vs-8*vf),['1-Max(R)= ',num2str(1-zMaxR)]);
text(V(1)+(V(2)-V(1))*1/25,V(3)+(V(4)-V(3))*(1-vs-9*vf),['Half R BW=
',num2str(zHalfRBW,7),' m']);
%%text(V(1)+(V(2)-V(1))*1/25,V(3)+(V(4)-V(3))*(1-vs-10*vf),['1st S-Lobe Level=
',num2str(zSLlevel)]);

text(V(1)+(V(2)-V(1))*2/3,V(3)+(V(4)-V(3))*(1-vs),['# Slices = ',num2str(maxSlice)]);


if toggleProf==1
   text(V(1)+(V(2)-V(1))*2/3,V(3)+(V(4)-V(3))*(1-vs-2*vf),['Profile is Guassian-->']);
   text(V(1)+(V(2)-V(1))*2/3,V(3)+(V(4)-V(3))*(1-vs-3*vf),['delnbar=
',num2str(alpha),'*(n-nSiO2) *']);
   text(V(1)+(V(2)-V(1))*2/3,V(3)+(V(4)-V(3))*(1-vs-3.5*vf),['   exp ( -4 ln2 z^2 /
FWHM^2 )']);
   text(V(1)+(V(2)-V(1))*2/3,V(3)+(V(4)-V(3))*(1-vs-4*vf),['z= -L/2 to L/2']);
   text(V(1)+(V(2)-V(1))*2/3,V(3)+(V(4)-V(3))*(1-vs-5*vf),['FWHM= ',num2str(FWHM),' m']);
else
if toggleProf==2
   text(V(1)+(V(2)-V(1))*2/3,V(3)+(V(4)-V(3))*(1-vs-2*vf),['Profile is Raised Cosine--
>']);
   text(V(1)+(V(2)-V(1))*2/3,V(3)+(V(4)-V(3))*(1-vs-3*vf),['delnbar=
',num2str(alpha),'*(n-nSiO2) *']);
   text(V(1)+(V(2)-V(1))*2/3,V(3)+(V(4)-V(3))*(1-vs-3.5*vf),['   0.5*(1+cos( pi*z/FWHM )
']);
   text(V(1)+(V(2)-V(1))*2/3,V(3)+(V(4)-V(3))*(1-vs-4*vf),['z= -L/2 to L/2']);
   text(V(1)+(V(2)-V(1))*2/3,V(3)+(V(4)-V(3))*(1-vs-5*vf),['FWHM= ',num2str(FWHM),' m']);
else
   text(V(1)+(V(2)-V(1))*2/3,V(3)+(V(4)-V(3))*(1-vs-2*vf),['Profile is Uniform']);
   text(V(1)+(V(2)-V(1))*2/3,V(3)+(V(4)-V(3))*(1-vs-3*vf),['delnbar=
',num2str(alpha),'*(n-nSiO2)']);
end; % if toggleProj==2
end; % if toggleProf==1
```

```
if ZeroDC==1
   text(V(1)+(V(2)-V(1))*2/3,V(3)+(V(4)-V(3))*(1-vs-6*vf),['"dc" index change = zero']);
   text(V(1)+(V(2)-V(1))*2/3,V(3)+(V(4)-V(3))*(1-vs-7*vf),['v= ',num2str(v/LargeNum)]);
else
   text(V(1)+(V(2)-V(1))*2/3,V(3)+(V(4)-V(3))*(1-vs-6*vf),['"dc" index change =
nonzero']);
   text(V(1)+(V(2)-V(1))*2/3,V(3)+(V(4)-V(3))*(1-vs-7*vf),['v= ',num2str(v)]);
end; % if ZeroDC



%%%save Refcorun4 zMaxR zHalfRBW zGratLambda zSLlevel ActualCenterL L alpha...
%%%n1 n2 n3 n4 a1
```

apod1L2apod2LVarDC.m

```
% original design is Ergodan's example of a chirped grating
% run apodv2ErgDes.m first

% profile of single apodizing function of original design is zero-dc

%%%%%%%%%%

   %  j = Centerindex;

   % Kl1ReadyMult drops with increasing lambdao by .21 percent over the range
   % of lambdao of interest and is larger that Kl3ReadyMult which drops by only
   % .15 percent.  Since the difference Kl1(z) - Kl3(z) is very small at edges,
   % to avoid it going negative for some values of lambdao, compute PerturbL1
   % and PerturbL3 with lambdao equal its largest value, corresponding to j=200.

   j = length(Bbar(:,count,toggleNum))
   lambdao=minLambdao+delLambdao*(j-1);
   BbarP=Bbar(j,count,toggleNum);

   [M,U]=UevalM(BbarP,lambdao,toggle);
   Mpeice2=M(1:5,2:6);
   Mpeice1=M(1:5,1);
   A(1)=1;
   A(2:6)=inv(Mpeice2)*(-1)*Mpeice1*A(1);

   P=2*.5*BbarP/377*quad8('eysqr',0,10*a3,[],[],A,U,BbarP,lambdao);
   A=A/sqrt(P);

   maxsigma=2*.5*2*pi/lambdao/377* (
N(1)*delnL1*quad8('eysqr',a(1),a(2),[],[],A,U,BbarP,lambdao) ...
   + N(2)*delnL2*quad8('eysqr',a(2),a(3),[],[],A,U,BbarP,lambdao) ...
   + N(3)*delnL3*quad8('eysqr',a(3),a(4),[],[],A,U,BbarP,lambdao) ...
   + N(4)*delnL4*quad8('eysqr',a(4),10*a(4),[],[],A,U,BbarP,lambdao) );

   if ZeroDC==1
      maxsigma = maxsigma/LargeNum;
   end; % if ZeroDC

   maxK = v/2 * 2*.5*2*pi/lambdao/377* (
N(1)*delnL1*quad8('eysqr',a(1),a(2),[],[],A,U,BbarP,lambdao) ...
   + N(2)*delnL2*exp(sqrt(-1)*pl2mpl1)*quad8('eysqr',a(2),a(3),[],[],A,U,BbarP,lambdao)
...
   + N(3)*delnL3*exp(sqrt(-1)*pl3mpl1)*quad8('eysqr',a(3),a(4),[],[],A,U,BbarP,lambdao)
...
   + N(4)*delnL4*exp(sqrt(-
1)*pl4mpl1)*quad8('eysqr',a(4),10*a(4),[],[],A,U,BbarP,lambdao) );

   % omega = 2*pi*f = 2*pi*c / lambdao;
   PerturbL1divisor = 2*pi / lambdao /377 /4 * 2 * ...
                      N(1)*quad8('eysqr',a(1),a(2),[],[],A,U,BbarP,lambdao);
   PerturbL3divisor = 2*pi / lambdao /377 /2 * ...
                      N(3)*quad8('eysqr',a(3),a(4),[],[],A,U,BbarP,lambdao);

   if ZeroDC==1
```

```
      maxK = maxK/LargeNum;
   end; % if ZeroDC

%%%%%%%%%%%

maxSlice4plotting = 200;
deltaz=L/maxSlice4plotting;

for Slice=1:maxSlice4plotting

   % Guassian profile
   if toggleProf==1
      term = exp( -4 * log(2) * (L/2 -Slice*deltaz +deltaz/2)^2 / FWHM^2 );
   else
   % Raised-Cosine Profile
   if toggleProf==2
      term = .5 * ( 1+cos(pi* (L/2 -Slice*deltaz +deltaz/2) / FWHM ));
      termTrack(Slice) = term;
   else
      term = 1;
   end; % if toggleProj==2
   end; % if toggleProf==1

%   sigma = maxsigma * term;
   K(Slice) = maxK * term;

   BbarP=Bbar(Centerindex,count,toggleNum);
   derLambdaoD = -1 * 1e-9/1e-2;
   Phi(Slice) = .5 * -4*pi*Bbar(Centerindex,count,toggleNum)* (L/2 -Slice*deltaz
+deltaz/2)^2 / ...
                (CenterLambdao^2) * derLambdaoD;

   z(Slice) = (L/2 -Slice*deltaz +deltaz/2);

   derPhi(Slice) = -4*pi*Bbar(Centerindex,count,toggleNum)* (L/2 -Slice*deltaz +deltaz/2)
/ ...
                   (CenterLambdao^2) * derLambdaoD;


end; % for Slice = 1:maxSlice4Plotting;

   % assume PhiL1(z)=0, PhiL3(z)=pi;
   Kl1 = ( K - .25*derPhi ) / 2;
   Kl3 = ( -K - .25*derPhi ) / 2;
   minPartial = min( [Kl1 Kl3] );

   Kl1 = Kl1 - minPartial;
   Kl3 = Kl3 - minPartial;

   % find delnL1bar * fL1 * v for layers
   PerturbL1 = Kl1 / PerturbL1divisor;
   PerturbL3 = Kl3 / PerturbL3divisor;


   figure; subplot(3,1,2);
   plot( z,PerturbL1.*( ones(1,length(z)) + cos( 2*pi/ (L/60) * z + 0 ) ) );
   title('Perturbation within layer 1 (gratings exist in layers 1 and 3)');
   xlabel('z (meters)');
   ylabel('delta n (unitless)');

   subplot(3,1,3);
   plot( z,PerturbL3.*( ones(1,length(z)) +cos( 2*pi/ (L/60) * z + pi) ) );
   title('Perturbation within layer 3');
   xlabel('z (meters)');
   ylabel('delta n (unitless)');

   subplot(3,1,1);
   plot( z,delnL1*termTrack.*cos( 2*pi/ (L/60) * z + Phi ) );
   title('Variation of the index change for original design');
   xlabel('z (meters)');
```

apod2LVarDC.m

```
% first run apodv2ErgDesChirp.m, then apod1L2apod2LZeroDC.m

minPartialAt155 = -9.451237885844486e2;
GratLambda=pi/( Bbar(Centerindex,1,1)*2*pi/ActualCenterL + 2 * -2 * minPartialAt155 );

for j=1:S(1)

   lambdao=minLambdao+delLambdao*(j-1);
   BbarP=Bbar(j,count,toggleNum);

   [M,U]=UevalM(BbarP,lambdao,toggle);
   Mpeice2=M(1:5,2:6);
   Mpeice1=M(1:5,1);
   A(1)=1;
   A(2:6)=inv(Mpeice2)*(-1)*Mpeice1*A(1);

   P=2*.5*BbarP/377*quad8('eysqr',0,10*a3,[],[],A,U,BbarP,lambdao);
   A=A/sqrt(P);

   % omega = 2*pi*c/lambdao
   Kl1ReadyMult = 2*pi/lambdao /377 /2 *
N(1)*quad8('eysqr',a(1),a(2),[],[],A,U,BbarP,lambdao);
   Kl1ReadyMultTrack(j) = Kl1ReadyMult;
   Kl3ReadyMult = 2*pi/lambdao /377 /2 *
N(3)*quad8('eysqr',a(3),a(4),[],[],A,U,BbarP,lambdao);
   Kl3ReadyMultTrack(j) = Kl3ReadyMult;

   PhiL1 = 0;
   PhiL3 = pi;

   delE = BbarP*2*pi/lambdao-pi/GratLambda;

   maxSlice = maxSlice4plotting;

   deltaz=L/maxSlice;
   if deltaz<10*GratLambda
      disp('Error: decrease maxSlice !!!');
   end; % if deltaz

   RoverS = [1; 0];

   for Slice=1:maxSlice

      Kl1 = Kl1ReadyMult * PerturbL1(Slice);
      Kl1Track(Slice) = Kl1;
      Kl3 = Kl3ReadyMult * PerturbL3(Slice);
      Kl3Track(Slice) = Kl3;

      ZeroDC4MultLayer = 0;
      if ZeroDC4MultLayer~=1
         v=1;
         sigma = 2 /v * (Kl1 + Kl3);
      else
         sigma = 0;
      end; % if ZeroDC4MultLayer

      %Ksa = Kl1*exp(i*PhiL1) + Kl3*exp(i*PhiL3);
      Ksa = Kl1 - Kl3;
      KsaTrack(Slice) = Ksa;
      K = abs(Ksa);
      Phi(Slice) = angle(Ksa);

   end; % for Slice=

   Phi = unwrap(Phi);
   Phi = fliplr( Phi ); % Slices were ordered from L/2 to -L/2
   derPhiTemp1 = diff(Phi) / deltaz;
   derPhiTemp2 = interp( derPhiTemp1, 2);
   derPhiTemp3 = derPhiTemp2( 2:2:length(derPhiTemp2) );
```

```
   derAtNegLDiv2 = interp( fliplr(derPhiTemp1), 2 );
   derAtNegLDiv2 = derAtNegLDiv2( length(derAtNegLDiv2) );
   derPhi = [ derAtNegLDiv2 derPhiTemp3 ];
   derPhi = fliplr(derPhi); % Slices are again ordered from L/2 to -L/2
   if j==1
      derPhiTrack = derPhi;
   end;

   % check
   if length(derPhi) ~= maxSlice
      disp('Error: length(derPhi) ~= maxSlice');
   end;

   RoverS = [1; 0];
   for Slice=1:maxSlice

      Kl1 = Kl1ReadyMult * PerturbL1(Slice);
      Kl3 = Kl3ReadyMult * PerturbL3(Slice);

      ZeroDC4MultLayer = 0;
      if ZeroDC4MultLayer~=1
         v=1;
         sigma = 2 /v * (Kl1 + Kl3);
      else
         sigma = 0;
      end; % if ZeroDC4MultLayer

      Ksa = Kl1*exp(i*PhiL1) + Kl3*exp(i*PhiL3);
      K = abs(Ksa);
      if j==1
         KTrack(Slice) = K;
      end; % if j==1

      sigmahat = delE + sigma -.5*derPhi(Slice);

      gamma = sqrt( (abs(K))^2 - sigmahat^2);
      F = [ cosh(gamma*deltaz) - i*sigmahat/gamma*sinh(gamma*deltaz) ...
            -i*K/gamma*sinh(gamma*deltaz);
            i*conj(K)/gamma*sinh(gamma*deltaz) ...
            cosh(gamma*deltaz) + i*sigmahat/gamma*sinh(gamma*deltaz) ];
      RoverS = F*RoverS;
   end; % for Slice=

R(j) = ( abs( RoverS(2)/RoverS(1) ) )^2;
PhaseRho1(j) = angle( RoverS(2)/RoverS(1) );
PhaseRho2(j) = angle( RoverS(2)/RoverS(1) ) - (-2*delE*L/2);

end; % for j=1:S(1)



lambdao=minLambdao+delLambdao*((1:j)-1);
PhaseRho1 = unwrap(PhaseRho1);
temp1 = [ lambdao(1:length(lambdao)-1); lambdao(2:length(lambdao)) ];
temp2 = [ -1*PhaseRho1(1:length(PhaseRho1)-1); PhaseRho1(2:length(PhaseRho1)) ];
for index=1:length(temp1)
   lambdaoDT(index) = sum( temp1(:,index) )/2;
   DelayTime(index) = -1*lambdaoDT(index)^2 / (2*pi*3e8) * sum( temp2(:,index)
)/delLambdao;
end; % for index=

temp1 = [ lambdaoDT(1:length(lambdaoDT)-1); lambdaoDT(2:length(lambdaoDT)) ];
temp2 = [ -1*DelayTime(1:length(DelayTime)-1); DelayTime(2:length(DelayTime)) ];
for index=1:length(temp1)
   lambdaoDis(index) = sum( temp1(:,index) )/2;
   Dispersion(index) = sum( temp2(:,index) ) / delLambdao;
end; % for index=


plot(lambdao,R);
title('Reflection Coefficient versus Wavelength');
```

```
xlabel('Lambdao'); ylabel('R');
axis([minLambdao max(lambdao) 0 1]);
V=axis;

vertfrac=1/14;
vertstart=1/12;
vf=vertfrac; vs=vertstart;
text(V(1)+(V(2)-V(1))*1/25,V(3)+(V(4)-V(3))*(1-vs),['n1= ',num2str(n1,5)]);
text(V(1)+(V(2)-V(1))*1/6,V(3)+(V(4)-V(3))*(1-vs),['n2= ',num2str(n2,5)]);
text(V(1)+(V(2)-V(1))*1/25,V(3)+(V(4)-V(3))*(1-vs-vf),['n3= ',num2str(n3,5)]);
text(V(1)+(V(2)-V(1))*1/6,V(3)+(V(4)-V(3))*(1-vs-vf),['n4= ',num2str(n4,5)]);
text(V(1)+(V(2)-V(1))*1/25,V(3)+(V(4)-V(3))*(1-vs-2*vf),['a1= ',num2str(a1),' m']);
if n2==n3 & n3==n4
   text(V(1)+(V(2)-V(1))*1/25,V(3)+(V(4)-V(3))*(1-vs-3*vf),['a2= irrelevant']);
   text(V(1)+(V(2)-V(1))*1/25,V(3)+(V(4)-V(3))*(1-vs-4*vf),['a3= irrelevant']);
else
   text(V(1)+(V(2)-V(1))*1/25,V(3)+(V(4)-V(3))*(1-vs-3*vf),['a2= ',num2str(a2),' m']);
   text(V(1)+(V(2)-V(1))*1/25,V(3)+(V(4)-V(3))*(1-vs-4*vf),['a3= ',num2str(a3),' m']);
end; % if n2==

text(V(1)+(V(2)-V(1))*1/25,V(3)+(V(4)-V(3))*(1-vs-5*vf),['Length= ',num2str(L),' m']);
text(V(1)+(V(2)-V(1))*1/25,V(3)+(V(4)-V(3))*(1-vs-6*vf),['GratLambda=
',num2str(GratLambda),' m']);

      zMaxR=max(R);
      dummy=R-zMaxR/2; dummy=dummy+abs(dummy);
      mloop=1;
      while dummy(Centerindex+mloop)>0
         mloop=mloop+1;
      end; % while dummy(
      nloop=1;
      while dummy(Centerindex-nloop)>0
         nloop=nloop+1;
      end; % while nloop
      zHalfRBW=delLambdao*(mloop+nloop);
%%    zGratLambda=GratLambda;
%     mloop=1;
%     while R(Centerindex+mloop)<R(Centerindex+mloop-1)
%        mloop=mloop+1;
%     end; % while mloop
%     nloop=1;
%     while R(Centerindex-nloop)<R(Centerindex-nloop+1)
%        nloop=nloop+1;
%     end; % while nloop
%     zSLlevel=max(R.*[ones(1,Centerindex-nloop) zeros(1,mloop+nloop-2+1) ...
%     ones(1,length(R)-Centerindex-mloop+1)]);

text(V(1)+(V(2)-V(1))*1/25,V(3)+(V(4)-V(3))*(1-vs-7*vf),['Measurements:']);
text(V(1)+(V(2)-V(1))*1/25,V(3)+(V(4)-V(3))*(1-vs-8*vf),['1-Max(R)= ',num2str(1-zMaxR)]);
text(V(1)+(V(2)-V(1))*1/25,V(3)+(V(4)-V(3))*(1-vs-9*vf),['Half R BW=
',num2str(zHalfRBW,7),' m']);
%%text(V(1)+(V(2)-V(1))*1/25,V(3)+(V(4)-V(3))*(1-vs-10*vf),['1st S-Lobe Level=
',num2str(zSLlevel)]);

text(V(1)+(V(2)-V(1))*2/3,V(3)+(V(4)-V(3))*(1-vs),['# Slices = ',num2str(maxSlice)]);


if toggleProf==1
   text(V(1)+(V(2)-V(1))*2/3,V(3)+(V(4)-V(3))*(1-vs-2*vf),['Profile is Guassian-->']);
   text(V(1)+(V(2)-V(1))*2/3,V(3)+(V(4)-V(3))*(1-vs-3*vf),['delnbar=
',num2str(alpha),'*(n-nSiO2) *']);
   text(V(1)+(V(2)-V(1))*2/3,V(3)+(V(4)-V(3))*(1-vs-3.5*vf),['   exp ( -4 ln2 z^2 /
FWHM^2 )']);
   text(V(1)+(V(2)-V(1))*2/3,V(3)+(V(4)-V(3))*(1-vs-4*vf),['z= -L/2 to L/2']);
   text(V(1)+(V(2)-V(1))*2/3,V(3)+(V(4)-V(3))*(1-vs-5*vf),['FWHM= ',num2str(FWHM),' m']);
else
if toggleProf==2
   text(V(1)+(V(2)-V(1))*2/3,V(3)+(V(4)-V(3))*(1-vs-2*vf),['Profile is Raised Cosine--
>']);
   text(V(1)+(V(2)-V(1))*2/3,V(3)+(V(4)-V(3))*(1-vs-3*vf),['delnbar=
',num2str(alpha),'*(n-nSiO2) *']);
```

```
   text(V(1)+(V(2)-V(1))*2/3,V(3)+(V(4)-V(3))*(1-vs-3.5*vf),['   0.5*(1+cos( pi*z/FWHM )
']);
   text(V(1)+(V(2)-V(1))*2/3,V(3)+(V(4)-V(3))*(1-vs-4*vf),['z= -L/2 to L/2']);
   text(V(1)+(V(2)-V(1))*2/3,V(3)+(V(4)-V(3))*(1-vs-5*vf),['FWHM= ',num2str(FWHM),' m']);
else
   text(V(1)+(V(2)-V(1))*2/3,V(3)+(V(4)-V(3))*(1-vs-2*vf),['Profile is Uniform']);
   text(V(1)+(V(2)-V(1))*2/3,V(3)+(V(4)-V(3))*(1-vs-3*vf),['delnbar=
',num2str(alpha),'*(n-nSiO2)']);
end; % if toggleProj==2
end; % if toggleProf==1

if ZeroDC==1
   text(V(1)+(V(2)-V(1))*2/3,V(3)+(V(4)-V(3))*(1-vs-6*vf),['"dc" index change = zero']);
   text(V(1)+(V(2)-V(1))*2/3,V(3)+(V(4)-V(3))*(1-vs-7*vf),['v= ',num2str(v/LargeNum)]);
else
   text(V(1)+(V(2)-V(1))*2/3,V(3)+(V(4)-V(3))*(1-vs-6*vf),['"dc" index change =
nonzero']);
   text(V(1)+(V(2)-V(1))*2/3,V(3)+(V(4)-V(3))*(1-vs-7*vf),['v= ',num2str(v)]);
end; % if ZeroDC



%%%save Refcorun4 zMaxR zHalfRBW zGratLambda zSLlevel ActualCenterL L alpha...
%%%n1 n2 n3 n4 a1
```

Bibliography

[1] T. Erdogan, "Fiber Grating Spectra," *Journal of Lightwave Technology*, Vol. 15, No. 8, pp. 1277-1294, August 1997.

[2] K. O. Hill and G. Meltz, "Fiber Bragg Grating Technology Fundamentals and Overview," *Journal of Lightwave Technology*, Vol. 15, No. 8, pp. 1263-1276, August 1997.

[3] C. C. Chang, "Coupled-Waveguide Fabry-Perot Resonator," M.S. thesis, Virginia Tech, December 1992.

[4] H. N. Rourke, S. R. Baker, K. C. Byron, R. S. Baulcomb, S. M. Ojha, and S. Clements, "Fabrication and Characterisation of Long, Narrowband Fibre Gratings by Phase Mask Scanning," *Electronics Letters*, Vol. 30, No. 16, pp. 1341-1342, August 4, 1994.

[5] M. Ibsen, J. Hubner, J. E. Pedersen, R. Kromann, L. U. A. Andersen, and M. Kristensen, "30 dB Sampled Gratings in Germanosilicate Planar Waveguides," *Electronics Letters*, Vol 32, No. 24, pp. 2233-2235, November 21, 1996.

[6] H. Nishihara, M. Haruna, and T. Suhara, *Optical Integrated Circuits*, McGraw-Hill Optical and Electro-Optical Engineering Series, New York, 1985.

[7] C. W. Haggans, H. Singh, W. F. Varner, L. Yaowen, and M. Zippin, "Narrow-band Rejection Filters With Negligible Backreflection Using Tilted Photoinduced Gratings in Single-Mode Fibers," *IEEE Photonics Technology Letters*, Vol. 10, No. 5, pp. 690-692, May 1998.

[8] A. Yariv, "Coupled-Mode Theory for Guided-Wave Optics," *IEEE Journal of Quantum Electronics*, Vol. QE-9, pp. 919-933, 1973.

[9] H. Kogelnik, "Theory of Optical Waveguides," *Guided-Wave Optoelectronics*, T. Tamir, Ed. New York: Springer-Verlag, 1990.

[10] V. Mizrahi and J. E. Sipe, "Optical Properties of Photosensitive Fiber Phase Gratings," *Journal of Lightwave Technology*, Vol. 11, No. 10, pp. 1513-1517, October 1993.

[11] R. C. Lawson, “A Study of Periodic Gratings in Planar Dielectric Waveguides,” M.S. thesis, Virginia Tech, December 1994.

[12] A. Safaai-Jazi, notes

[13] H. A. Haus, Waves and Fields in Optoelectronics, Prentice-Hall, New Jersey, 1984.

[14] B. J. Eggleton, P. A. Krug, L. Poladian, and F. Ouellette, “Long Periodic Superstructure Bragg Gratings in Optical Fibers,” *Electronics Letters*, Vol. 30, pp. 1620-1622, 1994.

[15] J. Martin, M. Tetu, C. Latrasse, A. Bellemare, and M. A. Duguay, “Use of a Sampled Bragg Grating as an In-Fiber Optical Resonator for the Realization of a Referencing Optical Frequency Scale for WDM Communications,” Optical Fiber Communications Conference, Dallas, TX, Feb. 16-21, 1997, paper ThJ5.

[16] J. E. Sipe, L. Poladian, C. Martijn de Sterke, “Propagation Through Nonuniform Grating Structures,” *Journal of the Optical Society of America*, Vol. 11, No. 4, pp. 1307-1320, April 1994.

[17] J. Albert, K. O. Hill, B. Malo, S. Theriault, F. Bilodeau, D. C. Johnson, and L. E. Erickson, “Apodisation of the Spectral Response of Fibre Bragg Gratings Using a Phase Mask with Variable Diffraction Efficiency,” *Electronics Letters*, Vol. 31, No. 3, pp. 222-223, February 2, 1995.

[18] B. Malo, S. Theriault, D. C. Johnson, F. Bilodeau, J. Albert, and K. O. Hill, “Apodised In-Fibre Bragg Grating Reflectors Photoimprinted Using a Phase Mask,” *Electronics Letters*, Vol. 31, No. 3, pp. 223-225, February 2, 1995.

[19] K. O. Hill, B. Malo, F. Bilodeau, D. C. Johnson, and J. Albert, “Bragg Gratings Fabricated in Monomode Photosensitive Optical Fiber by UV Exposure Through a Phase Mask,” *Applied Physics Letters*, Vol. 62, No. 10, pp. 1035-1037, March 8, 1993.

[20] K. O. Hill, S. Theriault, B. Malo, F. Bilodeau, T. Kitagawa, D. C. Johnson, J. Albert, K. Takiguchi, T. Kataoka, and K. Hagimoto, “Chirped In-Fibre Bragg Grating Dispersion Compensators: Linearisation of Dispersion Characteristic and Demonstration of Dispersion Compensation in 100 km, 10 Gbit/s Optical Fibre Link,” *Electronics Letters*, Vol. 30, No. 21, pp. 1755-1756, October 13, 1994.

[21] K. O. Hill, F. Bilodeau, B. Malo, T. Kitagawa, S. Theriault, D. C. Johnson, J. Albert, and K. Takiguchi, "Aperiodic In-Fiber Bragg Gratings For Optical Fiber Dispersion Compensation," Technical Digest Postdeadline Papers, Optical Fiber Communications Conference 1994, (Postdeadline Paper PD2).

[22] J. Martin and F. Ouellette, "Novel Writing Technique of Long and Highly Reflective In-Fibre Gratings," *Electronics Letters*, Vol. 30, pp. 811-812, May 12, 1994.

[23] D. Z. Anderson, V. Mizrahi, T. Erdogan, and A. E. White, "Production of In-Fibre Gratings Using a Diffractive Optical Element," *Electronics Letters*, Vol. 29, No. 6, pp. 566-568, March 18, 1993.

[27] B. Eggleton, P. A. Krug, L. Poladian, "Dispersion Compensation By Using Bragg-Grating Filters With Self-Induced Chirp," Optical Fiber Communications Conference 1994, pp. 227, (Paper ThK3).

[28] K. Sugden, I. Bennion, A. Molony, and N. J. Cooper, "Chirped Gratings Produced in Photosensitive Optical Fibres by Fibre Deformation During Exposure," *Electronics Letters*, Vol. 30, No. 5, pp. 440-442, March 3, 1994.

[29] R. Kashyap, P. F. McKee, R. J. Campbell, and D. L. Williams, "Novel Method of Producing All Fibre Photoinduced Chirped Gratings," *Electronics Letters*, Vol. 30, No. 12, pp. 996-997.

[30] J. Martin, J. Lauzon, S. Thibault, and F. Ouellette, "Novel Writing Technique of Long Highly Reflective in Fibre Bragg Gratings and Investigation of the Linearly Chirped Component," Technical Digest Postdeadline Papers , Optical Fiber Communications Conference 1994, (Postdeadline Paper PD29-1).

[31] R. Kashyap, H. G. Froehlich, A. Swanton, and D. J. Armes, "1.3 m Long Super-Step-Chirped Fibre Bragg Grating With a Continuous Delay of 13.5 ns and Bandwidth 10 nm for Broadband Dispersion Compensation," *Electronics Letters*, Vol. 32, No. 19, pp. 1807-1809, September 12, 1996.

[32] I. Bennion, J. A. R. Williams, L. Zhang, K. Sugden, and N. J. Doran, "UV-Written In-Fibre Bragg Gratings," *Optical and Quantum Electronics*, Vol. 28, pp. 93-135, 1996.

[33] R. Kashyap, H. G. Froehlich, A. Swanton, and D. J. Armes, “Super-Step-Chirped Fibre Bragg Gratings,” *Electronics Letters*, Vol. 32, No. 15, pp. 1394-1396, July 18, 1996.

[34] R. Kashyap, A. Swanton, and D. J. Armes, “Simple Technique for Apodising Chirped and Unchirped Fibre Bragg Gratings,” *Electronics Letters*, Vol. 32, No. 13, pp. 1226-1228, June 20, 1996.

[35] R. Kashyap, G. D. Maxwell, and B. J. Ainslie, “Laser Trimmed Four-Port Bandpass Filter Fabricated in Singlemode Planar Waveguides,” *IEEE Photonics Technology Letters*, Vol. 51, No. 2, pp. 191-194, 1993.

[36] A. Asseh, H. Storoy, B. E. Sahlgren, S. Sandgren, and R. A. H. Stubbe, “A Writing Technique for Long Fiber Bragg Gratings with Complex Reflectivity Profiles,” *Journal of Lightwave Technology*, Vol. 15, No. 8, pp. 1419-1423, August 1997.

Vita

Thomas L. Gradishar was born in Woodbury, N. J., on September 10, 1971. He received National Merit and Robert C. Byrd scholarships, and matriculated at Virginia Tech in August, 1989, in the Bradley Department of Electrical Engineering. He cooped at E. I. du Pont de Nemours and Company in Washington, W.V., where he was raised. He obtained a B.S. in May, 1994, and enrolled in the M.S. program in electrical engineering at Virginia Tech. He was a teaching assistant from August, 1996 through December, 1998, and received the EE department's 1997-98 graduate teaching assistant award. Mr. Gradishar will begin work at Motorola in Boynton Beach, Fl., in the spring of 1999.